DOCTOR OF PHILOSOPHY

Defining the mechanism of arsenic-induced degradation of PML

Hands, Katherine J.

Award date:
2012

DOCTOR OF PHILOSOPHY

Defining the mechanism of arsenic-induced degradation of PML

Katherine J. Hands

2012

University of Dundee

Defining the mechanism of arsenic-induced degradation of PML

by

Katherine J Hands

Thesis submitted for the degree of

Doctor of Philosophy

University of Dundee

August 2012

Acknowledgements

I would like to thank my supervisor, Ron Hay, for the opportunity to undertake my PhD research in his laboratory, and for all his help and guidance. Thanks also to all members of the Hay lab, past and present, for their help and friendship.

I am grateful to the Wellcome Trust for funding my research, and to the directors of the Clinical PhD programme in Dundee: Sara Marshall, Doreen Cantrell and Jerry Lambert for their support throughout my studies. I would also like to acknowledge the haematology department at Ninewells Hospital for their support while I pursued my interest in research.

To perform the work presented in this thesis I learned a multitude of new skills. Thanks to all who helped me learn these. In particular, thanks to Sam Swift, Callum Thomson and Markus Posch for help with microscopy, Manu de Rycker and Paul Andrews for introducing me to high content imaging, and Adel Ibrahim and Amit Garg for help with siRNA screening.

Finally, thank you to my friends and family, especially Sam, for all their support over the past three years.

Declaration

I hereby declare that the following thesis is based on the results of investigations conducted by me, and that this thesis is of my own composition. Work other than my own is clearly indicated in the text by reference to the relevant researchers or their publications. All references cited have been consulted by me. This thesis has not, in whole or part, been previously accepted for a higher degree.

Katherine J Hands

I certify that the work of which this thesis is a record was performed by Katherine Hands. The conditions of the relevant Ordinance and Regulations have been fulfilled.

Professor Ronald T Hay

Contents

Acknowledgements **2**

List of figures **9**

List of tables **9**

Abbreviations **14**

Abstract **19**

1 Introduction **21**

1.1 Ubiquitin 21

1.1.1 Ubiquitin like proteins 21

1.1.2 Ubiquitin conjugation 21

1.1.3 Ubiquitin chains 23

1.2 SUMO 24

1.2.1 SUMO conjugation 25

1.2.2 SUMO interaction motif 27

1.3 PML 27

1.3.1 PML Isoforms 28

1.3.2 PML and SUMO modification 28

1.3.3 PML nuclear bodies 30

1.3.3.1 Cell cycle variation 31

1.3.3.2 Antiviral response 32

1.3.3.3 Apoptosis control 32

1.3.3.4 Control of transcription 33

1.3.3.5 Cellular senescence 33

1.4 Acute promyelocytic leukaemia 34

1.4.1 Pathogenesis of APL 34

1.4.2 Treatment of APL 36

1.5 Mechanism of arsenic induced degradation of PML 38

1.5.1 The role of RNF4 40

1.5.2 Resistance to arsenic therapy 42

2 Materials and methods 43

2.1 DNA and RNA techniques 43

2.1.1 Constructs used in this study 43

2.1.2 DNA sequencing 43

2.1.3 Transformation of competent E coli cells 43

2.1.4 Small scale preparation of plasmid DNA (miniprep) 43

2.1.5 RNA preparation 44

2.1.6 Reverse transcription of RNA 44

2.1.7 RT qPCR 45

2.1.7.1 RT qPCR primer sequences (5'→ 3') 46

2.2 Protein techniques 47

2.2.1 SDS-PAGE 47

2.2.2 Coomassie Blue staining 47

2.2.3 Western blot analysis 48

2.2.4 Antibodies used in this study 49

2.3 Cell culture and lysates....51
2.3.1 Cell lines....51
2.3.2 Generation of eYFP HeLa cell line....52
2.3.3 DNA transfections....52
2.3.4 siRNA transfections....52
2.3.5 Cell treatments....53
2.3.6 Cell lysis....53
2.3.7 Lysis of NB4 cells....54
2.3.8 ATP based survival assay....54
2.4 Immunoprecipitation....56
2.4.1 GFP-IP of YFP-PML isoforms....56
2.4.2 GFP-IP of YFP-PML for mass spectrometry....56
2.5 Microscopy techniques....57
2.5.1 Cell culture on coverslips....57
2.5.2 Cytospin preparations....58
2.5.3 Cell fixation and immunolabelling....58
2.5.3.1 Adherent cells....58
2.5.3.2 Suspension cells....59
2.5.4 Imaging....59
2.5.5 Image analysis....60
2.6 Structured illumination imaging....60
2.7 High content imaging....61

2.7.1 Tissue culture 61

2.7.2 siRNA transfection in 96 well plates 61

2.7.3 Cell treatments 61

2.7.4 Cell fixation and staining 62

2.7.5 Imaging 62

2.7.6 Image analysis 63

2.8 siRNA screening 63

2.8.1 Screen setup 63

2.8.1.1 siRNA library 63

2.8.1.2 Quality control 64

2.8.1.3 Preparation 65

2.8.1.4 Dispensing of siRNA 65

2.8.1.5 Arsenic treatment 66

2.8.1.6 Cell fixation and staining 67

2.8.1.7 Imaging and image analysis 67

2.9 Data analysis and hit identification 68

2.10 Follow up screen 68

3 Development of a high content siRNA screen 69

3.1 Introduction 69

3.1.1 RNA interference 69

3.1.1.1 Off-target effects of siRNA 72

3.1.2 Good practice in siRNA screening 73

3.2 Results 76

3.2.1 Characterisation of an affinity purified anti-PML antibody 76

3.2.2 PML is degraded in response to arsenic treatment..... 79

3.2.3 RNF4 is required for arsenic mediated degradation of PML..... 81

3.2.4 Characterisation of YFP-PML HeLa cell line..... 85

3.2.5 YFP-PML is degraded in an RNF4 dependent manner following arsenic treatment..... 87

3.2.6 Quantitation of YFP-PML fluorescence after RNF4 depletion and arsenic treatment..... 89

3.2.7 Development of an assay suitable for high content screening 93

3.2.7.1 High content imaging and image analysis 93

3.2.7.2 Z' factor assessment of assay..... 97

3.2.7.3 Test plates 99

3.2.8 Primary screen- ubiquitome siRNA library 101

3.2.8.1 Data analysis and quality control..... 103

3.2.8.2 Results..... 105

3.2.8.3 Hits selected for further follow up..... 109

3.2.9 Deconvolution screen- ubiquitome siRNA library 112

3.2.9.1 Data analysis and quality control..... 112

3.2.9.2 Results..... 113

3.2.9.3 Hits selected for further follow up..... 115

3.2.10 Primary screen- kinome siRNA library..... 116

3.2.10.1 Data analysis and quality control..... 116

3.2.10.2 Results....117

3.2.11 Conclusions....119

3.3 Discussion....121

3.3.1 Rationale for use of a high content screen....121

3.3.2 Appraisal of the screening assay....123

3.3.3 Other applications of the HCS assay....125

3.3.4 Selection of hits for further follow up....125

3.3.4.1 CHD4 and BAZ1B....126

3.3.4.2 UBE4B....127

3.3.4.3 OTUD5....128

3.3.4.4 CUL3 and DCUN1D1....129

4 A CUL3 ubiquitin ligase complex regulates PML....130

4.1 Introduction....130

4.1.1 Cullin RING ligases....130

4.1.2 NEDD8 mediated regulation of CRL ubiquitin ligase activity....131

4.1.3 The role of DCUN1D1 in regulation of CRL activity....133

4.1.4 Cullin 3 specific functions....133

4.2 Results....136

4.2.1 siRNA screening data demonstrates Cullin 3 depletion results in PML accumulation....136

4.2.2 Confirmation of CUL3 siRNA phenotype....138

4.2.3 DCUN1D1 depletion results in decreased neddylation of CUL3 and accumulation of PML....142

4.2.4 MLN4924 treatment results in accumulation of PML 144

4.2.5 Cell cycle analysis following CUL3 depletion 145

4.2.6 Attempts to identify BTB adaptor protein 147

4.2.6.1 Investigation of the role of LZTR1 in PML stabilisation 147

4.2.6.2 Targeted siRNA screen: BTB domain containing proteins 150

4.2.6.3 Deconvolution siRNA screen- BTB domain containing proteins ... 152

4.2.6.4 Further experiments with siRNA 153

4.2.6.5 GFP IP and mass spectrometry to identify YFP PML interaction partners 155

4.2.7 MLN4924 treatment of leukaemia cell lines 157

4.2.8 Conclusions 160

4.3 Discussion 161

4.3.1 CUL3 depletion leads to PML accumulation 161

4.3.2 Attempts at rescue experiments 163

4.3.3 BTB domain adaptor protein identification 164

4.3.4 PML, CUL3 and disease 165

5 Degradation characteristics of PML isoforms in response to arsenic 167

5.1 Introduction 167

5.2 Results 168

5.2.1 PML isoforms degrade at different rates in response to arsenic treatment 168

5.2.2 PML and the PML-RARα oncoprotein degrade at similar rates in response to arsenic treatment 169

5.2.3 Characterisation of cell lines expressing only a single PML isoform.....171

5.2.4 Characterisation of the response of individual PML isoforms to arsenic treatment.....174

5.2.5 High content imaging and quantification of YFP PML fluorescence.....177

5.2.6 Super resolution imaging reveals differences in PML body structure....183

5.2.7 All PML isoforms are SUMO and ubiquitin modified following arsenic treatment.....188

5.2.8 The effect of RNF4 depletion on arsenic mediated degradation of PML isoforms I-VI.....191

5.2.9 Conclusions.....194

5.3 Discussion 196

5.3.1 Characterisation of the response of the major PML isoforms to arsenic treatment.....196

5.3.2 Susceptibility to arsenic mediated degradation.....196

5.3.3 Localisation of PML after arsenic treatment.....198

5.3.4 Differences in PML body structure.....199

5.3.5 RNF4 is required for degradation of all PML isoforms.....202

5.3.6 Implications for treatment of APL? 203

References 206

List of figures

Figure 1.1.1. Ubiquitin conjugation cascade....22

Figure 1.3.1. The exon assembly of PML (Adapted from Jensen et al., 2001) 29

Figure 1.3.2. PML nuclear bodies are punctate nuclear structures 31

Figure 1.4.1. PML-RARα isoforms 36

Figure 1.5.1. A model of the role of RNF4....41

Figure 3.1.1. Mechanism of siRNA induced gene silencing 70

Figure 3.2.1. Characterisation of a chicken anti PML antibody 77

Figure 3.2.2. siRNA mediated depletion of PML confirms chicken anti PML antibody specificity....79

Figure 3.2.3. PML is degraded following arsenic treatment in an RNF4 dependent manner....80

Figure 3.2.4. Immunofluorescence demonstrates PML accumulates in PML bodies in cells depleted of RNF4 prior to arsenic treatment 82

Figure 3.2.5. Immunofluorescence characterisation of YFP-PML HeLa cells....86

Figure 3.2.6. YFP-PML is degraded in an RNF4 dependent manner in response to arsenic treatment 88

Figure 3.2.7. Quantification of YFP-PML fluorescence following RNF4 depletion and arsenic treatment 91

Figure 3.2.8. Screenshot example of IN Cell Investigator software analysis of PML nuclear bodies....94

Figure 3.2.9. Automated quantification of YFP-PML fluorescence following RNF4 depletion and arsenic treatment....96

Figure 3.2.10. Testing the high content screening assay 100

Figure 3.2.11. Composition of the ubiquitome siRNA library 101

Figure 3.2.12. Plate layout and workflow for high content screening assay 102

Figure 3.2.13. Quality control for primary ubiquitome library siRNA screen 104

Figure 3.2.14. Quality control for deconvolution ubiquitome siRNA screen 113

Figure 3.2.15. Quality control for primary kinome library siRNA screen 117

Figure 4.1.1. Schematic of a CUL3-BTB protein complex 131

Figure 4.2.1. siRNA screen data for CUL3 siRNA 137

Figure 4.2.2. CUL3 depletion results in accumulation of PML 138

Figure 4.2.3. Quantification of YFP PML fluorescence following CUL3 depletion 140

Figure 4.2.4. DCUN1D1 depletion results in decreased CUL3 neddylation and PML accumulation 143

Figure 4.2.5. MLN 4924 treatment results in accumulation of PML 145

Figure 4.2.6. Cell cycle analysis following CUL3 depletion 146

Figure 4.2.7. The effects of siRNA mediated LZTR1 depletion 149

Figure 4.2.8. Quality control for BTB domain siRNA screen 151

Figure 4.2.9. Analysis of knockdown efficiency and effects on PML of siRNAs targeting BTB domain containing proteins. 154

Figure 4.2.10. Mass spectrometry analysis of YFP PML interacting proteins 156

Figure 4.2.11. MLN4924 treatment of leukaemia cell lines 159

Figure 5.2.1. PML isoforms appear to respond differently to arsenic treatment. 169

Figure 5.2.2. PML-RARα and PML degrade at similar rates following arsenic treatment 170

Figure 5.2.3. Western blotting of HepaRG cells expressing a single PML isoform.....172

Figure 5.2.4. Fluorescence microscopy of HepaRG cells expressing a single PML isoform 173

Figure 5.2.5. Western blotting of PML isoform expressing cells treated with arsenic.175

Figure 5.2.6. Immunofluorescence analysis of PML isoform expressing cells treated with arsenic 176

Figure 5.2.7. Screenshot of high content imaging analysis protocol 178

Figure 5.2.8. High content imaging and quantification of eYFP PML fluorescence following arsenic treatment: analysis of PML body size.....180

Figure 5.2.9. High content imaging and quantification of eYFP PML fluorescence following arsenic treatment: analysis of number of PML bodies per cell 182

Figure 5.2.10. Super- resolution imaging of PML isoform expressing cells treated with arsenic 185

Figure 5.2.11. Super resolution imaging of cytoplasmic PML inclusions following arsenic treatment 187

Figure 5.2.12. GFP immunoprecipitation confirms all PML isoforms are SUMO and ubiquitin modified in response to arsenic 190

Figure 5.2.13. Effect of RNF4 depletion on the response of PMLI and PML II to arsenic treatment……192

Figure 5.2.14. Effect of RNF4 depletion on the response of PML III and PML IV to arsenic treatment 193

Figure 5.2.15. Effect of RNF4 depletion on the response of PML V and PML VI to arsenic treatment 193

List of tables

Table I. Z' factor calculations 97

Table II. Ubiquitome screen: putative hits in non drug treated dataset which increase PML expression 106

Table III. Ubiquitome screen: putative hits in non drug treated dataset which decrease PML expression 107

Table IV. Ubiquitome screen: putative hits in arsenic treated dataset which increase PML expression 108

Table V. Ubiquitome screen: putative hits in arsenic treated dataset which decrease PML expression 109

Table VI. Ubiquitome screen follow up: putative hits in non drug treated dataset selected for further investigation in deconvolution screen 110

Table VII. Ubiquitome screen follow up: putative hits in arsenic treated dataset selected for further investigation in deconvolution screen 110

Table VIII. Deconvolution screen: siRNAs confirmed to increase PML expression following arsenic treatment 114

Table IX. Deconvolution screen: siRNAs confirmed to decrease PML expression following arsenic treatment 114

Table X. Deconvolution screen: siRNAs confirmed to decrease PML expression in the absence of arsenic 114

Table XI. Deconvolution screen: siRNAs confirmed to increase PML expression in the absence of arsenic 115

Table XII. Kinome screen: putative hits from non drug treated dataset 118

Table XIII. Kinome screen: putative hits from arsenic treated dataset.....119

Table XIV. Deconvolution screen: results for LZTR1 148

Table XV. BTB domain siRNA primary screen: putative hits 152

Table XVI. BTB domain siRNA deconvolution screen: results.....152

Table XVII. Proteins found to specifically interact with YFP PML by immunoprecipitation and mass spectrometry.....157

Equation 3.1. Z’ factor calculation.....98

Abbreviations

2D	two dimensional
3D	three dimensional
3D-SIM	three dimensional structured illumination microscopy
aa	amino acid
ABTB2	ankyrin repeat and BTB (POZ) domain containing 2
ANKFY1	ankyrin repeat and FYVE domain containing 1
APL	acute promyelocytic leukaemia
ATP	adenosine 5’-(tetrahydrogen triphosphate)
ATRA	all trans retinoic acid
BSA	bovine serum albumin
BTB	bric-a-brac, tramtrack, broad-complex
CAND1	cullin-associated and neddylation-dissociated 1
cDNA	complementary deoxyribonucleic acid
CREBBP	CREB binding protein
CRL	cullin RING ligase
CUL3	cullin 3
CyPN	cytoplasmic assemblies of PML and nucleoporins
DAPI	4',6-diamidino-2-phenylindole

DAXX	death domain associated protein
DCUN1D1	defective in cullin neddylation 1 dopmain containing 1
DMEM	Dulbecco's Modified Eagle Medium
DMSO	dimethyl sulfoxide
DNA	deoxyribonucleic acid
DSTT	Division of signal transduction therapy
DTT	dithiothreitol
DUB	deubiquitylating enzyme
EMCCD	electron multiplying charge coupled device
eYFP	enhanced yellow fluorescence protein
FBS	fetal bovine serum
FRAP	fluorescence recovery after photobleaching
GFP	green fluorescence protein
HECT	Homologous to the E6-AP Carboxyl Terminus
HRP	horse radish peroxidase
HSV1	herpes simplex virus 1
IC50	half maximal inhibitory concentration
IgY	immunoglobulin Y
IP	immunoprecipitation

ISG15	Interferon-induced 17 kDa protein
KCNC1	potassium voltage-gated channel, member 1
kD	kilodalton
KLHL25	kelch-like 25 (Drosophila)
LB	Luria-Bertani medium
LZTR1	leucine-zipper-like transcription regulator 1
MAPP	mitotic accumulations of PML
MDM2	Mdm2 murine double minute 2
MOPS	3-morpholinopropane-1-sulfonic acid
mRNA	messenger RNA
NAE	NEDD8 activating enzyme
NEDD8	Neural precursor cell expressed, developmentally down-regulated 8
NLS	nuclear localisation signal
NT	non-targeting
p300	E1A binding protein p300
p53	tumour protein p53
PAGE	polyacrylamide gel electrophoresis
PBS	phosphate buffered saline
PFA	paraformaldehyde

PIAS1	protein inhibitor of activated STAT, 1
PLZF	promyelocytic leukaemia zinc finger
PML	promyelocytic leukaemia protein
PML I-VI	PML isoform I-VI
PML-NB	PML nuclear body
PONY	potentiating neddylation
PVDF	polyvinylidene difluoride
QC	quality control
RARα	retinoic receptor alpha
Rb	retinoblastoma 1
RBX1/2	ring box protein 1/2
RING	really interesting new gene
RIPA	radioimmunoprecipitation assay buffer
RISC	RNA induced silencing complex
RNA	ribonucleic acid
RNF4	ring finger protein 4
rpm	revolutions per minute
RT-qPCR	real- time quantitative polymerase chain reaction
RXR	retinoid x receptor

SAE1/2	SUMO-activating enzyme 1/2
SCILLS	Scottish Institute for Cell Signalling
SDS	sodium dodecylsulphate
SENP	sentrin specific protease
shRNA	short hairpin RNA
SIM	SUMO-activating enzyme 1/2
siRNA	short interfering RNA
SP100	SP100 nuclear antigen
STUbL	SUMO targeted ubiquitin ligase
SUMO	small ubiquitin like modifier
TBS	tris buffered saline
TRIM	tripartite motif
Tris	tris(hydroxymethyl)aminomethane
UBA	ubiquitin associated
UBC	ubiquitin conjugating enzyme
Ubl	ubiquitin like protein
UTR	untranslated region
YFP	yellow fluorescent protein

Abstract

Arsenic trioxide is a clinically effective treatment for the disease acute promyelocytic leukaemia (APL) which is caused by the chromosomal translocation t(15;17) which fuses the promyelocytic leukaemia (PML) protein to the retinoic receptor alpha (RARα). The PML-RARα oncoprotein disrupts normal retinoic acid signalling and the function of PML nuclear bodies (PML-NBs), subnuclear protein complexes with roles in control of apoptosis and cellular senescence. Treatment with arsenic induces rapid post translational modification of PML and with the small ubiquitin like modifier (SUMO). SUMO modification of PML recruits the SUMO targeted ubiquitin E3 ligase RNF4 via four SUMO interaction motifs within the N-terminal region of RNF4. PML is then ubiquitylated and targeted for proteasomal degradation. In APL, these events trigger degradation of PML-RARα, curing the disease.

To further investigate the process of arsenic induced degradation of PML, a high content siRNA screen was designed to monitor the fate of a YFP linked version of PML after siRNA mediated knockdown of components of the ubiquitin system and arsenic treatment. RNF4 depletion prior to arsenic treatment prevented PML degradation and resulted in accumulation of PML in large, bright PML-NBs. This was used as a positive control. A library of siRNAs targeting 1067 gene products were screened to identify those which perturbed the process of arsenic mediated degradation of PML, and those which affected the stability of PML in untreated cells. A number of putative hits were identified. Depletion of the cullin RING ligase scaffold CUL3, and the NEDD8 E3 ligase DCUN1D1 resulted in striking accumulation of PML, suggesting PML may be a substrate of a CUL3 RING ligase complex. Further experiments using the inhibitor of neddylation, MLN4924 support this hypothesis.

PML is expressed as various isoforms which encode a unique C-terminal region, due to alternative splicing. The second part of this study investigated the role of this variable C-terminal region in the response of the six major PML isoforms to arsenic treatment. Using a system in which only a single eYFP-linked PML isoform is expressed, differences in the localisation of PML isoforms following arsenic treatment were identified, with PML I, II and VI found to accumulate in the cytoplasm following arsenic treatment, whereas PML III, IV and V did not. A high content imaging assay identified PML V as the isoform most readily degraded following arsenic treatment, and PML IV as relatively resistant to degradation. Using siRNA it was demonstrated that arsenic induced degradation of all PML isoforms is dependent on the ubiquitin E3 ligase RNF4. Intriguingly, depletion of RNF4 resulted in marked accumulation of PML V, suggesting this isoform is an optimal substrate for RNF4. Thus the variable C-terminal domain influences the rate and location of degradation of PML isoforms following arsenic treatment.

1 Introduction

1.1 Ubiquitin

1.1.1 Ubiquitin like proteins

The founding member of the family of ubiquitin like proteins is ubiquitin itself, a 76 amino acid protein which is responsible for the post translational modification of a vast array of substrate proteins (Kim et al., 2011). The covalent attachment of ubiquitin to a substrate protein, a process named ubiquitylation, is best characterised in the targeting of modified proteins for degradation by the 26S proteasome, a large multi-protein protease responsible for the regulated degradation of ubiquitylated proteins (Bedford et al., 2010).

Ubiquitin has a characteristic three dimensional structure, the β grasp fold, which is the hallmark structure of members of the ubiquitin like protein family, though the degree of sequence similarity to ubiquitin varies between family members (Hochstrasser, 2009). Other ubiquitin like proteins include Small Ubiquitin Like Modifier (SUMO), NEDD8, ISG15, FAT10 and ATG8. Like ubiquitin, SUMO is conjugated to hundreds of substrate proteins (Golebiowski et al., 2009). Each of these ubiquitin like proteins is conjugated to a target protein via a similar pathway, but each uses its own specific set of enzymes.

1.1.2 Ubiquitin conjugation

Ubiquitin is conjugated to target proteins via an enzymatic cascade involving three key enzymes (**Figure 1.1.1.**). The first step in this process involves the activation of the C- terminal glycine motif of ubiquitin by an E1 activating enzyme. Ubiquitin is then conjugated to a cysteine residue in an E2 conjugating enzyme via a thioester bond,

thus the E2 enzyme is ‘charged’ with ubiquitin. The charged E2 is subsequently bound by an E3 ligase enzyme, which also binds the target substrate, and ubiquitin is covalently linked to an amino group, most commonly the ε- amino group of a target lysine residue, in the substrate via an isopeptide bond. In humans, there are two ubiquitin E1 enzymes, approximately 30 E2 enzymes and more than 600 E3 ligases (Komander, 2009). There are two main classes of E3 enzyme: RING (Really Interesting New Gene) domain containing, and those with a HECT (Homologues to E6-AP C-terminus) domain. The mechanism of catalysis of ubiquitylation differs for the two classes of enzyme. E3 ligases with a HECT domain form a covalent intermediate with ubiquitin, whereas those with a RING domain catalyse the direct transfer of ubiquitin from the charged E2 enzyme to substrate.

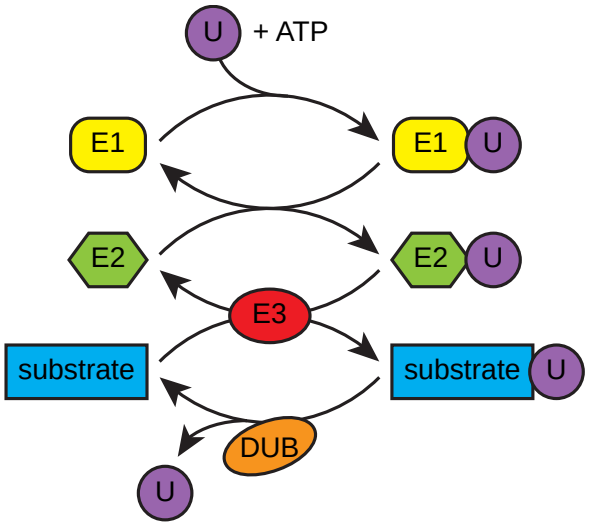

Figure 1.1.1. Ubiquitin conjugation cascade

Initially, ubiquitin is activated by the formation of a thioester bond between ubiquitin and the E1 activating enzyme, a process which is dependent on ATP. Ubiquitin is then transferred to an E2 conjugating enzyme. The final step in the ubiquitylation cascade is facilitated by a ubiquitin E3 ligase which recruits both substrate and ubiquitin charged E2 enzyme, and results in the formation of an isopeptide bond between the C- terminus of ubiquitin and the ε-amino group of a lysine side chain of the substrate protein. Deubiquitylating enzymes (DUBs) reverse this process.

1.1.3 Ubiquitin chains

The manner of ubiquitin modification modulates the effects of this modification on the substrate protein. A single ubiquitin molecule may be conjugated to a single lysine residue on the substrate protein, a process called monoubiquitylation, or single ubiquitin molecules may be conjugated to many lysine residues on the substrate protein: multiple monoubiquitylation. Monoubiquitylation is involved various cellular processes including endocytosis of membrane receptors (Haglund et al., 2003), the DNA damage response and the subcellular localisation of substrate proteins. (Haglund and Dikic, 2005). Monoubiquitylation may also serve as a starting point for polyubiquitin chain formation, with different E2 enzymes catalysing the initial and subsequent ubiquitylation events (Rodrigo-Brenni and Morgan, 2007; Windheim et al., 2008).

Ubiquitin itself has seven lysine residues (Lys6, 11, 27, 29, 33, 48 and 63), each of which can be modified with another ubiquitin moiety to form polymeric ubiquitin chains. Alternatively, linear ubiquitin chains are formed by the fusion of another ubiquitin molecule to the ubiquitin N terminus. The physiological role of some of these chain types is better characterised than of others. The most abundant of these are Lys48 linked chains, which comprise approximately one third of all ubiquitin chains (Xu et al., 2009). Lys48 linked ubiquitin chains are the best characterised ubiquitin chain, with a minimum of four Lys48 linked ubiquitin moieties functioning to target the substrate protein for degradation by the 26S proteasome (Thrower et al., 2000). Lys11 chains are almost as abundant as Lys48 chains (Xu et al., 2009), and also function as a signal for proteasomal degradation (Wickliffe et al., 2011). In contrast, Lys63 chains do not function as a signal for degradation. Rather, they have been implicated in endocytosis, the DNA damage response and cell signalling (Chen and Sun, 2009).

The process of ubiquitylation is reversible, through the action of deubiquitylating enzymes (DUBs). There are approximately 90 DUBs encoded by the human genome, which are attributed to five different families, classified by their protease domains (Ventii and Wilkinson, 2008). The majority are cysteine proteases which attack the lysine- glycine isopeptide bonds present in ubiquitylated proteins and ubiquitin chains (Sowa et al., 2009). DUBs can counteract the activity of E3 ligases by removing ubiquitin from substrates, or by editing ubiquitin chains and are also found at the proteasome where they are involved in the recycling of ubiquitin (Ventii and Wilkinson, 2008).

1.2 SUMO

The Small Ubiquitin like Modifier (SUMO) is a member of the family of ubiquitin like proteins, though it shares only 20% sequence identity with ubiquitin (Geoffroy and Hay, 2009; Hay, 2005). Like ubiquitin, SUMO is reversibly conjugated to ε- amino groups of a lysine residue of a substrate protein. There is one SUMO gene expressed in lower eukaryotes but three paralogues in vertebrates, termed SUMO1, SUMO2 and SUMO3. All three of these paralogues are expressed as larger, precursor molecules which are processed by proteases to reveal the diglycine motif which forms the isopeptide link to substrate (Hay, 2005; Melchior et al., 2003). The processed forms of SUMO2 and SUMO3 differ by only three amino acids at the N- terminus, and are difficult to functionally differentiate, and are therefore often referred to as SUMO2/3. SUMO1 shares only 50% sequence identity with SUMO2/3, but the proteins have both shared and distinct substrates (Vertegaal et al., 2006). There is redundancy between SUMO1 and SUMO2/3, because SUMO1 deficient mice are viable (Evdokimov et al., 2008; Zhang et al., 2008), but mice deficient in the SUMO conjugating enzyme UBC9

are not (Nacerddine et al., 2005), suggesting SUMO2/3 can take over at least some of the functions of the absent SUMO1.

SUMO modification has been implicated in the control of many cellular functions, including control of gene expression, maintenance of genome integrity, protein stability and intracellular transport (Hay, 2005; Melchior et al., 2003). More recently, SUMO has been characterised as a signal to recruit ubiquitin E3 ligases (Lallemand-Breitenbach et al., 2008; Tatham et al., 2008; Yin et al., 2012). Post translational modification with SUMO, as for modification with other Ubls, creates additional surfaces for protein- protein interactions.

1.2.1 SUMO conjugation

The process of SUMO conjugation to a substrate, termed sumoylation, proceeds through an enzymatic cascade similar to that for ubiquitin, but using a discrete set of enzymes (Hay, 2005). SUMO precursors are first processed to reveal the C terminal diglycine motif which is subsequently conjugated to the ε- amino group of a target lysine residue in the substrate protein. There is one SUMO E1 activating enzyme, a heterodimer of SAE1 and SAE2 (Desterro et al., 1999). Unlike the ubiquitin system, there is only one SUMO E2 enzyme, UBC9 (Desterro et al., 1997), which is often capable of transferring SUMO to the substrate in the absence of an E3 ligase, but the process is made more efficient in the presence of an E3 ligase (Johnson and Gupta, 2001; Pichler et al., 2002).

In general, the lysine residues modified with SUMO lie within a SUMO consensus motif, which most commonly consists of the sequence ψ-K-X-E, where ψ is a bulky hydrophobic residue, and X is any residue (Matic et al., 2010; Rodriguez et al., 2001). This consensus motif is recognised by UBC9, with residues within the motif

stabilising the interaction between UBC9 and substrate, thus facilitating sumoylation (Bernier-Villamor et al., 2002).

Like ubiquitylation, modification with SUMO can take several forms: a single SUMO molecule may be conjugated to a single lysine residue, or to multiple lysine residues within the same substrate proteins. Polymeric SUMO chains may be formed because SUMO2 and SUMO3 encode a SUMO consensus motif within the flexible N-terminal region, and can therefore be modified with further SUMO moieties to form SUMO2/3 chains (Tatham et al., 2001). Though SUMO1 lacks the SUMO consensus motif, there is evidence it can also be incorporated into polymeric SUMO chains, probably as a chain terminator (Matic et al., 2008).

SUMO modification is a dynamic, reversible process, which is modified by the action of six SUMO specific cysteine proteases, SENP1, 2, 3, 5, 6 and 7 (Hay, 2007; Melchior et al., 2003). SENPs function at different stages of SUMO conjugation. Prior to conjugation, SENPs use C- terminal hydrolase activity to process precursor SUMO molecules, revealing the C- terminal diglycine motif required for conjugation to substrate. Following SUMO conjugation, SENPs can modify the process in two ways. Firstly, SENP activity can edit polymeric SUMO chains by removing SUMO molecules from the chain. Secondly, SUMO specific protease activity can function to deconjugate SUMO from the substrate (Gareau and Lima, 2010; Hay, 2007; Melchior et al., 2003). The different SENP family members exhibit differences in SUMO paralogue specificity, subcellular localisation and response to cell stress, and thus regulate the modification of discrete substrates (Gareau and Lima, 2010; Hay, 2007; Melchior et al., 2003).

1.2.2 SUMO interaction motif

In addition to covalent modification of substrate proteins with SUMO, non-covalent protein- SUMO interactions may be mediated by a SUMO interaction motif (SIM). SIMs consist of a stretch of four hydrophobic residues, (V/I/L)-X-(V/I/L)-(V/I/L), often flanked by acidic residues, and insert into a hydrophobic groove on SUMO (Hecker et al., 2006; Song et al., 2005). Many proteins have been demonstrated to have SIMs, for example promyelocytic leukaemia protein (PML) and other PML body constituents such as DAXX and SP100, and enzymes of the SUMO conjugation pathway (Kerscher, 2007). The class of SUMO targeted ubiquitin E3 ligases (STUbLs) contain a number of SIM domains as well as a RING domain, and are thus recruited to SUMO modified proteins, which are then ubiquitylated (Geoffroy and Hay, 2009). SIMs therefore serve to recruit effector proteins to SUMO modified substrates, and thus mediate the effects of SUMO modification.

1.3 PML

The promyelocytic leukaemia protein (PML) was first identified in the disease Acute Promyelocytic Leukaemia (APL), in which it is fused to the retinoic acid receptor alpha (RARα) (De The et al., 1991; Kakizuka et al., 1991). PML is a member of the tripartite motif (TRIM) family of proteins, and as such contains three cysteine rich zinc binding domains, a RING and two B Boxes, and a coiled- coil domain at its N- terminus (Jensen et al., 2001b). The coiled- coil domain mediates protein- protein interactions, and in the case of PML facilitates homodimerisation of PML and heterodimerisation of PML with PML-RARα in APL (Kastner et al., 1992). PML is predominantly a nuclear protein which localises to punctate nuclear structures called PML nuclear bodies (PML-NBs) (Bernardi and Pandolfi, 2007). The molecular function of PML remains poorly understood, though it has been implicated in a many biological processes including the

control of apoptosis, response to viral infection and regulation of transcription (Bernardi and Pandolfi, 2007)

1.3.1 PML Isoforms

The PML gene consists of nine exons, which undergoes alternative splicing, resulting in the expression of six major nuclear PML isoforms, and one cytoplasmic isoform (Jensen et al., 2001b). Each of the nuclear isoforms share a common N-terminus, encoded by exons 1-6, but differ at the C- terminus due to the expression of various combinations of exons 7-9 (**Figure 1.3.1., panel A**). The TRIM motif is encoded within the common N- terminus (**Figure 1.3.1., panel B**), as is a nuclear localisation signal encoded within exon 6, which suggests that any functions related to these elements should be common to all isoforms, with isoform specific interactions or functions dependent on the varying C- terminal region.

1.3.2 PML and SUMO modification

PML was one of the first identified SUMO substrates (Boddy et al., 1996), and was further characterised to have three sumoylation sites: Lys65, Lys160 and Lys490 (Kamitani et al., 1998). Each of these sumoylation sites lies within the common N-terminal region of all the PML isoforms (**Figure 1.3.1., panel B**), and two, Lys160 and Lys490, lie within SUMO consensus motifs. In addition to these sites of covalent PML-SUMO modification, exon 7a of the primary PML transcript encodes a SUMO interaction motif (Shen et al., 2006). PML isoforms I-V therefore contain a SIM enabling non- covalent PML- SUMO interactions, whereas PML VI does not.

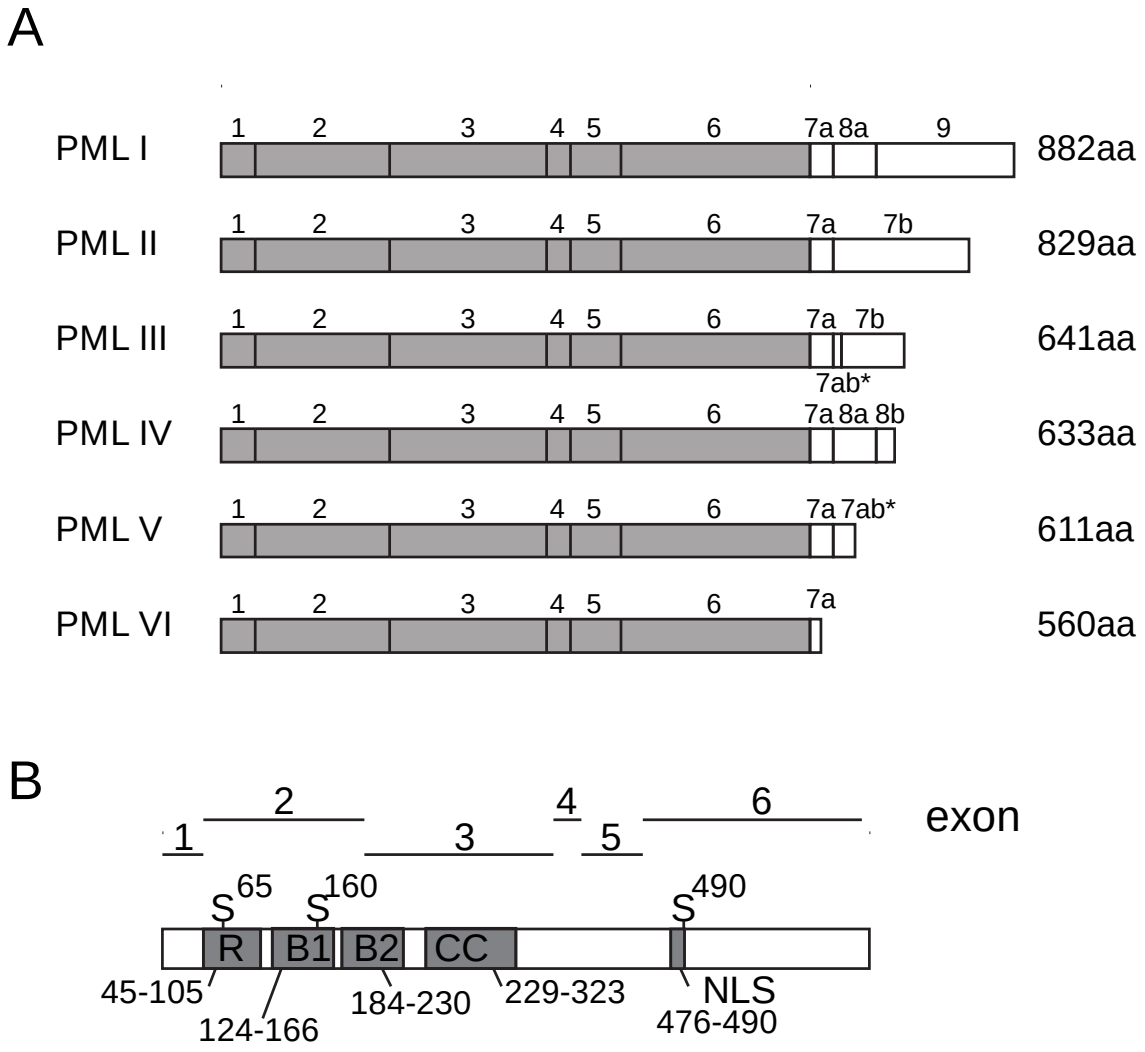

Figure 1.3.1. The exon assembly of PML (Adapted from Jensen et al., 2001)

A. Schematic representation of the exon structure of the six nuclear PML isoforms. All isoforms encode exons 1-6, but alternative splicing of exons 7-9 result in varying C-termini as shown. The length of each isoform is shown on the right. Asterisk indicates a retained intron.

B. All components of the PML TRIM are encoded within exons 1-6: RING domain (R), B Boxes 1 and 2 (B1 and B2) and the coiled coil motif (CC). The nuclear localisation signal (NLS) is also encoded by all six isoforms. Sumoylation sites are found at Lys65 within the RING domain, Lys160 in B box 1 and Lys490 in the nuclear localisation signal.

There is some evidence to suggest that PML itself may function as a SUMO E3 ligase: PML has a RING domain, and expression of human PML in yeast stimulates SUMO conjugation, a process dependent on its RING domain, suggesting that the RING has SUMO E3 ligase activity (Quimby et al., 2006); the RING domain of PML has been demonstrated to interact with the SUMO E2 conjugating enzyme UBC9 (Duprez et al., 1999); PML was also noted to enhance SUMO modification of the known SUMO substrates p53 and MDM2, primarily using mammalian overexpression systems, a process again noted to be dependent on its RING domain (Chu and Yang, 2011).

1.3.3 PML nuclear bodies

PML nuclear bodies are discrete nuclear foci (**Figure 1.3.2**), of approximately 0.2-1μm in diameter which are present in mammalian cells, and represent multiprotein complexes. Typically, there are between 1 and 20 PML-NBs per nucleus (Bernardi and Pandolfi, 2007; Salomoni and Pandolfi, 2002), but this varies under different cellular conditions. PML is required for the formation of PML nuclear bodies, because in cells derived from $PML^{-/-}$ mice, PML-NBs do not form (Ishov et al., 1999). Moreover, SUMO modification of PML is required for formation of mature PML bodies (Ishov et al., 1999; Lallemand-Breitenbach et al., 2001), as is the SIM domain present in exon 7a (Shen et al., 2006), indicating that both covalent and non covalent PML-SUMO interactions are required to form PML-NBs. Many other proteins are associated with PML-NBs, either constitutively or transiently, and many of these proteins are SUMO substrates. DAXX and SP100 are two well characterised PML-NB associating proteins. Both are SUMO substrates and contain SIM domains (Jang et al., 2002; Knipscheer et al., 2008; Lin et al., 2006; Sternsdorf et al., 1997). These observations regarding the requirement for SUMO modification of PML from PML-NB formation, the presence of

multiple other sumoylated proteins at PML-NBs, and the potential for PML to function as SUMO E3 ligase discussed above have led to a hypothesis that PML-NBs may function as sites of protein sumoylation, possibly through the action of PML as a SUMO E3 ligase. Alternatively, PML-NBs may act as 'depots' for SUMO modified proteins (Bernardi and Pandolfi, 2007).

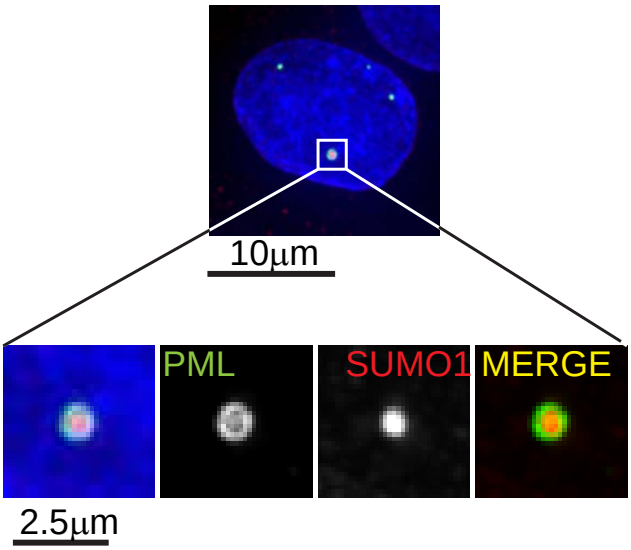

Figure 1.3.2. PML nuclear bodies are punctate nuclear structures

HeLa cells were fixed and immunolabelled with antibodies specific for PML and SUMO1, and appropriate fluorescently labelled secondary antibodies. DNA was stained with DAPI. PML is shown in green, SUMO1 in red and DAPI in blue. The top image shows four PML nuclear bodies (PML-NBs) in a cell nucleus; the lower panels are magnified images of the PML-NB indicated. Images represent maximal intensity projections of multiple z sections.

1.3.3.1 Cell cycle variation

As cells progress through S phase, the number of PML bodies increases (Dellaire et al., 2006a), but the most striking changes are seen when cells enter mitosis, when PML accumulates in fewer, larger aggregates termed MAPPs (mitotic accumulations of PML protein), which lack normal PML-NB components (Dellaire et al., 2006b; Everett et al., 1999). The formation of MAPPs coincides with a decrease in

sumoylation of PML, suggesting that cell cycle related regulation of SUMO modification of PML plays a role in the control of PML body formation, and therefore potentially PML-NB function throughout the cell cycle. The PML contained in MAPPs is then recycled from the cytoplasm into PML-NBs during G1 (Dellaire et al., 2006b).

1.3.3.2 Antiviral response

PML transcription is increased in response to interferon which leads to a marked increase in the number and size of PML bodies (Bernardi and Pandolfi, 2007; Everett and Chelbi-Alix, 2007), implicating PML-NBs in host antiviral defence. Indeed, some viruses target PML and PML-NB components to subvert their anti- viral effects: PML depletion increases Herpes simplex virus 1 (HSV-1) infection efficiency (Everett et al., 2006) and HSV-1 expresses a SUMO targeting ubiquitin E3 ligase which targets SUMO modified PML for degradation (Boutell et al., 2011). Interestingly, a study of the role of the individual PML isoforms in restriction of HSV-1 replication demonstrated though expression of PML I or PML II partially reverses the increase in HSV-1 replication observed in PML depleted cells, no individual isoform completely rescued the phenotype (Cuchet et al., 2011). This suggests that PML-NBs comprised of all PML isoforms are required for the antiviral response.

1.3.3.3 Apoptosis control

The study of $PML^{-/-}$ mice suggests a role for PML in tumour suppression. $PML^{-/-}$ cells grow faster than control cells (Gang Wang et al., 1998), whereas PML overexpression slows cell growth (Koken et al., 1995). $PML^{-/-}$ mice were more susceptible to tumours, in particular lymphomas (Gang Wang et al., 1998). PML expression is often lost in human cancers, and its loss correlates with tumour progression, again supporting the role of PML as a tumour suppressor (Gurrieri et al.,

2004). The response to apoptotic stimuli is altered in PML$^{-/-}$ cells, which are more resistant to caspase induced apoptosis than control cells (Wang et al., 1998). PML exerts these effects both via interactions with the tumour suppressor p53, and independently of p53 (Bernardi and Pandolfi, 2007).

1.3.3.4 Control of transcription

PML has been identified as both a transcriptional co activator and a corepressor. Many transcription factors localise to PML-NBs, including CREBBP and p300. There is some suggestion that PML and PML-NBs may regulate the activity of such transcription factors, either by sequestering them within PML-NBs or by controlling post translational modification of transcription factors, thus controlling their function (Zhong et al., 2000).

1.3.3.5 Cellular senescence

Cellular senescence describes the state of irreversible growth arrest which cells enter in response to various stimuli, for example DNA damage, oncogenic signalling or loss of telomeric integrity. This growth arrest prevents the proliferation of potential cancer cells and is therefore a mechanism for tumour suppression (Rodier and Campisi, 2011). Both PML expression and the number of PML-NBs are increased in response to oncogenic ras overexpression, a potent inducer of senescence, and overexpression of PML induces senescence via interactions with p53 and Rb (Bischof et al., 2002; Ferbeyre et al., 2000). PML triggered senescence promotes localisation of Rb and E2F transcription factors to PML-NBs, thus inhibiting the transcriptional activation activities of E2F proteins. E2F targets include many genes responsible for cell proliferation, and therefore PML induced suppression of transcription results in cell growth arrest (Vernier et al., 2011). PML-NBs also regulate the formation of senescence associated

heterochromatin foci, an important early event in cells approaching senescence (Zhang et al., 2005).

1.4 Acute promyelocytic leukaemia

Acute promyelocytic leukaemia (APL) is a rare but distinct subtype of acute myeloid leukaemia characterised by the accumulation of myeloid progenitor cells, promyelocytes, in the bone marrow and peripheral blood, a severe bleeding tendency and the balanced t(15;17) chromosomal translocation which results in the fusion of PML with the retinoic receptor α (RARα) (Lallemand-Breitenbach et al., 2012; Wang and Chen, 2008). The t(15;17) translocation is present in the vast majority of cases of APL, but less than 2% have variant chromosomal translocations involving chromosome 17, the most common being t(11;17) encoding the PLZF-RARα fusion. APL is now an eminently curable disease, with approaching 90% of patients achieving cure with treatments which target the PML-RARα fusion for degradation: all-trans retinoic acid (ATRA) and arsenic trioxide (Ablain and de The, 2011; de Thé and Chen, 2010). Sequential monitoring of patient bone marrow or peripheral blood samples for PML-RARα transcripts by RT-qPCR allows both assessment of treatment response and early identification of patients undergoing disease relapse, and enables reinstitution of anti-leukaemia therapy prior to frank relapse (Grimwade et al., 2009).

1.4.1 Pathogenesis of APL

The t(15;17) translocation and formation of PML-RARα fusion is the causative genetic lesion in APL, because expression of PML-RARα in mouse myeloid precursors causes development of a disease which closely resembles APL (Brown et al., 1997; Grisolano et al., 1997; He et al., 1997; Westervelt et al., 2003). Variation in the breakpoint in the PML gene leads to the formation of one of three PML-RARα isoforms

(**Figure 1.4.1.**): bcr1, the commonest, long isoform with the PML breakpoint within intron 6; bcr2, the variant isoform, with the breakpoint in exon 6; and bcr3, the short isoform with the breakpoint in PML intron 3 (Melo et al., 2006). The RARα breakpoint is consistently in intron 2, leading to the fusion of exons 3-9 to PML. The resulting PML-RARα isoforms therefore encode all components of the PML TRIM, of which the coiled- coil domain has been shown to be essential for the transforming potential of PML-RARα, allowing both PML-RARα homodimerisation and interaction of PML-RARα with PML (Occhionorelli et al., 2011). PML-RARα also encodes the functional elements of RARα, including the DNA binding, hormone binding and RXR binding domains. APL incidence is increased in patients previously treated with the topoisomerase II targeting agents etoposide, mitoxantrone and epirubicin for diseases such as multiple sclerosis and breast cancer. Interestingly, these agents predispose to specific breakpoint hot spots within both the PML and RARα genes, which correspond to regions of DNA preferentially cleaved by the DNA damaging agents in vitro (Hasan et al., 2008; Mays et al., 2010; Mistry et al., 2005).

Under normal circumstances, RARα interacts with RXR to act as a retinoic acid responsive transcription factor. PML-RARα forms heterotetramers with RXR, which bind RARα-RXR targets as well as DNA sequences not usually targeted by RARα-RXR complexes, leading to widespread deregulation of transcription (Martens et al., 2010). This deregulation of transcription leads to the block in myeloid progenitor differentiation demonstrated by the accumulation of promyelocytes, and also to increased self renewal properties (de Thé and Chen, 2010).

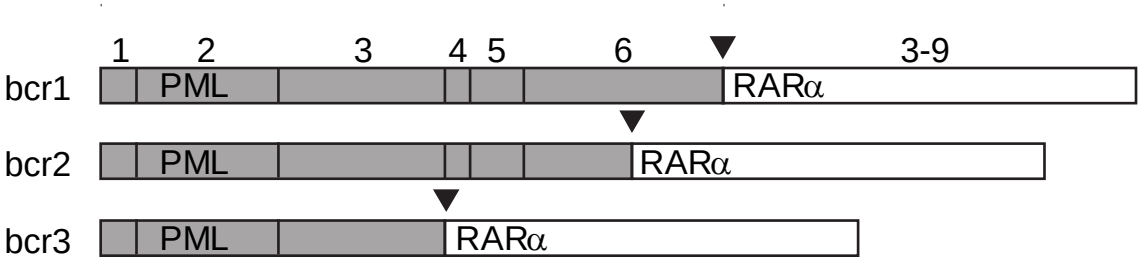

Figure 1.4.1. PML-RARα isoforms

The chromosomal translocation t(15;17) results in fusion of PML and RARα. Different breakpoints in chromosome 15 result in three PML-RARα isoforms, indicated by arrowheads. The breakpoint in bcr1 is within PML intron 6, bcr2 within exon 6 and bcr3 within intron 3. The breakpoint in chromosome 17 is invariably in RARα intron 2, thus all PML-RARα isoforms encode RARα exons 3-9.

PML-RARα also interferes with the normal functions of PML. PML-NBs are disrupted in APL due to PML- PML-RARα interactions, and are observed as characteristic nuclear speckles rather than punctate PML-NBs when assessed by immunofluorescence (de Thé and Chen, 2010; de The et al., 2012; Koken, 1994). This disrupts PML pro-apoptotic functions in leukaemic cells, leading to enhanced survival.

1.4.2 Treatment of APL

APL is an excellent example of a disease with molecularly targeted treatments. Initial treatment with conventional chemotherapeutic agents such as anthracyclines was complicated by the severe bleeding tendency conferred by APL cell overexpression of activators of coagulation and fibrinolysis (Breen et al., 2012), and cure rates were in the range of 35-45% (Wang and Chen, 2008). The identification of all trans retinoic acid (ATRA) as an agent which stimulated differentiation of leukaemic promyelocytes was a major breakthrough in the treatment of APL, and its use in combination with

conventional chemotherapy increased survival rates to approaching 90% (Wang and Chen, 2008).

PML-RARα is insensitive to physiological levels of retinoic acid which would normally stimulate dissociation of RARα-RXR co-repressor complexes and the recruitment of co-activator complexes. However, treatment with pharmacological concentrations of ATRA leads to proteasomal degradation of PML-RARα, allowing release of PML-RARα induced transcriptional repression, with a marked increase in histone acetylation observed at PML-RARα binding sites after ATRA treatment (Martens et al., 2010). This leads to activation of genes required for myeloid differentiation, and induces differentiation of leukaemic cells (de Thé and Chen, 2010). ATRA induced degradation of PML-RARα also abolishes PML-RARα interactions with PML and allows the reformation of normal PML-NBs (de The et al., 2012). It seems ATRA induced differentiation alone is insufficient for cure of APL, because despite complete differentiation, cure of leukaemia is rarely observed in the absence of other chemotherapeutic agents, or arsenic trioxide therapy (Ablain and de The, 2011).

Arsenic trioxide was first identified as an active agent in the treatment of APL through its use in traditional Chinese medicine, and is probably the single most active agent in treating the disease (Chen et al., 2011). Its clinical efficacy in APL was first reported in the 1990s, with striking response rates even in patients refractory to treatment with ATRA and chemotherapy (Shen et al., 1997). It is administered intravenously, and is well tolerated in the majority of patients, with little in the way of myelosuppression, or other toxicities (Chen et al., 2011). Arsenic induces degradation of PML-RARα by targeting the PML moiety for proteasomal degradation, the mechanism of which will be discussed in detail below. Having confirmed the efficacy of arsenic trioxide in the treatment of relapsed APL, clinical trials are now addressing

the role of arsenic treatment in newly diagnosed APL, and indeed assessing treatment regimens consisting of only ATRA and arsenic, thus abrogating the side effects of conventional chemotherapeutic agents (Lengfelder et al., 2012).

1.5 Mechanism of arsenic induced degradation of PML

Studies using the APL derived NB4 cell line (Lanotte et al., 1991) which expresses PML-RARα, as well as engineered mammalian cells have delineated the early effects of arsenic treatment on PML and PML-RARα. Shortly after arsenic treatment, PML is redistributed from the nucleoplasm to PML-NBs (Geoffroy et al., 2010; Zhu et al., 1997). PML is also rapidly sumoylated after arsenic treatment (Lallemand-Breitenbach et al., 2001), though recruitment of PML to PML-NBs is not SUMO dependent, because PML mutants which cannot be sumoylated are also redistributed to PML-NBs after arsenic treatment (Lallemand-Breitenbach et al., 2001). This may however be due to interaction of these mutants with SUMO modified PML-NB components. SUMO modification of PML is essential for the process of arsenic mediated degradation: mutational analyses demonstrate that sumoylation of PML Lys160 is required for degradation to take place (Lallemand-Breitenbach et al., 2001).

Two recent studies have investigated the mechanism of PML targeting to PML-NBs, and suggest that both direct arsenic binding and arsenic induced oxidative stress induce crosslinking of PML molecules which are targeted to PML-NBs (Jeanne et al., 2010; Zhang et al., 2010). Zhang and colleagues have demonstrated that the organic arsenical ReAsh, which fluoresces when bound to a tetracysteine motif, labels PML bodies, implying that arsenic binds directly to PML or another PML body component via cysteine residues. Using deletion mutants, ReAsH fluorescence at PML-NBs is demonstrated to be dependent on the RING domain and B2 domain of the PML TRIM, both of which are cysteine rich, zinc binding domains. The authors propose direct

binding of arsenic to these cysteine rich domains results in multimerisation of PML. Using a variety of techniques, for example nuclear magnetic resonance and circular dichroism, to examine the effects of arsenic on the secondary structure of a zinc depleted, isolated RING domain of PML, the authors conclude that arsenic binds directly to the PML RING in place of zinc atoms, and that this binding promotes multimerisation of PML and PML-RARα which in turn promotes SUMO modification. Zinc atoms stabilise the structure of the RING domain (Zheng et al., 2000), and these experiments may therefore be confounded by misfolding and subsequent aggregation of the zinc depleted PML RING, which may mimic multimerisation.

The second paper, by Jeanne and colleagues focusses on the role of PML oxidation in its targeting to PML-NBs. It is demonstrated PML accumulates in nuclear matrix associated, high molecular weight species under non- reducing conditions following arsenic treatment, and that the addition of the reducing agent DTT abrogates this multimerisation, implicating the formation of intermolecular disulfide bridges in the targeting of PML to the nuclear matrix. The direct binding of arsenic and PML is demonstrated using similar techniques to Zheng et al, but a dicysteine motif within the PML B2 domain is implicated as the site of binding. PML mutants in which one of these cysteine residues are mutated, C212 or C213, demonstrate decreased arsenic binding, decreased sumoylation under basal conditions, are predominantly nucleoplasmic and fail to form normal PML-NBs. Following arsenic treatment, these mutants are not sumoylated and are not degraded. Since these mutants fail to form normal PML-NBs under basal conditions and are not targeted to PML-NBs after arsenic treatment, the mutation of these cysteine residues themselves are likely to interfere with PML sumoylation in response to arsenic which takes place at PML-NBs, regardless of whether or not the cysteine residues directly bind arsenic.

The SUMO E3 ligase responsible for PML sumoylation triggered by arsenic therapy is yet to be confirmed. A single study reports the SUMO E3 ligase PIAS1 to be required for arsenic mediated degradation of PML (Rabellino et al., 2012). shRNA mediated depletion of PIAS1 impaired degradation of PML-RARα in NB4 cells, whereas overexpression of PIAS1 plus SUMO1 or 2 enhanced arsenic induced degradation of overexpressed PML-RARα in HEK293T cells. The overexpression experiments were performed using a system in which both PIAS1 and SUMO were overexpressed, Further confirmation of these findings is required. Given the evidence that PML itself may have SUMO E3 ligase function, another possibility is that arsenic activates autosumoylation activity of PML (Chu and Yang, 2011; Quimby et al., 2006). Alternatively, arsenic induced inhibition of SUMO proteases, for example SENP6 of which PML is a substrate (Hattersley et al., 2011), could result in the increased sumoylation of PML observed after arsenic treatment.

1.5.1 The role of RNF4

Ring finger protein 4 (RNF4) is a ubiquitin E3 ligase which encodes four SUMO interaction motifs in its N-terminal region, and a C-terminal RING domain, and thus targets SUMO modified proteins for ubiquitylation (Tatham et al., 2008). Arsenic treatment of cells depleted of RNF4 results in the accumulation of high molecular weight PML species, demonstrating that RNF4 is essential for arsenic mediated degradation of PML and PML-RARα (Lallemand-Breitenbach et al., 2008; Tatham et al., 2008). Under basal conditions, RNF4 is predominantly distributed in the nucleoplasm, but following arsenic treatment it is rapidly recruited to PML-NBs in a SUMO dependent manner, because RNF4 mutants lacking the N- terminal SIM domains do not relocalise to PML-NBs following arsenic treatment (Geoffroy et al., 2010), nor does wild type RNF4 colocalise with PML mutants which cannot be

sumoylated following arsenic treatment (Lallemand-Breitenbach et al., 2008). Indeed, PML modified with polymeric SUMO2 chains, but not unmodified PML is efficiently ubiquitylated by RNF4 in vitro (Tatham et al., 2008). These data demonstrate that sumoylation of PML in response to arsenic treatment recruits RNF4 to PML-NBs, where it subsequently ubiquitylates PML, targeting it for proteasomal degradation (**Figure 1.5.1.**) (Lallemand-Breitenbach et al., 2008; Tatham et al., 2008). It is established that inhibition of the proteasome prevents arsenic induced degradation of PML (Lallemand-Breitenbach et al., 2001). PML accumulates in PML bodies following combined arsenic treatment and proteasome inhibition, and after RNF4 depletion followed by arsenic treatment, suggesting that arsenic induced PML degradation by the proteasome takes place in PML-NBs (Geoffroy et al., 2010; Lallemand-Breitenbach et al., 2008; Tatham et al., 2008). In the case of APL, the PML-RARα oncoprotein is degraded via the same, SUMO dependent, ubiquitin mediated proteolytic pathway as PML, leading to cure of the disease.

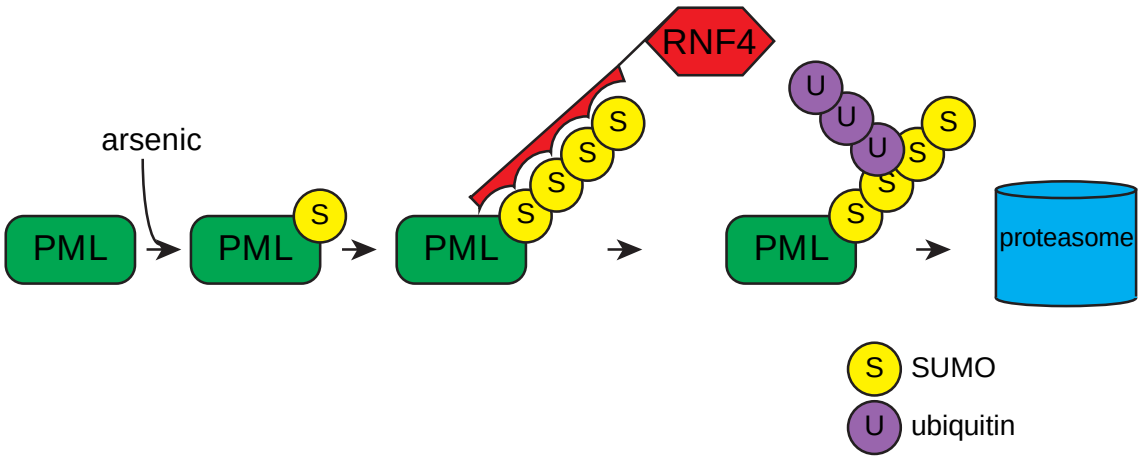

Figure 1.5.1. A model of the role of RNF4

Following arsenic treatment, PML is modified with polymeric SUMO chains which recruit RNF4 via its SIM domains. RNF4 then ubiquitylates the SUMO chains, targeting PML for degradation by the proteasome.

1.5.2 Resistance to arsenic therapy

The vast majority of patients who receive arsenic trioxide as a first line treatment reach a complete remission (Ghavamzadeh et al., 2011; Ravandi et al., 2009). There are therefore few reports detailing investigation of the mechanism of resistance to therapy. One report details the investigation of one patient in whom clinical resistance developed after prolonged arsenic treatment, and one patient who was primarily refractory to arsenic treatment (Goto et al., 2011). Studies revealed missense mutations in the B2 domain of the PML moiety of the PML-RARα fusion. Functional studies were then performed using PML-RARα constructs containing the two mutations, A216V and L218P. These revealed impaired SUMO modification and degradation of PML-RARα in the presence of these mutations, and notably both constructs localised to the cytoplasm (Goto et al., 2011). The mutated residues are close to the dicysteine motif proposed to directly bind arsenic (Jeanne et al., 2010), and it is suggested mutations may interfere with this arsenic binding. Alternatively, these mutations may disrupt the structure of the B2 domain of PML-RARα, interfering with PML-RARα interactions with, for example, the sumoylation machinery.

2 Materials and methods

2.1 DNA and RNA techniques

2.1.1 Constructs used in this study

The pGD-EYFP-C1 is a vector for mammalian expression, and was a kind gift from Professor Roger Everett, University of Glasgow.

2.1.2 DNA sequencing

Plasmid DNA was submitted for sequencing to the DNA Sequencing Service, University of Dundee.

2.1.3 Transformation of competent E coli cells

50ng of plasmid DNA was added to 50µl of competent DH5α *E. coli* cells which were then incubated on ice for 30 minutes. Cells were then subjected to heatshock at 42ºC in a water bath for 1 minute 15 seconds. Cells were incubated on ice for a further 3 minutes and then 1ml of LB medium was added. This cell suspension was incubated at 37ºC for 1 hour with constant shaking at 220 rpm. 100-900µl of this cell suspension was then spread on agar plates with appropriate antibiotic selection and incubated at 37ºC overnight.

2.1.4 Small scale preparation of plasmid DNA (miniprep)

5ml of LB medium with appropriate antibiotic (ampicillin was used at a final concentration of 100µg/ml, kanamycin at a final concentration of 50µg/ml) was inoculated with a single colony from an agar plate and incubated overnight at 37ºC with constant rotation at 220 rpm. The bacteria were then pelleted by centrifugation at 2800 x

g for 10 minutes at room temperature, and plasmid DNA purified from the cell pellet using the QIAprep Spin Miniprep Kit (Qiagen) according to manufacturer's instructions.

2.1.5 RNA preparation

Mammalian cells were cultured in triplicate wells in 6 well plates. Cells were washed once with PBS and lysed using RNA lysis buffer from the SV Total RNA Isolation System (Promega). RNA was then extracted from lysates using the SV Total RNA Isolation System (Promega) according to manufacturer's instructions, and stored at -80ºC.

2.1.6 Reverse transcription of RNA

RNA was prepared as in section 2.1.5 and the concentration determined using a NanoVue spectrophotometer (GE Healthcare). 1µg of RNA and 4µl of qScript cDNA Supermix (Quanta Biosciences) were added to an eppendorf tube, with the final reaction volume made up to 20µl with nuclease free water.

- **Reverse transcription reaction**

  25ºC for 5 minutes

  42ºC for 50 minutes

  85ºC for 5 minutes

Resulting cDNA was diluted 1:4 by the addition of 60µl of nuclease free water and stored at -20ºC.

2.1.7 RT qPCR

Triplicate samples were lysed and RNA extracted as described in section 2.1.5, and reverse transcribed as described in 2.1.6.

Specific primer pairs for each gene of interest were designed using Primer3 software, ordered from MWG Eurofins and reconstituted to a stock concentration of 100µM. A 2µM, working aliquot of forward and reverse primers was prepared by mixing 2µl of forward and reverse primers, with 96µl of nuclease free water.

Primer tests were performed by creating a 2 fold dilution curve (undiluted, 1/2, 1/4, 1/8, 1/16, 1/32) of cDNA which was assayed with each of the primer pairs to be tested. Duplicate reactions were performed in 96 well plates. The cDNA concentration resulting in a threshold cycle of 24 was selected for each primer, and subsequently cDNA was diluted by this factor for use with the primers.

RT qPCR reactions were performed in duplicate. Mastermixes of SYBR green, ROX reference dye and primer were prepared for each primer pair to be tested, and 9µl of this mix was pipetted into 96 well reaction plates. 6µl of each cDNA, diluted to the concentration required for the primer pair was then added. Plates were then sealed and centrifuged for 1 minute at 1000rpm before assaying using an ABI7500 real-time PCR machine.

- **1 X RT qPCR reaction**

  7.5µl Perfecta SYBR Green Fastmix (Quanta Biosciences)

  0.03 µl ROX reference dye (Invitrogen)

  1.5µl forward/ reverse primer 2µM mix

  6µl cDNA

- **Reaction protocol**

  95ºC for 2 minutes

  95ºC for 10 seconds/ 60ºC for 30 seconds, for 40 cycles

  Dissociation step

Results were processed using Applied Biosystems sequence detection system software and analysed using the ddCT method. Samples transfected with non- targeting control siRNA were used as the reference samples, and actin expression as the housekeeping gene.

2.1.7.1 RT qPCR primer sequences (5'→ 3')

- **PML** **F**- GGAACATCCTCGGCAGTAGA

  R- AGTCGGTGCGTGAGTTCC

- **RNF4** **F**- GTGAGCAGTGACGATGA

  R- GGAGGCACTGGCTACAG

- **LZTR1** **F**- GACCGCCACCTCTATGTGTT

  R- CCAAACACATCTCGGGACTT

- **KCNC1** **F**- GAGGACGAGCTGGAGATGAC

  R- AAGGTGGTGATGGAGACCAG

- **ABTB2** **F**- GAGGACAGCTATGCGGAGAC

  R - TGGCTGAAGCAGTTCATGTC

- **ANKFY1** **F**- GCTCCTCAGGGAGAGATGTG

  R- ATCCTCCTTCCTCAGGTCGT

- **KLHL25** **F-** CACAAGGCCAAGGAGATCAT

  R- TACGGTGTCGTACACCCAGA

- **actin** **F-** CAACTCCATCATGAAGTGTGACG

  R- CAGGGCAGTGATCTCCTTCTG

2.2 Protein techniques

2.2.1 SDS-PAGE

Samples for sodium dodecylsulphate-polyacrylamide gel electrophoresis (SDS-PAGE) were separated in NuPAGE Novex Bis-Tris 4-12% gels using MOPS buffer. Gels were run at a constant voltage of 150V until adequate separation of proteins was achieved (usually 90 minutes).

2.2.2 Coomassie Blue staining

After electrophoretic separation, gels were incubated in Coomassie blue staining solution for 30 minutes with constant rocking. Gels were then incubated in destaining solution I for 1 hour, and destaining solution II overnight.

- **Coomassie blue staining solution**

  Coomassie brilliant blue R-250 (1 g) was dissolved in 400 ml of methanol.

  Subsequently, distilled water and 70 ml of acetic acid were added to the final volume of 1 litre. The solution was filtered through a filter paper.

- **Destaining solution I**

  40% (v/v) methanol

  7% (v/v) acetic acid

- **Destaining solution II**

  5% (v/v) methanol

  7% (v/v) acetic acid

2.2.3 Western blot analysis

Proteins were separated by SDS-PAGE and transferred to PVDF membrane (Immobilon-P Transfer Membrane, Millipore). Gel- sized pieces of PVDF membrane were incubated for 5 minutes in methanol before equilibration for 10 minutes in Transfer buffer. A wet transfer was performed using the Mini Trans-Blot Cell (Bio-Rad) system, at 25mA overnight, or 300mA for 1.5 hours.

- **Transfer buffer**

  24 mM Tris

  193 mM glycine

  20% methanol

Following protein transfer, membranes were blocked in 5% Marvel non-fat milk powder in PBS/ 0.1% Tween 20 (milk/ PBST) for 30 minutes. Primary antibodies were diluted in milk/ PBST and membranes incubated for 2 hours at room temperature, or 4ºC overnight. Following 3 washes with PBST, membranes were incubated with secondary antibodies diluted in milk/ PBST for 1 hour at room temperature. Membranes were washed a further 3 times with PBST, twice with PBS and then incubated with ECL and exposed to x-ray film.

2.2.4 Antibodies used in this study

- **anti PML** (chicken polyclonal; raised in house) 1:5000 in milk/PBST for western blotting, 1:1000 in BSA/PBST for immunofluorescence
- **anti PML 5E10** (mouse, monoclonal, from Roel van Driel, Amsterdam) 1:20 in BSA/PBST for immunofluorescence.
- **anti SUMO 1** (sheep, polyclonal; raised in house) 1:1000 in milk PBST for western blotting, 1:100 in BSA/ PBST for immunofluorescence
- **anti SUMO 2** (sheep, polyclonal; raised in house) 1:1000 in milk/ PBST for western blotting, 1:100 in BSA/ PBST for immunofluorescence
- **anti SUMO 2** (rabbit, polyclonal; Zymed) 1:2000 in milk/ PBST for western blotting
- **anti ubiquitin** (rabbit, polyclonal; DAKO) 1:1000 in BSA/ PBST for western blotting
- **anti RNF4** (chicken, polyclonal, generated in house) 1:5000 in milk/ PBST for western blotting
- **anti RARα 115** (rabbit, polyclonal, gift from Cecily Egly) 1:1000 in milk/ PBST for western blotting
- **anti GFP** (mouse, monoclonal, Roche) 1:1000 in BSA/ PBST for western blotting
- **anti actin** (mouse, monoclonal; Sigma) used 1:25 000 in milk/ PBST for western blotting
- **anti CUL3** (rabbit, polyclonal, kind gift from Matthias Peter, ETH Zurich) 1:1000-1:2000 in BSA/ PBST for western blotting
- **anti tubulin** (mouse,) used 1:5000 in milk/ PBST for western blotting

- **anti chicken, HRP conjugated** (Sigma) 1:10 000 in milk/ PBST for western blotting
- **anti sheep, HRP conjugated** (Sigma) 1:4000 in milk/ PBST for western blotting
- **anti rabbit, HRP conjugated** (Sigma) 1:3000 in milk/ PBST for western blotting
- **anti mouse, HRP conjugated** (Sigma) 1:3000 in milk/ PBST for western blotting
- **anti sheep, Dylight594 conjugated** (Jackson) 1:150 in BSA/PBST for immunofluorescence
- **anti sheep, Cy5 conjugated** (Jackson) 1:150 in BSA/ PBST for immunofluorescence
- **anti chicken, Alexafluor488 conjugated** (Invitrogen) 1:300 in BSA/ PBST for immunofluorescence
- **anti chicken, Dylight594 conjugated** (Jackson) 1:150 in BSA/ PBST for immunofluorescence
- **anti sheep, FITC conjugated** (Jackson) 1:300 in BSA/ PBST for immunofluorescence
- **anti mouse, Alexafluor594 conjugated** (Invitrogen) 1:300 in BSA/ PBST for immunofluorescence

2.3 Cell culture and lysates

2.3.1 Cell lines

All cell lines were maintained in culture at 37ºC in 5% CO_2.

HeLa and U2OS cells were from Hay lab stocks, and maintained in Dulbecco's Modified Eagle's Medium (DMEM) medium plus Glutamax (Invitrogen) supplemented with 10% fetal bovine serum (FBS) and 100U/ml penicillin and streptomycin.

HeLa cells stably expressing YFP-PML (Geoffroy et al., 2010) were maintained in DMEM plus Glutamax with 10% FBS, 100U/ml penicillin and streptomycin plus blasticidin 1µg/ml.

HeLa cells stably expressing eYFP were generated as described in Section 2.3.2 and maintained in DMEM plus Glutamax with 10% FBS, 100U/ml penicillin and streptomycin plus 250µg/ml G418.

NB4 leukaemia cells were from Hay lab stocks and maintained in RPMI medium (Invitrogen) supplemented with 10% FBS, 2mM glutamine and 100U/ml penicillin and streptomycin.

HL60 (Gallagher et al., 1979) and P39 (Nagai et al., 1984) leukaemia cells were a kind gift from Mary Hepburn and Sudhir Tauro, University of Dundee. Cells were maintained in RPMI medium (Invitrogen) supplemented with 10% FBS, 2mM glutamine and 100U/ml penicillin and streptomycin.

HepaRG hepatocytes expressing enhanced yellow fluorescent protein (eYFP) linked PML isoforms were a kind gift from Professor Roger Everett, University of Glasgow (Cuchet et al., 2011). Cells were cultured in Williams Medium E (Gibco), with 10% fetal bovine serum gold (PAA), 2mM glutamine, 5µg/ml insulin, 0.5µM

hydrocortisone and 100U/ml penicillin and streptomycin. Cells were maintained under antibiotic selection with G418 and puromycin. Parental HepaRG hepatocytes were cultured under the same conditions, without antibiotic selection.

2.3.2 Generation of eYFP HeLa cell line

HeLa cells were transfected with the pGD-EYFP-C1 vector, a kind gift from Professor Roger Everett, University of Glasgow, as described in Section 2.3.3. 24 hours after transfection, antibiotic selection was commenced with 500µg/ml G418. Medium containing G418 was replaced every 24 hours and stable colonies were selected approximately two weeks later. Colonies were then screened by fluorescence microscopy and western blotting to identify those stably expressing eYFP.

2.3.3 DNA transfections

Cells were seeded in 6 well plates and transfected the following day at 70% confluency. 1µg of plasmid DNA was added to 50µl of OptiMEM serum free medium (Invitrogen) and vortexed briefly. 3µl of Fugene HD (Roche) transfection reagent was then added and vortexed briefly. This mixture was incubated at room temperature for 15 minutes before it was added to 2 ml of complete DMEM medium on the cells.

2.3.4 siRNA transfections

Cells were seeded in 6 well plates and transfected the following day at 20% confluency. 2.5µl of Lipofectamine RNAiMAX transfection reagent (Invitrogen) was diluted in 200µl of opti-MEM serum free medium (Invitrogen), and 1µl of 20µM stock siRNA diluted separately in 200µl of opti-MEM. These two solutions were mixed, and incubated at room temperature for 15 minutes, then added to 1.6mls of antibiotic free

DMEM medium on cells, giving a final siRNA concentration of 10nM and final volume of 2ml. Cells were then incubated for at least 48 hours prior to analysis.

2.3.5 Cell treatments

Cells were treated with drugs diluted in DMEM culture medium. Arsenic trioxide (Sigma) was used at 1µM final concentration. MG132 was used at a final concentration of 5 or 10µM. MLN 4924 was obtained from SCILLS, and used at various concentrations as documented in the text.

- **Preparation of arsenic stock solution**

  110mg arsenic trioxide was dissolved in 2ml 1M sodium hydroxide to give 280mM stock

  35.7µl of this 280mM stock was then diluted in 10ml TBS to give 1mM working stock

  1mM stock was then filter sterilised, aliquoted and stored at -20ºC.

2.3.6 Cell lysis

For whole cell lysis, cells were washed twice with PBS, and then lysed in 2 X SDS lysis buffer. Samples were then sonicated to shear DNA, incubated at 100ºC for 5 minutes and cleared by centriguation at 17 000 x g for 10 minutes. Protein concentration of the lysate was estimated using the DC Assay (Biorad). B- mercaptoethanol was added to samples at a final concentration of 0.5M after protein concentration estimation for samples to be separated by SDS-PAGE.

- **2 X SDS lysis buffer**

  50mM Tris pH6.8

  2% (v/v) SDS

  10% (v/v) glycerol

  0.005% (w/v) bromophenol blue

2.3.7 Lysis of NB4 cells

Western blotting analysis of NB4 cells lysed in 2 X SDS lysis buffer using the anti RARα-115 antibody demonstrated poor PML-RARα extraction. NB4 cells were therefore lysed in 8M urea containing lysis buffer which resulted in enhanced PML-RARα extraction, as previously reported (Isakson et al., 2010). Cells were washed twice in PBS and lysed in urea lysis buffer. Protein concentration of lysates was measured using the Biorad Protein Assay (Bio-Rad)according to manufacturer's instructions.

- **Urea lysis buffer**

  8M urea

  0.5% triton

  0.1M DTT

Lysates were diluted 1:3 with 2 X SDS lysis buffer for SDS-PAGE and western blotting analysis.

2.3.8 ATP based survival assay

This protocol relies on the ATP-dependent action of firefly luciferase and the direct correlation between the obtained luminescence values and ATP levels in the reaction. A buffer containing the required components for the reaction except ATP is

used. The reaction rate is therefore dependent on ATP levels, which are directly proportional to the number of live cells in the assay.

Cells were cultured in white, flat bottomed 96 well plates (Greiner). Typically $1x10^5$ HL60 or P39 cells were cultured per well in 100µl of culture medium. For drug treatment, identical aliquots of cells were centrifuged at 1000rpm to pellet cells, and resuspended in culture medium containing the appropriate concentration of drug. A multichannel pipette was then used to dispense 100µl of the well mixed cell suspension into 8 replicate wells.

72 hours later, cells were lysed by pipetting 100µl of 2 X ATP lysis buffer into each well using a multichannel pipette. Plates were then sealed with an adhesive plate seal and incubated at room temperature on an optical shaker at 750rpm for 10 minutes. Luminescence signal was then assayed using an EnVision Multilabel reader (Perkin-Elmer).

- **2 X ATP lysis buffer**

  50 mM Tris/Phosphate pH 7.8
  16 mM MgCl2
  2 mM DTT
  2% v/v Triton-X-100
  30% v/v (37.8% w/v) Glycerol
  1% w/v BSA

  (Dissolved completely in distilled water before addition of Luciferin.)

  0.25 mM D-Luciferin
  8 µM Sodium Pyrophosphate Tetra-basic Decahydrate
  500 ng/ml Luciferase

The average luminescent signal for each drug concentration was calculated from replicate wells, and calculated as a surviving fraction of untreated control cells.

2.4 Immunoprecipitation

2.4.1 GFP-IP of YFP-PML isoforms

PML isoform expressing HepaRG cells were cultured in 10cm plates and treated with arsenic as described in section 2.3.5 prior to harvesting by scraping after 2 washes with PBS/ 100mM iodoacetamide on ice. Typically, two 10cm plates were cultured for each time point. Cells were pelleted by centrifugation at 400 x g and lysed in ice cold RIPA buffer (see below) with 100mM iodoacetamide with end over end rotation for 20 minutes at 4 °C. Lysates were clarified by centrifugation at 17 000 x g for 10 minutes and precleared by incubation with sepharose beads for one hour, followed by overnight incubation with agarose beads coupled to a recombinant, single chain, camelid anti GFP antibody (a kind gift from the Division of Signal Transduction Therapy, University of Dundee) with constant end over end mixing at 4°C. Beads were then washed three times with RIPA buffer and bound proteins eluted in 2x SDS lysis buffer, and analysed by SDS- PAGE and western blotting.

- **RIPA buffer**

  50mM Tris pH7.5
  150mM NaCl
  1% NP-40
  0.5% deoxycholate

2.4.2 GFP-IP of YFP-PML for mass spectrometry

HeLa cells stably expressing either eYFP or YFP-PML were each cultured in 10, 15 cm tissue culture plates. When cells reached confluency, cells were harvested by scraping after 2 washes with PBS/ 100mM iodoacetamide on ice. Cells were pelleted by centrifugation at 400 x g and lysed in ice cold lysis buffer (see below) with 100mM

iodoacetamide with end over end rotation for 20 minutes at 4 °C. Lysates were clarified by centrifugation at 17 000 x g for 10 minutes and incubated with agarose beads coupled to a single chain anti-GFP antibody (a kind gift from the DSTT, University of Dundee) for 2 hours with constant end over end mixing at 4ºC. Beads were then washed twice in lysis buffer without NP40 and bound proteins eluted in 2X SDS lysis buffer.

- **Lysis buffer**

  50mM Tris pH7.5
  150mM NaCl
  0.5% NP-40

All material eluted was loaded into a single lane of a pre-cast bis-tris gel for each cell line. Proteins were then separated by SDS-PAGE, and the gel Coomassie stained as described in Section 2.2.2. At all stages, contamination was minimised by using sterile, single use equipment, and commercially prepared reagents, for example MOPs running buffer.

Microwave assisted, in- gel tryptic digestion of peptides for mass spectrometry was performed by Dr Mike Tatham, as was mass spectrometric analysis.

2.5 Microscopy techniques

2.5.1 Cell culture on coverslips

Adherent cells were cultured on 13mm glass coverslips in individual wells of six well plates. DNA or siRNA transfections were performed as described in Sections 2.3.3 and 2.3.4.

2.5.2 Cytospin preparations

Suspension cells were cultured in 6 well plates, then centrifuged at 400 x g and resuspended in 1ml of media. 100µl of cell suspension was then loaded into disposable sample chambers and centrifuged at 300rpm on a Cytospin3 centrifuge (Shandon), to distribute cells onto glass microscope slides. Slides were then air dried and stored at room temperature prior to fixation.

2.5.3 Cell fixation and immunolabelling

- **4% paraformaldehyde (PFA) (10ml)**

  0.4g PFA
  0.2mM NaOH
  8.6ml H_2O
  } Heated to 70ºC until dissolved

  1ml 10 x PBS added after PFA dissolved

- **Blocking buffer**

  5% BSA
  0.1% Tween 20
  PBS

- **Washing buffer**

  1% BSA
  0.1% Tween 20
  PBS

2.5.3.1 Adherent cells

Cells were washed twice with PBS and then fixed in 4% paraformaldehyde for 10 minutes at 37ºC. Cells were washed a further three times with PBS, and at this point may have been temporarily stored at 4ºC. Cells were permeabilised by incubation with 0.2% triton in PBS for 10 minutes at room temperature and then washed a further three times in PBS. Cells were then blocked in blocking buffer for 30 minutes at room

temperature before coverslips were transferred to a Saran wrap ‘wet room’ on the benchtop.

Primary antibody was diluted in washing buffer, and coverslips incubated for 1 hour at room temperature. Cells were washed three times with wash buffer, and incubated with secondary antibody, also diluted in wash buffer, for 45 minutes at room temperature. After three further washes, cells were incubated with DAPI, 0.1µg/ml to stain DNA for 5 minutes before five further washes. Cells were aspirated dry and mounted onto glass microscopy slides using Vectashield mounting media (Vector labs), and the edges sealed with nail varnish. Slides were then stored at -20ºC until imaging.

2.5.3.2 Suspension cells

A hydrophobic pen was used to circle the area of microscope slides with the cytospin cell preparations. Cells within the area marked were rehydrated by incubation with PBS for 10 minutes at room temperature, then fixed, permeabilised and immunolabelled as described for adherent cells.

Cells were aspirated dry and mounted with Vectashield mounting media, covered with a 20mm glass coverslip, and the edges sealed with nail varnish.

2.5.4 Imaging

Immunofluorescence samples were imaged by widefield microscopy using a Deltavision DV3 microscope (Applied Precision). Typically, images of multiple z-sections were captured using a Coolsnap HQ2 camera (12 bit, Roper scientific) and 40x and 60x oil immersion lenses.

2.5.5 Image analysis

Images were deconvolved using the Spinlock deconvolution cluster. Deconvolved images were analysed using Softworx software (Applied precision). For analysis of PML body fluorescence, the 2D polygon finder tool was used to identify pixel clusters above a given fluorescence threshold in maximal intensity projections of multiple z-sections. This threshold was maintained for the analysis of all images in a given experiment.

2.6 Structured illumination imaging

Cells were cultured on coverslips, fixed and antibody stained as described in section 2.5. Imaging was performed using the OMX version 2 system (Applied Precision). Images were acquired using a 100X, 1.4NA, oil immersion objective lens (Olympus, Center Valley,PA) and back-illuminated Cascade II 512 · 512 electron-multiplying charge-coupled device (EMCCD) camera (Photometrics, Tucson,AZ) on the OMX version 2 system (Applied Precision) equipped with 405-, 488-, and 593-nm solid-state lasers. Samples were illuminated by a coherent scrambled laser light source that had passed through a diffraction grating to generate the structured illumination by interference of light orders in the image plane to create a 3D sinusoidal pattern, with lateral stripes approximately 0.2 μm apart. The pattern was shifted laterally through five phases and through three angular rotations of 60’ for each Z-section, separated by 0.125 μm. Exposure times were typically between 200 and 500 ms, and the power of each laser was adjusted to achieve optimal intensities of between 2,000 and 4,000 counts in a raw image of 16-bit dynamic range, at the lowest possible laser power to minimize photo bleaching. Raw images were processed and reconstructed to reveal structures with greater resolution (Gustafsson, 2008). The channels were then aligned in x, y, and

rotationally using predetermined shifts as measured using a target lens and the Softworx alignment tool (Applied Precision).

2.7 High content imaging

2.7.1 Tissue culture

Cells for high content imaging were cultured in black, clear bottomed 96 well plates (Corning CellBIND) under standard tissue culture conditions. Typically, cells were cultured in 100µl of medium per well.

2.7.2 siRNA transfection in 96 well plates

For transfection of up to five 96 well plates, transfections were performed manually using multichannel pipettes. siRNA was diluted to 200nM in 1X siRNA buffer (Dharmacon). 10µl of this solution was pipetted into the desired wells of a 96 well plate. Lipofectamine RNAiMAX transfection reagent (Invitrogen) was diluted 1:50 in optiMEM serum free medium (Invitrogen) and 10ul of the resulting solution added to the 96 well plate using a multichannel pipette. This mixture of siRNA and transfection reagent was mixed by gently pipetting up and down three times. The plate was incubated at room temperature, with a sterile lid in place to prevent evaporation, for twenty minutes. Cells were trypsinised and typically 5000- 7500 cells were seeded to each well in 100µl of culture medium.

2.7.3 Cell treatments

For arsenic treatment, 10µl of 11µM arsenic trioxide dilute in culture medium was added to wells using a multichannel pipette, to give a final concentration of 1µM.

2.7.4 Cell fixation and staining

At the desired time point, culture medium was aspirated from wells using a benchtop aspirator. Cells were washed twice in 100µl per well of PBS and fixed with 40µl per well 4%PFA/PBS as described in section 2.5.3. Following fixation, cells were washed three times with 100µl per well of PBS, and then permeabilised with 40µl per well of 0.2% triton/PBS. Cells were washed a further three times with PBS prior to incubation with 40µl per well of 0.1µg/ml DAPI for 3 minutes. Cells were washed a further 5 times with PBS and 100µl of PBS left in each well. Plates were then sealed using adhesive microplate seals and plates stored at 4ºC prior to imaging.

2.7.5 Imaging

Cells in 96 well plates were imaged using an INCell 1000 automated microscope, or an INCell 2000 automated microscope (GE Healthcare) in the Drug Discovery Unit, University of Dundee. Robotics were used to enable automated, sequential analysis of multiple 96 well plates, which were loaded and unloaded from the microscope by a robotic arm.

Imaging protocols were developed using INCell analyser software to capture YFP and DAPI fluorescence with a 10x/0.45 plan Apo lens or a 20x/0.45 lens. At least two fields of view were captured per well, using laser autofocus before each image to ensure images were in focus. Exposure times for each wavelength were adjusted to provide optimal signal strength of 1000-1500 pixel intensity units. Individual images were saved as tif files onto a dedicated server, with images from a single plate stored in a folder labelled with the date and time of imaging.

2.7.6 Image analysis

Images were analysed using INCell Investigator software (GE healthcare). Protocols were developed according to the desired features to be analysed. For analysis of PML nuclear body fluorescence, cell nuclei were first identified in the DAPI channel using multi-scale top hat transformation. PML nuclear body fluorescence was then identified in the YFP channel, again using a multi-scale top hat transformation to identify pixel clusters above a specified threshold. The number of, size and location (nuclear or cytoplasmic, based on nuclear DAPI staining) of PML bodies was then reported for each cell analysed. Plates could be analysed in batches if required, for example when multiple plates formed one experiment.

The results of the analysis for each plate was exported as an Excel file. Thus, the number of Excel files generated corresponded to the number of plates analysed. These contained a summary document which contained a well by well summary of all cells analysed within the wells. Cell by cell data for each cell analysed was also available within the document. Raw images were reviewed using OMERO software, which allowed upload of images in a 96 well plate format.

2.8 siRNA screening

2.8.1 Screen setup

2.8.1.1 siRNA library

The ubiquitome siRNA library was purchased from Dharmacon, and consisted of 15, 96 well plates. Each well contained a pool of four siRNAs targeting a single gene. A total of 1067 genes were targeted in the library. The siRNA within the library plates was at a concentration of 200nM, and plates were thermally sealed and stored at -20ºC.

Each plate had a unique barcode, which allowed tracking of the number of freeze- thaw cycles for each plate, and the volume remaining in each well using a spreadsheet managed by Amit Garg, data manager and updated by each user.

2.8.1.2 Quality control

Where possible, the various steps undertaken in the siRNA screen were automated to increase precision. Prior to setup of the siRNA screen, quality control checks were performed for each piece of liquid handling equipment to be used. The Fluid X liquid handling robot which has 96 pipette tips was arranged to aspirate from, or dispense into a 96 well plate. This was programmed to aspirate and dispense 10µl of 10mM Orange G into triplicate clear 96 well plates. The WellMate (Thermo scientific) liquid handling device which dispenses liquid into the eight wells which make up one column of a 96 well plate at one time, was programmed to dispense both 80µl of 1mM Orange G or 10µl of 10mM Orange G into triplicate clear 96 well plates. The plates were then sealed, and absorbance measured for each well of the plates. The resulting absorbance values for each well of three plates for each piece of equipment were then assessed. Equipment passed this quality control test if the average percentage coefficient of variation of the three plates was less than 5%. This indicated that the liquid handling equipment was accurately and reproducibly dispensing the desired volume.

A quality control plate was to be assayed at the beginning and at the end of the assay plates containing the siRNA library in the siRNA screen. Each well of the QC plate was transfected with the positive control siRNA, in this case RNF4 siRNA. By assaying identical plates at the beginning and end of the screen, the consistency of the assay can be assessed.

2.8.1.3 Preparation

The number of plates to be assayed was calculated and unique barcode labels printed for each plate. These allowed tracking of each plate and identification of which siRNAs produce interesting phenotypes in the screen. In this case there were 34 plates in all: an arsenic treated set consisting of 2 QC plates and 15 assay plates, and an identical vehicle treated set.

Control siRNA was prepared as a batch to be used for all plates. RNF4 siRNA, PML siRNA and NT siRNAs were diluted from 20µM stock to 200nM working concentration in 1X siRNA buffer (Dharmacon). The siRNAs were pipetted into a reservoir 96 well plate in the layout which they would appear on each assay plate: filling columns 1 and 12 of each assay plate. A reservoir plate for the QC plates was also prepared with RNF4 siRNA in each well.

2.8.1.4 Dispensing of siRNA

The 15 siRNA library plates were thawed on the bench for one hour and then centrifuged at 3000rpm for 1 minute. 34 black, clear bottomed assay plates (Corning CellBIND) were labelled with the barcode stickers. Plates were moved into a laminar flow cabinet, and all subsequent steps took place under sterile conditions. Control siRNAs were dispensed using the Fluid X liquid handling device to aspirate siRNA from the reservoir plate and dispense 10µl of siRNA into the 30 assay plates. These control siRNAs occupy the outer-most columns of each 96 well plate, column 1 and 12. RNF4 siRNA was dispensed into each well of the 4 QC plates.

The 200nM concentration library siRNAs were then dispensed using the Fluid X liquid handling device. 10µl of siRNA was aspirated from each well of each library plate (columns 1 and 12 are empty in the library plates) and dispensed into the two

corresponding assay plates which already contained the control siRNAs. Lids were placed onto the assay plates immediately to prevent siRNA evaporation. Pipette tips were changed between each library plate to prevent cross contamination of siRNAs.

A 50:1 optiMEM serum free medium: lipofectamine RNAiMAX transfection reagent mix was prepared and gently mixed. This was then added to each plate using a multichannel pipette and gently pipetted up and down three times with fresh pipette tips for each well. This step was done in this way because siRNA transfection was unsuccessful when the transfection reagent was dispensed using the WellMate liquid handling device, probably due to siRNA binding the CellBIND coating on the assay plates. Plates were then incubated at room temperature for 15 minutes.

Tubing for the WellMate liquid handling device was flushed with first sterile water, then 70% ethanol, then finally further flushed with sterile water. Cells were trypsinised and a cell suspension prepared at a concentration of $6.25x10^4$ cells per ml. 80µl of this well mixed cell suspension was then dispensed into each well of the assay plates using the WellMate liquid handling device, a total of 5000 cells per well. This resulted in a final siRNA concentration of 20nM in a volume of 100µl. Plates were then incubated at 37ºC for 48 hours, in a dedicated tissue culture incubator to avoid unnecessary changes in environment due to frequent opening of the incubator.

2.8.1.5 Arsenic treatment

48 hours after transfection, cells were treated with arsenic or vehicle. Arsenic trioxide stock solution (see section 2.3.5) was diluted in culture medium to a concentration of 11µM. Vehicle solution was diluted in the same way. The WellMate liquid handling device was then used to dispense 10µl of arsenic solution or vehicle to each well of the 17 corresponding assay and QC plates. Cells were then incubated at 37ºC for a further 24 hours.

2.8.1.6 Cell fixation and staining

Plates were taken from the tissue culture incubator in batches of four for fixation. Using the Fluid X liquid handling device, media was aspirated from each plate and replaced with 100µl of PBS from a reservoir plate. This was aspirated and replaced with fresh PBS once more to wash cells. PBS was then aspirated and replaced with 40µl of 4%PFA/PBS and incubated at room temperature for 10 minutes. Cells were washed three times with PBS and plates stored at 4ºC. While the first batch of plates were incubating with PFA, a second batch were removed from the incubator and the same procedure commenced.

When all plates were fixed, the Fluid X liquid handling device was again used to aspirate PBS and dispense 0.2% triton to permeabilise cells. This was performed in batches of four plates. Following 10 minutes incubation, cells were washed three times before 5 minutes incubation with DAPI. Cells were then washed a final three times and 100µl of PBS was dispensed into each well. Plates were then sealed using a thermal sealer and stored at 4ºC until imaging.

2.8.1.7 Imaging and image analysis

Imaging was performed as described in section 2.7.5, using an INCell 1000 automated microscope with 10x/0.45 Plan apo lens. This took approximately 36 hours.

Image analysis was performed using INCell Investigator software, as described in section 2.7.6. The resulting data files were saved on a dedicated high content imaging server. Raw images were reviewed using OMERO software, which allowed upload of images in a 96 well plate format.

2.9 Data analysis and hit identification

Data analysis was performed by Amit Garg, SCILLS data manager using ActivityBase software (IDBS), and is discussed in detail in section 3.2.8.1.

2.10 Follow up screen

To follow up putative hits, the four individual siRNAs which made up the pool of siRNAs tested in the initial screen were ordered from Dharmacon, in 96 well plate format. Each siRNA occupied one well of a 96 well plate with, making a total of two 96 well plates. siRNAs were reconstituted to 200nM concentration and assayed using the same method as described in section 2.7.

3 Development of a high content siRNA screen

3.1 Introduction

The aim of this project was to investigate the mechanism of arsenic mediated degradation of PML. To do this a high content siRNA screen was developed to identify gene products which, when depleted using RNA interference, altered the fate of the PML protein in response to arsenic, implicating the gene product in the process. Initial steps in assay development involved characterisation of the reagents and cell lines required. Suitable controls were then identified, allowing development and validation of an assay suitable for use in high throughput screening. Ultimately, an siRNA screen was performed, and a number of putative hits identified and further validated. All steps in this process will be summarised in this chapter.

3.1.1 RNA interference

RNA interference is a conserved mechanism of post translational control of gene expression. Two types of short, non-coding RNAs, short interfering RNAs (siRNAs) and microRNAs induce silencing of target genes via the RNA interference machinery. siRNAs induce silencing by inducing degradation of target mRNA transcripts (Meister and Tuschl, 2004), while microRNAs effect silencing via translational inhibition and mRNA degradation (Huntzinger and Izaurralde, 2011).

Long double stranded RNAs which may be endogenous or exogenously introduced into cells, for example during viral infection, are processed in the cytoplasm by the enzyme Dicer into short, 21-22 nucleotide siRNAs (**Figure 3.1.1.**). The two strands of the siRNA play different roles in the silencing process. The guide strand of the siRNA is loaded onto the RNA interference silencing complex (RISC) while the passenger strand is degraded following RISC binding.

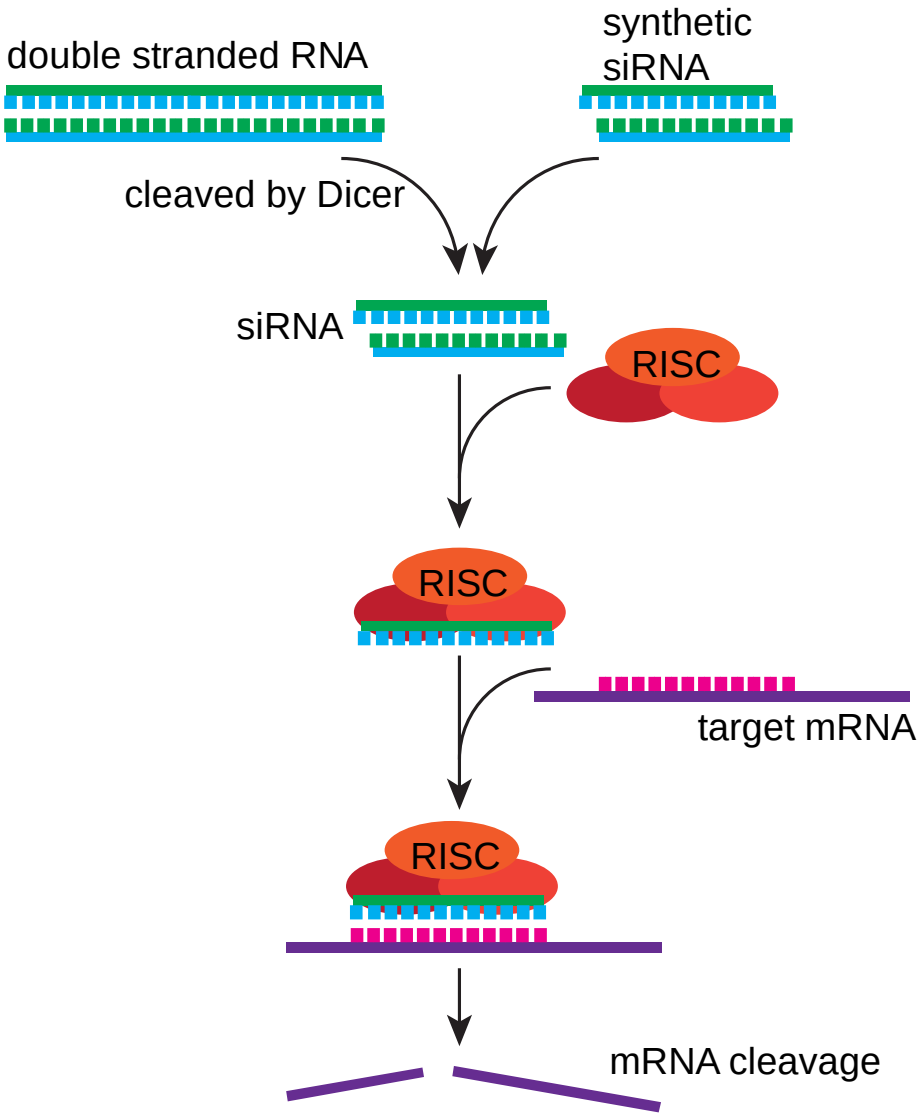

Figure 3.1.1. Mechanism of siRNA induced gene silencing

Long, double stranded RNA molecules are processed by the enzyme Dicer into 21- 22 nucleotide short interfering RNAs (siRNAs). The guide strand of the siRNA duplex is loaded onto the RNA interference silencing complex (RISC) which guides the silencing complex to mRNA sequences which are complementary to the guide strand. Synthetic siRNAs do not require cleaveage by Dicer and are loaded directly onto the RISC. Complementary mRNAs are then cleaved by Argonaute, the catalytic element of the RISC.

The RISC complex is then guided to mRNAs with sequences complementary to the siRNA guide strand which are targeted for cleavage by Argonaute, the enzymatic component of the RISC (**Figure 3.1.1.**). Target gene expression is thus reduced in a sequence specific manner. The RNA interference machinery can be used to experimentally reduce expression of a target gene through the introduction of synthetic siRNAs. Work by Fire and Mello confirmed that in order to achieve maximal gene knockdown, these synthetic siRNAs should be double stranded (Fire et al., 1998). Further investigation confirmed optimal knockdown with siRNA duplexes of 21 nucleotides in length (Elbashir et al., 2001). Synthetic siRNAs are now a widely used research tool, allowing examination of loss of function phenotypes on a large, even whole genome scale, through the use of libraries of siRNAs.

microRNAs are endogenous, non coding RNAs which are expressed as long, double stranded RNAs. These are processed, first in the nucleus and then in the cytoplasm, by a series of enzymes. The guide strand of the resulting short, double stranded microRNA is loaded onto the RISC which guides the silencing complex to the 3’ UTR of target mRNA, which may inhibit mRNA translation or induce mRNA degradation (Huntzinger and Izaurralde, 2011). In contrast to siRNA mediated silencing, microRNA induced silencing relies on only partial complementarity between microRNA and target mRNA sequences. Each microRNA therefore controls expression of multiple transcripts, each with 3’ UTR sequence similarity to the microRNA sequence. The post transcriptional regulation enforced by microRNAs has functions in many physiological processes, for example control of developmental transitions (Ebert and Sharp, 2012). There is also increasing evidence of the involvement of microRNAs in disease processes, with some microRNAs functioning as biomarkers for diseases such as cancers and autoimmune disorders (Pritchard et al., 2012).

3.1.1.1 Off-target effects of siRNA

Advances in the understanding of the mechanism of siRNA and microRNA induced silencing has allowed for greater understanding of the unintended side effects of siRNAs. These so called 'off-target effects' can be divided into two main groups: sequence specific off-target effects mediated by microRNA like activities and off-target effects due to an siRNA induced inflammatory response (Jackson and Linsley, 2010; Kassner, 2008; Sachse and Echeverri, 2004).

In addition to the intended target of a given siRNA, each siRNA has a sequence specific profile of unintended targets. These microRNA- like off- target effects are mediated by sequence similarity between the 5' region of the siRNA sequence and the sequence of the 3' UTR of mRNAs. mRNAs with 3' UTR sequences which display some, but not complete complementarity to the siRNA sequence may be targeted for cleavage in addition to the intended, perfectly complementary target. This process is similar to the targeting of multiple mRNAs by the seed region of a single microRNA (Birmingham et al., 2006; Jackson et al., 2006b). The repression of these off- target mRNAs tends to be less significant than those of the intended target (Birmingham et al., 2006; Jackson et al., 2006b), but are still sufficient to cause false positive results in siRNA screens (Echeverri et al., 2006). siRNAs with different sequences targeting the same gene product will have a different profile of sequence specific off-target gene regulation. This difference in off target profile can be exploited to confirm that a phenotype observed following transfection of a single siRNA duplex is due to repression of the desired target mRNA. If the same phenotype is induced by multiple siRNAs with distinct sequences but the same target gene, it is likely that the phenotype is due to knockdown of the target gene, because the only mRNA target shared by the

individual siRNAs is the intended target (Echeverri et al., 2006; Jackson and Linsley, 2010; Kassner, 2008; Sachse and Echeverri, 2004).

The other classes of off-target effects of siRNAs tend to be less problematic. siRNAs can induce changes in gene transcription which are due to stimulation of the innate immune system by exogenous siRNA. Some siRNAs appear to stimulate the immune system to a greater extent than others, suggesting that some sequences are more immunogenic. There is also evidence that chemical modification of siRNAs can reduce the likelihood of immune stimulation, and that the likelihood of such stimulation can be minimised by using the lowest possible concentrations of reagents (Jackson and Linsley, 2010).

3.1.2 Good practice in siRNA screening

For an siRNA screen to produce meaningful data, siRNA must be transfected into cells with high efficiency, and such transfection must result in profound and specific knockdown of the intended gene product. To this end, there are a number of considerations to take into account when designing an siRNA screen or screening service.

The siRNAs contained in libraries for screening should be designed in such a way that off target effects are minimised. Chemical modification by 2'-*O*-methyl ribosyl substitution at position 2 of the seed sequence of the guide strand of siRNA duplexes has been demonstrated to reduce off target transcriptional repression by 66% (Jackson et al., 2006a). siRNAs which have been modified in this way should therefore be used. The seed sequence of the guide strand of an siRNA duplex can also influence the likelihood of off target silencing via microRNA like mechanisms. A bioinformatics analysis of all possible six nucleotide seed sequences revealed wide variation in the

number of 3'UTR complementary regions in the genome for a given sequence (Anderson et al., 2008). Validation of this data confirmed significantly less off target silencing for siRNA seed sequences with low frequency seed region complementarity. It is therefore prudent to avoid siRNA sequences with high frequency seed region complementarity, which can be achieved using bioinfomatic tools (Anderson et al., 2008).

The use of a pool of siRNAs each with a distinct sequence enhances target gene silencing while reducing sequence specific off target effects (Echeverri and Perrimon, 2006; Sharma and Rao, 2009). This is likely to allow a decrease in the total siRNA concentration required to achieve optimal silencing, which has been shown to decrease off target effects (Jackson and Linsley, 2010). The lowest effective siRNA concentration should therefore be used when performing siRNA screens (Hannon and Rossi, 2004). Optimisation of transfection protocols should be performed with the transfection reagents to be used, which are usually lipid based, to monitor for related cellular toxicity, as well as transfection efficiency (Echeverri and Perrimon, 2006).

The SCILLS siRNA library consists of Dharmacon ON-TARGET*plus* siRNAs which are chemically modified and subject to the sequence design considerations mentioned above. The library consists of 1067 pools of siRNAs. Each is made up of four siRNAs with distinct sequences targeting the same gene product. These are transfected at a low concentration of 10-20nM to minimise off target effects.

A number of approaches can be used to validate hits obtained in a primary siRNA screen. To confirm the phenotype obtained, replicates can be performed using the same pooled siRNAs as used in the primary screen. Subsequently, each of the siRNAs which constituted the pool can be assayed individually. It is generally accepted that the desired 'hit' phenotype should be reproduced by transfection of at least two

individual siRNAs targeting the gene of interest (Echeverri et al., 2006; Hannon and Rossi, 2004). This allows identification of off target effects of siRNAs, due to both microRNA like repression of genes other than the desired target and due to immune stimulation. Correlation between the phenotype obtained and the degree of gene product knockdown increases confidence that a hit is due to an on target effect of the siRNA. RT qPCR can be employed to assay target mRNA transcript expression levels and successful knockdown can also be confirmed at protein level by western blotting, though this requires the availability of good quality antibodies.

The gold standard approach for validation of siRNA mediated phenotypes is to demonstrate that the siRNA mediated phenotype can be rescued by the expression of a construct expressing the gene of interest that is resistant to the test siRNA (Echeverri et al., 2006; Hannon and Rossi, 2004). This can be performed by reintroduction of a construct expressing the target gene which has been rendered resistant to the siRNA by virtue of silent point mutations within the siRNA target sequence. An alternative approach is to design siRNAs which target the 3'UTR of the target gene, and then rescuing expression using a construct which lacks the 3'UTR and is therefore resistant to the siRNA. It may also be possible to confirm the specificity of a hit phenotype using a small molecule that confers the same effects as the test siRNA, for example use of a kinase inhibitor to confirm the phenotype observed with siRNA mediated knockdown of the kinase of interest (Mohr et al., 2010). In addition, if mice are available in which the gene of interest has been disrupted in the genome, experiments can be repeated in cells which lack the gene product identified in the siRNA screen (Sharma and Rao, 2009).

3.2 Results

3.2.1 Characterisation of an affinity purified anti-PML antibody

Initial experiments sought to confirm the reactivity and specificity of a newly generated anti-PML antibody. Until this point, the mouse monoclonal PML5E10 antibody (Zhu et al., 1997) was used for immunofluorescence experiments, but was ineffective for western blotting. Chickens were therefore immunised with recombinant PML isoform VI (PML VI), the shortest PML isoform encoded by 560 amino acids, the sequence of which is shared by all the major PML isoforms(Jensen et al., 2001a) . The polyclonal IgY anti-PML antibody was subsequently purified from egg yolk and affinity purified by Ellis Jaffray, and its sensitivity towards recombinant PML VI was initially confirmed by dot blots (data not shown).

To assess the reactivity and specificity of the new anti- PML antibody, paraformaldehyde- fixed U2OS cells were incubated with either the purified antibody or IgY purified from the yolk of eggs laid prior to immunisation, followed by incubation with a fluorescently labelled anti chicken secondary antibody. Cells were then imaged by deconvolution microscopy. While the purified antibody identified punctate nuclear structures consistent with PML bodies, the preimmune IgY did not **(Figure 3.2.1, panel A)**. Similarly, U2OS whole cell extracts were analysed by western blotting with the purified antibody or pre immune IgY. Western blotting with the purified antibody but not the preimmune IgY identified a series of PML species consistent with the various PML isoforms and their post-translationally modified forms **(Figure 3.2.1, panel B)**.

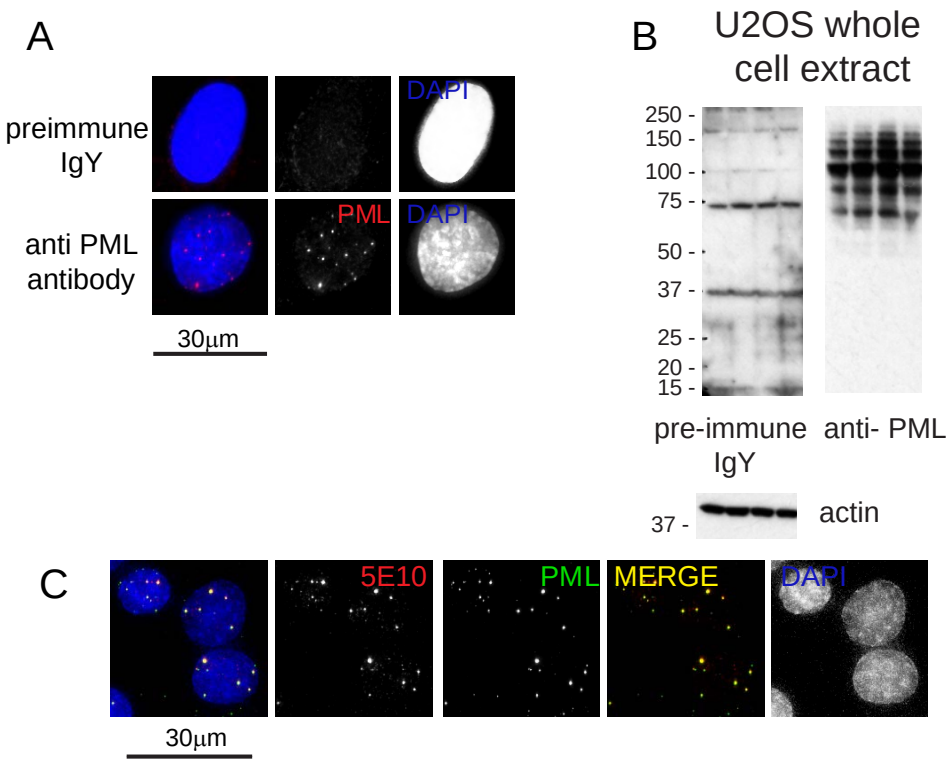

Figure 3.2.1. Characterisation of a chicken anti PML antibody

(A) U2OS cells were incubated with either preimmune IgY purified from egg yolk (top panels) or affinity purified chicken anti PML antibody (lower panels) followed by incubation with a fluorescently labelled anti chicken secondary antibody shown in red. DNA was stained with DAPI. Images presented are maximal projections of multiple z-sections.

(B) U2OS whole cell extracts (four replicates) were analysed by western blotting with either preimmune IgY (left panel) or purified anti PML antibody (right panel). An anti actin antibody was used as a loading control.

(C) U2OS cells were immunolabelled with mouse 5E10 anti PML antibody and purified chicken anti PML antibody, followed by fluorescently labelled secondary antibodies. DNA was stained with DAPI. Images presented are maximal projections of multiple z-sections. 5E10 PML is shown in red, chicken PML in green.

To investigate the specificity of the new antibody, U2OS cells cultured on coverslips were fixed in paraformaldehyde prior to double immunolabelling with the previously characterised monoclonal PML 5E10 antibody (Zhu et al., 1997) and the new chicken anti PML antibody. As expected, the PML 5E10 antibody identified endogenous PML primarily in punctate PML-NBs (**Figure 3.2.1, panel C, shown in red**). The chicken anti PML antibody also labelled PML-NBs (**Figure 3.2.1, panel C, shown in green**), precisely colocalising with the PML 5E10 labelled structures, demonstrating that the chicken anti PML antibody is immunoreactive to endogenous PML in this cell line.

To further confirm the specificity of the anti PML antibody, the effects of siRNA mediated depletion of PML on the pattern of species identified by western blotting were assessed. In cells depleted of PML by siRNA, the multiple species identified by the antibody in control, non- targeting siRNA treated cells all but disappeared (**Figure 3.2.2, panel A**). Immunofluorescence microscopy following PML siRNA demonstrates the disappearance of PML-NBs labelled by both the PML 5E10 antibody and the new chicken anti PML antibody (**Figure 3.2.2, panel B).**

These data confirm the newly generated antibody to be reactive to endogenous PML in both HeLa and U2OS cells, and the RNA interference data in **Figure 3.2.2** demonstrate the antibody to be specific for the PML protein. Thus the antibody is suitable for use in further immunoblotting and immunofluorescence experiments.

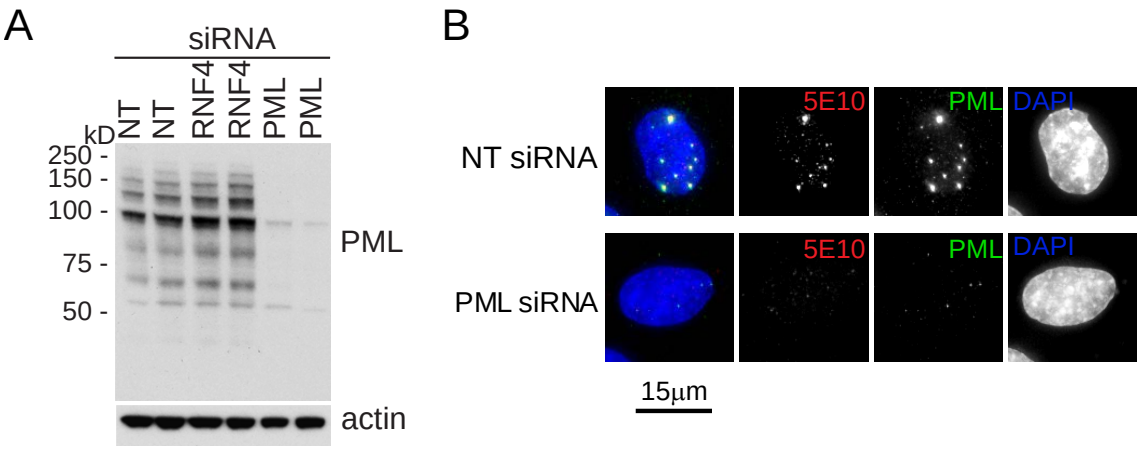

Figure 3.2.2. siRNA mediated depletion of PML confirms chicken anti PML antibody specificity

(A) U2OS cells were transfected in duplicate with pools of 4 siRNA duplexes targeting RNF4, PML or a non- targeting (NT) control duplex. Cells were lysed 48 hours after transfection and cell extracts analysed by western blotting with chicken anti PML and actin antibodies.
(B) U2OS cells were transfected with a pool of 4 siRNA duplexes targeting PML or a non- targeting (NT) control duplex. Cells were fixed 48 hours after transfection and labelled with 5E10 PML and chicken anti PML antibodies and fluorescently labelled secondary antibodies. DNA was stained with DAPI. Images presented are maximal projections of multiple z-sections. 5E10 PML is shown in red, chicken anti PML in green.

3.2.2 PML is degraded in response to arsenic treatment

It is well established that PML is SUMO modified and then degraded by the proteasome in response to arsenic treatment (Lallemand-Breitenbach et al., 2001; Muller et al., 1998). To help plan the timing of analysis for the siRNA screen, a kinetic analysis of PML degradation in response to arsenic was performed. U2OS cells were treated with arsenic and cells harvested at various time points. Whole cell extracts were then resolved by SDS-PAGE and analysed by immunoblotting (**Figure 3.2.3, panel A**).

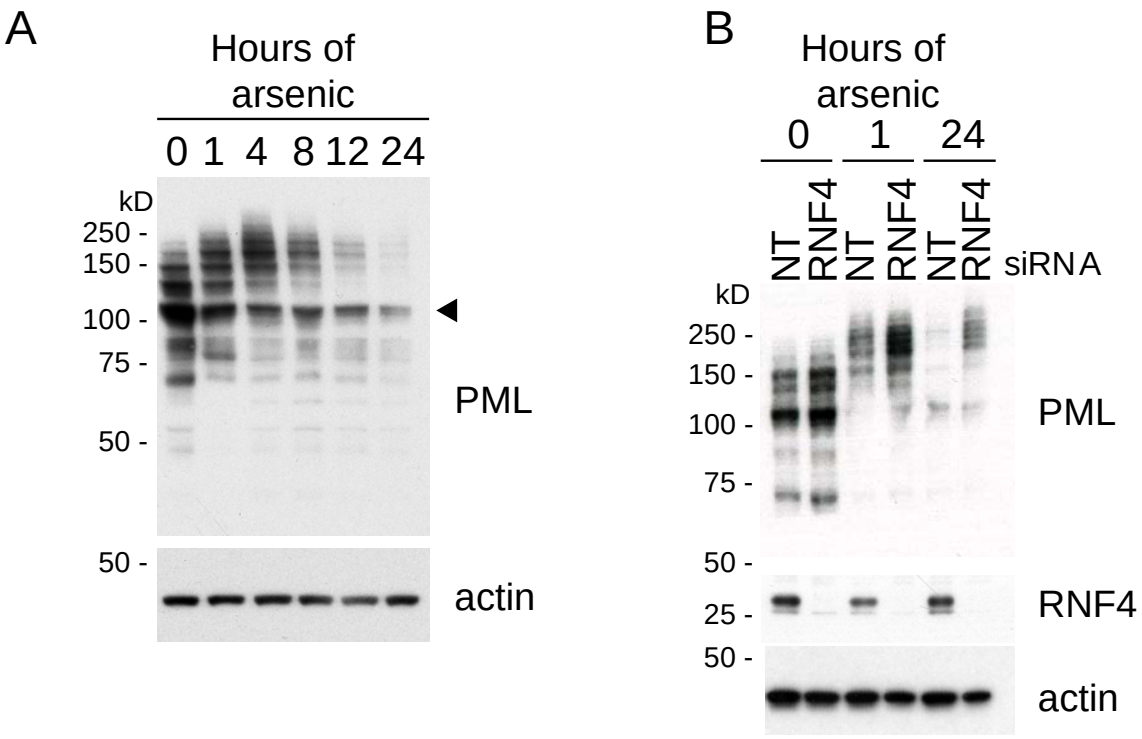

Figure 3.2.3. PML is degraded following arsenic treatment in an RNF4 dependent manner

(A) U2OS cells were treated with 1µM arsenic trioxide and lysed at the time points indicated. Cell extracts were then analysed by western blotting with chicken anti PML and actin antibodies.
(B) U2OS cells were transfected with a pool of 4 siRNA duplexes targeting RNF4 or a non targeting (NT) control duplex. 48 hours after transfection, cells were treated with 1µM arsenic trioxide and cell lysates analysed by western blotting using chicken anti PML, chicken anti RNF4 and mouse anti actin anitbodies.

After a short arsenic treatment of 1 to 4 hours, post translational modification of PML is demonstrated by the accumulation of high molecular weight PML species which represent the SUMO modification of the various PML isoforms (**Figure 3.2.3, panel A**). At later time points, a marked decrease in PML species is apparent, with near disappearance after 24 hours of treatment. This indicated arsenic induced degradation of PML was virtually complete after 24 hours of treatment. Some PML species appeared

to persist, indicating that some PML species are more susceptible to degradation than others (**Figure 3.2.3, panel A, arrowhead**).

3.2.3 RNF4 is required for arsenic mediated degradation of PML

The SUMO targeting ubiquitin E3 ligase RNF4 has been demonstrated to be essential for arsenic mediated degradation of PML (Lallemand-Breitenbach et al., 2008; Tatham et al., 2008). U2OS cells were transfected with either a non- targeting (NT) siRNA duplex or a pool of 4 siRNAs targeting RNF4. 48 hours later cells were treated with arsenic. Cells were harvested at various time points and whole cell extracts examined by western blotting (**Figure 3.2.3, panel B**). RNF4 depletion was confirmed by western blotting with an anti RNF4 antibody. Cells depleted of RNF4 express more PML than control cells prior to arsenic treatment, suggesting RNF4 may also regulate PML expression in the absence of arsenic (**Figure 3.2.3, panel B**). Following 1 hour of arsenic treatment, accumulation of high molecular weight PML species is observed in both control and RNF4 depleted cells. However, striking differences are noted following 24 hours of arsenic treatment. PML was almost completely degraded in control cells, whereas in RNF4 depleted cells there was accumulation of very high molecular weight PML species. These results confirmed that RNF4 is required for arsenic induced degradation of PML.

The process of arsenic mediated degradation of PML can also be monitored by immunofluorescence. The siRNA screening assay was to be performed using fixed cells, because the automated microscope to be used did not have facilities for live cell imaging. Preliminary experiments were therefore performed using cells fixed at various time points.

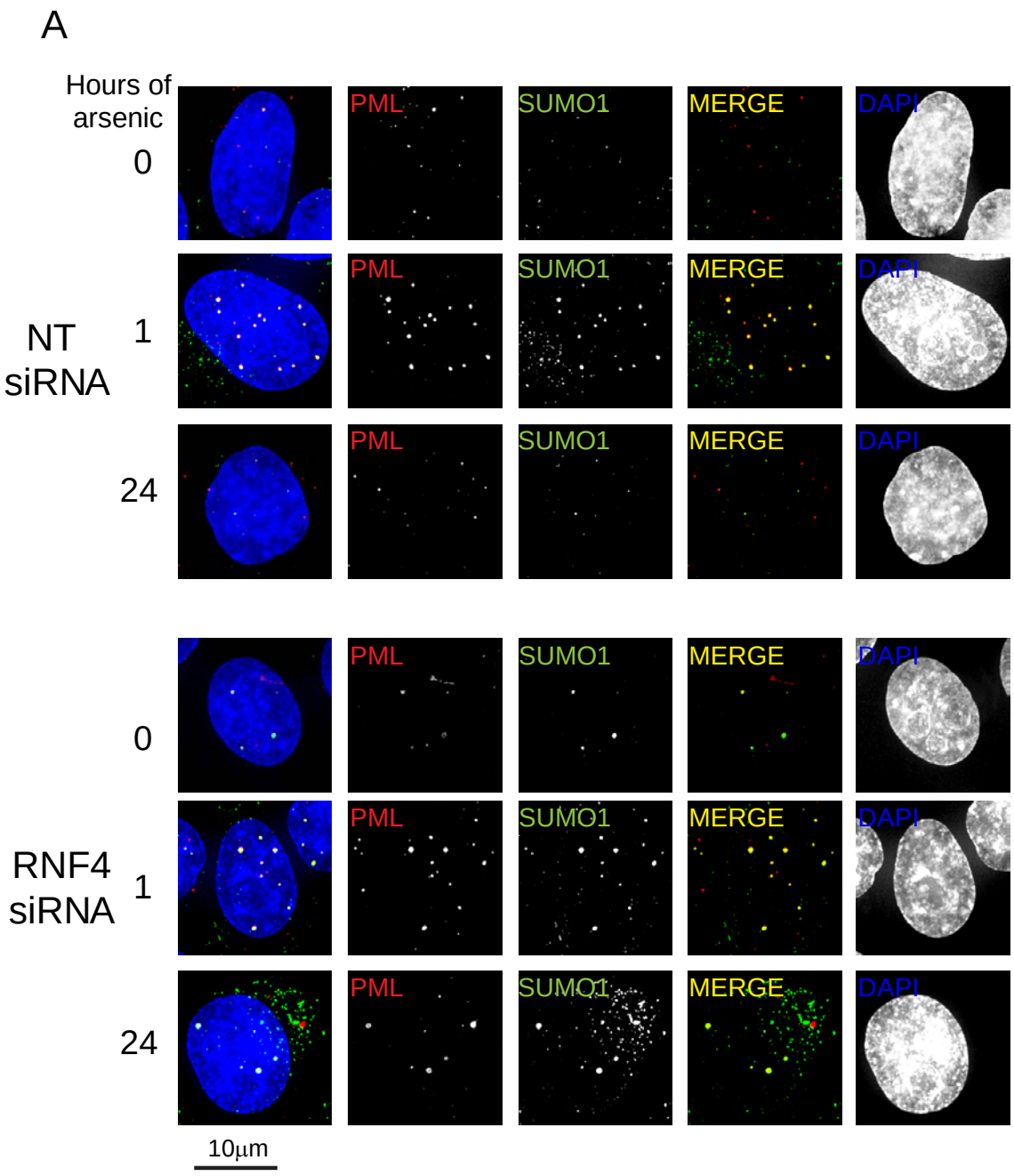

Figure 3.2.4. Immunofluorescence demonstrates PML accumulates in PML bodies in cells depleted of RNF4 prior to arsenic treatment

(A) HeLa cells were transfected with a pool of 4 siRNA duplexes targeting RNF4 or a non targeting control (NT) duplex. 48 hours after transfection cells were treated with 1μM arsenic for 0, 1 or 24 hours. Cells were fixed and stained with chicken anti PML (red) and sheep anti SUMO1 (green) antibodies. DNA was stained with DAPI. Immunofluorescence images presented are maximal projections of multiple z-sections.

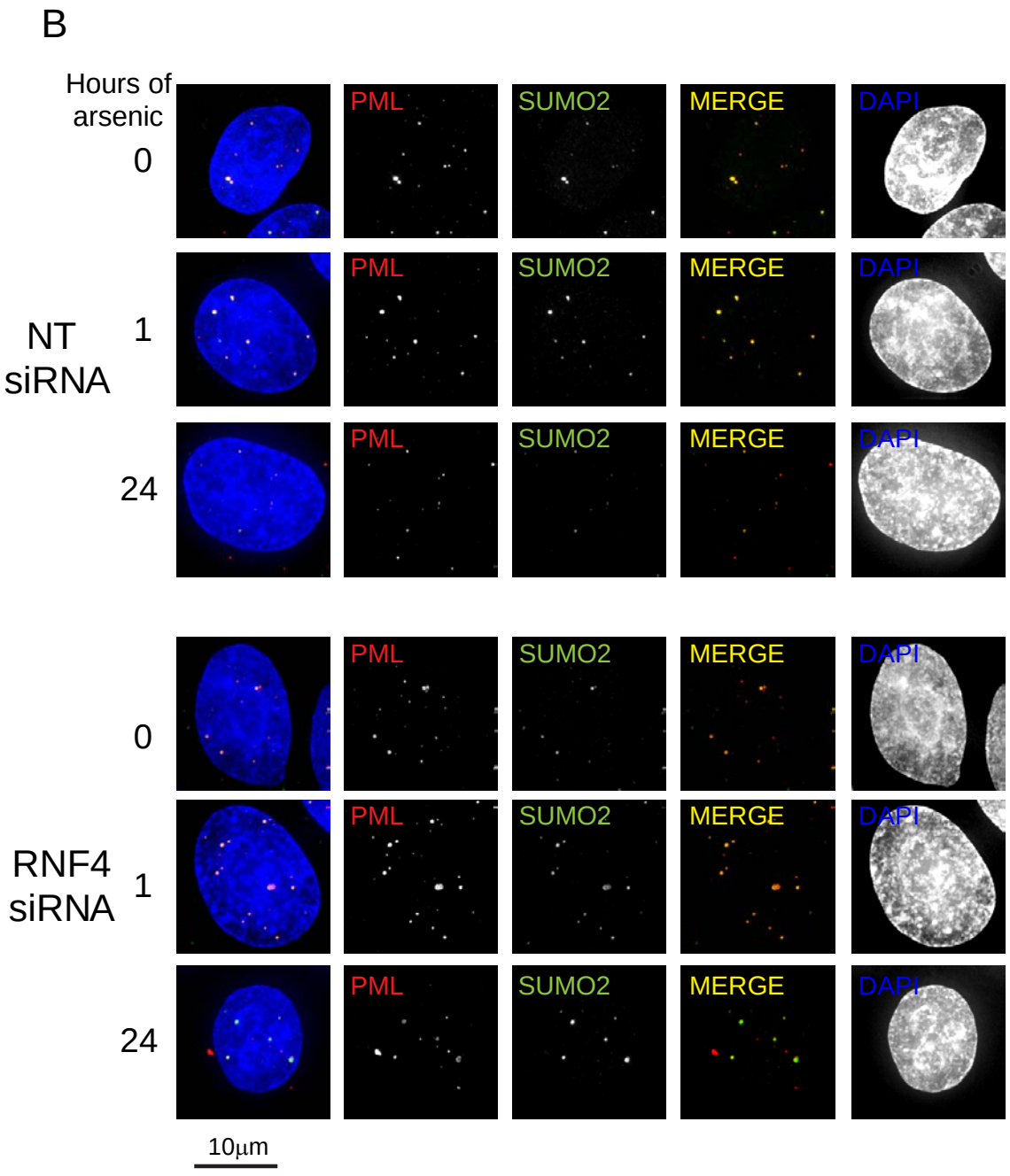

Figure 3.2.4. Immunofluorescence demonstrates PML accumulates in PML bodies in cells depleted of RNF4 prior to arsenic treatment

(B) HeLa cells were transfected and treated with arsenic as in (A). Cells were fixed and stained with chicken anti PML (red) and sheep anti SUMO2/3 (green) antibodies. DNA was stained with DAPI. Immunofluorescence images presented are maximal projections of multiple z-sections

To investigate the effects of RNF4 depletion on the localisation and degradation of PML resulting from arsenic treatment, HeLa cells were transfected with either control NT siRNA or RNF4 siRNA and then treated with arsenic. Cells were fixed at various time points and immunostained with an anti PML antibody plus either anti SUMO1 (**Figure 3.2.4, panel A**) or anti SUMO2/3 (**Figure 3.2.4, panel B**) antibodies. In NT siRNA transfected control cells prior to arsenic treatment, there is a small amount of SUMO1 (**Figure 3.2.4, panel A**) and SUMO2/3 (**Figure 3.2.4, panel B**) associated with PML, as identified by colocalisation of the proteins by immunofluorescence. After 1 hour of arsenic treatment, there is an increase in the number of PML-NBs and in the amount of associated SUMO1 and SUMO2/3. After 24 hours of treatment, there are virtually no PML-NBs remaining, and very little SUMO associated (**Figures 3.2.4, panels A and B**), indicative of SUMO modified PML having been degraded in response to arsenic. In cells depleted of RNF4, the initial response to arsenic treatment was similar to that of control cells, with an increase in the number of PML-NBs and in the amount of SUMO1 and SUMO2/3 associated. The striking differences identified between control and RNF4 depleted cells after 24 hours of arsenic treatment were confirmed in these immunofluorescence images. There was accumulation of PML and SUMO1 (**Figure 3.2.4, panel A**) and SUMO2/3 (**Figure 3.2.4, panel B**) in large, bright PML-NBs in RNF4 depleted cells, compared with the near complete absence of PML-NBs in NT siRNA transfected cells.

The striking difference in phenotype identified by immunofluorescence between cells transfected with NT siRNA and RNF4 siRNA suggested that it should be possible to screen for other proteins essential for the process of arsenic mediated degradation of PML by monitoring PML fluorescence. The aim of the siRNA screen would be to identify siRNAs which recreated the RNF4 siRNA phenotype after 24 hours of arsenic treatment. This suggested that RNF4 was likely to be an appropriate positive control for

a high content screening assay. Since NT siRNA did not interfere with arsenic mediated degradation of PML, it could be further employed as a negative control.

3.2.4 Characterisation of YFP-PML HeLa cell line

The aim of the siRNA screening experiment was to monitor the fate of the PML protein following siRNA mediated gene knockdown and arsenic treatment by immunofluorescence. This could be performed using the previously characterised anti-PML antibody to immunostain endogenous PML in a cell line of choice. However, given the scale of the screening experiment, this was likely to be extremely laborious. In order to keep the screening assay as simple and reproducible as possible it would be ideal to use a cell line expressing a fluorescent version of PML. This would eliminate the need for two step antibody staining of PML and the associated potential variation in PML detection. For these reasons, a HeLa cell line stably expressing PML isoform III-yellow fluorescent protein (YFP) fusion created by Marie-Claude Geoffroy (Geoffroy et al., 2010) was selected for characterisation. These cells express YFP-PML at close to endogenous levels, and the YFP-PML is efficiently incorporated into PML-NBs (**Figure 3.2.5, panel A**). When these cells are depleted of PML using siRNA, YFP fluorescence is abolished (**Figure 3.2.5, panel B**), confirming that all of the YFP is linked to PML. This experiment also confirms that these cells can be satisfactorily transfected with siRNA, another key characteristic of cells to be used in the screening experiment.

The readout of the siRNA screen was to be measures of YFP-PML fluorescence. It was therefore important that cell to cell variation in YFP-PML expression was minimised in order to obtain a robust assay. To ensure the population of these cells used for further experiments, including the screening experiment was as homogeneous as possible, a population of cells expressing a low level of YFP-PML was obtained by

fluorescence-activated cell sorting, performed by Dr Rosie Clarke, University of Dundee. These cells were used in the studies which follow.

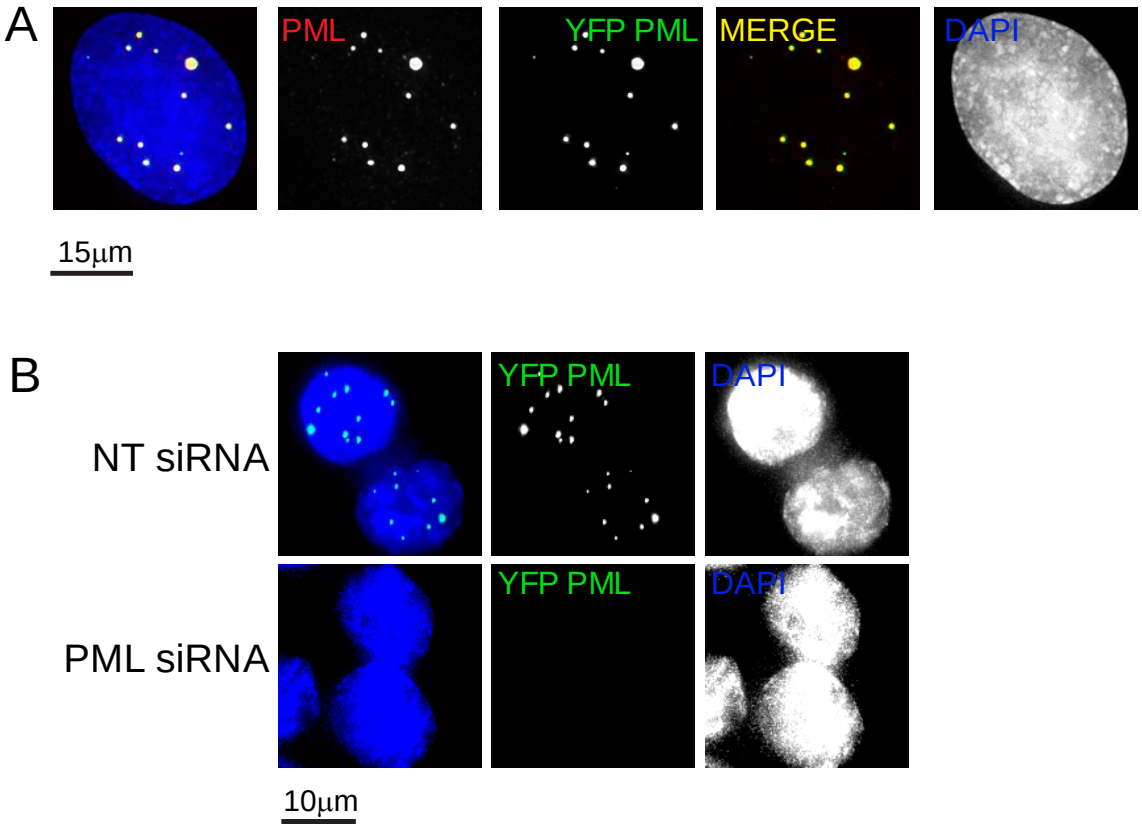

Figure 3.2.5. Immunofluorescence characterisation of YFP-PML HeLa cells

(A) YFP-PML HeLa cells were fixed and stained with chicken anti PML antibody. Cells were imaged by deconvolution microscopy. YFP-PML is shown in green, chicken anti PML antibody in red. DNA was stained with DAPI. Immunofluorescence images presented are maximal projections of multiple z-sections.

(B) YFP-PML HeLa cells were transfected with a pool of 4 siRNAs targeting PML or a control, non targeting (NT) duplex. Cells were fixed 48 hours after transfection and DNA was stained with DAPI. Images presented are maximal projections of multiple z- sections.

3.2.5 YFP-PML is degraded in an RNF4 dependent manner following arsenic treatment

Endogenous PML is degraded in an RNF4 dependent manner, as described in section 3.2.3. The next experiments sought to characterise the response of YFP-PML in the YFP-PML HeLa stable cell to arsenic treatment. Cells were transfected with a pool of four siRNAs targeting RNF4, and 48 hours later, treated with arsenic and lysed at various time points. Western blotting of whole cell extracts performed with an anti-RNF4 antibody confirms that RNF4 can be successfully depleted in these cells (**Figure 3.2.6, panel A**). The effects of this depletion on YFP-PML are similar to those observed when endogenous PML is assessed following RNF4 depletion and arsenic treatment. After a short 1 hour arsenic treatment, high molecular weight YFP-PML species accumulated, indicating that YFP-PML was post-translationally modified (**Figure 3.2.6, panel A, anti-GFP blot**). After 24 hours exposure to arsenic, in cells transfected with non-targeting (NT) control siRNA, YFP-PML was almost completely degraded. Conversley, in cells transfected with RNF4 siRNA high molecular weight YFP-PML species accumulated (**Figure 3.2.6, panel A, GFP blot, 24 hour time point**). This experiment confirmed that in response to arsenic treatment YFP-PML is degraded in an RNF4 dependent manner. This experiment was repeated with cells cultured on coverslips to examine the effects of RNF4 depletion and arsenic treatment on the localisation and intensity of YFP-PML fluorescence by deconvolution microscopy. In cells transfected with NT siRNA, an increase in YFP-PML fluorescence at PML-NBs was noted after 1 hour of arsenic treatment. The marked decrease in YFP-PML fluorescence after 24 hours of arsenic exposure (**Figure 3.2.6, panel B**) indicated that YFP-PML has been degraded. Conversely, in cells depleted of RNF4, YFP-PML

accumulated in large, bright PML-NBs following arsenic treatment (**Figure 3.2.6, panel B**).

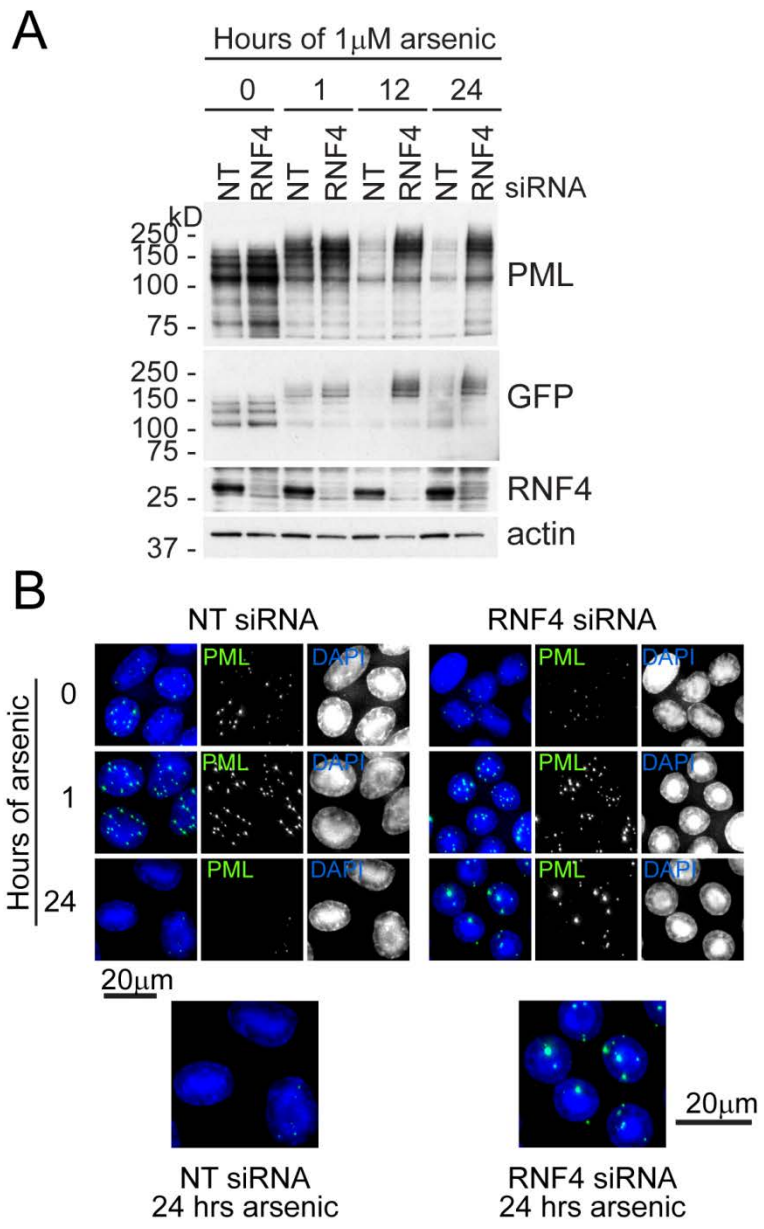

Figure 3.2.6. YFP-PML is degraded in an RNF4 dependent manner in response to arsenic treatment

(A) YFP-PML HeLa cells were transfected with a pool of siRNAs targeting RNF4 or a non-targeting (NT) control duplex. 48 hours after transfection, cells were treated with 1μM arsenic trioxide for the indicated periods of time prior to cell lysis. Cell lysates were analysed by western blotting with chicken anti PML, anti GFP (to detect YFP-PML only), anti RNF4 and actin antibodies.

(B) YFP-PML HeLa cells were transfected and arsenic treated as in **(A)**, before fixation with paraformaldehyde. DNA was stained with DAPI and cells were imaged by deconvolution microscopy. YFP-PML is shown in green. Immunofluorescence images presented are maximal projections of multiple z-sections.

This demonstrated that, like endogenous PML (section 3.2.3.), the most marked differences in YFP-PML fluorescence between control and RNF4 depleted cells are identified following 24 hours of arsenic treatment (**Figure 3.2.6, panel B, bottom panels**).

These results confirmed that HeLa cells stably expressing YFP-PML could be successfully transfected with siRNA, and that YFP-PML was degraded in an RNF4 dependent manner in response to arsenic treatment. The phenotype observed in YFP-PML HeLa cells depleted of RNF4 following 24 hours of arsenic treatment was the same as that observed for endogenous PML. YFP-PML HeLa cells were therefore a suitable system to use to investigate the effects of siRNA mediated gene knockdown on the process of arsenic mediated degradation of PML. The data also suggest that most appropriate time point at which to analyse cells in the screening assay would be after 24 hours of arsenic treatment.

3.2.6 Quantitation of YFP-PML fluorescence after RNF4 depletion and arsenic treatment

The images presented in **Figures 3.2.4. and 3.2.6., panel B,** demonstrated a marked difference in phenotype between cells transfected with control siRNA and cells transfected with RNF4 siRNA following 24 hours of arsenic treatment. This suggested that RNF4 siRNA may be an appropriate positive control to be used in the screening experiment. Knockdown of RNF4 prevented arsenic mediated degradation of PML, and

the aim of the screen was to identify siRNAs which perturbed this process. In order to transform this observation into an assay suitable for high content screening, a measure of YFP-PML fluorescence that characterised this difference was required, and the next experiments sought to identify such a measure.

Quantitation of YFP-PML fluorescence was performed by imaging cells cultured on coverslips using deconvolution microscopy. Maximal intensity projections of multiple z sections of deconvolved images were prepared and YFP-PML fluorescence quantified using Softworx software. Initially, the mean YFP fluorescence of entire cell nuclei was calculated for NT siRNA and RNF4 siRNA transfected cells at three different time points after arsenic treatment (**Figure 3.2.7, panel A**). This identified a 1.3 fold difference between the mean nuclear YFP fluorescence of NT siRNA treated and RNF4 siRNA treated cells after 24 hours of arsenic treatment (**Figure 3.2.7 panel A**). This small difference did not reflect the marked differences in phenotype identified in the images (**Figure 3.2.6, panel B**), and was unlikely to be sufficient to discriminate between siRNAs which perturbed the process of PML degradation and those which did not in a high content screening assay.

Subsequently, attempts at quantification of YFP-PML fluorescence were focussed on quantification of fluorescence of PML-NBs, because it appeared from images (**Figure 3.2.6, panel B**) that the main difference in the phenotype of YFP-PML fluorescence following RNF4 depletion appeared to be in the intensity, number and size of PML-NBs present after arsenic treatment. Once again, maximal intensity projections were made of multiple z sections of images and PML-NBs were identified as clusters of pixels with a YFP intensity above a specified threshold using Softworx software. The threshold used was maintained across all time points and siRNA conditions to allow comparisons to be drawn. This semi- automated approach was used because eventually

the aim was to produce an assay suitable for automated analysis of thousands of images, and manual quantification of fluorescence of individual PML-NBs would not be possible. This method of quantification did not identify a difference in PML-NB intensity (**Figure 3.2.7, panel B**).

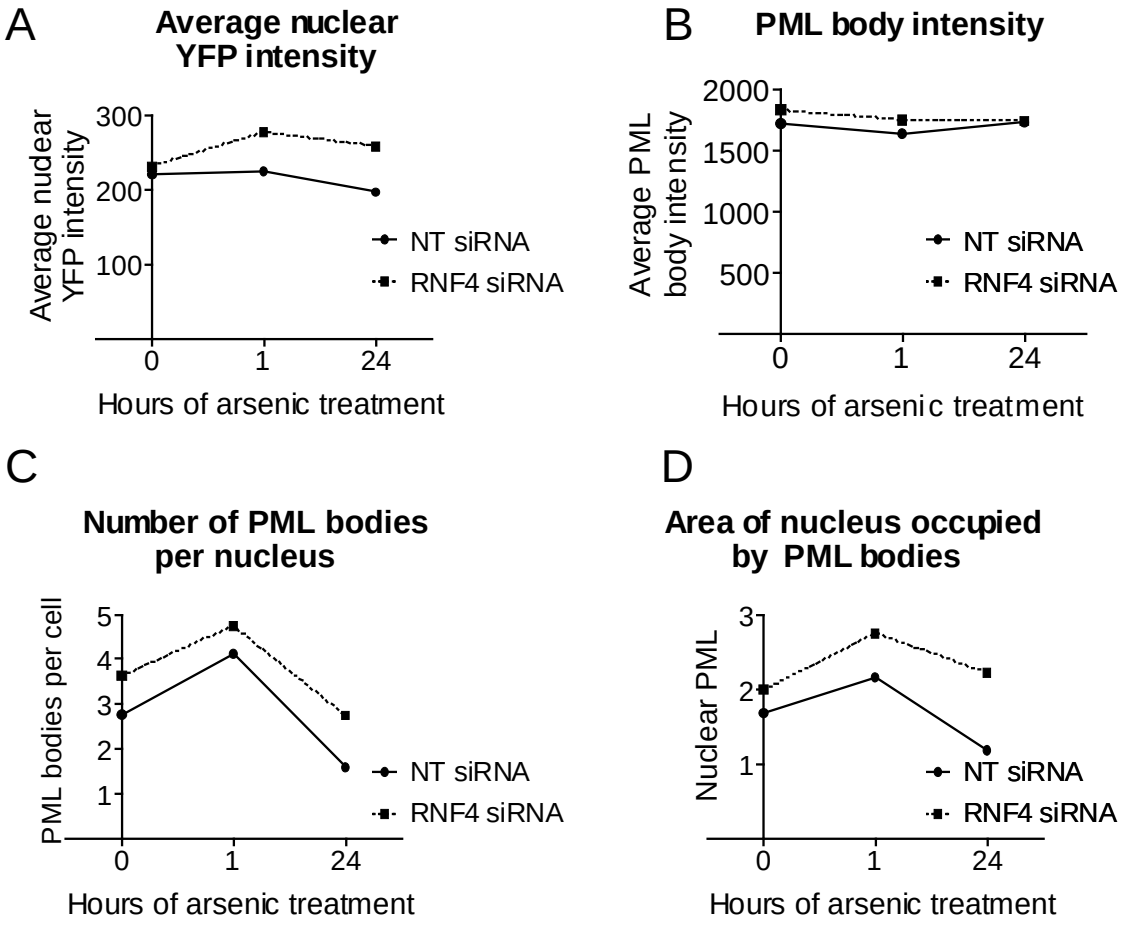

Figure 3.2.7. Quantification of YFP-PML fluorescence following RNF4 depletion and arsenic treatment

YFP-PML HeLa cells were transfected with a pool of 4 siRNA duplexes targeting RNF4, or a non- targeting (NT) control duplex. 48 hours after transfection, cells were treated with 1µM arsenic trioxide for 0, 1 or 24 hours. Cells were stained with DAPI and imaged using deconvolution microscopy. YFP-PML fluorescence was then quantified from maximal projections of multiple z sections.

(A) Comparison of YFP-PML fluorescence of whole cell nucleus. Data represents the average fluorescence of 50 cells analysed for NT or RNF4 siRNA transfected cells at each timepoint.

(B) The average pixel intensity of YFP-PML bodies was analysed. Data represents the average pixel intensity of PML bodies in 100 cells per condition.
(C) The number of YFP-PML bodies per nucleus was analysed for 100 cells per condition. Data represents the average number of PML bodies per nucleus for each condition.
(D) The sum of the area of all PML bodies in each cell nucleus was calculated for 100 cells per condition. Data represents the average total area of the nucleus occupied by PML bodies.

This is to be expected because in order to be identified as a PML-NB by the software, a cluster of YFP fluorescent pixels had to have a YFP intensity above the given threshold of YFP intensity. Thus, the mean intensity of very small pixel clusters with YFP intensity above the threshold identified in the NT siRNA treated cells is very similar to the mean intensity of the larger pixel clusters identified in RNF4 siRNA treated cells. More significant differences were identified in measures of PML-NB number and area (**Figure 3.2.7, panel C and panel D**). The average number of PML-NBs identified per nucleus in RNF4 siRNA treated cells was 1.7 times higher than that identified in control cells after 24 hours of arsenic treatment (**Figure 3.2.7, panel C**). The most discriminatory measure between RNF4 depleted and control cells was found to be the sum of the area of PML-NBs attributed to one nucleus, with RNF4 depleted cells having PML-NBs twice the area of control cells after 24 hours of arsenic treatment (**Figure 3.2.7, panel D**).

These experiments demonstrated that, in principle, a high content siRNA screen using NT siRNA as a negative control and RNF4 siRNA as a positive control, and the measure of the sum of the area of all PML-NBs in one cell, hereafter referred to as ‘PML body total area’, as the assay parameter, should be capable of identifying gene products which, when knocked down, influence the process of arsenic mediated degradation of PML.

3.2.7 Development of an assay suitable for high content screening

3.2.7.1 High content imaging and image analysis

The next experiments aimed to recreate the results summarised in sections 3.2.5 and 3.2.6 in an experimental format suitable for high throughput screening, and by doing so develop an assay suitable for use in a high content screen. A method was developed to perform reverse siRNA transfection of YFP-PML HeLa cells in black, clear bottomed 96 well plates which were suitable for automated microscope imaging. First the siRNA duplex, then transfection reagent and finally cells in culture medium were added to each well of the plate, and the cells incubated for 48 hours. Arsenic trioxide diluted in culture medium was then added to the plates, and cells incubated for a further 24 hours. Cells were then washed, fixed with paraformaldehyde and stained with DAPI.

Imaging of cells in 96 well plates was performed using an IN Cell 1000 automated microscope, using a 10x lens to obtain images of sufficient resolution to identify PML bodies, while maximising the number of cells imaged per field. Two fields of view were captured per well.

To analyse YFP-PML fluorescence in the images obtained, a protocol was designed using IN Cell Investigator software (GE Healthcare) which, like the semi-automated quantification of fluorescence described in section 3.2.6, identified PML-NBs when the YFP-PML fluorescence of a pixel cluster exceeded a given threshold above background intensity (**Figure 3.2.8**). This threshold was maintained for all plates imaged and analysed in a given experiment.

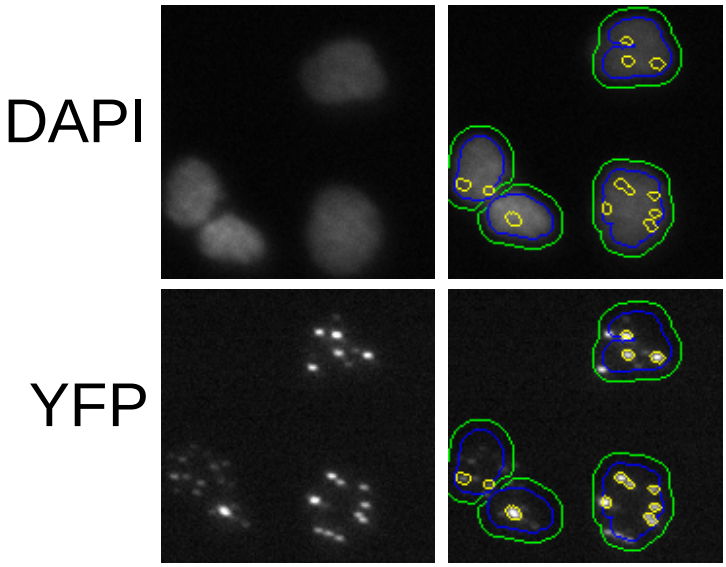

Figure 3.2.8. Screenshot example of IN Cell Investigator software analysis of PML nuclear bodies

YFP-PML HeLa cells were transfected with non targeting, control siRNA and cultured in 96 well plates prior to fixation and DAPI staining. Cells were imaged using the IN Cell 1000 automated microscope to capture YFP and DAPI fluorescence. Resulting images were analysed using a protocol designed to identify cell nuclei using DAPI fluorescence, and YFP-PML nuclear bodies within the nucleus. Left panels show raw images, and right panels the regions of interest selected by the analysis protocol: Blue lines encircle nuclei, green lines a cytoplasmic collar and yellow lines PML nuclear bodies.

The protocol captured data regarding the PML body total area, mean nuclear YFP fluorescence, the number of PML-NBs per cell, the intensity of PML-NBs and the number of cells analysed per well. The output from this analysis was a summary file with a value for each of the parameters listed, which was an average of all the individual cells analysed in a well, for each well of the 96 well plate analysed. Cell by cell data was also available in a separate file. Data analysis was performed in the assay development phase using Microsoft Excel software. It was also possible to review the images to ensure the cells appeared healthy, and to compare the data obtained from the analysis protocol to the phenotype identified by eye. At each stage, analysis was

discussed with Amit Garg, SCILLS Data Manager, who developed protocols in ActivityBase software (IDBS) which would be used to analyse siRNA screening data for hit identification.

Using the procedure outlined above, YFP-PML HeLa cells were transfected in multiple replicates with either NT or RNF4 siRNA in 96 well plates and 48 hours later treated with arsenic for 24 hours. Cells were imaged and analysed, and the results are presented in **Figure 3.2.9**. Approximately 10 000 cells were analysed for each of the two conditions. Data were very similar to that reported in **Figure 3.2.7**. There was no difference found in mean nuclear YFP intensity or mean PML-NB intensity between NT siRNA or RNF4 siRNA transfected cells (**Figure 3.2.9, panel A and panel B**). A 1.5 fold increase in the number of PML-NBs was noted for cells transfected with RNF4 siRNA compared to NT siRNA (**Figure 3.2.9, panel C**), and a two fold increase in the PML body total area (**Figure 3.2.9, panel D**).

The data obtained are very similar to that acquired from smaller scale experiments, and confirmed automation of this assay had been successful. Once again, the PML body total area was identified as the measure which best differentiated the control and RNF4 siRNA mediated phenotypes. These data confirm that the 96 well plate screening assay can discriminate between the phenotypes resulting from NT siRNA and RNF4 siRNA transfection prior to arsenic treatment, and are therefore encouraging in terms of using this assay to perform an siRNA screen searching for siRNAs which perturb the process of arsenic mediated degradation of PML.

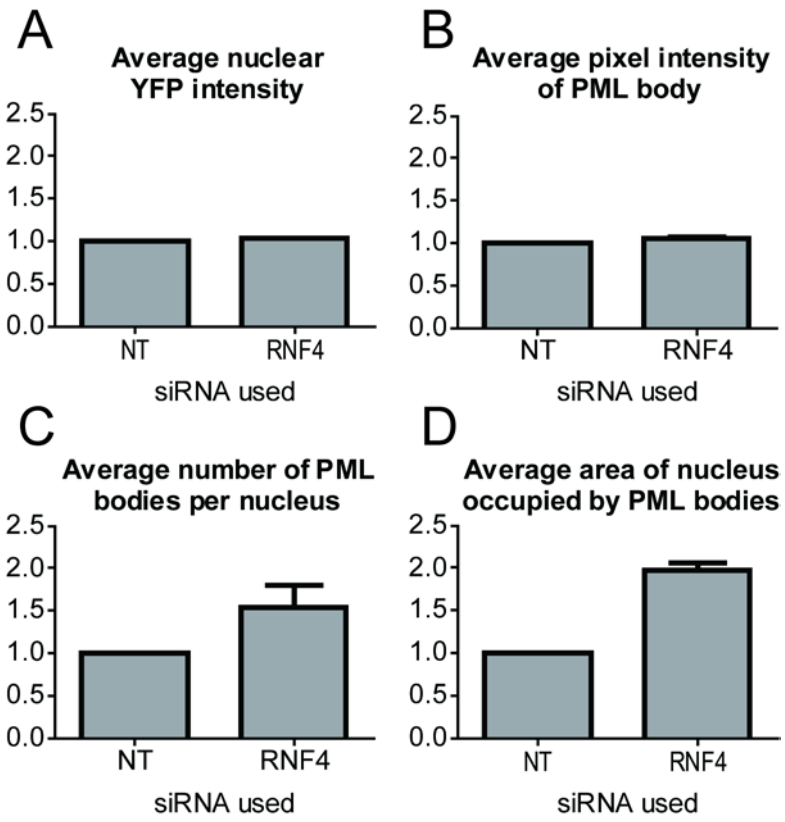

Figure 3.2.9. Automated quantification of YFP-PML fluorescence following RNF4 depletion and arsenic treatment

YFP-PML HeLa cells were transfected in 96 well plates with a pool of 4 siRNA duplexes targeting RNF4 or a non-targeting (NT) control duplex. 48 hours after transfection, cells were treated with 1µM arsenic for 24 hours. Cells were fixed and stained with DAPI. Imaging was performed using an IN Cell 1000 automated microscope and YFP-PML fluorescence in the resulting images analysed using IN Cell Investigator software.

(A) Average YFP-PML fluorescence of the cell nucleus was analysed for approximately 20 000 cells for NT and RNF4 siRNA transfected cells. Data were normalised to NT siRNA and represent the mean ± standard error of the mean.

(B) The average YFP-PML fluorescence intensity of PML bodies was analysed for approximately 20 000 cells. Data were normalised to NT siRNA and represent the mean ± standard error of the mean.

(C) The number of YFP-PML bodies per cell was analysed for 20 000 cells in each condition. Data were normalised to NT siRNA and represent the mean number of PML bodies per cell ± standard error of the mean.

(D) The total area of YFP-PML bodies per cell was analysed for 20 000 cells in each condition. Data were normalised to NT siRNA and represent the mean number of PML bodies per cell ± standard error of the mean.

3.2.7.2 Z' factor assessment of assay

To assess whether an assay is suitable for high throughput siRNA screening, a number of statistical parameters can be calculated which give an indication of whether the assay is robust enough to allow confident identification of hits (Birmingham et al., 2009). One of these statistical parameters, the Z' factor, is calculated using the mean and standard deviations of the positive and negative controls for a given parameter (Zhang et al., 1999), in this case each particular measure of YFP fluorescence. **Table I** shows the Z' factors calculated using the results obtained from arsenic treated, NT siRNA and RNF4 siRNA transfected cells analysed for the number of PML-NBs per cell, the average pixel intensity of PML-NBs and the PML body total area.

Table I. Z' factor calculations

Cells were transfected with either NT siRNA or RNF4 siRNA in 48 wells each of a 96 well plate. 48 hours after transfection, cells were treated with 1µM arsenic trioxide for 24 hours, and then fixed, DAPI stained and imaged using the automated high content screening assay. Z' factors were calculated using the resulting data for number of PML bodies per cell, PML body intensity and total area of the nucleus occupied by PML bodies in cells transfected with NT or RNF4 siRNA.

Z' factor NT vs RNF4 siRNA	
PML body number	**0.49**
PML body intensity	**-0.08**
PML body total area	**0.56**

$$\text{Z' factor} = 1 - \frac{3(\sigma_{hc} + \sigma_{lc})}{|\mu_{hc} - \mu_{lc}|}$$

Equation 3.1. Z' factor calculation

The Z' factor is calculated using the means of the high and low controls (μ_{hc} and μ_{lc} respectively), and the standard deviation of the two control populations (σ_{hc} and σ_{lc}) as demonstrated in **Equation 3.1**.

A Z' factor of greater than 0.5 identifies an assay which is statistically robust, in that there is sufficient separation of positive and negative controls to allow hit identification. A Z' factor of >0 is adequate, and a Z' factor of <0 demonstrating the assay is unsuitable for screening. Thus, the assay measurements of both PML- NB number and PML body total area produce statistically robust assays which should be suitable for use in a high content siRNA screen. Since the PML body total area had consistently yielded the best separation between negative and positive controls, it was selected as the primary measure to be used for siRNA screening.

3.2.7.3 Test plates

Prior to commencing the large scale siRNA screen, a number of test plates were analysed using the assay described above. RNF4 siRNA was transfected in 17 wells of a 96 well plate and NT siRNA in the remaining wells (**Figure 3.2.10, panel A**). Cells were treated with arsenic, fixed and stained before imaging and image analysis as previously described. The image analysis results were then interpreted by Amit Garg, data manager, without information as to which wells were transfected with RNF4 siRNA. All 17 wells were correctly identified using the measure PML body total area (**Figure 3.2.10, panel B**), and once again the PML body total area in RNF4 depleted cells was approximately twice that found in control cells.

At this stage, the high content screening assay had been tested on multiple occasions, all yielding similarly robust Z' factors calculated using the positive and negative controls. It was therefore decided to proceed with the siRNA screen, using the assay as described.

A

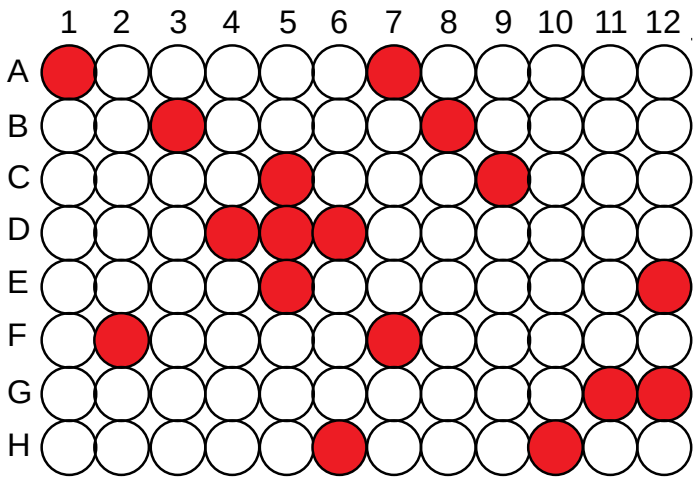

B

	1	2	3	4	5	6	7	8	9	10	11	12
A	14.721	8.661	7.942	8.741	8.018	8.32	16.412	8.726	8.808	8.384	8.718	9.341
B	9.364	9.117	16.843	8.382	8.126	7.802	7.649	16.167	8.401	8.484	8.391	8.974
C	9.443	8.525	8.633	7.66	16.056	7.638	7.689	7.698	16.192	7.741	8.573	9.444
D	9.297	8.389	8.078	16.29	15.272	16.077	8.43	7.869	8.245	7.892	8.056	9.068
E	8.844	8.344	8.026	7.758	16.475	7.724	8.02	7.293	7.639	8.061	9.053	17.375
F	8.968	15.728	8.318	8.235	8.199	7.296	16.268	7.859	7.511	8.419	8.731	9.514
G	9.704	8.733	8.452	7.746	7.376	6.808	7.712	8.145	7.788	8.243	17.158	16.982
H	10.158	8.834	8.777	8.987	8.603	15.842	8.361	8.232	7.977	16.956	9.169	9.67

Figure 3.2.10. Testing the high content screening assay

(A) RNF4 siRNA was transfected in 17 wells of a 96 well plate, highlighted in red. The remaining wells were transfected with NT siRNA.

(B) Cells transfected as in (A) were treated with 1μM arsenic 48 hours after transfection, and fixed with paraformaldehyde 24 hours later. Cells were then imaged and analysed using the automated assay. Data presented represent the mean total area of the nucleus occupied by PML bodies for all cells in the well. Approximately 4000 cells were analysed per well. Wells transfected with RNF4 siRNA are highlighted in orange.

3.2.8 Primary screen- ubiquitome siRNA library

The first siRNA library to be used in the screening assay was a library consisting of 1067 pools of 4 siRNAs targeting elements of the ubiquitin system, for example ubiquitin E1, E2 and E3 enzymes, deubiquitylases, RING domain containing proteins, SUMO E1, E2 and E3 enzymes and SUMO specific proteases (**Figure 3.2.11.**). This library is owned by SCILLS, and is distributed over 15 96-well plates.

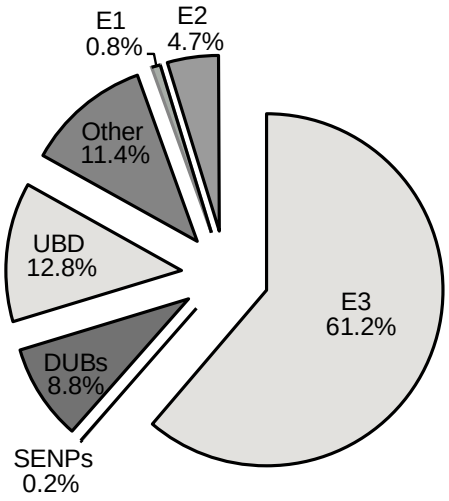

Figure 3.2.11. Composition of the ubiquitome siRNA library

The ubiquitome siRNA library is composed of siRNAs targeting proteins in the following categories: E1 enzymes, E2 enzymes, E3 enzymes, proteins with ubiquitin binding domains (UBD), deubiquitylating enzymes (DUBs) and SUMO specific proteases (SENPs). siRNAs targeting proteins not included in one of these categories are counted in 'Others'.

In order to identify siRNAs which influenced PML expression in the absence of arsenic, the screen was performed with and without arsenic treatment. Each assay plate contained both positive and negative siRNA controls (**Figure 3.2.12, panel A**) so the Z' factor could be calculated for each assay plate for quality control. These plate controls

also allowed normalisation of data so the results for all test siRNAs could be compared, despite the siRNAs being assayed in a number of different plates.

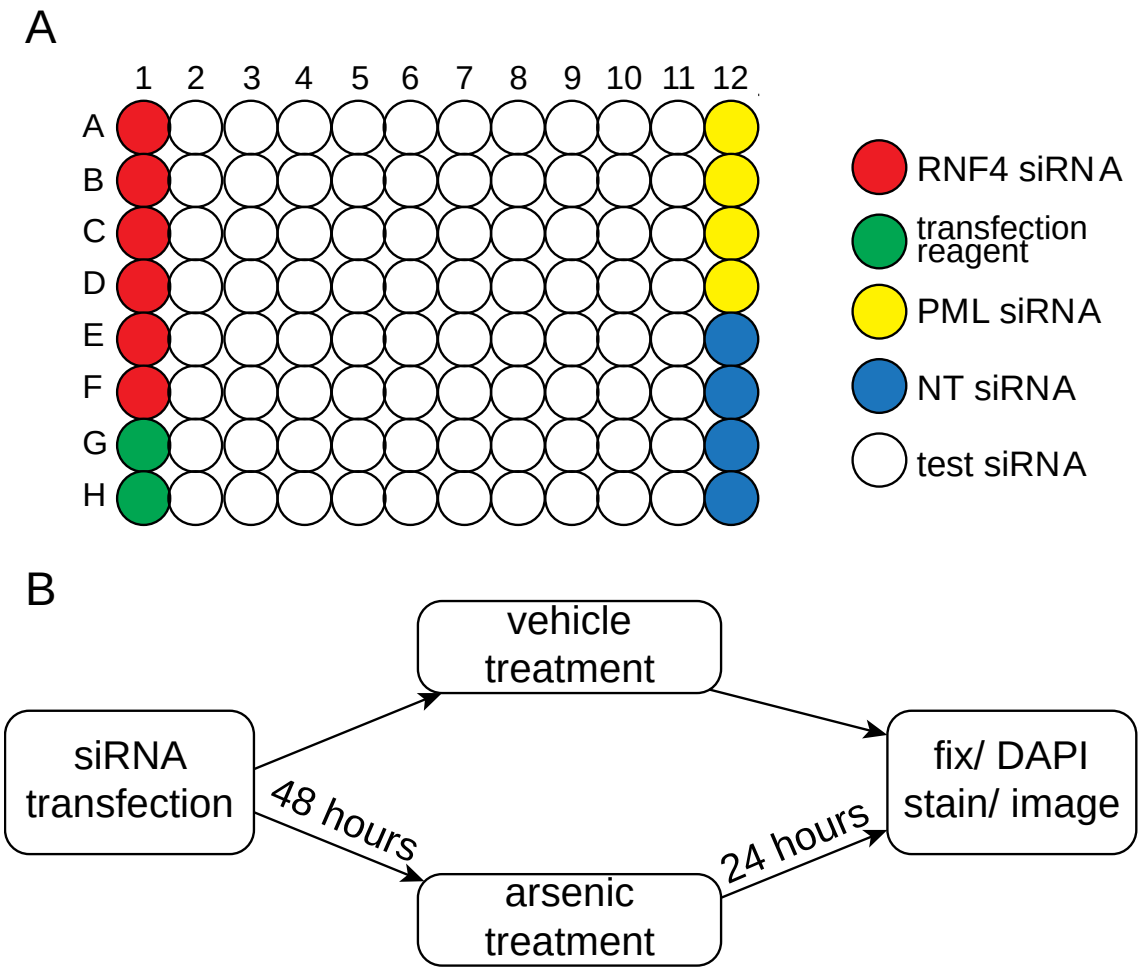

Figure 3.2.12. Plate layout and workflow for high content screening assay

(A) Each 96 well plate in the high content screen contains the following controls: RNF4 siRNA (red), PML siRNA (yellow), non targeting siRNA (blue) and a transfection reagent plus cells control (green). Test siRNAs fill the remaining wells.
(B) Schematic of workflow for high content screen.

Prior to commencing the screen, quality control experiments were performed using all liquid handling devices to be used for dispensing reagents and cells to ensure accuracy,

to minimise error introduced by inaccurate dispensing. These tests were all satisfactory. All plates were transfected with siRNA at the same time (**Figure 3.2.12, panel B**). 48 hours later, one set of 15 plates containing the siRNA library were treated with arsenic, and the other 15 plates were treated with vehicle solution at the same concentration. 24 hours later, cells were fixed and stained with DAPI, using robotics for liquid handling. The plates were then imaged using the automated microscope, and the resulting images analysed using the protocol described in section 3.2.7.1, to measure the PML body total area for each test siRNA.

3.2.8.1 Data analysis and quality control

The output data from the IN Cell investigator software was further analysed by Amit Garg, SCILLS data manager, using ActivityBase software. The Z' was calculated for each plate assayed to determine whether individual plates met quality control criteria (**Figure 3.2.13**). All plates in the arsenic treated dataset had Z' score of greater than 0.5 indicating they were suitable for further analysis. Six of the 15 plates in the vehicle treated dataset had Z' score of less than 0.5, but all were greater than 0.25 which was deemed acceptable (Birmingham et al., 2009). This is likely to be because RNF4 siRNA does not produce a particular phenotype in the absence of arsenic treatment (**Figure 3.2.6., 0hr time point**). All 30 plates were then analysed to identify potential hits.

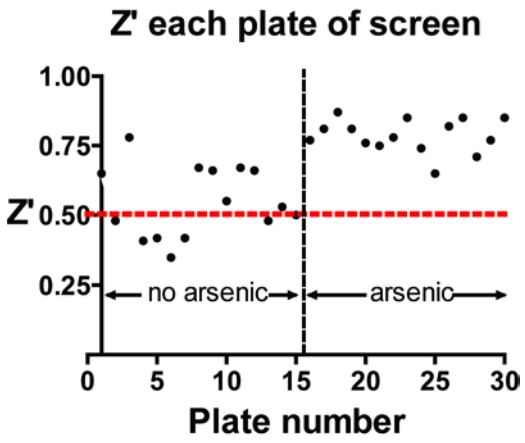

Figure 3.2.13. Quality control for primary ubiquitome library siRNA screen

The Z' factor was calculated for each plate in the siRNA screen using results from wells containing the negative control, non targeting siRNA and the positive control, RNF4 siRNA. Red line denotes optimal Z' threshold of 0.5.

YFP-PML fluorescence was analysed for each test siRNA, and the parameter used for hit identification was PML body total area. Potential hits were identified using two parameters: 'non target fold' and 'percent activity'. 'Non target fold' was calculated by dividing the PML body total area for a test siRNA by the result for NT siRNA control. 'Per cent activity' was derived by calculating the test siRNA PML body area as a percentage of that of the RNF4 positive control. Potential hits were selected as siRNAs with PML body total area greater than 2 standard deviations above or below the 'non target fold' or 'per cent activity' average. This resulted in four lists of putative hits; siRNAs which decreased PML expression in the absence of arsenic, siRNAs which increased PML expression in the absence of arsenic, siRNAs which decreased PML expression in response to arsenic and siRNAs which increased PML expression in response to arsenic.

3.2.8.2 Results

Tables II and III list the putative hits identified in the non- drug treated dataset, including the ‘non target fold’ value for each. In order to score as a hit in this dataset, the siRNA ‘non target fold’ was either less than 0.6 or greater than 1.32. The siRNAs included in the list with ‘non target fold’ values outside these limits were scored as hits because the ‘percent activity’ was outwith 2 standard deviations of the mean.

The arsenic treated dataset yielded the following list of potential hits (**Tables IV and V**). In order to score as a hit in this dataset, the ‘non target fold’ was less than 0.5 or greater than 1.175. ‘Percent activity’ thresholds for this dataset were 8.18 and 48.86% of RNF4 activity.

Table II. Ubiquitome screen: putative hits in non drug treated dataset which increase PML expression

Gene Symbol	Fold change compared to NT siRNA control
CUL3	2.40
BAZ1B	1.81
TRIM7	1.80
VPS11	1.61
DCUN1D1	1.55
NICE-4	1.52
COPS6	1.50
LZTR1	1.48
TRAF2	1.39
MARK1	1.34
UEVLD	1.33
BRPF3	1.32
CHD4	1.21
UCHL3	1.43
SHARPIN	1.38
USP15	1.40
UBQLN2	1.39
FBXO34	1.38
UFD1L	1.35
UBASH3A	1.35
USP18	1.34
TRIM60	1.33
TRIM62	1.33
FBXL19	1.33
RBX1	1.26
LOC643904	1.23
KRTAP5-9	1.20
PDZRN3	1.17
PHF11	1.15
BAHD1	1.15
PHF13	1.15
BRPF1	1.14
AIRE	1.13
BRCA1	1.11
CNOT4	1.11
EEA1	1.09
ANAPC11	1.09
MARCH-IX	1.09
LPXN	1.09
WDR71	1.08
C6ORF49	1.07
IBRDC2	1.07

Table III. Ubiquitome screen: putative hits in non drug treated dataset which decrease PML expression

Gene Symbol	Fold change compared to NT siRNA control
PML	0.24
RBBP6	0.34
SOCS2	0.38
LOC200933	0.41
DDB1	0.42
FBXL3A	0.45
PCF11	0.45
KIAA1536	0.47
DNAJB2	0.47
RYBP	0.47
TRIM33	0.49
FBXO43	0.49
CBLL1	0.50
SPOP	0.50
MGC10198	0.53
LOC124402	0.59
REV1L	0.60
TRIM48	0.60
FBXW12	0.48
RAB40C	0.50
FBXW7	0.52
FBXW2	0.54
SHFM3	0.54
KIAA0644	0.57
LMX1B	0.57
KLHL15	0.64
KIAA0363	0.65

Table IV. Ubiquitome screen: putative hits in arsenic treated dataset which increase PML expression

Gene Symbol	Fold change compared to NT siRNA control
RNF4	1.69
CHD4	1.59
BAZ1B	1.55
FBXO44	1.52
UBE4B	1.51
LOC644006	1.46
VPS11	1.42
ZNF364	1.40
LZTR1	1.29
MYO6	1.23
STAM	1.19
EPN3	1.09
UBE2V2	1.29
UEVLD	1.28
RNF165	1.26
NPL4	1.26
LPXN	1.24
SENP1	1.23
TOPORS	1.23
KCTD15	1.22
LNX2	1.19
UFD1L	1.19
LMX1B	1.18
LRRC29	1.26
KIAA0804	1.23
INTS12	1.22
LOC200933	1.19
TRIM45	1.19
40245	1.18
ANAPC2	1.17
DKFZP761G2113	1.16
USP37	1.13
KIAA1536	1.13
EIF2AK4	1.09
EPN2	1.08
CDC27	1.04
DMRT3	1.03

Table V. Ubiquitome screen: putative hits in arsenic treated dataset which decrease PML expression

Gene Symbol	Fold change compared to NT siRNA control
CNOT4	0.04
RNF6	0.05
FSD1L	0.10
DTX3L	0.11
PML	0.37
CXXC1	0.49
RBX1	0.49
UBE1	0.50
PCF11	0.46
OTUD5	0.58
IBRDC3	0.08
EDD1	0.37
TRIP12	0.44
RAB40C	0.45
DDB1	0.46
RBBP6	0.46
HUWE1	0.46
SMURF1	0.48
RYBP	0.50
BRE	0.50
USP20	0.53

3.2.8.3 Hits selected for further follow up

The raw images for each of the putative hits listed in tables **Tables II, III, IV and V** were examined to assess the YFP-PML fluorescence. In each case, the data analysis results corresponded to the phenotype seen in the images.

The top hits, that is those producing the most pronounced phenotypes for each dataset, were selected for further analysis in the deconvolution screen. There was some crossover between the hits identified in the vehicle and arsenic treated datasets (**Tables VI and VII**).

Table VI. Ubiquitome screen follow up: putative hits in non drug treated dataset selected for further investigation in deconvolution screen

Gene Symbol	Fold change compared to NT siRNA control
CUL3	2.40
BAZ1B	1.81
TRIM7	1.80
VPS11	1.61
DCUN1D1	1.55
PML	0.24
RBBP6	0.34
SOCS2	0.38

Table VII. Ubiquitome screen follow up: putative hits in arsenic treated dataset selected for further investigation in deconvolution screen

Gene Symbol	Fold change compared to NT siRNA control
RNF4	1.69
CHD4	1.59
BAZ1B	1.55
FBXO44	1.52
UBE4B	1.51
LOC644006	1.46
VPS11	1.42
ZNF364	1.40
LZTR1	1.29
STAM	1.19
EPN3	1.09
UBE2V2	1.29
UEVLD	1.28
RNF165	1.26
TOPORS	1.23
CNOT4	0.04
RNF6	0.05
FSD1L	0.10
DTX3L	0.11
PML	0.37
CXXC1	0.49
OTUD5	0.58
IBRDC3	0.08
USP20	0.53

3.2.9 Deconvolution screen- ubiquitome siRNA library

The aim of the deconvolution screen was to identify siRNAs which give a true phenotype and to exclude those which produce a phenotype through an off target effect. In order to do this, four individual siRNAs for each target gene were assayed. When two or more of these duplexes produced the same phenotype, a true hit was identified, whereas if only one of the four produced a phenotype, this gene target was rejected as an off target effect of that individual siRNA.

For each of the putative hits identified listed in tables VI and VII, the four individual siRNA duplexes making up the pool of siRNA tested in the primary screen were ordered. A screen was then performed in exactly the same way as described in section 3.2.4 using these 96 siRNA duplexes targeting 24 individual genes, distributed in two 96 well plates. Positive and negative controls were included in each plate. Once again, duplicate plates were treated with either arsenic or vehicle, and imaged and analysed using the automated microscopy system.

The deconvolution experiments for CUL3 and DCUN1D1 were performed in the non-automated assay described in section 3.2.6, because siRNA duplexes were available in the lab, and were therefore not ordered in 96 well plate format.

3.2.9.1 Data analysis and quality control

Amit Garg, SCILLS data manager performed initial data analysis using ActivityBase software. The Z' was calculated for each of the four plates assayed using the RNF4 and NT siRNA controls **(Figure 3.14)**, and for the arsenic treated plates, Z' were highly satisfactory at 0.8, indicating the data were suitable for further analysis. The Z' in the vehicle treated plates were once again lower, but deemed to be acceptable as they were greater than 0 in both cases.

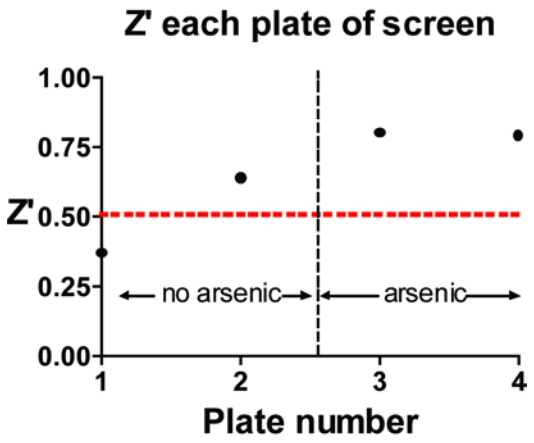

Figure 3.2.14. Quality control for deconvolution ubiquitome siRNA screen

The Z' factor was calculated for each plate in the siRNA screen using results from wells containing the negative control, non targeting siRNA and the positive control, RNF4 siRNA. Red line denotes optimal Z' threshold of 0.5.

3.2.9.2 Results

As mentioned previously, the purpose of this experiment was to investigate whether phenotypes identified in the primary siRNA screen were off target effects of the pools of siRNA tested. Once again, the data were allocated into four datasets: siRNAs which increased PML expression in the presence of arsenic, those which decreased PML expression in the presence of arsenic, those which increased PML expression in the absence of drug and those which decrease expression in the absence of drug. Twelve target genes were validated as potential regulators of PML in the presence of arsenic; nine raising PML expression (**Table VIII**) and three decreasing expression (**Table IX**). At least two oligosiRNAs targeting each of these genes reproduced the phenotype identified in the primary screen. All four oligosiRNAs targeting CUL3 and DCUN1D1 caused marked accumulation of PML in the absence of arsenic treatment (**Table X**), but no other targets were validated in this dataset. siRNAs targeting two of the genes identified to decrease PML expression in the presence of arsenic were also

validated to decrease PML expression in the absence of arsenic (**Table XI**). For the remaining target genes examined, only one siRNA recreated the phenotype identified in the primary screen and were therefore excluded from further follow up.

Table VIII. Deconvolution screen: siRNAs confirmed to increase PML expression following arsenic treatment

Gene Symbol	Fold change compared to NT siRNA control			
	Oligo 1	Oligo 2	Oligo 3	Oligo 4
UEVLD	1.79	0.96	0.72	1.23
FBXO44	1.36	0.79	1.07	1.52
BAZ1B	0.96	1.14	1.80	1.05
CHD4	0.91	1.45	1.04	2.01
LOC644006	1.35	1.24	1.13	0.97
TOPORS	1.18	0.83	1.25	1.32
UBE4B	1.24	1.47	1.57	1.19
VPS11	0.72	0.87	1.57	1.47
EPN3	0.73	0.87	1.16	1.17

Table IX. Deconvolution screen: siRNAs confirmed to decrease PML expression following arsenic treatment

Gene Symbol	Fold change compared to NT siRNA control			
	Oligo 1	Oligo 2	Oligo 3	Oligo 4
CXXC1	0.70	0.36	0.49	0.57
RBBP6	0.34	0.39	0.34	0.42
OTUD5	0.27	0.49	0.52	0.41

Table X. Deconvolution screen: siRNAs confirmed to decrease PML expression in the absence of arsenic

Gene Symbol	Fold change compared to NT siRNA control			
	Oligo 1	Oligo 2	Oligo 3	Oligo 4
CXXC1	0.77	0.41	0.54	0.49
RBBP6	0.35	0.41	0.19	0.41

Table XI. Deconvolution screen: siRNAs confirmed to increase PML expression in the absence of arsenic

Gene Symbol	Fold change compared to NT siRNA control			
	Oligo 1	Oligo 2	Oligo 3	Oligo 4
CUL3	8.11	5.16	4.89	5.65
DCUN1D1	5.11	2.94	1.75	2.54

3.2.9.3 Hits selected for further follow up

The next step was to decide which of the validated gene targets to follow up with further experiments to attempt to characterise the role of the gene product in the regulation of PML. The phenotype induced by siRNAs targeting CUL3 and DCUN1D1 were particularly striking and therefore they were selected for further investigation, detailed in Chapter 4.

3.2.10 Primary screen- kinome siRNA library

There is evidence to suggest that phosphorylation of PML influences its stability (Gresko et al., 2008), and that PML is phosphorylated in response to arsenic treatment (Hayakawa and Privalsky, 2004). The screening assay was therefore repeated using a library of siRNAs targeting kinases, a subset of the Drug Discovery Unit whole genome siRNA library, to identify kinases involved in the process of arsenic mediated degradation of PML. This screen consisted of 12 assay plates which were tested with and without arsenic treatment using the same plate layout and controls as described in section 3.2.7.

3.2.10.1 Data analysis and quality control

Data were analysed by Amit Garg using ActivityBase software. The Z' for each assay plate was calculated using RNF4 and NT siRNA controls. The Z' for the arsenic treated datasets were highly satisfactory with all scoring approximately 0.7 (**Figure 3.2.15**). The Z' for the non- drug treated dataset were lower, with values ranging from 0.2 to 0.7. Hits were identified using the parameters of 'non target fold' and 'percent activity' as in the primary screen, and siRNAs giving a PML body total area of greater or less than two standard deviations from the mean for either or both of these parameters were determined to be hits.

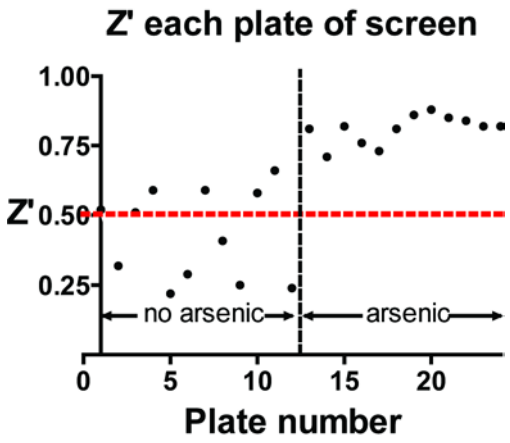

Figure 3.2.15. Quality control for primary kinome library siRNA screen

The Z' factor was calculated for each plate in the siRNA screen using results from wells containing the negative control, non targeting siRNA and the positive control, RNF4 siRNA. Red line denotes optimal Z' threshold of 0.5.

3.2.10.2 Results

Data were grouped into hits in the presence (**Table XIII**) or absence (**Table XII**) of arsenic treatment. Three siRNAs were hits in both datasets, NLK, PMVK and MGC26597, though the latter is a pseudogene.

The lists of hits were reviewed and links with PML sought from the literature. There were no clear links with PML, and therefore follow up experiments were concentrated on hits generated from the ubiquitome siRNA screen.

Table XII. Kinome screen: putative hits from non drug treated dataset

Gene Symbol	Fold change compared to NT siRNA control
CDK5RAP1	0.32
MGC26597	0.40
SGKL	0.40
TTBK1	0.44
CDK9	1.40
PCK1	1.57
EPHA6	1.66
GFRA2	1.66
PMVK	1.69
BLNK	1.73
MAP4K5	1.78
CAMKK2	1.85
APEG1	2.04
NLK	2.04
AKAP3	2.40

Table XIII. Kinome screen: putative hits from arsenic treated dataset

Gene Symbol	Fold change compared to NT siRNA control
MGC26597	0.24
AGTR2	0.26
PANK4	0.31
AKT2	0.31
ITPKA	0.38
CKB	1.26
CLK1	1.27
NRBP2	1.28
MAP3K1	1.29
MYLK	1.32
PIP5K2B	1.32
FGFR4	1.32
TAO1	1.34
CHKB	1.36
CALM3	1.37
AMHR2	1.39
PIK3CA	1.39
NLK	1.47
STK23	1.54
MAP2K7	1.56
PMVK	1.59

3.2.11 Conclusions

The aim of this project was to investigate the mechanism of arsenic induced degradation of PML using a high content siRNA screen. Initial experiments characterised the various reagents required. A new, chicken anti-PML antibody was demonstrated to identify endogenous PML by both western blotting and immunofluorescence. The kinetics of arsenic mediated degradation of PML were then assessed and demonstrated to be near complete after 24 hours of arsenic treatment. siRNA mediated depletion of RNF4 prior to arsenic treatment prevented PML degradation, which resulted in accumulation of PML within PML-NBs demonstrated by immunofluorescence. This suggested other siRNAs which influence the pathway of

arsenic induced degradation of PML may be identified by monitoring PML-NBs by immunofluorescence.

An assay suitable for high content siRNA screening was then developed, using RNF4 siRNA as a positive control. A YFP linked version of PML stably expressed in HeLa cells was demonstrated to degrade in an RNF4 dependent manner as for endogenous PML. These cells were selected for use in the siRNA screen as two step antibody staining of endogenous PML was not then required. Quantitation of YFP fluorescence was performed following transfection with RNF4 siRNA and arsenic treatment and PML body total area was noted as the measure which best discriminated between control cells and those depleted of RNF4.

A high content siRNA screen was then performed, using the YFP PML HeLa cell line and a library of 1067 pools of siRNA targeting components of the ubiquitin system. The screen was performed with and without arsenic treatment. Cells were transfected with siRNA and 48 hours later treated with arsenic or vehicle for 24 hours before fixation. Cells were imaged using an automated microscope and YFP PML fluorescence quantified using a protocol developed to quantify the size of PML-NBs. Data was then analysed and a number of potential hits identified. Putative hits were further validated in a deconvolution screen in which 4 individual siRNAs targeting each putative hit were assayed. A number of hits were validated in this way. The most striking phenotypes were noted in the absence of arsenic treatment when CUL3 and DCUN1D1 were depleted. Further follow up experiments are discussed in the chapter which follows.

3.3 Discussion

3.3.1 Rationale for use of a high content screen

Despite the widespread clinical use of arsenic trioxide in the treatment of acute promyelocytic leukaemia, the mechanism of its action has only recently been elucidated, and unanswered questions remain. Arsenic treatment induces proteasomal degradation of PML and PML-RARα (Lallemand-Breitenbach et al., 2008; Lallemand-Breitenbach et al., 2001; Tatham et al., 2008). Shortly after arsenic treatment, PML is recruited to PML-NBs, where it is SUMO modified. This SUMO modification recruits the SUMO targeted ubiquitin E3 ligase, RNF4 to PML-NBs (Geoffroy et al., 2010). RNF4 ubiquitylates SUMO modified PML targeting it for degradation by the 26S proteasome (Lallemand-Breitenbach et al., 2008; Tatham et al., 2008). A number of questions remain regarding this process: what is the SUMO E3 ligase responsible for SUMO modification of PML?; do SUMO specific proteases modify the process of arsenic induced sumoylation of PML and if so which ones?; which deubiquitylating enzymes counteract the actions of RNF4?; are there other ubiquitin mediated regulators of PML? This project set out to investigate this process using siRNA screening to identify components of the ubiquitin system that influence the process of arsenic mediated degradation of PML.

High content screening refers to the use of automated microscopy to capture images of intact cells as the read out of a high throughput assay (Giuliano et al., 1997). Assays may use live or fixed cells, and often capture images of multiple fluorescently labelled cellular structures or proteins. The advantage of using such an assay is that various parameters can be quantitavely assessed to define the effect of a given treatment. For example, the intensity, distribution and size of regions of fluorescent signal can be assayed. The morphology of cells can also be evaluated, which may allow

identification of drugs or siRNAs which have particularly toxic effects. Thus, a huge amount of data can be gleaned from a single assay. Advances in the quality of automated microscopy equipment have allowed interrogation of various cellular processes using this technology. High content screening can be used for drug discovery, for example previous screens have identified compounds with efficacy against the tropical disease Leishmaniasis (Siqueira-Neto et al., 2012), and compounds which induce mitotic arrest (Wilson et al., 2006). The use of siRNA coupled with high content screening allows examination of loss of function phenotypes on a genome wide scale, which can help define key proteins in cellular processes (Adamson et al., 2012; Lipinski et al., 2010; Orvedahl et al., 2011).

Arsenic induced degradation of PML can be monitored using fluorescence microscopy (**Figures 3.2.4., 3.2.6**). Disruption of this pathway induced by depletion of RNF4 results in a striking phenotype, with accumulation of PML in PML-NBs (**Figures 3.2.4., 3.2.6.**) (Geoffroy et al., 2010; Lallemand-Breitenbach et al., 2008; Tatham et al., 2008). This suggested that it may be possible to identify other gene products involved in this process by monitoring the appearance of PML-NBs after siRNA mediated gene knockdown and arsenic treatment. A cell line expressing a YFP linked version of PML isoform III was characterised. Experiments confirmed YFP PML degraded in an RNF4 dependent manner in response to arsenic, recapitulating the phenotype identified for endogenous PML. This cell line was selected for use in further experiments because YFP PML fluorescence could be directly visualised, thus removing the need for two step antibody labelling of PML. The difference in whole cell YFP fluorescence was not significantly altered in cells depleted of RNF4 following arsenic treatment compared to control cells (**Figure 3.2.7., panel A**) Measuring whole cell fluorescence using a plate reader was therefore unlikely to be sensitive enough to detect small changes in whole cell PML fluorescence induced by blocking arsenic mediated degradation of PML in

this way. High content siRNA screening was therefore an attractive option to investigate the role of a large number of gene products in the process of arsenic mediated degradation of PML, because the size, number and location of PML-NBs could be monitored allowing identification of siRNAs which perturbed the process of PML degradation.

3.3.2 Appraisal of the screening assay

The aim of this assay was to identify gene products which influenced PML degradation in response to arsenic treatment. To assess whether gene products were associated with changes in PML-NB stability exclusively in the presence of arsenic treatment, the assay was also performed without arsenic. The majority of assay development was performed using arsenic treated cells, and in particular, the positive control siRNA RNF4 only produces a pronounced PML phenotype in cells treated with arsenic (**Figure 3.2.6.**) The Z' quality control measure was calculated for all plates using the positive (RNF4) and negative (non targeting) siRNA controls. Because there was not a significant difference between the positive and negative controls in the absence of arsenic, plates assayed in the absence of arsenic had lower Z' scores (**Figures 3.2.12., 3.2.13. and 3.2.14.**). The Z' of arsenic treated plates was consistently very good at approximately 0.75, indicating the assay was robust. RNF4 siRNA was included within the siRNA library and was identified as the top hit in the arsenic treated data set (**Table IV**). This confirmed the ability of the assay to robustly identify the phenotype of PML-NB accumulation of PML following arsenic treatment induced by RNF4 depletion. To increase confidence in the assay in the absence of arsenic, the screen could be repeated using CUL3 siRNA as the positive control, which was identified to induce marked accumulation of PML in the absence of arsenic (discussed in detail in Chapter 4 of this thesis).

PIAS1, the SUMO E3 ligase reported to be required for arsenic induced degradation of PML (Rabellino et al., 2012) was not identified as a hit in this screen. If one assumes PIAS1 is indeed the ligase required, there are a number of technical reasons why this may not have been identified. These reasons also apply to the reporting of other potential false negatives. siRNA transfection efficiency may not have been optimal in the well containing the pool of siRNAs targeting PIAS1. The quality control plates performed at the beginning and end of the screen have positive control siRNA transfected in each well of the 96 well plate. By assaying these, any well specific transfection problems, for example due to a blocked pipette tip on the liquid handling device, should have been identified. This does not however exclude a problem with transfection in a single well. This could be investigated by performing further replicates of the primary siRNA screen to increase confidence in the hits identified and to confirm siRNAs which do not produce a phenotype. This assay was performed at one time point only, with the end point of the assay 72 hours after siRNA transfection. The efficiency of siRNA mediated knockdown at a protein level depends on the half life of the protein translated from the targeted mRNA. Therefore, if the half life of the targeted protein is longer than 72 hours, the effects of siRNA mediated knockdown are unlikely to be identified as a hit by this assay. This could be avoided by performing the screen at different time points. Where multiple proteins contribute to a cellular process, redundancy between these proteins may mean that siRNA mediated depletion of a single factor does not cause a phenotype sufficient for hit identification in the screening assay. Finally, the screen was performed using a cell line expressing YFP linked PML isoform III in HeLa cells which also express endogenous PML (Geoffroy et al., 2010). It is possible that PML isoform III specific effects may be identified using this cell line, though interactions between YFP PML III and endogenous PML may preclude this. The screen could be repeated using the cell lines employed in Chapter 5 of this thesis, which

express only a single PML isoform (Cuchet et al., 2011) to identify isoform specific phenotypes. Alternatively immunofluorescence labelling of endogenous PML could be employed to assess the effects of siRNA knockdown on the degradation of endogenous protein.

3.3.3 Other applications of the HCS assay

Yip and colleagues developed a high content screen to identify compounds which induced formation of PML-NBs, using a measure of the number of PML-NBs present within the cell nucleus as the read out, and interferon stimulation as a positive control (Yip et al., 2011). The assay described in this thesis could be used to identify compounds which induce degradation of PML-NBs, using arsenic as a positive control. Compounds identified by such a screen may be clinically useful in patients with APL for whom arsenic treatment is contraindicated. Compounds identified in this way would not necessarily act via the same mechanism as arsenic, and therefore may be useful in the treatment of patients whose disease has become refractory to arsenic therapy. It would also be possible to identify compounds which induce PML accumulation in PML-NBs using this assay. Though such compounds would not be useful in the treatment of APL, they be useful in other cancers in which PML expression is lost, as the loss of PML is associated with increased tumour invasion (Gurrieri et al., 2004). Compounds which increase PML expression may therefore help to rescue this phenotype, and be useful as anti- cancer treatments.

3.3.4 Selection of hits for further follow up

The first step after the screen had been performed and data analysed was to decide which putative hits to follow up in the deconvolution screen. In the main, these were siRNAs which had induced the most pronounced phenotypes either in the presence

or absence of arsenic treatment. There were some siRNAs which scored as hits in both datasets, suggesting that the gene product targeted exerted effects on PML independent of arsenic treatment.

Hits were validated in the deconvolution screen when 2 of more siRNAs with distinct sequences targeting the same gene induced the same PML phenotype. This was the case for 14 target gene products (**Tables VIII, IX, X, and XI**), the vast majority of which were not previously reported to influence PML stability or the process of arsenic mediated degradation of PML. Of the gene products noted to impair arsenic mediated degradation of PML, LOC644006 is an RNF4 pseudogene. The sequence of LOC644006 and RNF4 are very similar, and it is therefore likely that siRNAs designed to target the sequence of LOC644006 also targeted RNF4 mRNA for degradation. Western blotting analysis of cell extracts transfected with the pool of siRNAs targeting LOC644006 confirmed reduced RNF4 expression (data not shown), and thus explain the phenotype detected in the screen.

3.3.4.1 CHD4 and BAZ1B

Depletion of the transcription factors CHD4 and BAZ1B was noted to impair arsenic mediated degradation of PML (**Table VIII**). Both are implicated in disease processes. A proportion of patients with dermatomyositis have autoantibodies to CHD4 (Seelig et al., 1995), and BAZ1B (also known as WSTF) is commonly deleted in patients with William's syndrome (Lu et al., 1998). CHD4 is part of a large multi-protein complex which has both chromatin remodelling effects and histone deacetylase function, and maintains gene repression. BAZ1B is a member of three chromatin remodelling complexes, which have diverse roles in transcriptional control of a number of processes. Cells derived from BAZ1B deficient mice were obtained (Yoshimura et al., 2009), however unfortunately the chicken anti PML antibody was not reactive to

endogenous PML in these cells, precluding further investigations. The mechanism of how these transcription factors and related complexes may regulate arsenic mediated degradation of PML is not immediately clear. The phenotype identified in the screen may be due to a direct effect on PML expression, or via regulation of one or more intermediates. Initial steps in follow up for these siRNA phenotypes would include the use of RT qPCR to assess the effects of depletion of CHD4 or BAZ1B on PML expression. It would also be useful to quantify expression of other known components of the pathway of arsenic mediated degradation of PML, for example RNF4.

3.3.4.2 UBE4B

The ubiquitin fusion degradation (UFD) pathway is a ubiquitin mediated proteolytic pathway first identified in yeast. The yeast homologue of UBE4B, UFD2 was identified in a screen searching for mutations which impaired degradation of a ubiquitin- glutathione S-transferase (ubi-GST) fusion (Johnson et al., 1995). UFD2 is a RING domain containing protein which functions as a so called ubiquitin E4 enzyme. UFD2 is not required for the initiation of ubiquitylation of ubi-GST, but its addition greatly enhances the formation of polyubiquitin chains (Koegl et al., 1999). It has been further demonstrated that UFD2 functions in a pathway which escorts ubiquitylated proteins to the proteasome for degradation (Richly et al., 2005). p97 (CDC48 in yeast) is a member of the AAA ATPase family which has been demonstrated to have roles in multiple cellular processes including the degradation of misfolded proteins, autophagosome maturation (Ju et al., 2009; Tresse et al., 2010), and membrane transport (Ye et al., 2001). p97/ CDC48 exerts functions to remodel ubiquitylated substrate proteins to facilitate downstream events, and binds to UFD2 and recruits oligoubiquitylated substrates for further ubiquitylation by UFD2 (Richly et al., 2005).

The E4 activity of UBE4B has been demonstrated to enhance MDM2 mediated ubiquitylation and degradation of p53 (Wu and Leng, 2011; Wu et al., 2011).

Depletion of UBE4B in the siRNA screen impaired degradation of PML in response to arsenic treatment. This is consistent with a model in which UBE4B mediated ubiquitylation of PML following arsenic treatment enhances proteasomal degradation of PML via a CDC48 mediated pathway. Thus, depletion of UBE4B would impair PML ubiquitylation and degradation, leading to the phenotype identified in the screen. This may be an additional mechanism by which PML is degraded in response to arsenic treatment. A specific inhibitor of p97 ATPase activity, DBeQ, has recently been reported (Chou et al., 2011). Preliminary experiments performed using this compound demonstrated accumulation of PML after treatment with DBeQ suggesting PML may be a substrate of a p97 mediated degradative pathway (data not shown). Attempts to use this compound to investigate the role of p97 in arsenic mediated degradation of PML were limited by toxicity of the combination of DBeQ and arsenic trioxide treatments. An alternative approach to investigate this process would be to use an in vitro system to investigate whether PML is a substrate of UBE4B/ p97. It would be interesting to investigate whether any ubiquitylation activity of UBE4B/ p97 toward PML was dependent on SUMO modification of PML, as is true for RNF4 (Lallemand-Breitenbach et al., 2008; Tatham et al., 2008).

3.3.4.3 OTUD5

OTUD5 (also known as DUBA) is a member of the ovarian tumour domain class of deubiquitylase enzymes. OTUD5 activity is regulated by phosphorylation, and phosphorylated OTUD5 undergoes marked structural changes on ubiquitin binding (Huang et al., 2012). OTUD5 was previously identified as a negative regulator of the innate immune system (Kayagaki et al., 2007), where it suppresses type 1 interferon

production. Depletion of OTUD5 was noted to enhance arsenic mediated degradation of PML (**Table IX**). If PML were a substrate of the deubiquitylating activity of OTUD5, it would be anticipated that depletion of OTUD5 would lead to enhanced PML degradation, as was observed in the screen. Some preliminary follow up experiments were performed to test this hypothesis. It was noted however that depletion of OTUD5 resulted in accumulation of RNF4 (data not shown). This increase in RNF4 expression is likely to account for the phenotype identified in the screen. The mechanism by which OTUD5 depletion results in increased RNF4 expression is unclear, but cannot be explained by an increase in Lys48 linked ubiquitin chains attached to RNF4. It is possible that OTUD5 depletion leads to destabilisation of an intermediate which in turn leads to stabilisation of RNF4. OTUD5 was previously reported to have specificity for Lys63 linked ubiquitin chains (Kayagaki et al., 2007). Therefore OTUD5 depletion may lead to accumulation of ubiquitin chains of different linkage type attached to RNF4 or an intermediate which in turn stabilises the protein.

3.3.4.4 CUL3 and DCUN1D1

CUL3 depletion resulted in marked accumulation of PML in the primary screen. This phenotype was confirmed in the deconvolution screen (**Table XI**). DCUN1D1, a NEDD8 E3 ligase responsible for activation of cullin RING ligase complexes was also identified as a hit in the siRNA screen. Both phenotypes were identified in the absence of arsenic treatment, however accumulation was so striking that it was decided to follow up these hits further. This will be discussed in detail in chapter 4 of this thesis.

4 A CUL3 ubiquitin ligase complex regulates PML

4.1 Introduction

4.1.1 Cullin RING ligases

The cullin family of proteins, which in humans consists of six members, form the scaffold of multi subunit ubiquitin E3 ligase complexes called cullin RING ligases (CRL). The CRL complexes formed by different cullin proteins, denoted CUL1, 2, 3, 4a, 4b, and 5, contain the cullin protein as a central scaffold which binds a RING domain containing protein, RBX1 or RBX2, at the C terminus and a substrate adaptor protein at the N terminus (Zheng et al., 2002). The RING domain of RBX1 or 2 recruits ubiquitin charged E2 enzyme to the complex, and promotes ubiquitin transfer to the substrate. CRL complexes regulate a variety of cellular processes, by targeting substrate proteins for ubiquitylation and subsequent proteasomal degradation (Petroski and Deshaies, 2005).

Each cullin protein binds a distinct substrate adaptor protein which in turn binds substrate receptor proteins which confer substrate specificity to the complexes (Petroski and Deshaies, 2005; Zimmerman et al., 2010). CUL1 binds to the adaptor protein SKP1 which in turn binds to various F- box protein substrate receptors responsible for recruiting substrate (Bai et al., 1996). CUL2 binds the adaptor protein Elongin C, which in turn binds suppressor of cytokine signalling/ elongin- BC (SOCS/BC) box substrate receptor proteins (Kamura et al., 1998). CUL3 binds proteins which confer both CUL3 substrate adaptor and receptor function in a single polypeptide (Geyer et al., 2003; Pintard et al., 2003). These proteins consist of an N terminal Bric a brac, Tramtrack, Broad complex (BTB) domain, and recruit substrate via another protein- protein interaction domain at the C terminus (**Figure 4.1.1.**) (Stogios et al., 2005).

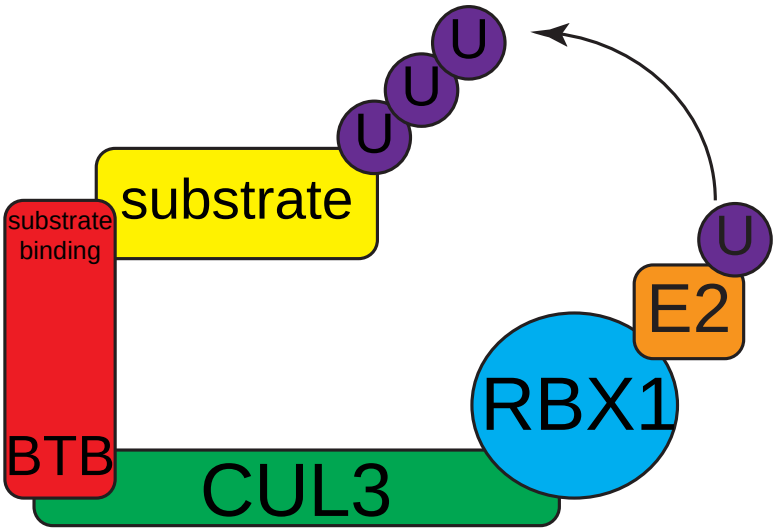

Figure 4.1.1. Schematic of a CUL3-BTB protein complex

CUL3 RING ligase complexes consist of a CUL3 scaffold which binds to the RING domain protein RBX1 at the c terminus. RBX1 binds the ubiquitin charged E2 enzyme. Substrates are bound via a BTB domain containing adaptor protein which binds the N terminus of CUL3 via an N terminal BTB domain, and substrate via a second protein interaction motif at the C terminus.

BTB domain containing proteins may dimerise via the BTB domain, and can therefore induce dimerization of CUL3 RING ligase complexes (Zhuang et al., 2009). There are approximately 350 BTB domain containing proteins in humans, though only around two thirds of these encode an additional protein- protein interaction domain. This suggests not all BTB proteins function as CUL3 adaptor proteins (Perez-Torrado et al., 2006).

4.1.2 NEDD8 mediated regulation of CRL ubiquitin ligase activity

The ubiquitin like protein NEDD8 is covalently linked to cullin proteins via an enzymatic cascade analogous to that of ubiquitin conjugation, termed neddylation (Gong and Yeh, 1999; Liakopoulos et al., 1998; Osaka et al., 1998). NEDD8 is first activated by a single E1 enzyme, NAE, which transfers NEDD8 to the catalytic cysteine residue of one of two E2 enzymes, UBE2M (UBC12) and UBE2F. These E2 enzymes

catalyse neddylation of specific cullins; UBE2M catalyses neddylation of CUL1-4 and UBE2F neddylation of CUL5. These E2 enzymes work with separate E3 ligases; UBE2M with RBX1, and UBE2F with RBX2, to catalyse transfer of NEDD8 from the E2 to a conserved lysine residue in the C terminus of the target cullin (Huang et al., 2009).

Neddylation of cullins stimulates CRL ubiquitylation activity. Insight into the mechanism by which cullin neddylation brings about this enhanced ubiquitylation activity has been gained by examining the structure of both unmodified and NEDD8 modified cullin-RBX complexes (Duda et al., 2008). In CRL complexes not modified by NEDD8, the cullin adopts a closed conformation, and the RING domain of RBX1 is in contact with the cullin C terminal domain. NEDD8 modification of the acceptor lysine residue in the cullin C terminus results in marked structural changes, with the RBX1 RING domain released from interactions with the cullin into an open conformation. The RBX1 RING domain can then rotate into multiple different orientations (Duda et al., 2008). This open conformation enhances cullin ubiquitylation activity through increased recruitment of ubiquitin loaded E2, by improving ubiquitin transfer from the E2 active site and by bringing E2 and substrate into proximity (Saha and Deshaies, 2008).

The process of cullin neddylation is inhibited by the protein CAND1, which binds to unmodified cullin-RBX1 complexes. The C terminal region of CAND1 binds to the cullin adaptor protein binding site preventing assembly of the CRL complex. The N terminal region of CAND1 binds to the RBX1 RING cullin interface that is present only when the cullin RBX1 complex is in the closed conformation. This locks the cullin in the closed conformation and obscures the NEDD8 acceptor lysine, preventing cullin neddylation (Duda et al., 2008; Goldenberg et al., 2004).

4.1.3 The role of DCUN1D1 in regulation of CRL activity

DCUN1D1, like RBX1 and RBX2, functions as a NEDD8 E3 ligase, potentiating cullin neddylation (Kurz et al., 2008; Kurz et al., 2005; Scott et al., 2010). DCUN1D1 binds to components of the CRL complex (Kim et al., 2008) and is overexpressed in squamous cell carcinoma, in which cancer cells may become addicted to high DCUN1D1 levels (Sarkaria et al., 2006). Structural studies using the yeast homologue Dcn1 demonstrate Dcn1 to contain a ubiquitin associated (UBA) and a potentiating neddylation (PONY) domain, the latter of which is sufficient to potentiate neddylation (Kurz et al., 2008) both in vitro and in vivo. Further analyses have demonstrated that Dcn1 binds the E2 enzyme Ubc12 and the yeast CUL1 homologue Cdc53, reducing the distance between RBX bound, NEDD8 charged E2 and the acceptor lysine on the cullin, facilitating neddylation (Scott et al., 2010). Depletion of DCUN1D1 using siRNA demonstrates decreased, but not abolished neddylation of CUL1, suggesting despite its role in facilitating neddylation, DCUN1D1 is not essential for cullin neddylation (Kim et al., 2008). There are four other DCUN1D family members, DCUN1D2-5, each of which encode a C terminal PONY domain, but vary at the N terminus. DCUN1D3 has previously been shown to both interact with CUL3 and to influence its neddylation, with siRNA mediated depletion of DCUN1D3 decreasing CUL3 neddylation (Meyer-Schaller et al., 2009).

4.1.4 Cullin 3 specific functions

CUL3 CRL complexes are less extensively studied than CUL1 counterparts. As discussed above, proteins with a BTB domain mediate the interaction between CUL3-RBX1 and substrate (Geyer et al., 2003; Pintard et al., 2004; Pintard et al., 2003). The BTB domain is a protein interaction domain which shares structural similarities with the

region of SKP1 which binds CUL1 (Schulman et al., 2000). BTB adaptor proteins may dimerize, thus inducing dimerization of CUL3 CRLs (Zimmerman et al., 2010). CUL3 CRL complexes are implicated in the regulation of many diverse cellular processes. The first CUL3 CRL complex characterised was in C elegans. A complex involving the BTB domain containing protein MEL26 is required for degradation of MEI1, an event which allows proper formation of the mitotic spindle in early embryos (Furukawa et al., 2003) . CUL3- BTB CRL complexes also play important roles in the control of mitotic progression and cytokinesis, where a complex involving CUL3 and KLHL9 and KLHL13 ubiquitylate the mitotic kinase Aurora B, controlling its proper localisation during mitosis (Sumara et al., 2007), and a KLHL21-CUL3 CRL complex is involved in Aurora B localisation during anaphase (Maerki et al., 2009). The transcription factor Nrf2 activates transcription of detoxifying enzymes in response to oxidative cell stress. Levels of Nrf2 are closely controlled by a CUL3 CRL complex which contains the BTB protein Keap1 (Zhang et al., 2004). Interestingly, a recent study described recurrent mutations in KLHL3, a BTB domain protein and CUL3 in patients with pseudohypoaldosteronism type II (PHA II), an inherited syndrome which results in hypertension, hyperkalaemia and metabolic acidosis, suggesting a CUL3- KLHL3 CRL complex plays a role in control of blood pressure, probably within the kidney (Boyden et al., 2012), though the substrate(s) affected remain so far uncharacterised.

One previous study implicated a CUL3 CRL complex in the regulation of PML specifically under hypoxic conditions. Using prostate cancer cell lines, it was demonstrated that hypoxia induced expression of the BTB adaptor protein KLHL20, which forms a CUL3 CRL complex responsible for ubiquitylation and degradation of PML, a process dependent on the phosphorylation of PML (Yuan et al., 2011). In contrast to RNF4 mediated degradation of PML, this process was not dependent on

SUMO modification of PML, because a PML mutant which could not be sumoylated was efficiently ubiquitylated by the CUL3-KLHL20 complex.

4.2 Results

4.2.1 siRNA screening data demonstrates Cullin 3 depletion results in PML accumulation

As discussed in detail in Chapter 3 of this thesis, an siRNA screen using a library of siRNAs to target various components of the ubiquitome was performed to identify gene knockdowns which affected the size of PML bodies either in the presence or absence of arsenic treatment. The most striking phenotype noted in the siRNA screen performed in the absence of arsenic was identified when Cullin 3 (CUL3) was depleted. Cells transfected with CUL3 siRNA contained numerous large, bright PML bodies (**Figure 4.2.1., panel A**). Analysis of these images using the automated screening assay, demonstrated a 2.4 fold increase in the PML body total area when CUL3 and control siRNA transfected cells were compared (**Figure 4.2.1., panel B**).

These data suggested that PML may be a substrate for a CUL3 ubiquitin E3 ligase complex. In the absence of CUL3, it would be anticipated that substrates of a CUL3 E3 ligase complex would fail to be ubiquitylated, and thus accumulate. This is consistent with the phenotype identified in the siRNA screen. In support of this hypothesis, siRNA mediated depletion of DCUN1D1, a protein which is required for the neddylation and therefore activation of cullins, resulted in a 1.5 fold increase in the total area of the nucleus occupied by PML bodies.

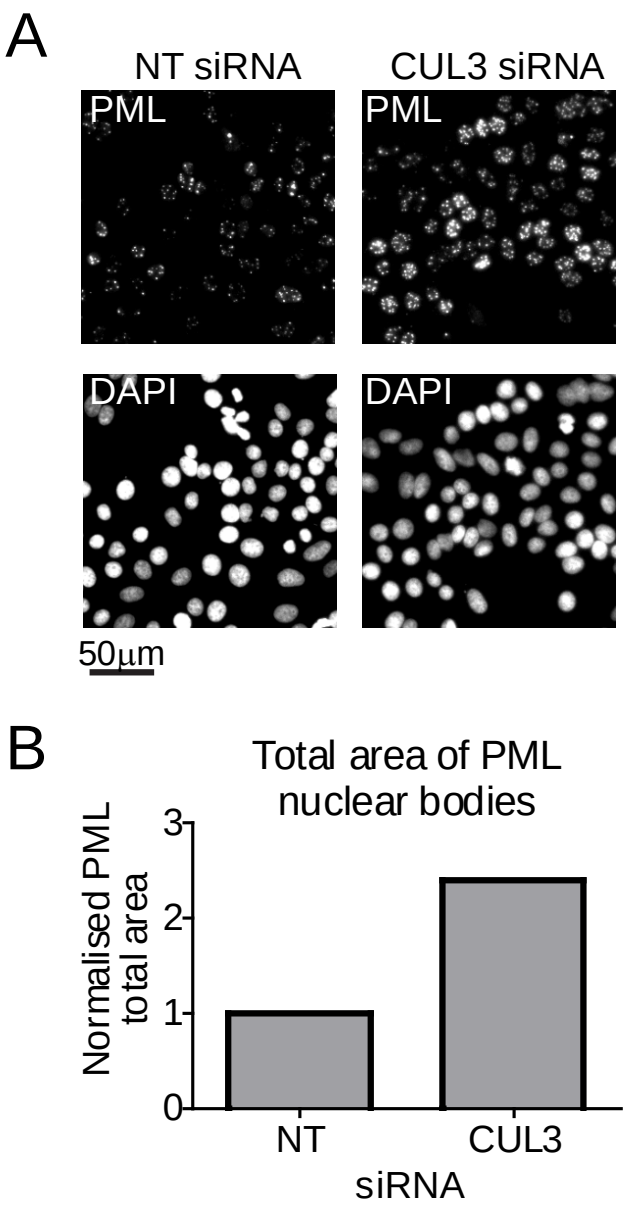

Figure 4.2.1. siRNA screen data for CUL3 siRNA

(A) Representative images of YFP-PML HeLa cells transfected with either control, non-targeting siRNA (left panels) or CUL3 siRNA (right panels) in the primary ubiquitome siRNA screen, as discussed in section 3.2.8. Cells were imaged with a 10x lens using an IN Cell 1000 automated microscope. Images represent individual z sections.

(B) The sum of the area of all PML bodies in a given cell nucleus were analysed using the automated analysis protocol described in section 3.2.7.1.. The values for all cells transfected with non- targeting siRNA (6890 cells analysed) or CUL3 siRNA (6317 cells analysed) were averaged, and normalised to the NT siRNA result, to give the data shown on the graph.

4.2.2 Confirmation of CUL3 siRNA phenotype

The data obtained in the initial siRNA screen used a pool of four siRNAs to target each test gene. Each of the four siRNA duplexes were then tested individually. This aimed to confirm that the phenotype identified in the primary screen was due to CUL3 depletion, and not due to an off target effect of an individual siRNA duplex.

Cells were transfected with a non- targeting siRNA duplex, the previously tested pool of siRNAs targeting CUL3, or one of four individual siRNA duplexes targeting CUL3. Western blotting of cells transfected with non targeting control siRNA with an anti CUL3 antibody demonstrated two CUL3 species. The higher molecular weight species represented neddylated CUL3, and the lower, unmodified CUL3 (**Figure 4.2.2., NT lane**).

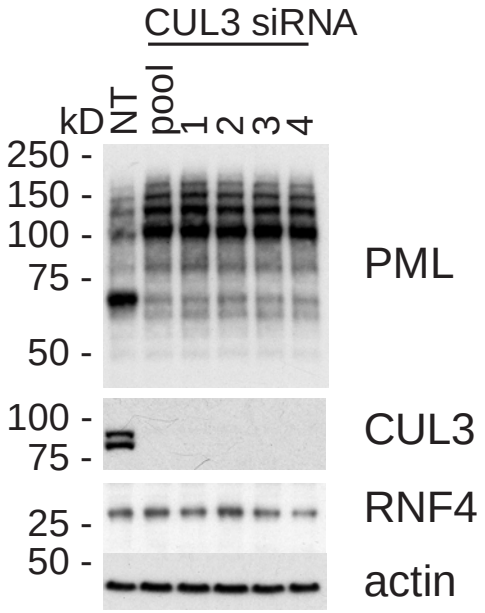

Figure 4.2.2. CUL3 depletion results in accumulation of PML

YFP PML HeLa cells were transfected with non-targeting, control siRNA or 4 individual siRNA duplexes targeting CUL3, or a pool of all 4 duplexes. 72 hours later cells were lysed and analysed by western blotting with antibodies specific for PML, CUL3, RNF4 and actin.

Transfection with the pool of CUL3 siRNAs, or any of the four individual duplexes reduced CUL3 protein to undetectable levels (**Figure 4.2.2., CUL3 siRNA lanes**).CUL3 depletion resulted in accumulation of primarily high molecular weight YFP-PML and endogenous PML species. RNF4 expression was unaffected by CUL3 depletion.

To quantify the accumulation of PML noted by western blotting, cells were cultured on coverslips prior to transfection with non targeting siRNA, a pool of CUL3 siRNAs or one of four individual siRNAs targeting CUL3. These cells were then imaged by deconvolution microscopy and YFP PML fluorescence quantified. Images demonstrated an increase in the number and size of PML nuclear bodies for cells transfected with the pool of CUL3 siRNAs or any of the four individual duplexes (**Figure 4.2.3., panel A**). The most pronounced increase in YFP PML fluorescence was noted in images of cells transfected with the pool of CUL3 siRNAs and the first individual siRNA duplex. Quantification of YFP PML fluorescence was then performed. Transfection of all four siRNA duplexes targeting CUL3 resulted in an increase in the PML body total area. The most pronounced effects were observed in cells transfected with oligo siRNA 1, for which an eight fold increase was noted (**Figure 4.2.3., panel B**). There was also an increase in the number of PML nuclear bodies detected, with transfection with any of the four individual CUL3 siRNAs increasing the number of PML bodies per cell two fold compared with control cells (**Figure 4.2.3., panel C**). This demonstrates that the increase in PML body total area noted in **Figure 4.2.3., panel B** is due to a combination of an increase in the number of PML bodies per nucleus and an increase in the size of these PML nuclear bodies. To investigate whether the increase in PML body number and size was due to redistribution of PML from the nucleoplasm to PML bodies, or whether there was an increase in the

total amount of PML present, the YFP PML fluorescence of the whole nucleus was quantified.

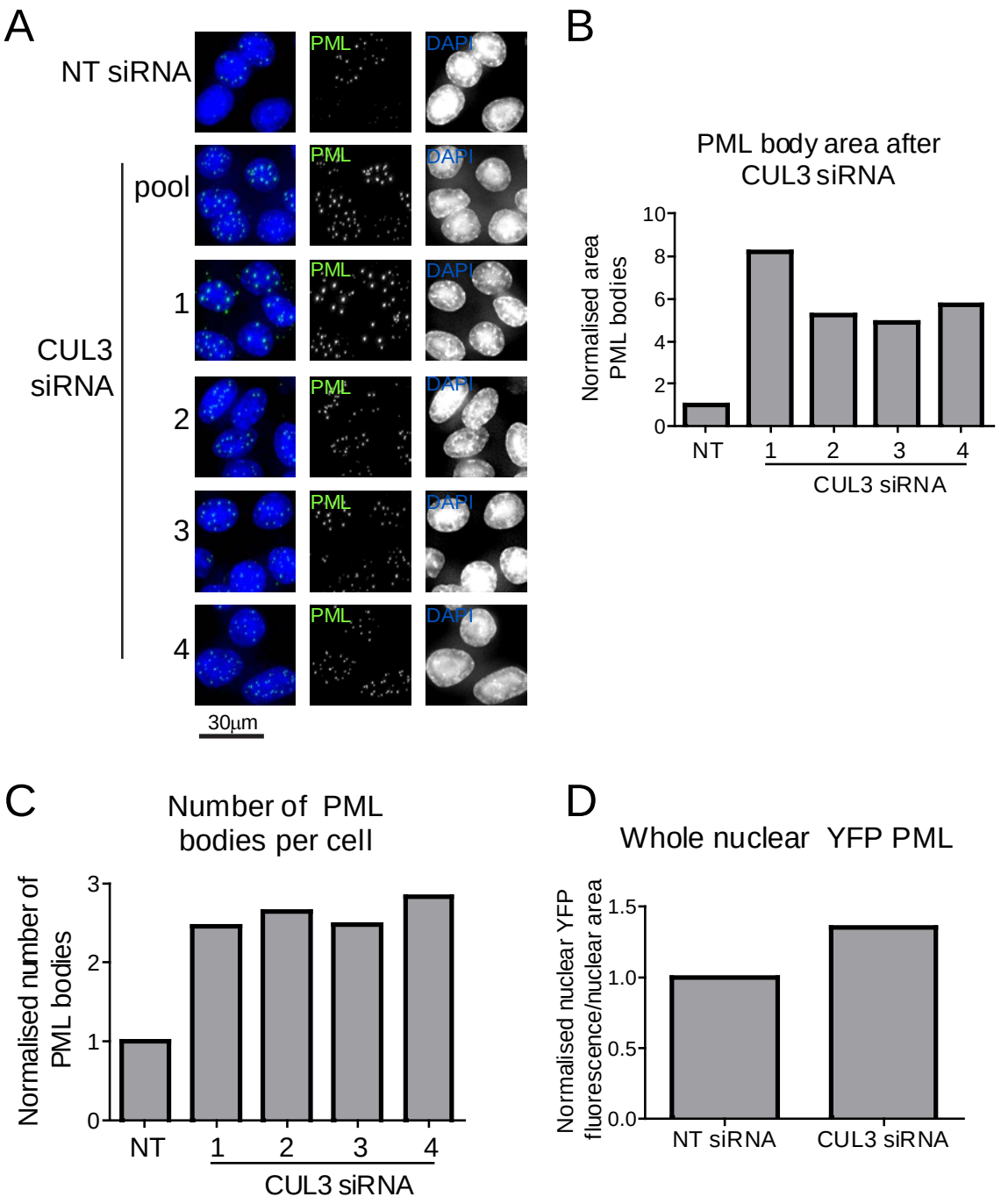

Figure 4.2.3. Quantification of YFP PML fluorescence following CUL3 depletion

(A) YFP PML HeLa cells were transfected with non- targeting control siRNA, a pool of 4 siRNAs targeting CUL3, or each of the individual duplexes in the pool. 72 hours later, cells were fixed with paraformaldehyde, stained with DAPI and

imaged using deconvolution microscopy. Immunofluorescence images represent maximal projections of multiple z sections.
(B) YFP PML HeLa cells were transfected with non-targeting, control siRNA or 4 individual siRNA duplexes targeting CUL3. Cells were fixed, stained with DAPI and imaged using deconvolution microscopy. Maximal intensity projections were prepared from multiple z sections, and quantitation of YFP PML fluorescence was performed to evaluate the size of PML nuclear bodies. The total area of PML nuclear bodies was calculated for each cell, and averaged for all cells analysed in each condition. Values were normalised to that found for NT siRNA transfected cells.
(C) YFP PML HeLa cells were transfected and imaged as described in (B). Maximal intensity projections were prepared from multiple z sections and the number of PML bodies per nucleus quantified. Data presented represents the average number of PML bodies per cell, normalised to the number of PML bodies present in NT siRNA transfected cells.
(D) YFP PML HeLa cells were transfected with control, non targeting (NT) siRNA or a pool of 4 siRNAs targeting CUL3. 72 hours later, cells were fixed and stained with DAPI prior to imaging using deconvolution microscopy. Maximal intensity projections of multiple z sections were prepared and the total YFP PML fluorescence per nucleus was calculated. This value was then divided by the area of the nucleus to normalise for nuclear size. Data presented is the average of all cells analysed for each condition, normalised to the value for NT siRNA.

This demonstrated a 1.3 fold increase in whole nuclear YFP PML fluorescence for cells transfected with CUL3 siRNA compared to control cells (**Figure 4.2.3., panel D**). This indicated an increase in the total amount of YFP PML present in the nucleus. This increase was modest compared to the increases noted in PML body total area and number, suggesting both accumulation and redistribution of YFP PML to PML-NBs take place in response to CUL3 depletion.

4.2.3 DCUN1D1 depletion results in decreased neddylation of CUL3 and accumulation of PML

As mentioned in section 4.2.1, DCUN1D1, a protein required for the neddylation and therefore activation of cullins was identified as a putative hit in the siRNA screen. To exclude the possibility that the phenotype identified in the screen was due to an off target effect of one of the siRNAs included in the pool of four tested, cells were transfected with each of the individual siRNA duplexes and the effects analysed by deconvolution microscopy. The resulting images revealed an increase in the number and size of PML nuclear bodies for all four of the individual duplexes tested (**Figure 4.2.4., panel A**). Quantification of YFP PML fluorescence was then performed. This confirmed an increase in the PML body total area for each of the DCUN1D1 siRNA duplexes tested. The most pronounced effects were observed in cells transfected with the first oligosiRNA, in which a five fold increase in total PML body area was noted compared to that of control cells (**Figure 4.2.4., panel B**). These data confirmed the phenotype identified in the screen was recapitulated for each of the individual siRNA duplexes tested and was therefore unlikely to be due to an off target effect.

To investigate whether the effects of DCUN1D1 depletion were mediated by effects of this depletion on CUL3, cells were transfected with a non targeting control siRNA duplex or a pool of four siRNAs targeting DCUN1D1. Western blotting analysis with an antibody specific for PML demonstrated accumulation of high molecular weight PML species in cells depleted of DCUN1D1 (**Figure 4.2.4., panel C**), similar to that identified in cells depleted of CUL3 (**Figure 4.2.3**). Analysis using a CUL3 specific antibody revealed a decrease in the high molecular weight, neddylated CUL3 species following DCUN1D1 depletion, and accumulation of the lower molecular weight CUL3

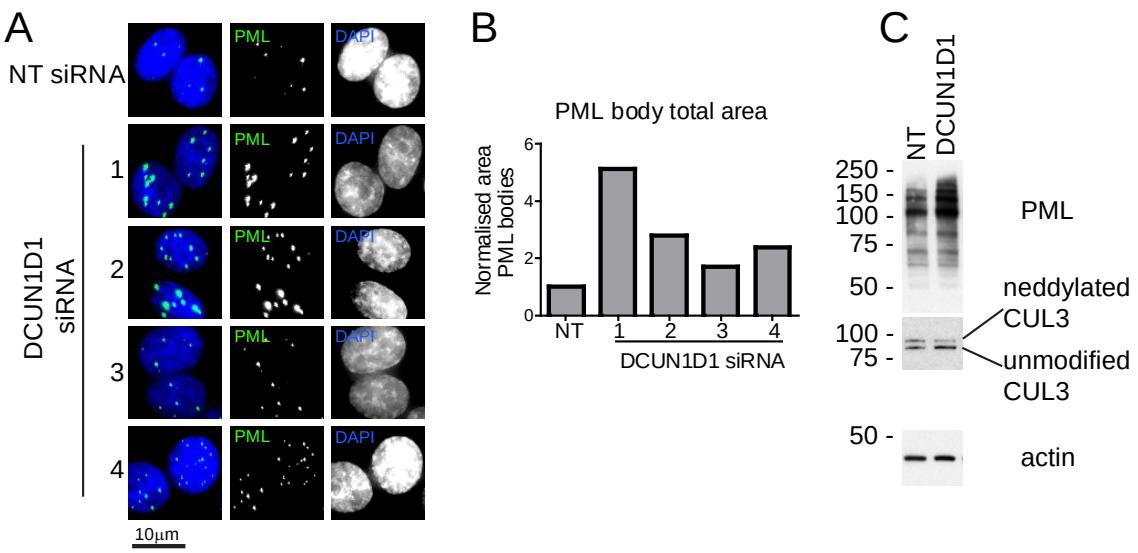

Figure 4.2.4. DCUN1D1 depletion results in decreased CUL3 neddylation and PML accumulation

(A) YFP PML HeLa cells were transfected with a non- targeting siRNA duplex or 4 individual siRNAs targeting DCUN1D1. 72 hours later, cells were fixed with paraformaldehyde and stained with DAPI. Cells were then imaged by deconvolution microscopy. Immunofluorescence images presented are maximal intensity projections of multiple z sections.

(B) YFP PML HeLa cells were transfected and imaged as in (A). YFP PML fluorescence in maximal intensity projections was quantified to calculate the total area of each cell nucleus occupied by PML bodies. This was then averaged for all cells analysed for each condition. Data presented represents the mean total PML body area per cell for each condition, normalised to the result for NT siRNA transfected cells.

(C) YFP PML HeLa cells were transfected with a non- targeting siRNA duplex or a pool of 4 siRNAs targeting DCUN1D1. 72 hours later, cells were lysed and analysed by western blotting with antibodies specific for PML, CUL3 and actin.

species (**Figure 4.2.3. panel C**). This demonstrates that DCUN1D1 is required, at least in part, for proper neddylation and therefore activity of CUL3. This suggests that the effects of DCUN1D1 depletion on PML identified in **Figures 4.2.4., panels A-C** are due to the resulting decrease in CUL3 CRL ubiquitin ligase activity. There is still a proportion of neddylated CUL3 present in cells depleted of DCUN1D1 (**Figure 4.2.4.**

panel C), which is likely to be why the accumulation of PML in cells depleted of DCUN1D1, maximally a five fold increase in PML body total area (**Figure 4.2.4., panel B**), is less than that observed in cells completely depleted of CUL3, in which up to an eight fold increase was identified (**Figure 4.2.3., panel B**).

4.2.4 MLN4924 treatment results in accumulation of PML

MLN4924 is a potent inhibitor of NEDD8 activating enzyme (NAE), and therefore prevents neddylation of cullins decreasing cullin-RING ligase activity leading to accumulation of their substrates (Soucy et al., 2009). If indeed PML is a substrate of a CUL3 ubiquitin ligase complex, it would therefore be expected that PML should accumulate in the presence of MLN4924. In order to test this hypothesis, YFP PML HeLa cells were incubated with MLN4924 for various periods of time, and the effects on PML monitored by western blotting and immunofluorescence. Western blotting with a CUL3 specific antibody confirms the loss of the high molecular weight CUL3 species and accumulation of the lower molecular weight CUL3 species following 24 hours of MLN4924 treatment, confirming the drug has inhibited neddylation of CUL3, and therefore inhibited its activity (**Figure 4.2.5., panel A**). An increase in total PML species is noted after MLN4924 treatment, with a particular increase in high molecular weight PML species (**Figure 4.2.5., panel A**). When assessed by deconvolution microscopy, an increase in the number and size of PML nuclear bodies is noted after twenty- four hours of MLN4924 treatment (**Figure 4.2.5., panel B**), and this phenotype persists after forty-eight hours of treatment. A change in phenotype was seen after 72 hours of MLN4924 treatment, with the accumulation of PML in numerous small PML nuclear bodies (**Figure 4.2.5., panel B**).

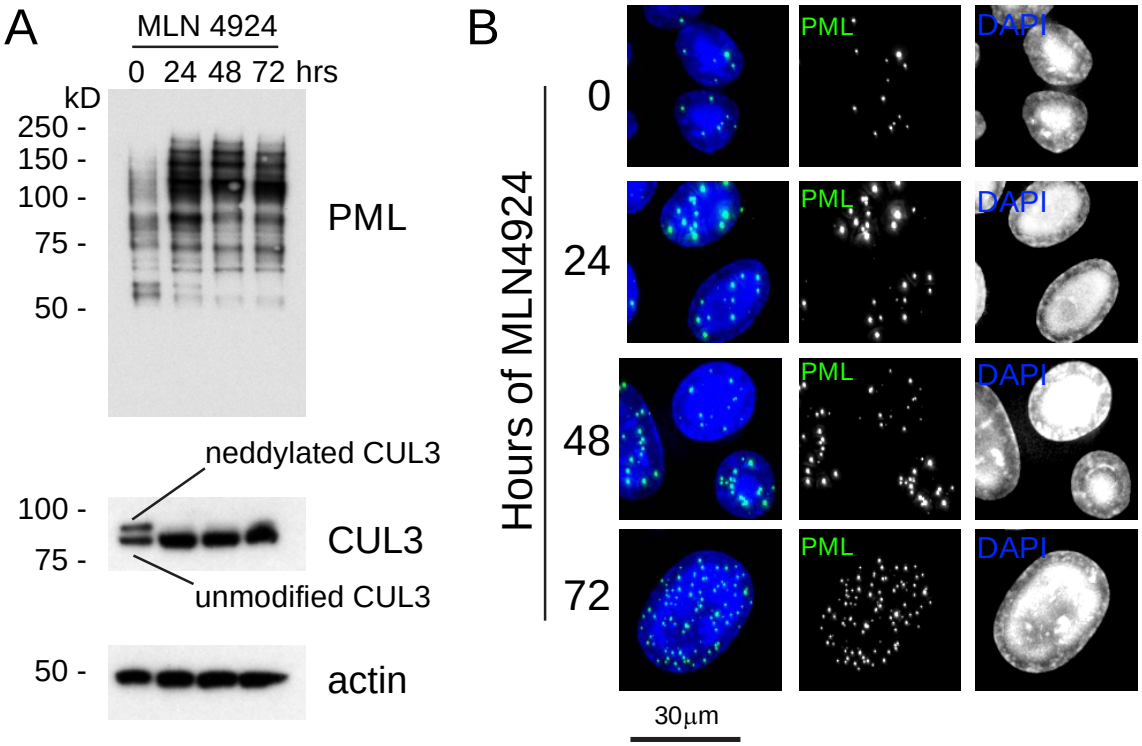

Figure 4.2.5. MLN 4924 treatment results in accumulation of PML

(A) YFP PML HeLa cells were treated with 5μM MLN 4924 and cells lysed at 0, 24, 48 and 72 hours. Whole cell extracts were then analysed by western blotting with antibodies specific for PML, CUL3 and actin.
(B) YFP PML HeLa cells were treated with 5μM MLN 4924 and cells fixed with paraformaldehyde at 0, 24, 48 and 72 hours. Cells were then stained with DAPI and imaged using deconvolution microscopy. Immunofluorescence images presented are maximal intensity projections of multiple z sections.

These data demonstrated that inhibition of neddylation resulted in accumulation of PML, and are consistent with the hypothesis that PML is a substrate of a CUL3 CRL ligase, but don't exclude that PML may be a substrate for other CRLs which would also be inhibited by MLN4924.

4.2.5 Cell cycle analysis following CUL3 depletion

The number and composition of PML nuclear bodies and posttranslational modifications of PML are reported to change throughout the cell cycle. An increase in

the number of PML bodies is identified in cells during S phase (Dellaire et al., 2006a), with a fall in the number of PML bodies as cells enter mitosis (Dellaire et al., 2006b).

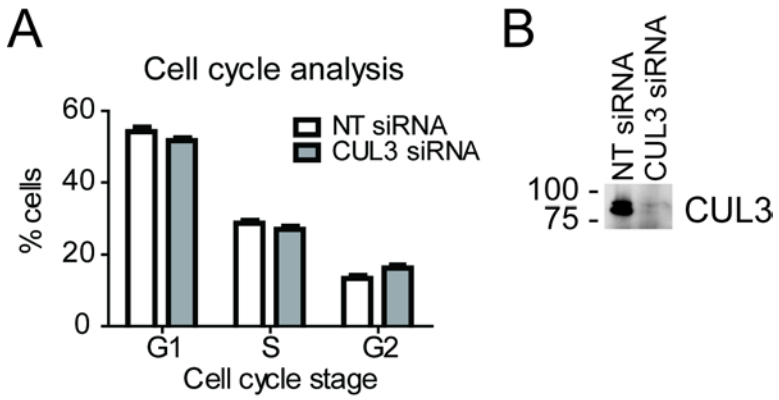

Figure 4.2.6. Cell cycle analysis following CUL3 depletion

(A) YFP PML HeLa cells were transfected in triplicate with either a non-targeting siRNA duplex or a pool of 4 siRNAs targeting CUL3. 72 hours later, cells were fixed in ethanol and DNA stained with propidium iodide. The cellular DNA content was then assessed by flow cytometry to determine cell cycle stage. Data demonstrates the average percentage of cells in G1, S or G2 phase of the cell cycle for NT siRNA and CUL3 siRNA transfected cells, ± the standard error of the mean.
(B) Whole cell extracts from cells transfected with siRNA as in (A) were analysed by western blotting with a CUL3 antibody.

CUL3 ubiquitin E3 ligase complexes have previously been demonstrated to regulate mitosis via ubiquitylation of key regulatory proteins (Maerki et al., 2009; Sumara and Peter, 2007; Sumara et al., 2007). Given the cell cycle dependent changes in PML and the potential disruption of mitosis secondary to CUL3 depletion, the cell cycle profile of YFP PML HeLa cells was determined in cells transfected with siRNA targeting CUL3. Cells were harvested and stained with propidium iodide 72 hours after siRNA transfection, the same time point that the accumulation of PML was noted after CUL3 depletion in the siRNA screen. CUL3 depletion was confirmed by western blotting of an aliquot of cells from each condition (**Figure 4.2.6.**). Flow cytometry

analysis of DNA content of the two populations of cells was performed by Dr Rosie Clarke, University of Dundee. Data obtained demonstrates only a slight increase in the percentage of cells in G2 phase of the cell cycle, with a corresponding decrease in G1 and S phase population (**Figure 4.2.6**). These results suggest the accumulation of PML identified following CUL3 depletion is not due to the accumulation of cells in a certain phase of the cell cycle leading to PML accumulation.

4.2.6 Attempts to identify BTB adaptor protein

As discussed in the introduction to this chapter, CUL3 ubiquitin ligases rely on a substrate specific BTB domain containing protein to bring substrate into proximity with the CUL3 ligase complex (Furukawa et al., 2003; Geyer et al., 2003; Xu et al., 2003). It was therefore important to attempt to identify the BTB domain containing protein involved in a CUL3 ligase complex responsible for the ubiquitylation of PML.

4.2.6.1 Investigation of the role of LZTR1 in PML stabilisation

Data from the original siRNA screen was re-examined to ascertain if any of the putative hits identified in the non drug treated dataset were BTB domain containing proteins (**Table II**). LZTR1 is a protein with six N-terminal kelch repeats and two BTB domains at the C- terminus (Nacak et al., 2006). This makes it an atypical BTB domain containing protein because the BTB domain is usually located at the N- terminus (Petroski and Deshaies, 2005). LZTR1 is commonly deleted in the congenital Di George syndrome (Kurahashi et al., 1995). Depletion of LZTR1 with a pool of four siRNAs in the initial siRNA screen resulted in a 1.5 fold increase in the total area of the nucleus occupied by PML bodies (**Table II**).

LZTR1 was also investigated in the deconvolution screen described in section 3.2.5 of this thesis. Four individual siRNAs targeting LZTR1 were transfected into YFP

PML HeLa cells and the total area of PML bodies measured 72 hours later. Only one of the four siRNA duplexes used recapitulated the phenotype identified in the primary screen (**Table XIV**). This initially led to the phenotype being disregarded as an off target effect, however given the increased interest in proteins containing a BTB domain, further investigations were performed.

Table XIV. Deconvolution screen: results for LZTR1

Gene Symbol	Fold change compared to NT siRNA control			
	Oligo 1	Oligo 2	Oligo 3	Oligo 4
LZTR1	0.62	2.50	0.91	1.01

To assess whether all of the four individual siRNAs were effective in targeting LZTR1 mRNA for degradation, RT qPCR was employed to assess LZTR1 mRNA levels following siRNA knockdown with each of the four individual siRNA duplexes. Parallel samples were prepared for immunofluorescence analysis, to allow correlation of the degree of mRNA knockdown achieved with effects on YFP PML fluorescence. All four of the siRNA duplexes examined reduced LZTR1 mRNA to 50% or less than the level identified in control cells (**Figure 4.2.7., unfilled bars**). However, the degree of knockdown did not correlate with the degree of PML accumulation identified by immunofluorescence (**Figure 4.2.7., grey bars**). These results did not correspond to the data produced from the siRNA screen either, in which the most pronounced phenotype was identified in cells transfected with the second siRNA duplex (**Table XIV**).

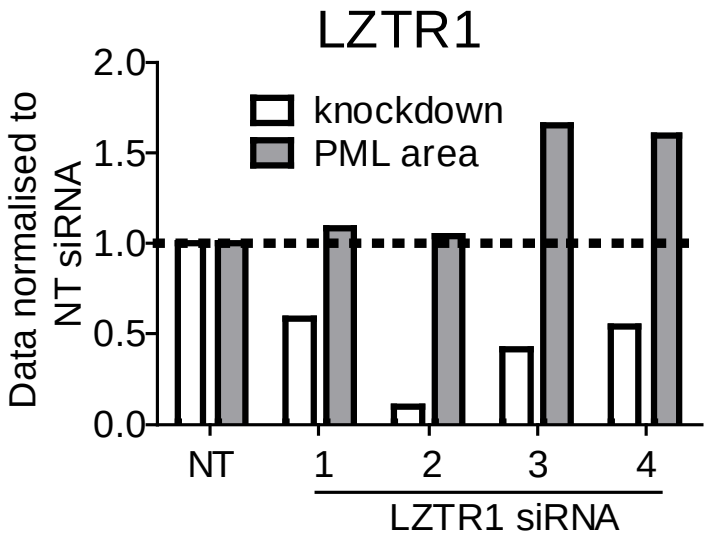

Figure 4.2.7. The effects of siRNA mediated LZTR1 depletion

YFP PML HeLa cells were transfected with either a non targeting control siRNA duplex or one of 4 individual siRNA duplexes targeting LZTR1. 72 hours later cells were lysed in RNA lysis buffer or fixed with paraformaldehyde. LZTR1 mRNA levels were then analysed by RT qPCR to assess knockdown efficiency of each LZTR1 duplex (unfilled bars) relative to control. Cells fixed in PFA were stained with DAPI and imaged using deconvolution microscopy. Maximal intensity projections of multiple z sections were prepared and YFP PML fluorescence of PML bodies was analysed to measure the total area of the nucleus occupied by PML bodies. Results were averaged for all cells in each condition and normalised to the result obtained for NT siRNA transfected cells (grey bars).

4.2.6.2 Targeted siRNA screen: BTB domain containing proteins

To attempt to identify BTB domain containing proteins that may be involved in a CUL3 ubiquitin ligase complex responsible for PML ubiquitylation, a repeat high content siRNA screen was performed, using 160 pools of siRNA targeting BTB domain containing proteins which are within the SCILLS ubiquitome siRNA library to transfect YFP PML HeLa cells. To widen the scope for hit identification, the screen was performed at two time points, with cells fixed at either 72 or 96 hours after transfection. Because the CUL3 siRNA phenotype was identified in cells not treated with arsenic, cells were not arsenic treated. The screen consisted of a total of four test plates, two at each time point, with non targeting and RNF4 siRNA controls on each plate as previously. Plates were imaged using an automated microscope and analysed using the same protocol as for the previous siRNA screens to identify the PML body total area for a given cell, averaged for all cells analysed for a particular siRNA.

The Z' factor was calculated for each of the assay plates, and the results are shown in **Figure 4.2.8.**. The Z' factor for plate 1 was satisfactory at over 0.6, but for the remaining plates was lower at 0.2. This is similar to the Z' factors calculated for the non- drug treated plates in the previous siRNA screens.

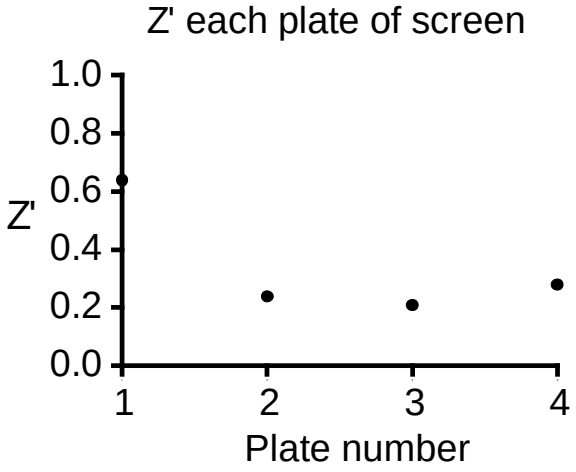

Figure 4.2.8. Quality control for BTB domain siRNA screen

The Z' factor was calculated for each plate in the siRNA screen using results from wells containing the negative control, non targeting siRNA and the positive control, RNF4 siRNA.

Due to the low number of siRNAs screened, slightly different criteria were adopted for hit identification, with siRNAs scoring as a hit if the total area of PML nuclear bodies was outwith 1.3 standard deviations of the mean. This resulted in an initial list of fourteen siRNA targets, which was further reduced following image analysis. A list of putative hits identified in this screen, and selected for further investigation is shown in **Table XV**. ABTB2 is included because although there was not significant accumulation of PML in cells transfected with ABTB2 siRNA, when reviewing the images, it was noted the cells contained numerous, small PML bodies, which was an interesting phenotype. LZTR1 was not further investigated because the experiments described in section 4.2.6.1 had already been performed.

Table XV. BTB domain siRNA primary screen: putative hits

Gene Symbol	Fold change compared to NT siRNA control
LZTR1	3.11
KCNC1	1.26
ABTB2	0.84
ANKFY1	1.09
KLHL25	1.39

4.2.6.3 Deconvolution siRNA screen- BTB domain containing proteins

Four individual siRNA duplexes targeting each of KCNC1, KLHL25, ANKFY1 and ABTB2 were ordered to allow deconvolution of the pools of siRNA tested in the primary screen. YFP PML HeLa cells were transfected with these siRNAs, and also with four siRNA duplexes targeting each of DCUN1D1 and CUL3 as positive controls, and to allow comparison of the phenotype observed in the images following depletion of the BTB domain containing proteins with those depleted of CUL3 or DCUN1D1.

The data from the deconvolution screen was inconclusive. Only one siRNA duplex targeting each of KCNC1, ANKFY1 and KLHL25 resulted in a PML body total area higher than that identified in control, non target siRNA transfected cells (**Table XVI, highlighted by red text**).

Table XVI. BTB domain siRNA deconvolution screen: results

Gene Symbol	Fold change compared to NT siRNA control			
	Oligo 1	Oligo 2	Oligo 3	Oligo 4
ABTB2	0.645	0.78	0.75	0.905
ANKFY1	0.875	0.84	0.83	**1.19**
KCNC1	0.88	**1.145**	0.785	0.64
KLHL25	**1.235**	0.615	0.915	0.955
CUL3	2.05	1.955	2.005	2.02
DCUN1D1	1.94	1.15	1.295	1.07

Transfection with positive control siRNAs targeting CUL3 and DCUN1D1 resulted in accumulation of YFP PML to a similar extent as previously identified in the high content screening assay.

4.2.6.4 Further experiments with siRNA

Rather than discount the phenotypes identified in the primary siRNA screen as off target effects following the deconvolution screen, attempts were made to correlate the degree of mRNA knockdown achieved for each of the siRNAs tested with the PML phenotype observed by immunofluorescence. Cells were transfected with the individual siRNA duplexes, and subsequent mRNA levels assessed using RT qPCR with specific primers for each gene target. Parallel samples were prepared for deconvolution microscopy, to allow quantification of PML body total area for each of the siRNAs tested.

Each of the siRNAs transfected targeting KCNC1 reduced KCNC1 to less than 50% of control levels (**Figure 4.2.9., panel A, unfilled bars**). Accumulation of PML was however only detected by immunofluorescence for the first siRNA tested, and this accumulation was only marginal (**Figure 4.2.9., panel A, grey bars**). The siRNAs targeting ABTB2 showed varying efficiency at reducing mRNA levels (**Figure 4.2.9., panel B, unfilled bars**), which did not correlate with the accumulation of PML. Three of the four siRNA duplexes targeting ANKFY1 resulted in accumulation of PML (**Figure 4.2.9., panel C, grey bars**).However, siRNA duplex 3 which resulted in the greatest mRNA knockdown did not lead to accumulation of PML (**Figure 4.2.9., panel C, unfilled bars**). All four of the siRNA duplexes targeting KLHL25 resulted in efficient mRNA knockdown (**Figure 4.2.9., panel D, unfilled bars**), but again, this degree of knockdown did not correlate with the degree of PML accumulation observed in the microscopy images (**Figure 4.2.9., panel D, grey bars**).

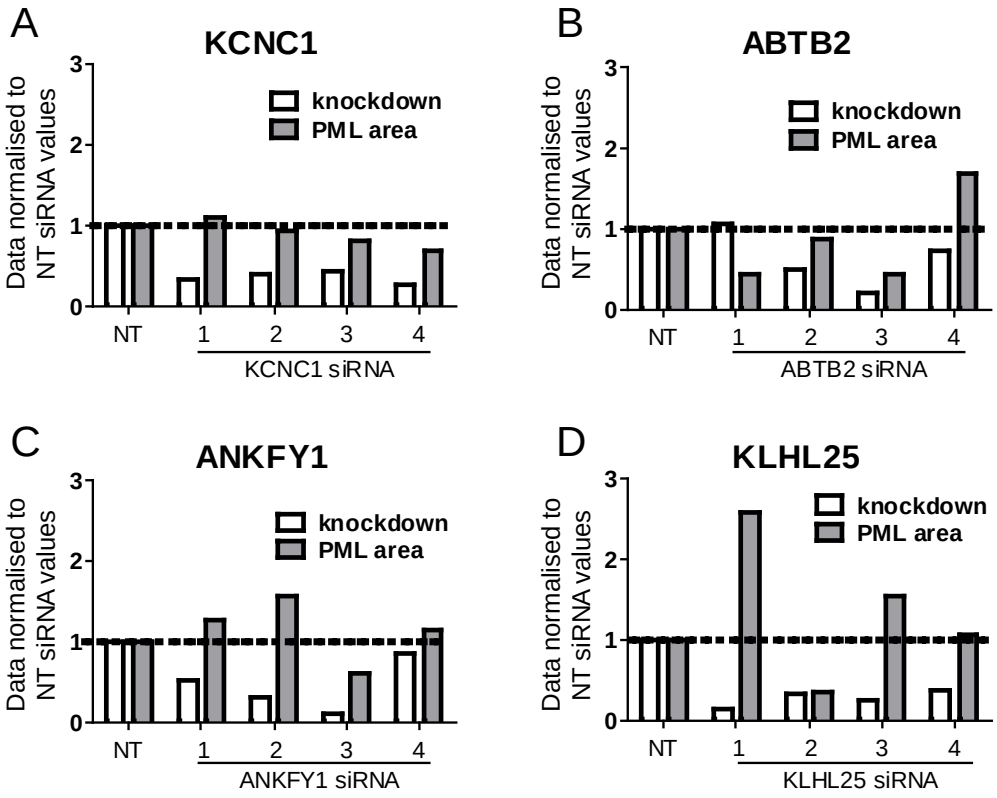

Figure 4.2.9. Analysis of knockdown efficiency and effects on PML of siRNAs targeting BTB domain containing proteins.

(A) YFP PML HeLa cells were transfected with either a non targeting control siRNA duplex or one of 4 individual siRNAs targeting KCNC1. 72 hours later cells were lysed with RNA lysis buffer or fixed with paraformaldehyde. KCNC1 mRNA levels were analysed by RT qPCR to assess KCNC1 siRNA knockdown efficiency relative to control siRNA (unfilled bars). Cells fixed in PFA were stained with DAPI and imaged by deconvolution microscopy. Maximal intensity projections of multiple z sections were prepared from the resulting images and YFP PML fluorescence of PML bodies was analysed to measure the total area of the nucleus occupied by PML bodies. Data were averaged for all cells analysed in each condition and normalised to the result obtained for NT siRNA transfected cells (grey bars).

(B) YFP PML HeLa cells were transfected with either a non targeting control siRNA duplex or one of 4 individual siRNAs targeting ABTB2. Cells were then analysed as in (A).

(C) YFP PML HeLa cells were transfected with either a non targeting control siRNA duplex or one of 4 individual siRNAs targeting ANKFY1. Cells were then analysed as in (A).

(D) YFP PML HeLa cells were transfected with either a non targeting control siRNA duplex or one of 4 individual siRNAs targeting KLHL25. Cells were then analysed as in (A).

Unfortunately, these data did not isolate a BTB domain containing protein as a likely component of a CUL3 ligase complex responsible for PML ubiquitylation. Further experiments were performed to assess the effect of overexpression of these proteins on PML stability (data not shown). These failed to demonstrate decreased stability of PML in the presence of the overexpressed BTB domain containing protein, nor did any of these proteins colocalise at PML nuclear bodies by immunofluorescence (data not shown).

4.2.6.5 GFP IP and mass spectrometry to identify YFP PML interaction partners

Following the limited success in identifying a BTB domain containing adaptor protein using siRNA to investigate loss of function phenotypes, a different approach was employed to attempt to identify components of an endogenous CUL3-PML complex by mass spectrometry.

Large scale cultures of YFP PML HeLa cells and control HeLa cells expressing YFP were lysed, and immunoprecipitation of YFP or YFP PML was performed using agarose beads coupled to a single chain, recombinant camelid anti GFP antibody. Eluted proteins were separated by SDS-PAGE, and in gel tryptic digestion was performed by Dr Mike Tatham, who also performed the mass spectrometry analysis. Approximately 3000 proteins which had intensity data in both the YFP and YFP PML samples were identified, and of these, 37 were found to be enriched in the YFP PML dataset, suggesting they were specific interaction partners of PML (**Figure 4.2.10.**).

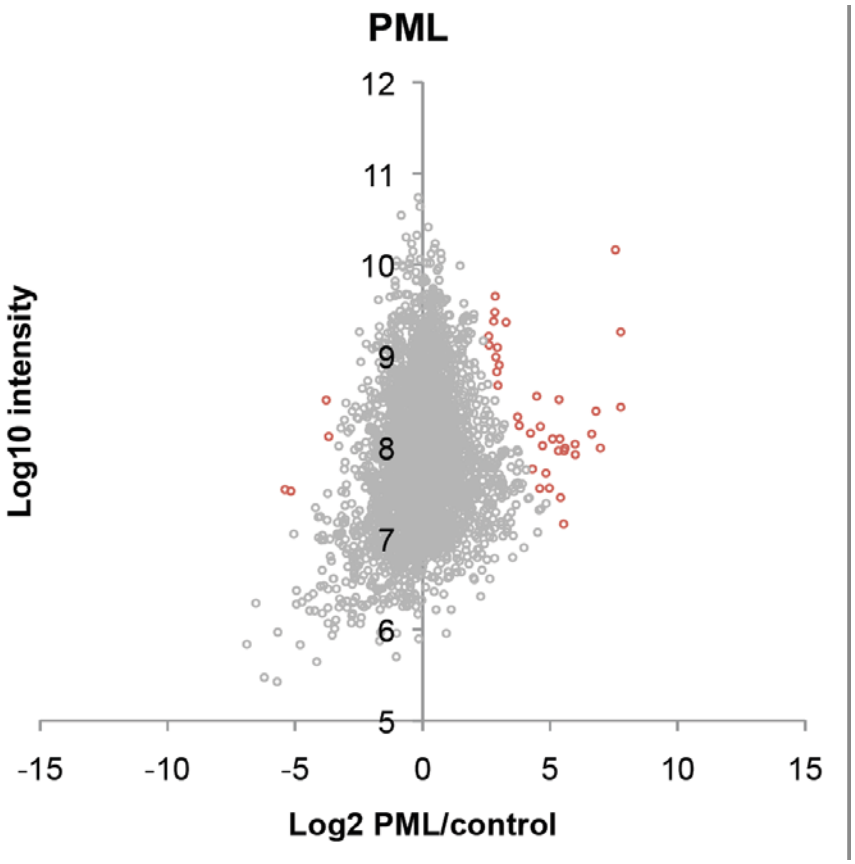

Figure 4.2.10. Mass spectrometry analysis of YFP PML interacting proteins

Control HeLa cells expressing YFP, and YFP PML HeLa cells were cultured in 10, 15cm tissue culture plates each, and lysed under non denaturing conditions when confluent. Lysates were then subjected to immunoprecipitation using agarose beads coupled to a single chain, recombinant, camelid antibody specific for GFP. Proteins eluted from the YFP and YFP PML immunoprecipitations were separated by SDS PAGE, and the gel excised into 5 slices, which were then subjected to tryptic digestion and peptide extraction. Samples were analysed by mass spectrometry and analysed using MaxQuant software. Intensity data for each protein identified were used to calculate the relative abundance of each protein in control YFP and YFP PML samples. The scatter plot displays ratios for all proteins identified, with proteins significantly enriched in the YFP PML sample highlighted in red.

Of the proteins enriched in the YFP PML IP (**Table XVII**), none have a BTB domain. Neither CUL3 nor known interaction partners of PML, for example SUMO,

Daxx or Sp100 were identified, which suggests the immunoprecipitation conditions may not have preserved these protein- protein interactions. Alternatively, it may be that the conditions used were not sufficient to extract PML from PML nuclear bodies which are relatively insoluble.

Table XVII. Proteins found to specifically interact with YFP PML by immunoprecipitation and mass spectrometry

Proteins enriched in YFP PML IP	
PML	RPL14
SYNE2	EMG1
EIF3A	PRPF31
CLPP	ARHGDIA
MYPN	RPL10A
NNMT	TRPS1
DROSHA	PRDX6
EXOSC5	FAM3C
KIAA1033	HIST2H2AA3
BCAP31	RPL19
DFFA	AK3
BAZ1A	EXO3CL1
TATDN1	AK2
TSN	PSMA3
IFI30	LAMTOR1
C1orf135	POLR3B
PSMA6	RPL13
GRPEL1	ANKRD5
HDHD3	

4.2.7 MLN4924 treatment of leukaemia cell lines

Recent publications have documented the sensitivity of leukaemia cell lines and primary leukaemia cells to treatment with the NEDD8 activating enzyme inhibitor MLN4924 (Swords et al., 2010; Tan et al., 2011). To assess whether accumulation of PML may contribute to the induction of apoptosis induced by MLN4924, leukaemia cell lines were examined by immunofluorescence after treatment with a therapeutically relevant concentration of MLN4924.

The myeloid leukaemia cell lines HL60 (Gallagher et al., 1979) and P39 (Nagai et al., 1984) were kindly gifted by Mary Hepburn and Sudhir Tauro, Department of Haematology, University of Dundee. Both of these cell lines consist of suspension cells which grow easily under standard tissue culture conditions. Initial experiments sought to characterise the sensitivity of these cells to MLN4924 treatment. Cells were exposed to various concentrations of MLN4924 for 72 hours and cell viability assayed using an ATP based viability assay. The surviving fraction was calculated for each cell line at each drug concentration and IC_{50} curves and values calculated using GraphPad Prism software (**Figure 4.2.11., panel A**). The IC_{50} for HL60 cells was found to be 170nM after 72 hours of MLN4924 treatment, with P39 cells more sensitive to MLN4924 treatment with an IC_{50} of 130nM.

Subsequent experiments were performed to assess the effects of MLN4924 treatment on PML in these cell lines. Using the data obtained from the IC_{50} calculations, a concentration of 150nM MLN4924 was used in subsequent experiments. HL60 and P39 cells were treated with MLN4924, using the same cell density as examined in the experiments performed to determine the IC_{50}. Following 72 hours of drug or control exposure, cells were cytospun onto microscopy slides and stained with antibodies specific for PML and SUMO2/3 and examined by deconvolution microscopy (**Figure 4.2.11., panel B**). PML bodies are present in control cells of both cell lines examined (**Figure 4.2.11., panels B and C, DMSO treated cells**). In control HL60 cells, the SUMO2/3 antibody identified diffuse nuclear staining with punctate accumulations of SUMO2/3 which colocalise with PML-NBs, suggesting PML, or other PML-NB components are SUMO2/3 modified in these cells (**Figure 4.2.11, panel B**).

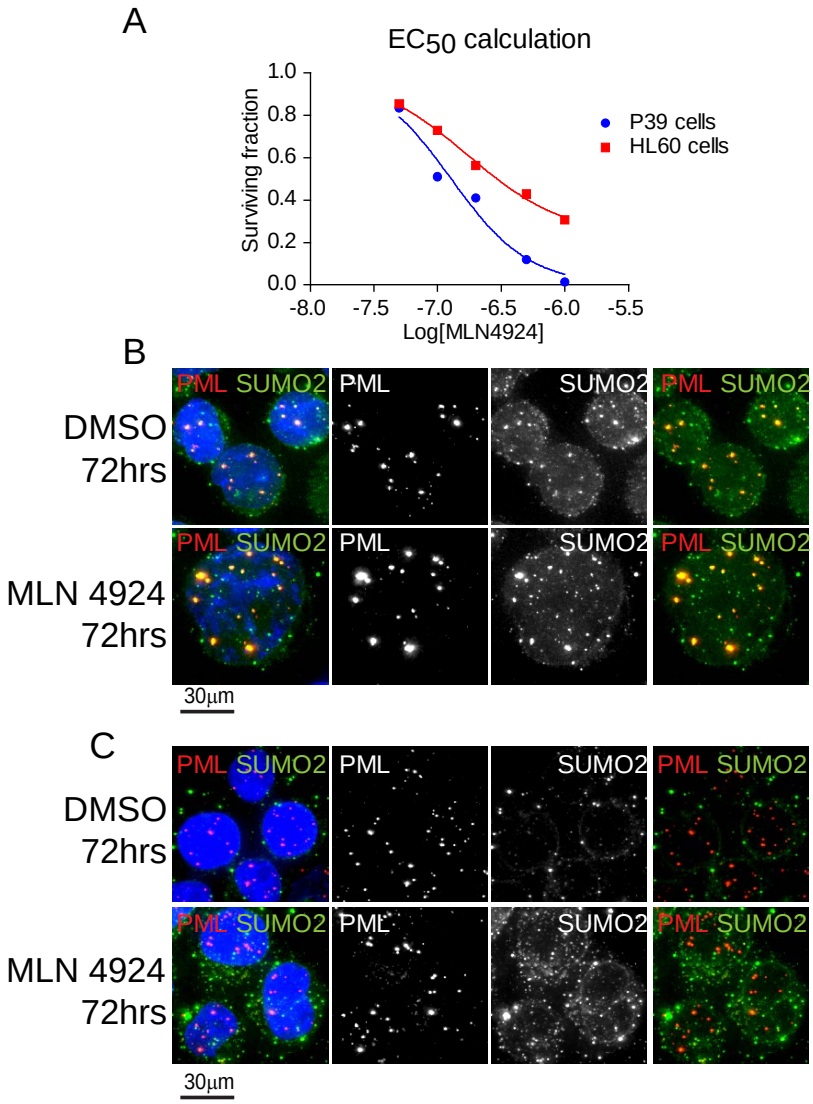

Figure 4.2.11. MLN4924 treatment of leukaemia cell lines

(A) HL60 and P39 leukaemia cell lines were treated with concentrations of MLN4924 varying from 50nM to 1µM for 72 hours in multiple replicates and cell viability assessed using an ATP based cell viability assay. The surviving fraction for each MLN4924 concentration was calculated and the IC50 for each cell line calculated using GraphPad Prism software.

(B) HL60 cells were treated with 150nM MLN4924 for 72 hours. Cells were cytospun onto microscope slides, fixed and incubated with anti PML and anti SUMO2/3 primary antibodies followed by fluorescently labelled secondary antibodies and DAPI staining. Immunofluorescence images presented are maximal intensity projections of multiple z sections, PML is shown in red, SUMO2/3 in green.

(C) P39 cells were treated and imaged as described in panel (B).

In contrast, very little nuclear SUMO2/3 was identified in P39 cells (**Figure 4.2.11., panel C**). Following MLN4924 treatment, HL60 cell nuclei enlarge and large, bright PML bodies are present, which demonstrate SUMO2/3 colocalisation (**Figure 4.2.11., panel B**). The number of PML nuclear bodies in P39 cells is increased after 72 hours of MLN4924 treatment, and there is increased diffuse nuclear SUMO2/3 staining, but only occasional colocalisation of SUMO2/3 at PML nuclear bodies (**Figure 4.2.11., panel C**). These results confirm that the localisation of PML is altered in leukaemia cell lines following MLN4924.

4.2.8 Conclusions

Through the use of a high content siRNA screen, CUL3 depletion was noted to result in significant accumulation of PML. Further experiments using four individual siRNA duplexes to target CUL3 mRNA for degradation demonstrated the same accumulation of PML as identified in the primary screen, and quantification of YFP PML fluorescence revealed CUL3 depletion resulted in an increase in total cell PML, primarily due to accumulation in PML nuclear bodies.

Depletion of DCUN1D1, a protein required for the neddylation of cullins, was also noted to result in accumulation of PML in the primary siRNA screen. Further experiments confirmed this to be a true phenotype, with all of four siRNA duplexes tested reproducing the phenotype identified in the screen. Western blotting analysis of cells depleted of DCUN1D1 revealed decreased neddylation of CUL3, demonstrating the effects of DCUN1D1 depletion on PML are likely to be mediated by the reduction in neddylated CUL3 capable of forming CRLs. This in turn suggests the ubiquitin ligase activity of CUL3 is required for PML accumulation, and a model is proposed in which, under basal conditions, PML is ubiquitylated by a CUL3 ubiquitin E3 ligase complex, targeting PML for degradation by the proteasome. Thus, the accumulation of PML

identified in the absence of CUL3 is due to decreased ubiquitylation of, and therefore stabilisation of PML.

Attempts to identify the BTB adaptor protein component of the CUL3 complex responsible for PML ubiquitylation have been so far unsuccessful. A targeted siRNA screen of BTB domain containing proteins yielded a list of putative hits which could not be confirmed in subsequent experiments. The use of immunoprecipitation of YFP PML plus mass spectrometry to attempt to identify BTB domain containing proteins which interact with PML was also unsuccessful, probably because PML was inadequately purified from cells, given that well characterised PML interaction partners were not identified either.

The inhibitor of neddylation, MLN4924 was identified to alter PML expression in both YFP PML HeLa cells and the leukaemia cell lines HL60 and P39. In all three cell lines, an increase in the number and size of PML nuclear bodies was identified in cells treated with MLN4924, which is likely to be, at least in part, due to the inhibition of CUL3 function by this inhibitor. PML is known to sensitise cells to apoptotic stimuli, and therefore this accumulation of PML may increase the susceptibility of leukaemia cells to MLN4924 induced apoptosis.

4.3 Discussion

4.3.1 CUL3 depletion leads to PML accumulation

The siRNA screen described in Chapter 3 of this thesis identified CUL3 as a potential regulator of PML. Deconvolution of the pool of siRNAs used in the siRNA screen confirmed that PML accumulated following CUL3 depletion with four different siRNA duplexes targeting CUL3 (**Figures 4.2.2 and 4.2.3.**), suggesting that indeed the phenotype identified was due to CUL3 depletion rather than an off target effect. In

support of this finding, depletion of DCUN1D1, a NEDD8 E3 ligase responsible for neddylation and therefore activation of cullins also resulted in accumulation of PML. Further experiments confirmed this effect to be independent of the siRNA sequence used to target DCUN1D1 (**Figure 4.2.4.**), and demonstrated decreased neddylation of CUL3 following DCUN1D1 depletion. CUL3 is therefore identified as a substrate of DCUN1D1. It is likely that the accumulation of PML identified following DCUN1D1 depletion is due to decreased activity of a CUL3 RING ligase complex. Of note, RBX1, a RING domain containing protein which confers E3 ligase activity to CRL complexes was also identified as a hit in the primary siRNA screen (**Table II**), though was not further validated.

CUL3 depletion results in marked accumulation of PML, which is predominantly of higher molecular weight than PML present in control cells (**Figures 4.2.2. and 4.2.4.**). This suggests that the PML which accumulates may be post translationally modified, and raises the possibility that a CUL3 CRL complex may specifically regulate post translationally modified forms of PML. PML is SUMO modified at three major sites (Kamitani et al., 1998). It may be that SUMO modification at one or more of these residues is required to recruit a CUL3 complex. This could be tested using a cell line stably expressing a PML mutant which cannot be sumoylated. If SUMO modified PML is the substrate of the CUL3 CRL, this PML mutant would not be expected to accumulate in the absence of CUL3. If confirmed, this SUMO specificity of the CRL complex would be similar to the SUMO specific recruitment of RNF4 to SUMO modified PML following arsenic treatment (Geoffroy et al., 2010; Lallemand-Breitenbach et al., 2008; Tatham et al., 2008). Post translational substrate modification, for example phosphorylation, of the CRL binding site on substrates has been previously demonstrated to regulate CRL binding (Wu et al., 2003). CUL3 CRL complexes interact with substrate via a BTB domain containing protein (Geyer et al., 2003). If SUMO

modified PML is a substrate of such a CRL, it is possible that this specificity for sumoylated PML may be conferred by SIM domains in the BTB domain containing protein. Thus the CUL3 CRL complex would be recruited to SUMO modified PML via SIM domain(s) located in the BTB adaptor protein. A bioinformatics analysis of BTB domain containing proteins could be undertaken to identify proteins with putative SIM domains. Any identified could then be tested experimentally using an in vitro system to test ubiquitylation activity of the resulting CUL3 CRL complex towards PML, or in vivo where overexpression of the BTB containing protein would be expected to result in PML degradation.

4.3.2 Attempts at rescue experiments

The gold standard method for validation of siRNA mediated phenotypes is demonstration that expression of an siRNA resistant version of the target gene rescues the siRNA mediated phenotype. To this end, attempts were made to create cell lines stably expressing an siRNA resistant version of CUL3. Two strategies were employed. In the first, YFP PML HeLa cells were transfected with constructs expressing either FLAG tagged wild type CUL3 or a version of CUL3 rendered resistant to one of the siRNA duplexes tested by virtue of three silent point mutations in the siRNA target sequence. In the second, parental HeLa cells were transfected with the same constructs. Each of these constructs was designed to express CUL3 at low levels, using the HSV-1 gD promoter to achieve this (Cuchet et al., 2011). Unfortunately, no colonies stably expressing these constructs were isolated following antibiotic selection. This may be due to toxicity conferred by CUL3 overexpression. It may therefore be possible to create stable cell lines expressing an inducible, siRNA resistant version of CUL3 for use in rescue experiments. Attempts were made to demonstrate rescue using transient transfections of DNA along with siRNA (data not shown). It proved extremely difficult

to achieve satisfactory expression of the siRNA resistant construct at the same time as achieving adequate siRNA mediated knockdown of endogenous CUL3.

Compounds which induced the same effect as siRNA depletion of a gene product can be used to validate siRNA mediated phenotypes (Mohr et al., 2010). The compound MLN4924 is a potent inhibitor of the NEDD8 activating enzyme. MLN4924 treatment therefore inhibits cullin neddylation, resulting in accumulation of the substrates of CRLs (Soucy et al., 2009). Treatment of YFP PML HeLa cells with MLN4924 resulted in inhibition of neddylation of CUL3 and accumulation of PML (**Figure 4.2.5.**). This supports the hypothesis that PML is a substrate of a CUL3 CRL complex. Of note, the phenotype identified after 24 hours of MLN4924 treatment closely resembled that of CUL3 depletion, with PML accumulating in large PML-NBs. After 72 hours of MLN4924 exposure, the appearance of PML-NBs changes, and many small PML-NBs were observed. It may be that the later phenotype is due to perturbation of other cellular processes induced by long-term inhibition of neddylation.

4.3.3 BTB domain adaptor protein identification

Unfortunately, this study failed to identify the BTB domain containing adaptor protein component of a CUL3-PML complex. Of note, KLHL20, the substrate adaptor previously reported to form part of a CUL3 CRL complex which ubiquitylates PML in response to hypoxia (Yuan et al., 2011) was not identified as a hit in the primary screen, nor in the rescreen of BTB domain containing proteins. This suggests that this CRL complex does not regulate PML under normoxic conditions. There may be redundancy between BTB adaptor proteins which may account for the failure to identify an adaptor using siRNA to screen loss of function phenotypes.

In a second approach to attempt to identify a BTB domain containing adaptor protein, YFP PML and interaction partners were immunoprecipitated from cells and subjected to mass spectrometric analysis. This yielded only a small list of interaction partners of PML (**Table XVII**) which did not include well characterised PML-NB components, SUMO or ubiquitin. CUL3 depletion results in accumulation of PML in PML-NBs, which suggests that CUL3 CRL mediated PML degradation may take place within PML-NBs. It may therefore be expected that CUL3 would be found associated with PML-NB located PML. Since other PML-NB components were not identified, it is possible that PML-NB PML was not extracted under the conditions used. Attempts to use increased concentrations of detergents to solubilise PML resulted in loss of all PML interacting proteins, when samples were analysed by mass spectrometry (data not shown). An alternative approach may be to attempt to purify intact YFP PML bodies using differential centrifugation followed by immunoprecipitation using the anti-GFP antibody used in this study. This would hopefully allow identification of all elements of a CUL3 CRL complex found at PML-NBs, but also provide information regarding other proteins present at PML-NBs.

4.3.4 PML, CUL3 and disease

CUL3 expression correlates with tumour stage in breast cancer, with increasing levels of CUL3 expression found as tumours progress (Haagenson et al., 2012). It would be interesting to assess PML expression in such samples. The data presented in this chapter suggests PML is a substrate of a CUL3 CRL complex. If this is indeed the case, one would anticipate PML expression to be reduced in tumours with high CUL3 expression. PML has tumour suppressor activities (Gang Wang et al., 1998), and therefore the increased CUL3 identified in tumours may drive tumour growth through loss of PML. Equally, it would be interesting to assess CUL3 expression in tumours

which have been demonstrated to have lost PML expression (Gurrieri et al., 2004) to confirm the reciprocal effects. Therapeutic agents that increase PML expression may be useful in the treatment of cancers in which PML expression is lost, and this study identifies MLN4924 as such a compound. The treatment of leukaemia cells with MLN4924 resulted in accumulation of PML in PML-NBs (**Figure 4.2.11.**) when MLN4924 was used at a concentration demonstrated to reduce cell viability by half. This accumulation of PML may contribute to the pro-apoptotic effects of MLN4924 previously described (Swords et al., 2010) by enhancing PML-p53 interactions. The contribution of PML accumulation to the cytotoxic effect of MLN4924 could be investigated in $PML^{-/-}$ mice.

5 Degradation characteristics of PML isoforms in response to arsenic

5.1 Introduction

PML is expressed as various isoforms due to alternative splicing. These isoforms share a common N terminus, encoded by exons 1-6, but vary at the C terminus due to varied expression of exons 7-9 (Jensen et al., 2001a). To assess the role of this variable C-terminal region in the response of an individual PML isoform to arsenic treatment, a series of cell lines expressing only one of the six major PML isoforms, PML I- VI, were treated with arsenic and the response monitored by western blotting, immunofluorescence and high content imaging. The post translational modifications of the isoforms were characterised by immunoprecipitation, and the effects of depletion of RNF4 analysed using RNA interference.

5.2 Results

5.2.1 PML isoforms degrade at different rates in response to arsenic treatment

It is now well established that PML undergoes SUMO dependent, ubiquitin mediated degradation in response to arsenic treatment (Geoffroy et al., 2010; Lallemand-Breitenbach et al., 2008; Tatham et al., 2008). When assessed by western blotting, PML is identified as multiple species representing the different isoforms and their post translationally modified forms (**Figure 5.2.1**). Following arsenic treatment at a therapeutically relevant concentration, PML rapidly accumulates as high molecular weight species (**Figure 5.2.1, 1 hour time point**). Previous work has demonstrated this to represent modification with SUMO (Geoffroy et al., 2010; Lallemand-Breitenbach et al., 2001) and ubiquitin (Geoffroy et al., 2010; Lallemand-Breitenbach et al., 2008; Tatham et al., 2008). At later time points, total PML species are reduced due to their proteasomal degradation (**Figure 5.2.1, 24 and 30 hour time points**). However, some PML species persist (**Figure 5.2.1, arrowhead**), indicating that not all forms of PML degrade at the same rate in response to arsenic treatment.

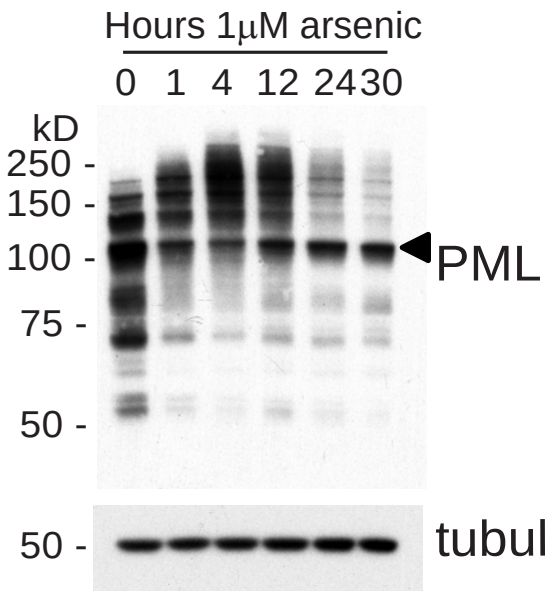

Figure 5.2.1. PML isoforms appear to respond differently to arsenic treatment.

HepaRG hepatocytes were treated with 1μM arsenic trioxide and lysed after 0, 1, 4, 12, 24 and 30 hours. Whole cell extracts were analysed by western blotting with chicken anti PML and anti tubulin antibodies.

5.2.2 PML and the PML-RARα oncoprotein degrade at similar rates in response to arsenic treatment

The NB4 acute promyelocytic leukaemia (APL) cell line expresses the PML-RARα fusion (Lanotte et al., 1991) and is a useful model system for investigating the effects of therapeutic agents used to treat APL, including all trans retinoic acid (Lanotte et al., 1991) and arsenic trioxide (Chen et al., 1996; Chen et al., 1997). The PML-RARα fusion product represents a unique PML isoform in which truncated PML is present at the N-terminus, with exons 3-9 of RARα forming the C-terminus of the oncoprotein. NB4 cells were treated with arsenic trioxide to compare the rates of degradation of PML-RARα and endogenous PML (**Figure 5.2.2.**). Western blotting performed with antibodies specific for PML and RARα demonstrated that both PML and the PML-

RARα fusion are post translationally modified at similar rates following arsenic treatment (**Figure 5.2.2., 0, 1, 4 hour time points**). Analysis after prolonged exposure to arsenic reveals similar degrees of degradation of endogenous PML isoforms and PML-RARα (**Figure 5.2.2., 12 hour time point**) which suggests that arsenic induced degradation of PML is not absolutely dependent on a sequence within the differentially spliced C- terminus of PML.

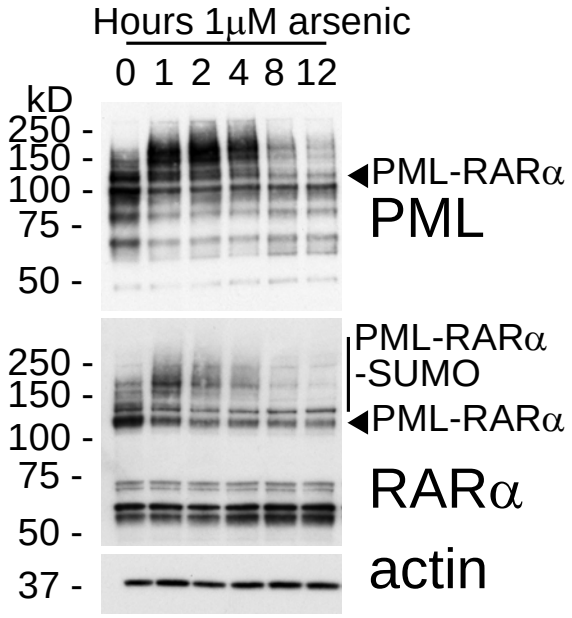

Figure 5.2.2. PML-RARα and PML degrade at similar rates following arsenic treatment

The NB4 acute promyelocytic leukaemia cell line which contains the PML-RARα fusion was treated with 1μM arsenic for 0, 1, 4, 8 and 12 hours prior to lysis. Whole cell extracts were analysed by western blotting with chicken anti PML, anti RARα and anti actin antibodies. The PML- RARα fusion protein is indicated by arrowheads.

5.2.3 Characterisation of cell lines expressing only a single PML isoform

To assess the role of the variable C- terminus of PML in determining response to arsenic treatment, six cell lines expressing only a single PML isoform were used. These cell lines were a kind gift from Roger Everett, MRC- University of Glasgow Centre for Virus Research, Glasgow, UK and were previously used to investigate the role of the various PML isoforms in repression of herpes virus replication (Cuchet et al., 2011). These cell lines were created using HepaRG hepatocytes (Gripon et al., 2002) which stably express a short hairpin RNA (shRNA) to deplete endogenous PML (Everett et al., 2008). Expression of a single eYFP PML isoform was then reconstituted at low levels using lentiviral transfection of a eYFP PML construct with expression from the HSV-1 gD gene promoter (Cuchet et al., 2011).

Initial experiments sought to characterise PML expression in these cell lines. Western blotting with an anti PML antibody demonstrated a different profile of PML species for each cell line, representing the expression of the various isoforms and their post translationally modified forms (**Figure 5.2.3., top panel**). Comparison of the PML antibody signal in the HALL lane with the HALP lane confirms the specificity of the chicken anti PML antibody, because HALP cells are depleted of PML. There was some variation in expression levels of the different isoforms, but none were hugely overexpressed when compared to endogenous PML expression (**Figure 5.2.3., cf. HALL with PML I- PML VI**). The profile of SUMO1 and SUMO2/3 conjugates did not vary significantly between cell lines (**Figure 5.2.3.**).

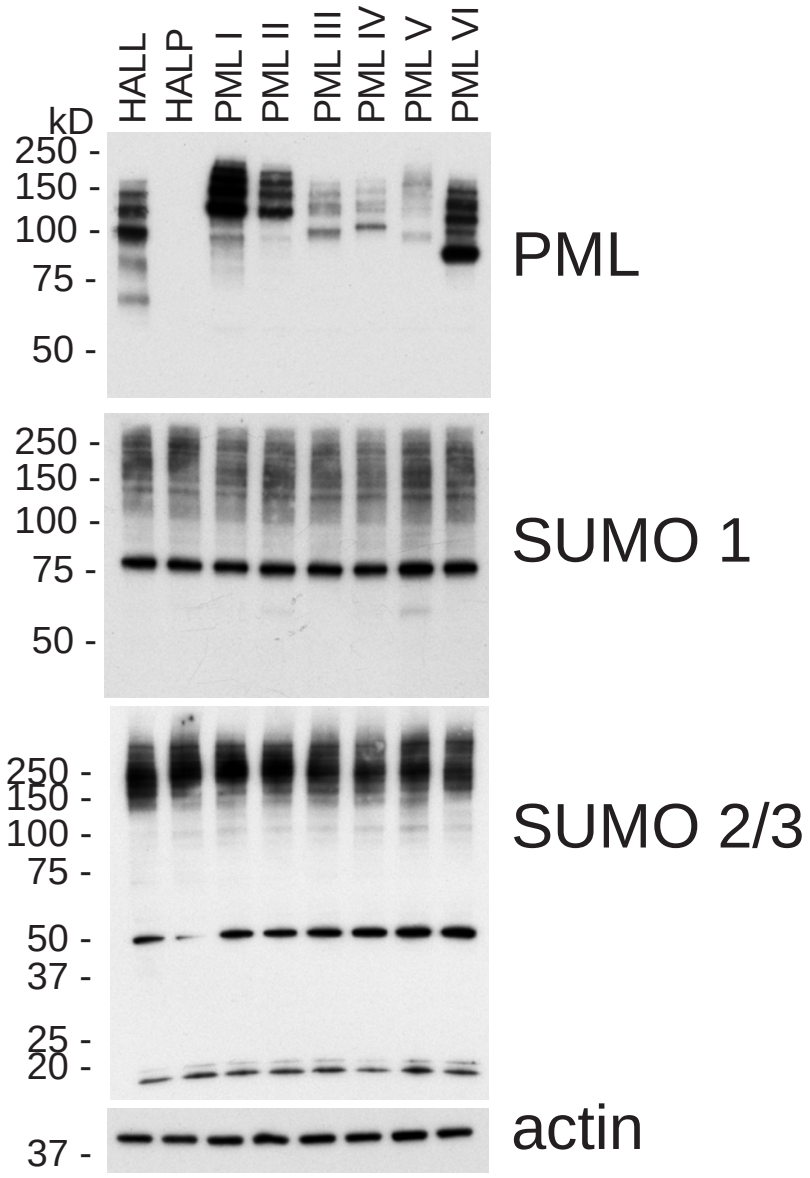

Figure 5.2.3. Western blotting of HepaRG cells expressing a single PML isoform

HepaRG cells stably expressing eYFP plus a control shRNA (HALL), eYFP plus an anti PML shRNA (HALP) or an anti PML shRNA plus a single shRNA resistant eYFP PML isoform fusion (PML I-PMLVI), were lysed and whole cell extracts analysed by western blotting with anti PML, anti SUMO1, anti SUMO2/3 and actin antibodies.

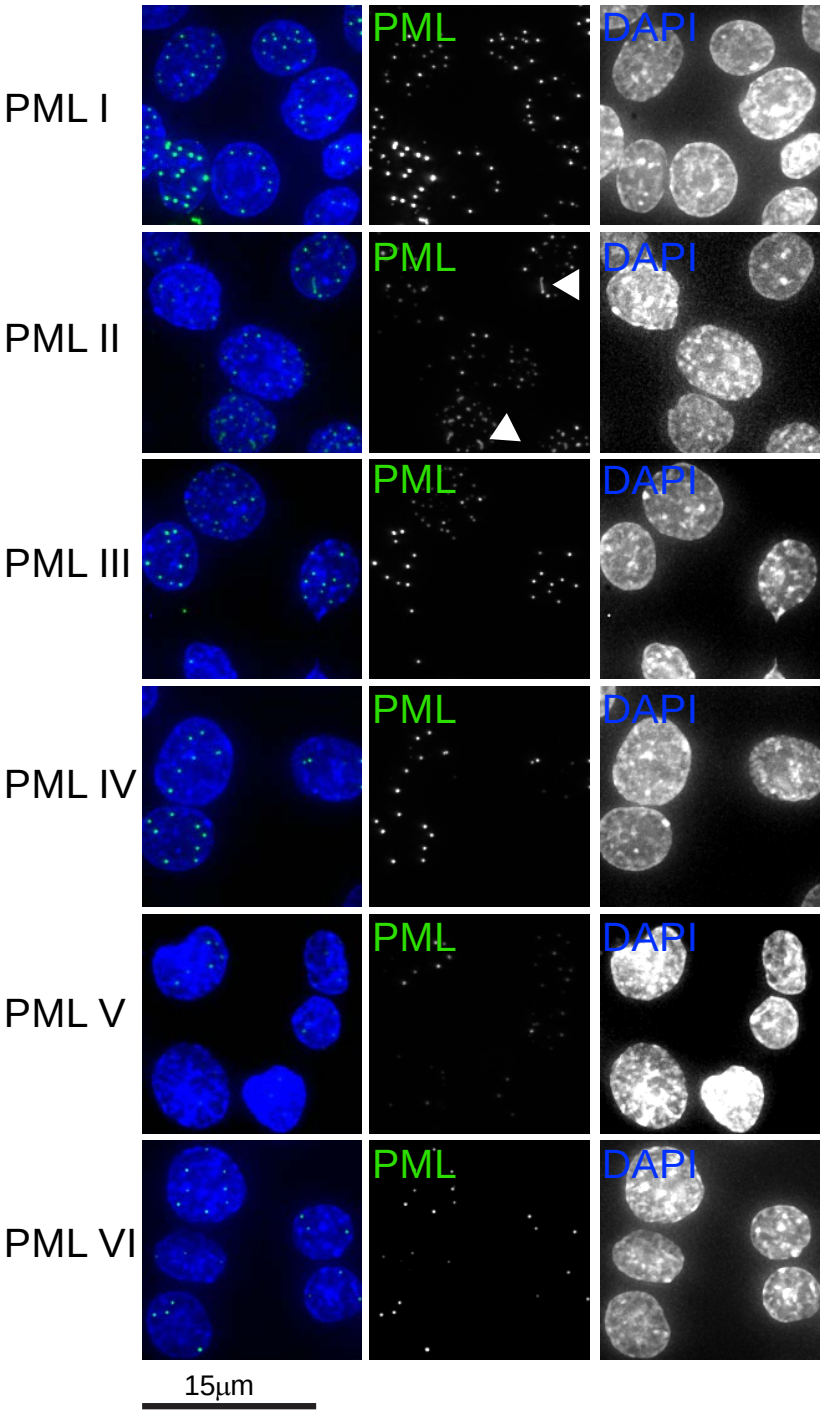

Figure 5.2.4. Fluorescence microscopy of HepaRG cells expressing a single PML isoform

HepaRG cells stably expressing an anti PML shRNA plus a single shRNA resistant eYFP PML isoform fusion were fixed and DNA stained with DAPI. Cells were then imaged by deconvolution microscopy. Images presented are maximal projections of multiple z- sections. eYFP PML is shown in green, DAPI in blue.

Cells were then examined by deconvolution microscopy (**Figure 5.2.4.**). Images obtained confirmed that all PML isoforms form PML nuclear bodies in the absence of other isoforms, presumably due to interaction between PML molecules of the same isoform. These images also demonstrated the differences in PML expression noted by western blotting in **Figure 5.2.3.** Cells expressing PML I had numerous, bright PML bodies, whereas cells expressing PML V had fewer, smaller PML bodies (**Figure 5.2.4.**). There were also some differences in the structure of PML nuclear bodies formed by the different PML isoforms. Analysis of cells expressing PML II revealed frequent cells displaying thread like structures of eYFP PML II (**Figure 5.2.4. arrowheads**), whereas cells expressing the other PML isoforms displayed punctate, round PML bodies. These data suggested that the variable C-terminus of PML influences interactions between PML molecules in the formation of PML nuclear bodies which in turn influences the structure of the PML bodies formed.

5.2.4 Characterisation of the response of individual PML isoforms to arsenic treatment

To assess the response of the different PML isoforms to arsenic treatment, cells expressing a single eYFP PML isoform were exposed to arsenic for various periods of time and whole cell extracts analysed by western blotting (**Figure 5.2.5.**). All of the PML isoforms analysed appeared to be post translationally modified in response to arsenic treatment, as demonstrated by a change in electrophoretic mobility of PML after one hour of arsenic exposure, with the appearance of high molecular weight PML species (**Figure 5.2.5.**). After twenty- four hours of arsenic treatment, some PML isoforms had degraded more than others. Treatment of PML IV resulted in the accumulation of high molecular weight PML species, but little or no apparent degradation. Conversely, PML V was efficiently degraded following arsenic treatment,

with almost no PML species identified after twenty- four hours arsenic exposure. PML I, II and VI displayed very similar patterns of response to arsenic treatment: they were initially modified, and these modified species were degraded, but there was reappearance of a major species that may represent the newly synthesised unmodified material that accumulates after twenty- four hours of treatment (**Figure 5.2.5.**).

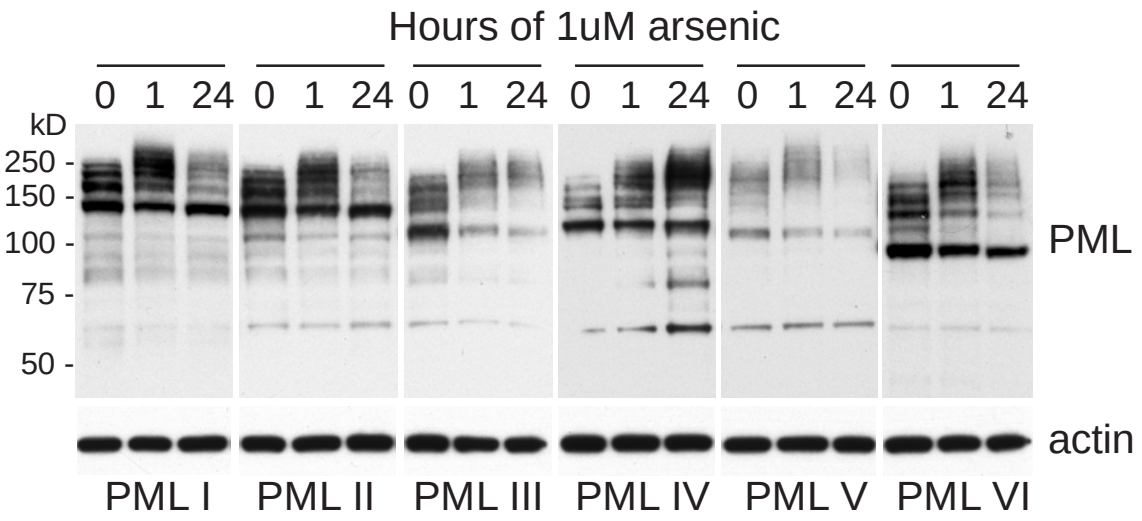

Figure 5.2.5. Western blotting of PML isoform expressing cells treated with arsenic

HepaRG cells stably expressing an anti PML shRNA plus a single shRNA resistant eYFP PML isoform fusion were treated with 1µM arsenic for 0, 1 or 24 hours prior to lysis. Whole cell extracts were analysed by western blotting with anti PML antibody and anti actin antibodies.

By exploiting the fact that these cells express a eYFP- linked PML isoform, deconvolution microscopy was employed to evaluate the subcellular localisation of the PML isoforms in response to arsenic. Immunofluorescence microscopy using an anti SUMO2/3 antibody reveals that SUMO2/3 colocalised with PML nuclear bodies in all cell lines in untreated cells (**Figure 5.2.6., panels A-F, 0 hour time point**). The initial response of all isoforms to arsenic treatment was similar.

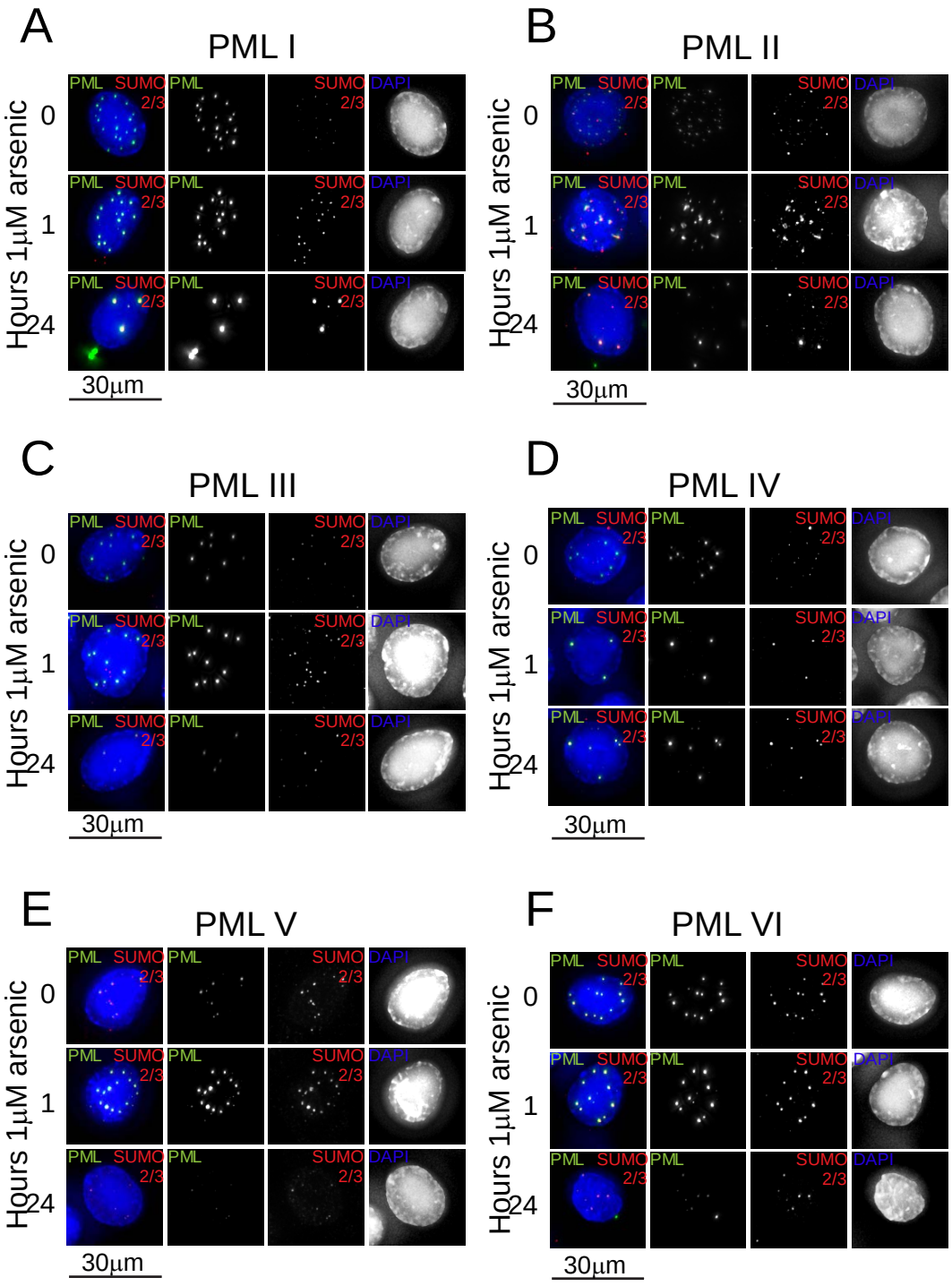

Figure 5.2.6. Immunofluorescence analysis of PML isoform expressing cells treated with arsenic

(A-F) HepaRG cells stably expressing an anti PML shRNA plus a single shRNA resistant eYFP-PML isoform fusion (PML I-PML VI) were treated with 1μM arsenic for 0, 1 or 24 hours prior to fixation with paraformaldehyde. Cells were then analysed by immunofluorescence using an anti SUMO2 antibody. eYFP PML is shown in green, SUMO2/3 in red and DAPI in blue. Images presented are maximal projections of multiple z- sections.

Following 1 hour of arsenic treatment, there was an increase in the number of PML nuclear bodies, and an increase in the amount of SUMO2/3 present at these PML bodies (**Figure 5.2.6., panels A-F, 1 hour time point**). This is consistent with the data presented in **Figure 5.2.5.** where an increase in high molecular weight PML species was demonstrated after 1 hour of arsenic treatment and suggests that at least part of this increase in molecular weight is due to SUMO modification. After 24 hours of arsenic treatment, differences in response became apparent. The number of PML bodies present was reduced following prolonged treated with arsenic, but PML I appeared to accumulate in fewer, larger PML bodies (**Figure 5.2.6., panel A**). PML I, II and VI accumulated in the cytoplasm following prolonged arsenic treatment. This cytoplasmic PML did not colocalise with SUMO2/3 suggesting that it had either been desumoylated or was newly synthesised and yet to be SUMO modified (**Figure 5.2.6., panels A, B and F, 24 hour time point**). It is possible that the reappearance of an apparently unmodified PML species noted in **Figure 5.2.5.** represents this non- SUMO modified cytoplasmic fraction. PML III and PML V appear to be efficiently degraded following prolonged arsenic treatment, with a decrease in the number and size of PML nuclear bodies observed, and no accumulation of PML in the cytoplasm (**Figure 5.2.6., panels C and E**). Consistent with the observation in **Figure 5.2.5.**, PML IV was not significantly degraded following arsenic treatment and accumulated in bright PML bodies which colocalise with SUMO2/3 (**Figure 5.2.6., panel D**).

5.2.5 High content imaging and quantification of YFP PML fluorescence

To quantify the differences identified in the response of the PML isoforms to arsenic, a high content imaging assay was developed to enable automated imaging and analysis of eYFP PML fluorescence. Cells were cultured in 96 well plates and treated

with arsenic for various lengths of time as indicated previously. Following fixation, cells were stained with DAPI and imaged using an IN Cell 2000 automated microscope. Resulting images were then analysed using an automated protocol designed to quantify the size, number and location of eYFP PML nuclear bodies or cytoplasmic inclusions (**Figure 5.2.7.**). This protocol identified clusters of pixels when eYFP intensity exceeded a given threshold above background intensity, and assigned these pixel clusters to the nucleus or cytoplasm based on whether they lay within the nucleus as defined by DAPI staining.

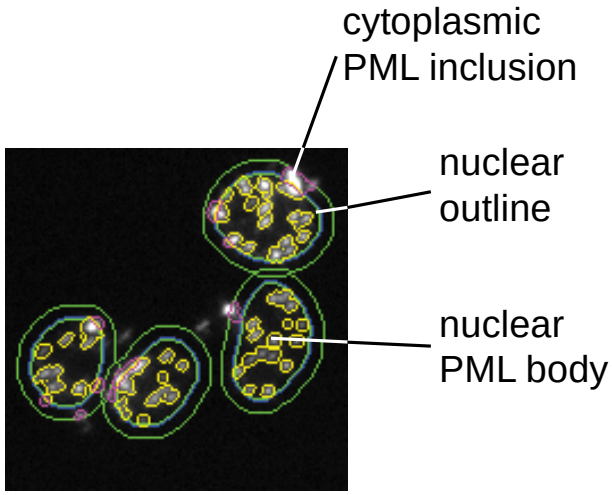

Figure 5.2.7. Screenshot of high content imaging analysis protocol

Cells cultured in 96 well plates were imaged using an IN Cell 2000 automated microscope, capturing images of eYFP and DAPI signal. Images were then analysed using IN Cell Investigator software with a protocol designed to identify PML nuclear bodies (yellow outlines) and PML cytoplasmic inclusions (pink outlines).

Analysis of the size of PML nuclear bodies and cytoplasmic inclusions demonstrated that the total area of the nucleus occupied by PML bodies decreased for all PML isoforms analysed except PML IV (**Figure 5.2.8., panels A-F, focus on panel D**). This decrease in PML body total area following 24 hours of arsenic treatment was statistically significant for isoforms PML I, II, V and VI. These data also confirmed the

cytoplasmic accumulation of PML noted in **Figure 5.2.6.**, with a two to four fold increase in the total area of cytoplasmic inclusions noted for PML I, II and VI over the course of a 24 hour arsenic treatment. PML V was readily degraded following arsenic treatment, with the nuclear PML body total area decreasing by two thirds following prolonged arsenic treatment **(Figure 5.2.8., panel E**), with no appearance of cytoplasmic PML.

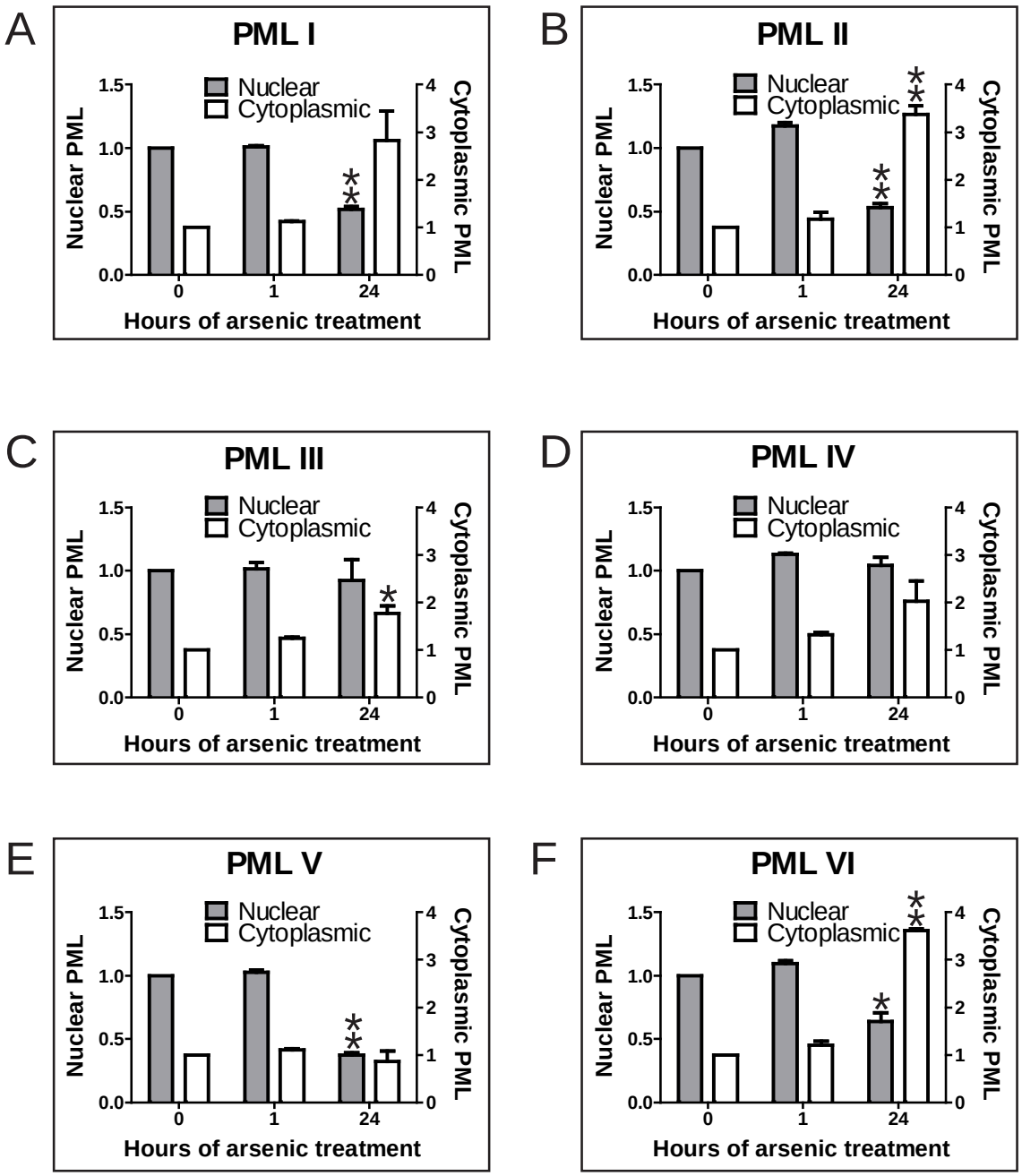

Figure 5.2.8. High content imaging and quantification of eYFP PML fluorescence following arsenic treatment: analysis of PML body size

(A-F) HepaRG cells stably expressing an anti PML shRNA plus a single shRNA resistant eYFP-PML isoform fusion (PML I-PML VI) were cultured in clear bottomed, black, 96 well plates prior to arsenic treatment for 0, 1 or 24 hours. Cells were then fixed and stained with DAPI prior to automated, high content imaging. Resulting images were analysed using an automated protocol (**Figure 5.2.7.**) to quantify the area of PML nuclear bodies or cytoplasmic inclusions. The sum of the area of all PML nuclear bodies or cytoplasmic inclusions per cell were averaged for all cells analysed at each time point. Data

was then normalised to the amount of nuclear or cytoplasmic PML present in untreated cells. Data presented represents the mean normalised total area of PML in the nucleus (grey bars, left y axis) or cytoplasm (unfilled bars, right y axis) at each time point, ± standard error of the mean. * $p<0.05$, ** $p<0.02$ students t test comparing 0 and 24 hour time points.

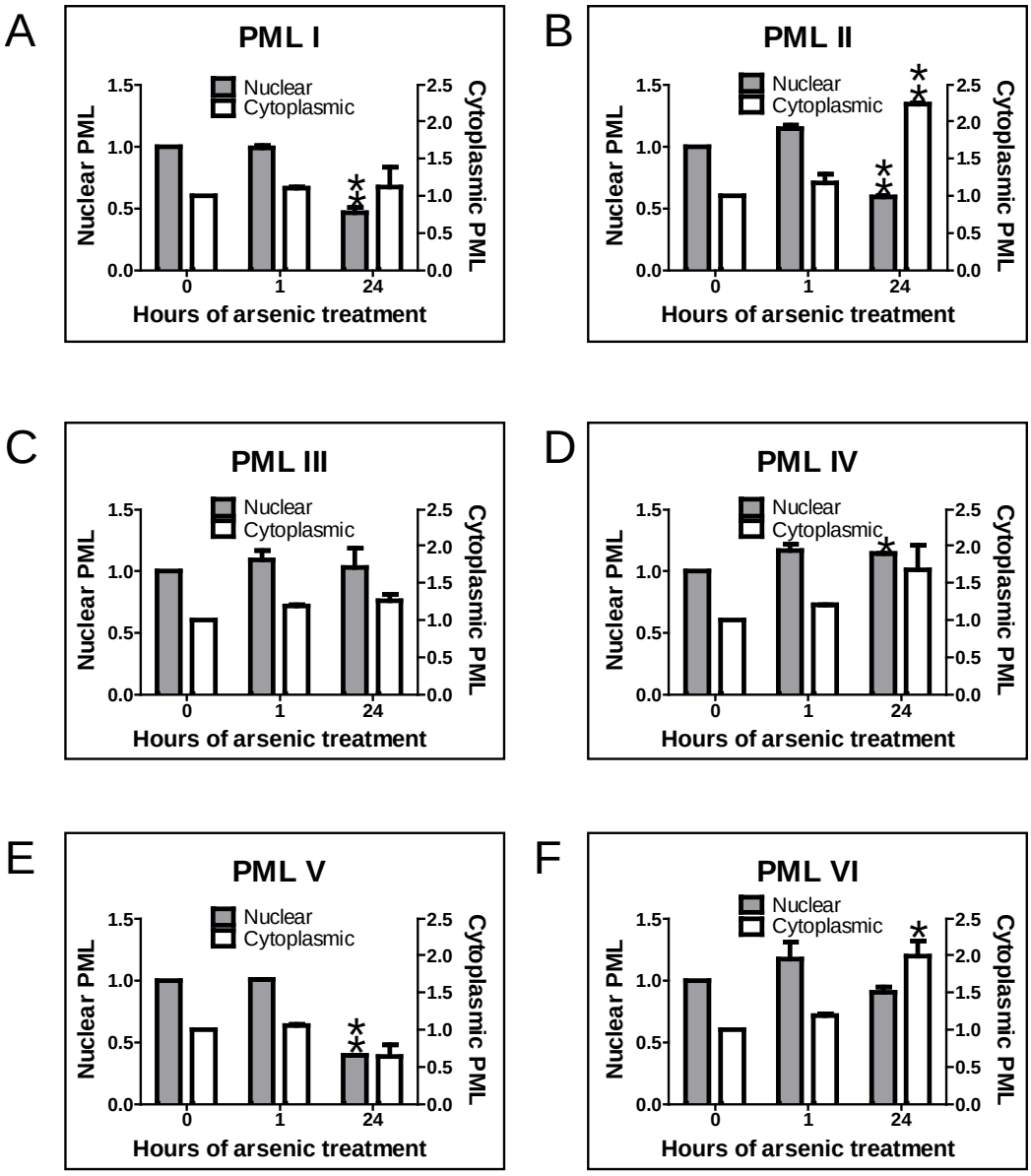

Figure 5.2.9. High content imaging and quantification of eYFP PML fluorescence following arsenic treatment: analysis of number of PML bodies per cell

(A-F) Cells were cultured, arsenic treated and imaged as in **Figure 5.2.8.**. Data were analysed using an automated protocol to count the number of PML nuclear bodies and cytoplasmic PML inclusions per cell, which was then averaged for all cells analysed for each time point. Data was then normalised to the number of PML nuclear bodies or cytoplasmic inclusions in untreated cells. Data presented represent the normalised mean number of PML nuclear bodies (grey bars, left y axis) and cytoplasmic inclusions (unfilled bars, right y axis) for each time point, ± standard error of the mean. * $p<0.05$, ** $p<0.02$ students t test comparing 0 and 24 hour time points

The number of PML nuclear bodies and cytoplasmic inclusions were also altered by arsenic treatment. Statistically significant decreases in the number of PML nuclear bodies present following 24 hours of arsenic treatment were quantified for PML I, II and V (**Figure 5.2.9., panels A, B and E**). Conversely, there was a statistically significant increase in the number of PML nuclear bodies present in cells expressing PML IV following the same treatment, again confirming PML IV to be the isoform most resistant to arsenic mediated degradation (**Figure 5.2.9., panel D**). Interestingly, the number of cytoplasmic inclusions in cells expressing PML I did not increase following arsenic treatment (**Figure 5.2.9., panel A**), demonstrating the increase in total area of cytoplasmic PML noted in **Figure 5.2.8., panel A** is due to the accumulation of a limited number of large cytoplasmic inclusions. On the other hand, the number of cytoplasmic inclusions counted in cells expressing PML II and PML VI increased two fold following arsenic treatment (**Figure 5.2.9., panel B and F**), suggesting the three fold increase in total cytoplasmic PML area noted in **Figure 5.2.8., panel B and F** was due to a combination of an increase both number and size of cytoplasmic inclusions.

5.2.6 Super resolution imaging reveals differences in PML body structure

As demonstrated in Figure 5.2.4. and 5.2.6., the individually expressed PML isoforms form PML nuclear bodies, and these are associated with SUMO modification. Previous work has investigated the structure of PML nuclear bodies. Electron microscopy with immunolabelling revealed PML bodies to be ring shaped (Boisvert et al., 2000; Koken, 1994; Lallemand-Breitenbach et al., 2001) and more recent work using high resolution microscopy (Hattersley et al., 2011; Lang et al., 2010) confirmed PML bodies to consist of a spherical shell of PML, with SUMO1 and SUMO2/3 found

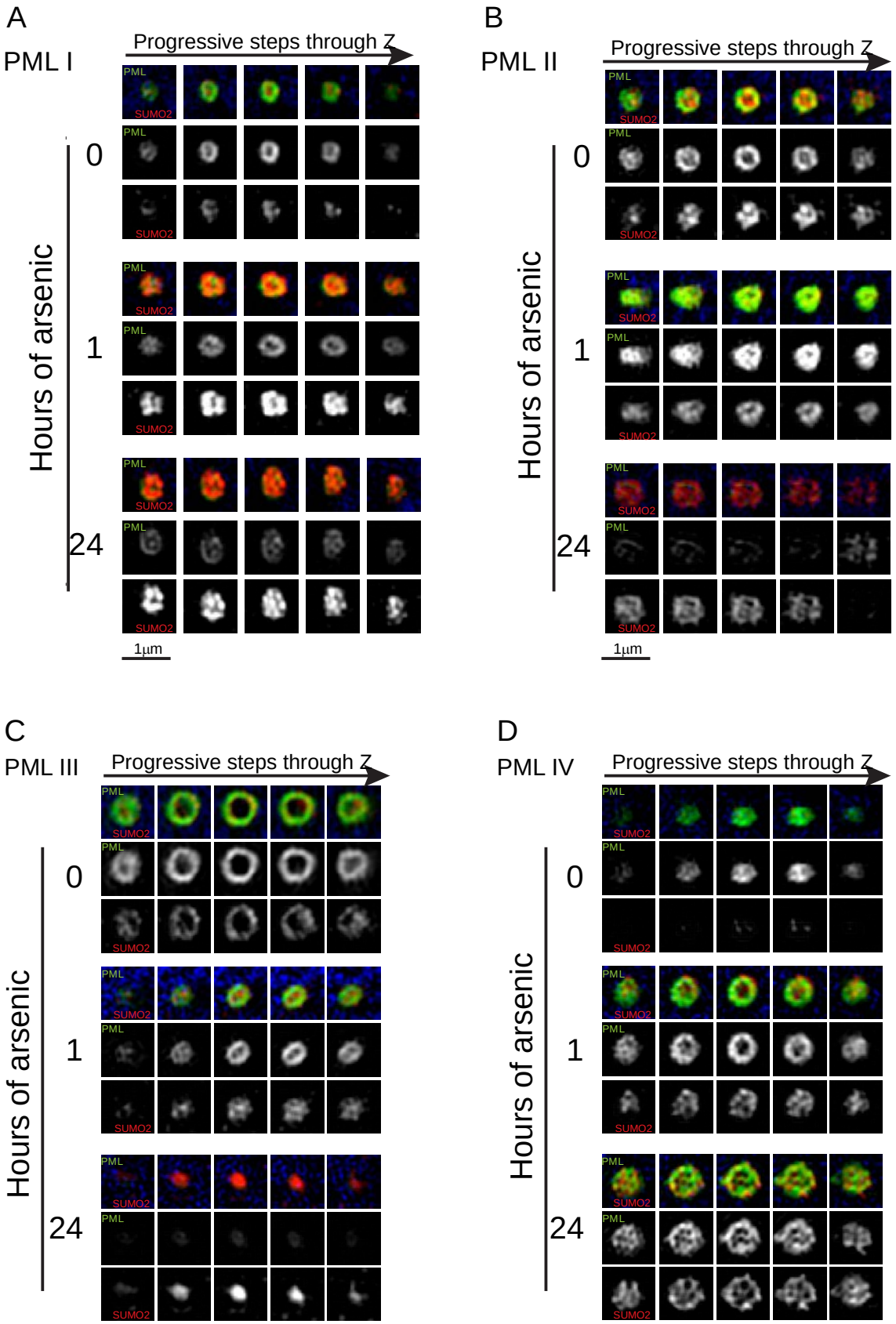
A
PML I
Progressive steps through Z
Hours of arsenic
0
1
24
PML
SUMO2
1µm
B
PML II
Progressive steps through Z
Hours of arsenic
0
1
24
PML
SUMO2
1µm
C
PML III
Progressive steps through Z
Hours of arsenic
0
1
24
PML
SUMO2
D
PML IV
Progressive steps through Z
Hours of arsenic
0
1
24
PML
SUMO2

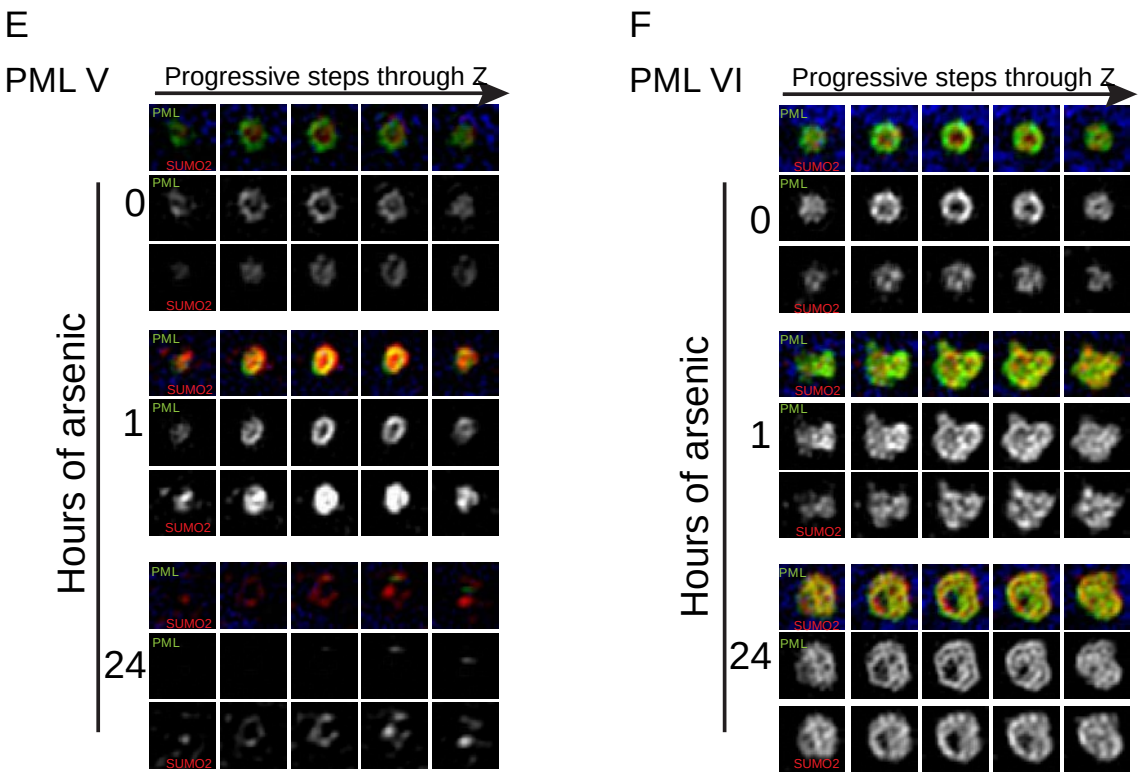

Figure 5.2.10. Super- resolution imaging of PML isoform expressing cells treated with arsenic

(A-F) HepaRG cells stably expressing an anti PML shRNA plus a single shRNA resistant eYFP-PML isoform fusion (PML I-PML VI) were treated with 1µM arsenic for 0, 1 or 24 hours prior to fixation with paraformaldehyde. Cells were immunolabelled using an anti SUMO2/3 antibody and a fluorescently labelled anti sheep secondary antibody. Cells were then analysed by structured illumination. eYFP PML is shown in green, SUMO2/3 in red and DAPI in blue. Images presented are progressive z sections though a representative PML nuclear body.

predominantly interspersed within the PML shell and in the central core of the PML body respectively. The structure of the PML bodies formed by the individual isoforms and the changes in structure induced by arsenic treatment was investigated using 3-dimensional structured illumination microscopy (3D SIM) to obtain super- resolution images. The images confirmed that all PML isoforms form nuclear bodies consisting of hollow, near spherical shells of PML and that SUMO2/3 is associated with these shells (**Figure 5.2.10., panels A-F**). However, the location of SUMO2/3 in relation to PML

differed between isoforms. In untreated cells, SUMO2/3 was found in the central core of PML bodies formed by PML I, II and V consistent with previous reports, but SUMO2/3 was incorporated into the PML outer shell of the nuclear bodies formed by PML III (**Figure 5.2.10., panel C**). PML VI nuclear bodies had SUMO2/3 in both locations (**Figure 5.2.10., panel F**). Following 1 hour of arsenic treatment, there was an increase in SUMO2/3 associated with all PML isoforms, but this was particularly marked in cells expressing PML I and V, where there was accumulation of SUMO2/3 associated with the outer shell of PML as well as in the central core (**Figure 5.2.10., panels A and E**). The most dramatic changes in nuclear body structure were seen after 24 hours of arsenic treatment. Nuclear bodies were still visible as essentially spherical structures consisting of PML and SUMO2/3, but the well defined outer shell of PML was no longer seen in cells expressing PML I, II, IV or VI. Rather, PML was present both in the outer part of and within the central area of the nuclear body and was seen to closely localise with SUMO2/3. Interestingly, in cells expressing PML V, the PML was efficiently degraded after twenty four hours of arsenic treatment but the remnants of PML nuclear bodies could be identified by a spherical hollow shell of SUMO2/3. This may represent a tiny fraction of very heavily SUMO2/3 modified PML, below the limit of detection of eYFP- fluorescence or SUMO modification of another component of the nuclear body, for example SP100.

When structured illumination was used to analyse the cytoplasmic inclusions of PML I following twenty four hours of arsenic treatment, it was apparent that these did not have the spherical structure of PML nuclear bodies (**Figure 5.2.11.**). Rather, these appeared to consist of a disordered mass of eYFP PML with no associated SUMO 2/3.

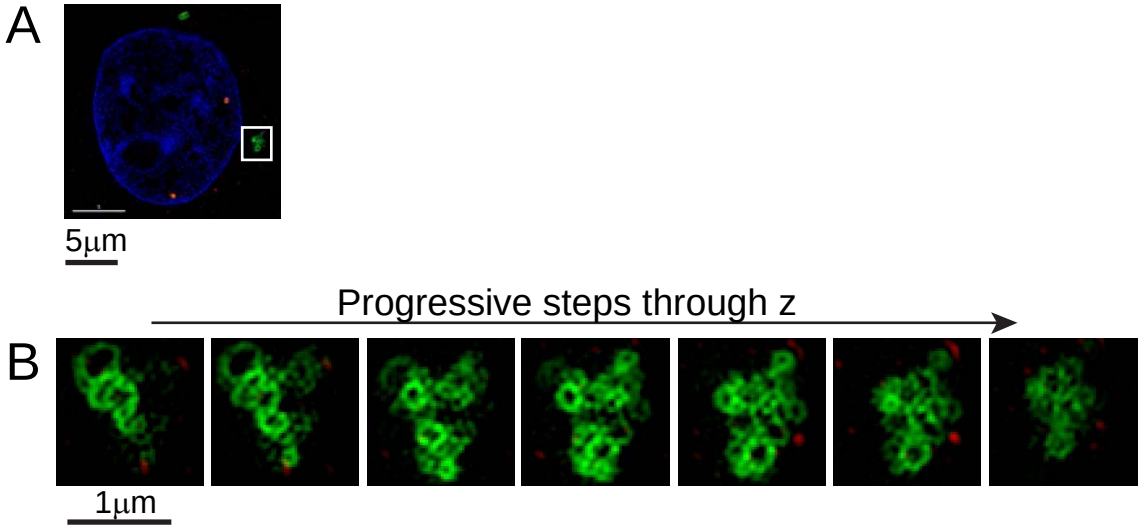

Figure 5.2.11. Super resolution imaging of cytoplasmic PML inclusions following arsenic treatment

(A) HepaRG cells stably expressing an anti PML shRNA plus an shRNA resistant eYFP-PML I fusion were treated with arsenic for 24 hours prior to fixation and immunolabelling with an SUMO2/3 antibody. Cells were analysed by structured illumination. eYFP PML Is shown in green, SUMO2/3 in red and DAPI in blue.

(B) Magnification of area outlined by white box in **(A)**. Images presented are progressive z sections through a representative cytoplasmic PML I inclusion.

5.2.7 All PML isoforms are SUMO and ubiquitin modified following arsenic treatment

The appearance of high molecular weight PML species following arsenic treatment seen for all isoforms examined (**Figure 5.2.5.**) suggested that all are post-translationally modified in response to arsenic treatment. Immunofluorescence experiments confirmed an increase in co-localisation of PML and SUMO2/3 following arsenic treatment (**Figure 5.2.6.**), suggesting each isoform is SUMO modified in response to arsenic treatment. To biochemically characterise the post- translational modifications of the PML isoforms, eYFP PML and its conjugates were immunoprecipitated from each of the isoform expressing cell lines after varying exposures to arsenic trioxide. The data presented in **Figure 5.2.12.** demonstrates that all isoforms were modified with SUMO1, SUMO2/3 and ubiquitin in response to arsenic treatment, although substantial differences between isoforms were noted. While it was difficult to compare the amount of SUMO modification between isoforms due to differences in PML expression levels, it was possible to analyse the differences in modification for any given isoform at different time points after arsenic treatment. While PML I, II and V showed a low level of SUMO2/3 modification (Figure **5.2.12., panels A, B and E**), PML III, IV and VI were essentially unmodified prior to arsenic treatment (**Figure 5.2.12., panels C, D and F**). In untreated cells, SUMO1 and SUMO2/3 modification of PML I and II was manifest as a number of distinct species, whereas SUMO modification of PMLV was apparent as a high molecular weight smear, suggesting it may be modified with polymeric SUMO chains.

There was a marked increase in SUMO1, and even more substantial increase in SUMO2/3 modification of PML I after one hour of arsenic treatment (**Figure 5.2.12. panel A**).

Figure 5.2.12. GFP immunoprecipitation confirms all PML isoforms are SUMO and ubiquitin modified in response to arsenic

(A-F) HepaRG cells stably expressing an anti PML shRNA plus a single shRNA resistant eYFP-PML isoform fusion (PML I-PML VI) were treated with 1μM arsenic for 0, 1 or 24 hours prior to lysis under conditions to maintain SUMO modification. eYFP PML was then immunoprecipitated from whole cell extracts and bound proteins eluted and analysed by western blotting with anti PML, anti SUMO1, anti SUMO2 and anti ubiquitin antibodies.

A very similar pattern was seen for PML II and PML VI (**Figure 5.2.12. panels B and F**). The increase in SUMO modification appeared slower for other isoforms, with the most marked SUMO1 and SUMO2/3 modification of PML III and PML IV taking place after 24 hours of arsenic treatment (**Figure 5.2.12. panels C and D**). Given that there was a decrease in the amount of eYFP PML I, II and III immunoprecipitated after 24 hours of arsenic treatment, the fact there was substantially more SUMO1 and SUMO2/3 co-immunoprecipitated at this time point suggests that this small amount of PML is extensively SUMO modified (**Figure 5.2.12. panels A, B and C**). Data in Figures 5.2.5., 5.2.6. and 5.2.8. identified PML IV as relatively stable in the presence of arsenic trioxide. The GFP- IP data (**Figure 5.2.12. panel D**) demonstrated that PML IV is modified by both SUMO1 and SUMO2/3 in response to arsenic. There was an increase in ubiquitin modification of PML IV after twenty four hours of arsenic treatment, but no decrease in the amount of eYFP PML IV immunoprecipitated, suggesting that despite ubiquitin modification, the protein is not efficiently degraded by the proteasome.

5.2.8 The effect of RNF4 depletion on arsenic mediated degradation of PML isoforms I-VI

Having confirmed that all PML isoforms studied are SUMO and ubiquitin modified in response to arsenic treatment, the effects of depletion of the SUMO specific ubiquitin E3 ligase RNF4 on the response of the different isoforms to arsenic was investigated. A pool of siRNAs was used to efficiently deplete cells of RNF4, prior to arsenic treatment. The fate of each PML isoform was then monitored by western blotting and immunofluorescence, and eYFP PML fluorescence was quantified using a high content imaging assay, modified such that cells were transfected with siRNA in 96 well plates prior to arsenic treatment. High content imaging was performed as described previously in the siRNA screening experiments discussed in Chapters 3 and 4 of this thesis.

RNF4 depletion prior to arsenic treatment resulted in the accumulation of high molecular weight PML species for all isoforms examined (**Figure 5.2.13., panels A and D, Figure 5.2.14., panels A and D, and Figure 5.2.15., panels A and D)**, which suggests that, indeed, RNF4 is required for ubiquitylation and subsequent degradation of each of the PML isoforms. When cells were examined by fluorescence microscopy, it was apparent that this accumulation of PML was within PML nuclear bodies, which are demonstrated to be larger and brighter following RNF4 depletion and arsenic treatment (**Figure 5.2.13., panels B and E, Figure 5.2.14., panels B and E, and Figure 5.2.15., panels B and E**). This was confirmed by quantification of eYFP PML fluorescence (**Figure 5.2.13., panels C and F, Figure 5.2.14., panels C and F, and Figure 5.2.15., panels C and F**).

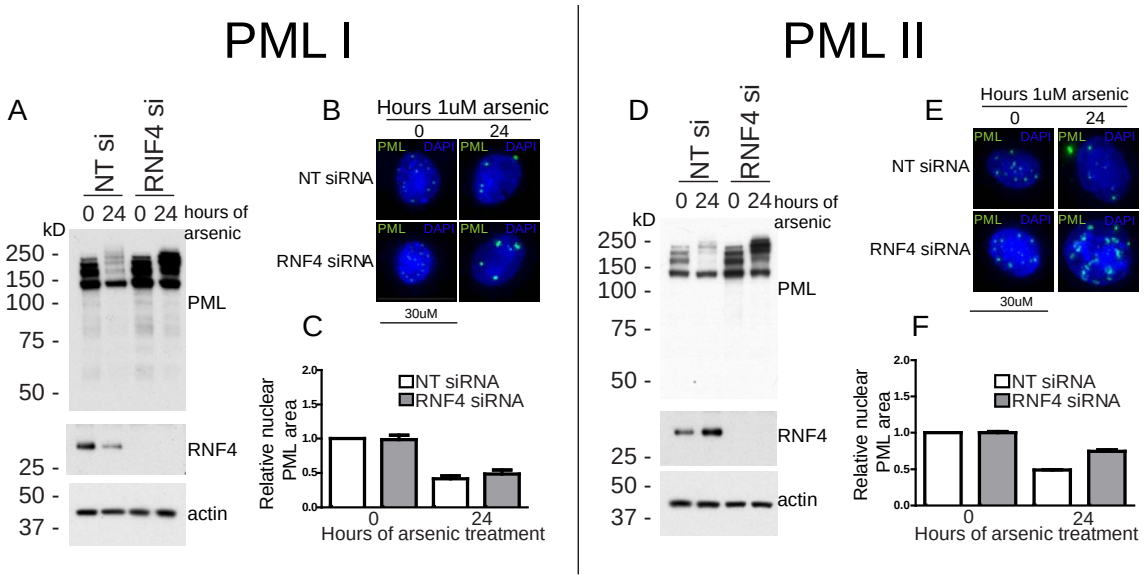

Figure 5.2.13. Effect of RNF4 depletion on the response of PMLI and PML II to arsenic treatment

(A, D) HepaRG cells stably expressing an anti PML shRNA plus either eYFP PML I (A) or eYFP PML II (D) were transfected with a pool of 4 siRNAs targeting RNF4 or a non targeting control siRNA. 48 hours after transfection cells were treated with arsenic for 0 or 24 hours. Whole cell extracts were then separated by SDS-PAGE and analysed by western blotting. RNF4 depletion was confirmed by immunoblotting with an anti RNF4 antibody.
(B, E) HepaRG cells stably expressing an anti PML shRNA plus either eYFP PML I (B) or eYFP PML II(E) were transfected with a pool of 4 siRNAs targeting RNF4 or a non targeting control siRNA. 48 hours after transfection cells were treated with arsenic for 0 or 24 hours. Cells were fixed and stained with DAPI prior to imaging by deconvolution microscopy. Representative mages are presented as maximal intensity projections of multiple z- sections.
(C, F) HepaRG cells stably expressing an anti PML shRNA plus either eYFP PML I(C) or eYFP PML II(F) were transfected with a pool of 4 siRNAs targeting RNF4 or a non targeting control siRNA in 96 well plates. 48 hours later, cells were treated with arsenic for 0 or 24 hours prior to fixation and DAPI staining. High content imaging was then performed and the resulting images were analysed using an automated protocol to quantify the size of PML nuclear bodies. The sum of the area of all nuclear bodies per cell was averaged for each condition and normalised to control siRNA transfected cells at the 0 hour time point. Normalised data are presented as the mean ± the standard error of the mean of data from two experiments.

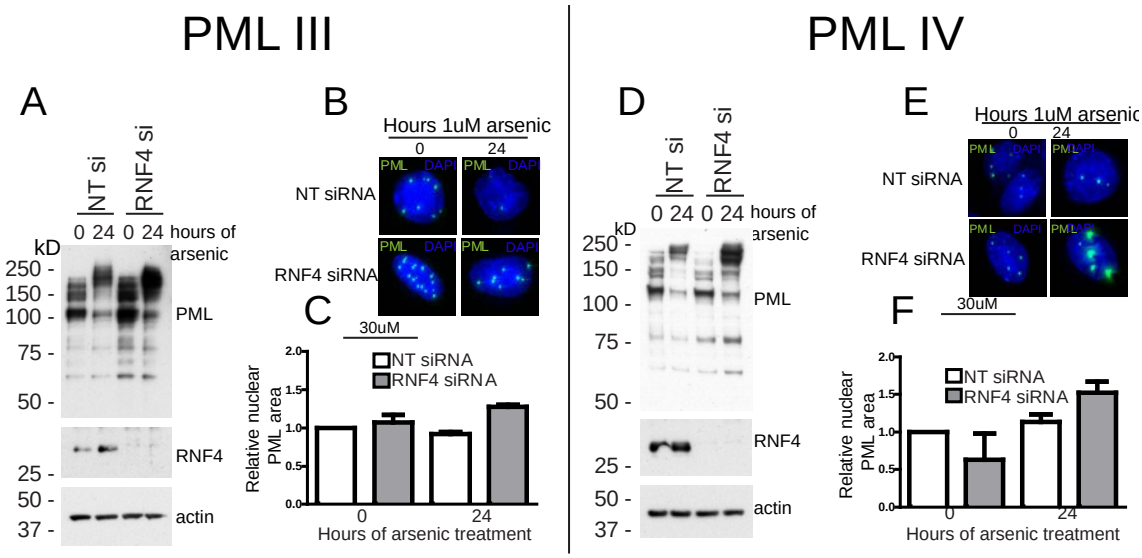

Figure 5.2.14. Effect of RNF4 depletion on the response of PML III and PML IV to arsenic treatment

(A- F) Experiments were performed as in Figure 5.2.13, but cells expressing eYFP PML III or eYFP PML IV were used.

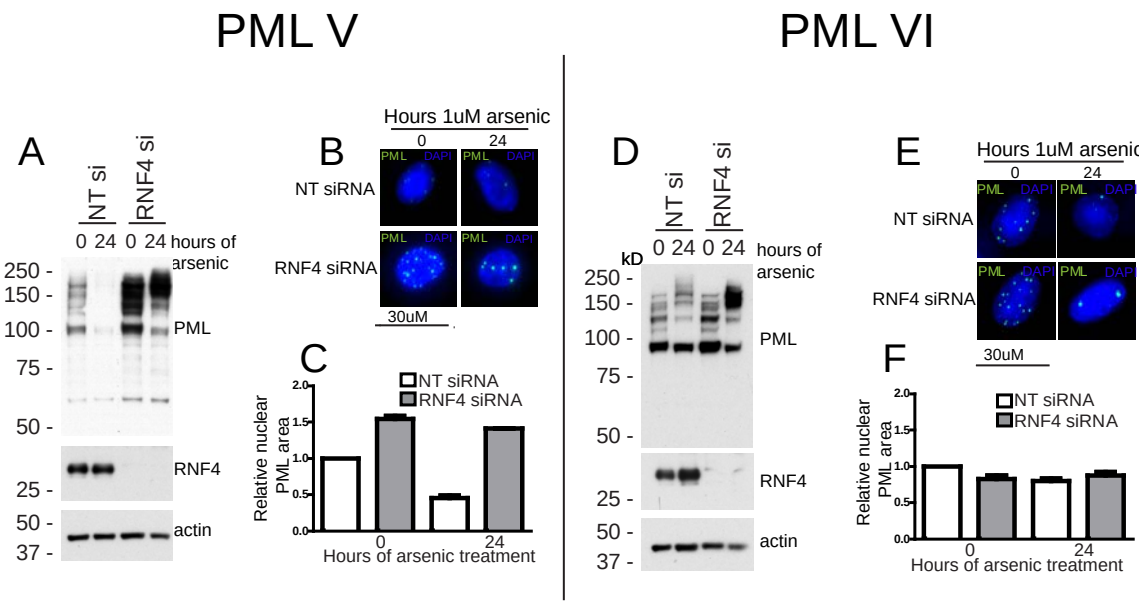

Figure 5.2.15. Effect of RNF4 depletion on the response of PML V and PML VI to arsenic treatment

(A- F) Experiments were performed as in Figure 5.2.13, but cells expressing eYFP PML V or eYFP PML VI were used.

The most striking observations were made when cells expressing PML V were depleted of RNF4 prior to arsenic treatment. Marked accumulation of PML V was observed following RNF4 depletion alone (**Figure 5.2.15, panels A-C**), which suggests PML V is subject to ubiquitylation by RNF4 and subsequent proteasomal degradation under basal conditions. This may account for the relatively low levels of PML V expression seen in untreated cells, and is also consistent with the observation that PML V is the most efficiently degraded isoform in response to arsenic treatment, because it appears to be a particularly good substrate for RNF4.

5.2.9 Conclusions

The contribution of the variable C- terminus of the various PML isoforms to the response of an individual PML isoform to arsenic trioxide treatment was investigated using a series of cell lines which express only a single PML isoform, thus allowing evaluation of the response of a single isoform in isolation. Western blotting demonstrated an accumulation of high molecular weight PML species for all isoforms shortly after arsenic treatment, suggesting all are post translationally modified in response to arsenic exposure. Following longer arsenic treatment, PML V was confirmed to be readily degraded whereas PML IV was not. Immunofluorescence experiments confirmed that all isoforms form PML nuclear bodies in the absence of other isoforms, and that SUMO2/3 colocalises with these PML nuclear bodies. Following arsenic treatment, this colocalisation was increased, suggesting all isoforms are modified with SUMO2/3 following arsenic treatment. PML I, II and VI were demonstrated to accumulate in the cytoplasm following arsenic treatment.

Quantification of changes in YFP PML fluorescence after arsenic treatment was performed using a high content imaging assay, which confirmed degradation of nuclear

PML for all isoforms except PML IV, and a two to four fold increase in cytoplasmic PML following arsenic treatment for PML I, II and VI.

Immunoprecipitation of YFP PML isoforms and their conjugates following arsenic treatment demonstrated that all are SUMO1, SUMO2/3 and ubiquitin modified after arsenic treatment, but that there is variation in the kinetics of this response. Finally, the effect of RNF4 depletion on the response to arsenic of the PML isoforms was evaluated using RNA interference. These experiments confirmed the requirement of RNF4 for arsenic induced degradation of each of the PML isoforms tested, because in the absence of RNF4, PML accumulated in large PML nuclear bodies following arsenic treatment. These accumulated PML species were confirmed to be high molecular weight species by western blotting, consistent with accumulation of SUMO modified PML. Cells expressing PML V showed a particularly dramatic phenotype following RNF4 depletion, with accumulation of PML V in the absence of arsenic treatment, suggesting PML V is constantly degraded in an RNF4 dependent manner in cells under basal conditions.

5.3 Discussion

5.3.1 Characterisation of the response of the major PML isoforms to arsenic treatment

SUMO dependent, ubiquitin mediated proteolysis of the PML-RARα fusion protein is responsible for cure in Acute Promyelocytic Leukaemia (Lallemand-Breitenbach et al., 2008; Tatham et al., 2008). Six major nuclear PML isoforms, PML I-VI are expressed as a result of alternative splicing of the primary PML transcript. These isoforms share a common N- terminal region, encoded by exons 1-6, but express unique C- termini (Jensen et al., 2001a). The response of endogenous PML isoforms II, III, IV and V to arsenic was assessed using isoform specific antibodies (Condemine et al., 2006). All isoforms were identified to degrade to similar extent following arsenic treatment. By examining endogenous PML isoforms, the response of a single isoform to arsenic cannot be clearly ascertained, because interactions between different isoforms may influence this process. To avoid such inter-isoform interactions, and allow investigation of the role of the unique C- terminal region in the response of individual PML isoforms to arsenic treatment, cell lines expressing only a single YFP- linked PML isoform (Cuchet et al., 2011) were treated with arsenic. The fate of PML isoforms was then monitored using western blotting, fluorescence microscopy and super resolution microscopy. The data presented in this thesis therefore represents the first comprehensive characterisation of the response of the individual PML isoforms to arsenic treatment.

5.3.2 Susceptibility to arsenic mediated degradation

It is now well established that PML undergoes proteasomal degradation in response to arsenic treatment (Lallemand-Breitenbach et al., 2008; Tatham et al., 2008).

The NB4 cell line examined in this study expresses the longest PML-RARα isoform, bcr1 (**Figure 1.4.1.**). The PML breakpoint in this PML-RARα isoform is within intron 6 and therefore exons 1-6 are encoded. This is equivalent to the common N-terminal region expressed by all PML isoforms examined in this study. Like PML VI, PML-RARα lacks the PML SIM domain. The C terminal region of PML-RARα is encoded by exons 3- 9 of RARα. This region includes the DNA binding, hormone binding and RXR binding motifs. PML-RARα was efficiently degraded in response to arsenic (Figure 5.2.2.). This demonstrates that none of the elements encoded within the RARα portion of PML-RARα interfere with this process, and also that no single element encoded within exons 7-9 of PML is absolutely required for arsenic induced degradation to take place.

Western blotting of endogenous PML after arsenic treatment revealed PML species that were relatively resistant to arsenic induced degradation, suggesting that different PML isoforms may respond differently to arsenic treatment (**Figure 5.2.1.**). Subsequent arsenic treatment of cells expressing only an individual PML isoform confirmed this hypothesis. PML IV was found to be relatively resistant to arsenic treatment, while PML V was very readily degraded (**Figures 5.2.5.**). Western blotting analysis of PML IV after prolonged arsenic treatment demonstrates the accumulation of high molecular weight PML species. This suggests PML IV is SUMO modified in response to arsenic treatment but that this modification fails to trigger degradation. Fluorescence microscopy demonstrates PML IV to accumulate in PML-NBs after arsenic treatment (**Figure 5.2.6.**). This is consistent with previous reports that degradation of PML takes place in PML-NBs (Geoffroy et al., 2010; Lallemand-Breitenbach et al., 2001). Immunoprecipitation analysis demonstrates PML IV is SUMO and ubiquitin modified following arsenic treatment (**Figure 5.2.12., panel D**). It is not therefore clear why degradation does not take place. One explanation is that

PML-NBs formed by PML IV may fail to recruit proteasomal subunits demonstrated to be recruited to PML-NBs after arsenic treatment (Lallemand-Breitenbach et al., 2001), thus preventing degradation. This would not be identified using a system in which PML IV was expressed with a background of endogenous PML expression (Condemine et al., 2006). Alternatively, PML IV may be ubiquitylated with ubiquitin chains other than Lys48 linked chains, for example Lys63 chains which would not target PML IV for degradation.

5.3.3 Localisation of PML after arsenic treatment

High content imaging was used to quantify YFP-PML fluorescence for each isoform after arsenic treatment (**Figure 5.2.8.**). PML is rapidly targeted to PML-NBs after arsenic treatment, where it accumulates in large PML-NBs if RNF4, the ubiquitin E3 ligase required for arsenic induced degradation of PML is depleted (Geoffroy et al., 2010; Lallemand-Breitenbach et al., 2008; Tatham et al., 2008). An assay was therefore developed to measure the size of PML-NBs as a measure of degradation, and also the size of any cytoplasmic inclusions of PML. This confirmed the differences in susceptibility of the different isoforms to arsenic treatment, with PML IV the least degraded after 24 hours of arsenic (**Figure 5.2.8., panel D**). The localisation of PML following arsenic treatment also differs between isoforms, with PML I, II and VI accumulating in the cytoplasm after prolonged arsenic treatment (**Figure 5.2.8., panels A, B and F**). A recent report (Lång et al., 2012) described the formation of cytoplasmic accumulations of PML and nucleoporins (CyPNs) following arsenic treatment in cells overexpressing PML I, both on a background of endogenous PML and in cells depleted of PML. Here, we identify formation of PML cytoplasmic inclusions for three of the six PML isoforms examined (**Figure 5.2.6. and Figure 5.2.8., panels A, B and F**). PML I, II and VI found in cytoplasmic foci following arsenic treatment did not appear to be

SUMO modified, because immunofluorescence analysis shows no colocalisation of SUMO2/3 with PML in these foci (**Figure 5.2.6.**). This was described for CyPNs reported previously (Jul-Larsen et al., 2009; Lång et al., 2012). The sequence of PML VI is common to all isoforms (Jensen et al., 2001a). It is therefore interesting that it localises differently to PML III, IV and V in response to arsenic treatment. This suggests that elements encoded by the C- terminal regions of PML III, IV and V preclude CyPN formation, whereas the C- terminal regions of PML I and II do not.

The function of CyPNs is not currently clear. In untreated cells, CyPNs appear following mitosis and gradually disappear as PML-NBs are reformed in G1 phase. This suggests PML is recycled from one generation to the next via storage in CyPNs. In contrast, when cells are treated with arsenic these CyPNs are stabilised and PML-NBs do not reform (Lång et al., 2012). This suggests PML translocation from cytoplasm to nucleus is impaired following arsenic treatment. The cytoplasmic PML isoform, PML VII, has previously been demonstrated to be required for transforming growth factor beta (TGFβ) signalling (Lin et al., 2004). A proportion of PML localises to the endoplasmic reticulum and mitochondrial associated membranes where it regulates cell survival by modulating calcium ion transport, thus regulating apoptosis (Giorgi et al., 2010). It is not clear whether arsenic induced cytoplasmic accumulation of PML I, II and VI contributes to these cytoplasmic functions of PML, or whether the sequestration exerts effects by preventing nuclear PML functions which are specific to these isoforms.

5.3.4 Differences in PML body structure

The structure of PML-NBs has previously been investigated using electron microscopy (Boisvert et al., 2000; Koken, 1994; Lallemand-Breitenbach et al., 2001) and more recently using high resolution microscopy (Hattersley et al., 2011; Lang et al., 2010). These studies demonstrated PML to form a spherical shell around a central core

which contains SUMO2. In contrast, in APL, the structure of PML-NBs is disrupted and vast numbers of small nuclear speckles are identified by immunofluorescent staining with an anti PML antibody (Daniel et al., 1993). Each of the individually expressed PML isoforms examined in this thesis formed PML-NBs. Differences in the structure of these PML-NBs was observed using deconvolution microscopy. PML II was noted to form thread like structures as well as punctate PML-NBs. This is in keeping with a previous report in which PML II was stably expressed in PML-/- cells (Condemine et al., 2006). The other PML isoforms formed punctate PML-NBs, all of which colocalised with SUMO2 by immunofluorescence. PML body formation was previously demonstrated to require both sumoylation of PML (Lallemand-Breitenbach et al., 2001) and the SIM domain of PML (Shen et al., 2006), which is encoded within exon 7a, and is therefore present in PML I-V but not PML VI. The current data therefore suggest the SIM is dispensable for PML-NB formation because PML VI forms PML-NBs which appear structurally similar to those formed by the other isoforms examined, with a near spherical outer shell of PML. The presence or absence of other PML-NB constituent proteins at PML-NBs formed by PML VI has not been assessed by this study but previous work reported robust Sp100, Daxx and ATRX colocalisation at PML-NBs formed by PML VI (Cuchet et al., 2011). A number of PML body components have SIM domains, and PML VI is sumoylated (**Figure 5.2.12.**). PML-NB formed by PML VI may therefore rely on interactions between the SIM of PML-NB components with SUMO modified PML VI.

To further investigate the structure of PML-NBs, 3D structured illumination microscopy was employed to obtain high resolution images of PML-NBs before and after arsenic treatment. This demonstrated that nuclear bodies formed by all isoforms consist of a spherical shell of PML, and are associated with SUMO2. The distribution of SUMO2 differed between isoforms. Consistent with previous reports (Hattersley et al.,

2011; Lang et al., 2010), SUMO2/3 was found in the central core of PML-NBs formed by PML I, II and V. However SUMO2/3 was incorporated into the outer PML shell of PML-NBs formed by PML III. A number of PML isoform specific interactions have been described (Fogal et al., 2000; Yu et al., 2010) and it is likely that isoform specific differences observed in PML-NB structures are due, at least in part, to differences in interacting proteins recruited to PML-NBs by the different isoforms. The difference in SUMO2/3 modification state of each PML isoform is also likely to influence the structure of PML-NBs.

It would be very interesting to use a quantitative proteomics approach to investigate PML isoform specific interactions using these cell lines. This would allow identification of isoform specific interactions and overcome the problem associated with inter-isoform interactions present in cells in which a single isoform is overexpressed on a background of endogenous PML. This would help define the contribution of the various isoforms to cellular processes in which PML has been implicated. This approach could be extrapolated to include assessment of PML isoform interaction partners before and after arsenic treatment, which may help confirm the identity of, for example, the SUMO E3 ligase(s) responsible for PML sumoylation after arsenic treatment. The single chain, recombinant, camelid, anti GFP antibody used in the present study provides an excellent method for immunoprecipitating YFP linked PML from cells, however previous problems in extracting PML adequately under conditions which maintain PML- interaction partner interactions would need to be addressed. One option may be purify intact YFP-PML-NBs from cells using the previously mentioned antibody.

5.3.5 RNF4 is required for degradation of all PML isoforms

The ubiquitin E3 ligase RNF4 is required for arsenic induced degradation of all six PML isoforms examined in this thesis, as siRNA mediated depletion of RNF4 prior to arsenic treatment blocks degradation and results in accumulation of high molecular weight PML species (**Figures 5.2.13., 5.2.14 and 5.2.15**). When RNF4 depleted cells were examined by fluorescence microscopy, it was apparent that each PML isoform accumulated in PML-NBs after arsenic treatment. This is consistent with previous reports (Geoffroy et al., 2010; Tatham et al., 2008)(this thesis) in which the localisation of endogenous PML or PML overexpressed on a background of endogenous PML was examined after RNF4 depletion and arsenic treatment.

An intriguing finding of this study was the dramatic effect of RNF4 depletion on PML V expression under basal conditions (**Figure 5.2.15., panel A**). RNF4 has been previously proposed to ubiquitylate PML under basal conditions because an increase in PML expression was identified following RNF4 depletion (Lallemand-Breitenbach et al., 2008). While there is a slight increase in expression of PML III following RNF4 depletion (**Figure 5.2.14, panel A**), there is marked accumulation of high molecular weight PML V species under basal conditions, which are increased further following arsenic treatment (**Figure 5.2.15., panel A**). This suggests PML V is a particularly good substrate for RNF4, and may account for the low levels of PML V observed in this (**Figure 5.2.3.**), and other studies (Bernardi and Pandolfi, 2007; Cuchet et al., 2011) . This is also consistent with the observation that PML V is the PML isoform most readily degraded in response to arsenic treatment (**Figures 5.2.5, 5.2.6., panel E and 5.2.8., panel E**). RNF4 is recruited to PML modified with polymeric SUMO chains in PML-NBs following arsenic treatment via four SUMO interaction motifs in the N-terminal region of the protein (Geoffroy et al., 2010; Lallemand-Breitenbach et al.,

2008; Tatham et al., 2008). PML V appears to be a particularly good substrate for RNF4 which suggests that PML V may be more SUMO modified when compared to other isoforms. This hypothesis is supported by the observation that when analysed by western blotting, PML V is identified as a high molecular weight smear (**Figure 5.2.3.**), and that immunoprecipitation of PML V and analysis of post- translational modifications revealed a similar smear of SUMO1 modification, suggesting PMLV is modified by multiple SUMO1 molecules (**Figure 5.2.12., panel E**). PML V has previously been suggested to act as a scaffold in PML-NBs, because it is particularly stable in PML-NBs when analysed by fluorescence recovery after photobleaching (FRAP) (Weidtkamp-Peters et al., 2008). Interestingly, PML mutants which cannot be sumoylated at Lys160 and Lys490 have dramatically reduced residence time in PML-NBs (Weidtkamp-Peters et al., 2008), and therefore the increased residence times observed for PML V may be due to its high levels of SUMO modification at one or both of these residues. PML V is one of only two PML isoforms conserved from mouse to humans (Condemine et al., 2006), which suggests functions dependent on the unique C-terminal region of PML V may be particularly important, perhaps including this potential function as a scaffold component for PML-NBs. The importance of this region of PML V is further supported by the observation that the C-terminal region of PML V is capable of forming punctate nuclear structures in the absence of other PML isoforms, and recruits other PML-NB components to these structures (Geng et al., 2012).

5.3.6 Implications for treatment of APL?

In APL, PML and PML-RARα interact via the PML coiled coil domain. This domain is encoded within the common N terminal region of all PML isoforms examined in this study, as well as all PML-RARα isoforms (**Figures 1.3.1. and 1.4.1.**),(Jensen et al., 2001a; Melo et al., 2006). This suggests that PML-RARα can interact with all PML

isoforms. Interactions between PML-RARα and PML result in the disruption of PML-NBs in APL (Daniel et al., 1993). This implies that these interactions interfere with the normal functions of the PML isoforms and PML-NBs, events which contribute to the pathogenesis of APL.

PML-RARα in NB4 cells is rapidly degraded following arsenic treatment (**Figure 5.2.2.**) (Muller et al., 1998). While the degradation of PML-RARα is important for cure of APL, it is not sufficient to induce cure, because single agent ATRA treatment, which induces degradation of PML-RARα, often results in only short term remissions (Huang et al., 1988). ATRA treatment does however result in the reformation of PML-NBs, but no degradation of PML. This is in contrast to arsenic treatment, following which PML-NBs are reformed prior to degradation of PML (Geoffroy et al., 2010; Zhu et al., 1997). Following treatment of the APL derived NB4 cell line, or cells engineered to overexpress PML-RARα with arsenic, PML and PML-RARα are rapidly redistributed from the characteristic nuclear speckles associated with APL into PML-NBs (Zhu et al., 1997). This also recruits other PML-NB components, for example Sp100, to PML-NBs. The reformation of PML-NBs has been postulated to contribute to arsenic induced cure of APL, because PML-NBs exert functions in control of apoptosis and induction of cellular senescence (de The et al., 2012). The work presented in this thesis demonstrates PML I- VI are recruited to PML-NBs following arsenic treatment (**Figure 5.2.6.**), but not all are then degraded. These data therefore raise the possibility that differential degradation of PML isoforms in response to arsenic treatment may contribute to disease response. PML V is very readily degraded in response to arsenic when expressed in isolation (**Figures 5.2.5. and 5.2.6., panel E**). It is therefore unlikely that PML V functions would contribute to cure, because PML V is almost completely degraded after 24 hours of arsenic treatment. Perhaps instead the lack of PML V results in activation of cellular processes which contribute to cure.

Alternatively, other factors recruited to PML-NBs by PML V may dissociate following PML V degradation and they may be important for disease response. Conversely, PML isoforms which are not readily degraded are likely to continue to function after arsenic treatment has been instituted. PML IV is the isoform identified as most resistant to arsenic induced degradation. It is therefore likely that the functions of PML IV and PML IV specific interactions would persist following arsenic treatment. PML IV has been previously shown to directly interact with p53 (Fogal et al., 2000). This interaction was dependent on the unique C terminal region of PML IV and resulted in increased p53 transactivation (Fogal et al., 2000). The persistence of this PML IV- p53 interaction may therefore contribute to arsenic induced apoptosis of leukaemia cells. This may be particularly important in leukaemic stem cells, which are relatively resistant to conventional chemotherapeutic agents.

This study therefore implicates differential degradation of PML isoforms, and the resulting effects on isoform specific interactions in the cure of APL following arsenic treatment. A comprehensive study of PML isoform specific interactions and functions as discussed in section 5.3.3 would help delineate the functional effects of differential degradation of the various PML isoforms in response to arsenic treatment.

References

Ablain, J. and de The, H. (2011). Revisiting the differentiation paradigm in acute promyelocytic leukemia. *Blood* 117, 5795-5802.

Adamson, B., Smogorzewska, A., Sigoillot, F. D., King, R. W. and Elledge, S. J. (2012). A genome-wide homologous recombination screen identifies the RNA-binding protein RBMX as a component of the DNA-damage response. *Nat Cell Biol* 14, 318-28.

Anderson, E. M., Birmingham, A., Baskerville, S., Reynolds, A., Maksimova, E., Leake, D., Fedorov, Y., Karpilow, J. and Khvorova, A. (2008). Experimental validation of the importance of seed complement frequency to siRNA specificity. *RNA* 14, 853-861.

Bai, C., Sen, P., Hofmann, K., Ma, L., Goebl, M., Harper, J. W. and Elledge, S. J. (1996). SKP1 connects cell cycle regulators to the ubiquitin proteolysis machinery through a novel motif, the F-box. *Cell* 86, 263-74.

Bedford, L., Paine, S., Sheppard, P. W., Mayer, R. J. and Roelofs, J. (2010). Assembly, structure, and function of the 26S proteasome. *Trends in Cell Biology* 20, 391-401.

Bernardi, R. and Pandolfi, P. P. (2007). Structure, dynamics and functions of promyelocytic leukaemia nuclear bodies. *Nature Reviews Molecular Cell Biology* 8, 1006-1016.

Bernier-Villamor, V., Sampson, D. A., Matunis, M. J. and Lima, C. D. (2002). Structural Basis for E2-Mediated SUMO Conjugation Revealed by a Complex between Ubiquitin-Conjugating Enzyme Ubc9 and RanGAP1. *Cell* 108, 345-356.

Birmingham, A., Anderson, E. M., Reynolds, A., Ilsley-Tyree, D., Leake, D., Fedorov, Y., Baskerville, S., Maksimova, E., Robinson, K., Karpilow, J. et al. (2006).

3[prime] UTR seed matches, but not overall identity, are associated with RNAi off-targets. *Nat Meth* 3, 199-204.

Birmingham, A., Selfors, L. M., Forster, T., Wrobel, D., Kennedy, C. J., Shanks, E., Santoyo-Lopez, J., Dunican, D. J., Long, A., Kelleher, D. et al. (2009). Statistical methods for analysis of high-throughput RNA interference screens. *Nat Methods* 6, 569-75.

Bischof, O., Kirsh, O., Pearson, M., Itahana, K., Pelicci, P. and Dejean, A. (2002). Deconstructing PML-induced premature senescence. *The EMBO journal* 21, 3358 - 3369.

Boddy, M. N., Howe, K., Etkin, L. D., Solomon, E. and Freemont, P. S. (1996). PIC 1, a novel ubiquitin-like protein which interacts with the PML component of a multiprotein complex that is disrupted in acute promyelocytic leukaemia. *Oncogene* 13, 971-82.

Boisvert, F.-M., Hendzel, M. J. and Bazett-Jones, D. P. (2000). Promyelocytic Leukemia (Pml) Nuclear Bodies Are Protein Structures That Do Not Accumulate RNA. *Journal of Cell Biology* 148, 283-292.

Boutell, C., Cuchet-Lourenco, D., Vanni, E., Orr, A., Glass, M., McFarlane, S. and Everett, R. D. (2011). A viral ubiquitin ligase has substrate preferential SUMO targeted ubiquitin ligase activity that counteracts intrinsic antiviral defence. *PLoS Pathog* 7, e1002245.

Boyden, L. M., Choi, M., Choate, K. A., Nelson-Williams, C. J., Farhi, A., Toka, H. R., Tikhonova, I. R., Bjornson, R., Mane, S. M., Colussi, G. et al. (2012). Mutations in kelch-like 3 and cullin 3 cause hypertension and electrolyte abnormalities. *Nature* 482, 98-102.

Breen, K. A., Grimwade, D. and Hunt, B. J. (2012). The pathogenesis and management of the coagulopathy of acute promyelocytic leukaemia. *British Journal of Haematology* 156, 24-36.

Brown, D., Kogan, S., Lagasse, E., Weissman, I., Alcalay, M., Pelicci, P. G., Atwater, S. and Bishop, J. M. (1997). A PMLRARα transgene initiates murine acute promyelocytic leukemia. *Proceedings of the National Academy of Sciences* 94, 2551-2556.

Chen, G., Zhu, J., Shi, X., Ni, J., Zhong, H., Si, G., Jin, X., Tang, W., Li, X., Xong, S. et al. (1996). In vitro studies on cellular and molecular mechanisms of arsenic trioxide (As2O3) in the treatment of acute promyelocytic leukemia: As2O3 induces NB4 cell apoptosis with downregulation of Bcl-2 expression and modulation of PML-RAR alpha/PML proteins. *Blood* 88, 1052-1061.

Chen, G. Q., Shi, X. G., Tang, W., Xiong, S. M., Zhu, J., Cai, X., Man, Z. G., Ni, J. H., Shi, G. Y., Jia, P. M. et al. (1997). Use of arsenic trioxide (As2O3) in the treatment of acute promyelocytic leukemia (APL): I. As2O3 exerts dose-dependent dual effects on APL cells. *Blood* 89, 3345-3353.

Chen, S.-J., Zhou, G.-B., Zhang, X.-W., Mao, J.-H., de Thé, H. and Chen, Z. (2011). From an old remedy to a magic bullet: molecular mechanisms underlying the therapeutic effects of arsenic in fighting leukemia. *Blood* 117, 6425-6437.

Chen, Z. J. and Sun, L. J. (2009). Nonproteolytic functions of ubiquitin in cell signaling. *Molecular Cell* 33, 275-86.

Chou, T.-F., Brown, S. J., Minond, D., Nordin, B. E., Li, K., Jones, A. C., Chase, P., Porubsky, P. R., Stoltz, B. M., Schoenen, F. J. et al. (2011). Reversible inhibitor of p97, DBeQ, impairs both ubiquitin-dependent and autophagic protein clearance pathways. *Proceedings of the National Academy of Sciences* 108, 4834-4839.

Chu, Y. and Yang, X. (2011). SUMO E3 ligase activity of TRIM proteins. *Oncogene* 30, 1108-1116.

Condemine, W., Takahashi, Y., Zhu, J., Puvion-Dutilleul, F., Guegan, S., Janin, A. and de The, H. (2006). Characterization of Endogenous Human Promyelocytic Leukemia Isoforms. *Cancer Research* 66, 6192-6198.

Cuchet, D., Sykes, A., Nicolas, A., Orr, A., Murray, J., Sirma, H., Heeren, J., Bartelt, A. and Everett, R. D. (2011). PML isoforms I and II participate in PML-dependent restriction of HSV-1 replication. *Journal of Cell Science* 124, 280-291.

Daniel, M., Koken, M., Romagne, O., Barbey, S., Bazarbachi, A., Stadler, M., Guillemin, M., Degos, L., Chomienne, C. and de The, H. (1993). PML protein expression in hematopoietic and acute promyelocytic leukemia cells. *Blood* 82, 1858-1867.

de Thé, H. and Chen, Z. (2010). Acute promyelocytic leukaemia: novel insights into the mechanisms of cure. *Nat Rev Cancer* 10, 775-783.

De The, H., Lavau, C., Marchio, A., Chomienne, C., Degos, L. and Dejean, A. (1991). The PML-RARα fusion mRNA generated by the t(15;17) translocation in acute promyelocytic leukemia encodes a functionally altered RAR. *Cell* 66, 675-684.

de The, H., Le Bras, M. and Lallemand-Breitenbach, V. (2012). The cell biology of disease: Acute promyelocytic leukemia, arsenic, and PML bodies. *Journal of Cell Biology* 198, 11-21.

Dellaire, G., Ching, R. W., Dehghani, H., Ren, Y. and Bazett-Jones, D. P. (2006a). The number of PML nuclear bodies increases in early S phase by a fission mechanism. *Journal of Cell Science* 119, 1026-1033.

Dellaire, G., Eskiw, C. H., Dehghani, H., Ching, R. W. and Bazett-Jones, D. P. (2006b). Mitotic accumulations of PML protein contribute to the re-establishment of PML nuclear bodies in G1. *Journal of Cell Science* 119, 1034-1042.

Desterro, J. M. P., Rodriguez, M. S., Kemp, G. D. and Hay, R. T. (1999). Identification of the Enzyme Required for Activation of the Small Ubiquitin-like Protein SUMO-1. *Journal of Biological Chemistry* 274, 10618-10624.

Desterro, J. M. P., Thomson, J. and Hay, R. T. (1997). Ubch9 conjugates SUMO but not ubiquitin. *FEBS Letters* 417, 297-300.

Duda, D. M., Borg, L. A., Scott, D. C., Hunt, H. W., Hammel, M. and Schulman, B. A. (2008). Structural Insights into NEDD8 Activation of Cullin-RING Ligases: Conformational Control of Conjugation. *Cell* 134, 995-1006.

Duprez, E., Saurin, A., Desterro, J., Lallemand-Breitenbach, V., Howe, K., Boddy, M., Solomon, E., de The, H., Hay, R. and Freemont, P. (1999). SUMO-1 modification of the acute promyelocytic leukaemia protein PML: implications for nuclear localisation. *Journal of Cell Science* 112, 381-393.

Ebert, Margaret S. and Sharp, Phillip A. (2012). Roles for MicroRNAs in Conferring Robustness to Biological Processes. *Cell* 149, 515-524.

Echeverri, C. J., Beachy, P. A., Baum, B., Boutros, M., Buchholz, F., Chanda, S. K., Downward, J., Ellenberg, J., Fraser, A. G., Hacohen, N. et al. (2006). Minimizing the risk of reporting false positives in large-scale RNAi screens. *Nat Meth* 3, 777-779.

Echeverri, C. J. and Perrimon, N. (2006). High-throughput RNAi screening in cultured cells: a user's guide. *Nat Rev Genet* 7, 373-384.

Elbashir, S. M., Harborth, J., Lendeckel, W., Yalcin, A., Weber, K. and Tuschl, T. (2001). Duplexes of 21-nucleotide RNAs mediate RNA interference in cultured mammalian cells. *Nature* 411, 494-498.

Evdokimov, E., Sharma, P., Loskett, S. J., Lualdi, M. and Kuehn, M. R. (2008). Loss of SUMO1 in mice affects RanGAP1 localization and formation of PML nuclear

bodies, but is not lethal as it can be compensated by SUMO2 or SUMO3. *Journal of Cell Science* 121, 4106-4113.

Everett, R., Rechter, S., Papior, P., Tavalai, N., Stamminger, T. and Orr, A. (2006). PML contributes to a cellular mechanism of repression of herpes simplex virus type 1 infection that is inactivated by ICP0. *Journal of Virology* 80, 7995 - 8005.

Everett, R. D. and Chelbi-Alix, M. K. (2007). PML and PML nuclear bodies: Implications in antiviral defence. *Biochimie* 89, 819-830.

Everett, R. D., Lomonte, P., Sternsdorf, T., van Driel, R. and Orr, A. (1999). Cell cycle regulation of PML modification and ND10 composition. *Journal of Cell Science* 112 (Pt 24), 4581-8.

Everett, R. D., Parada, C., Gripon, P., Sirma, H. and Orr, A. (2008). Replication of ICP0-Null Mutant Herpes Simplex Virus Type 1 Is Restricted by both PML and Sp100. *Journal of Virology* 82, 2661-2672.

Ferbeyre, G., de Stanchina, E., Querido, E., Baptiste, N., Prives, C. and Lowe, S. W. (2000). PML is induced by oncogenic ras and promotes premature senescence. *Genes and Development* 14, 2015-27.

Fire, A., Xu, S., Montgomery, M. K., Kostas, S. A., Driver, S. E. and Mello, C. C. (1998). Potent and specific genetic interference by double-stranded RNA in Caenorhabditis elegans. *Nature* 391, 806-811.

Fogal, V., Gostissa, M., Sandy, P., Zacchi, P., Sternsdorf, T., Jensen, K., Pandolfi, P. P., Will, H., Schneider, C. and Sal, G. D. (2000). Regulation of p53 activity in nuclear bodies by a specific PML isoform. *EMBO Journal* 19, 6185-6195.

Furukawa, M., He, Y. J., Borchers, C. and Xiong, Y. (2003). Targeting of protein ubiquitination by BTB-Cullin 3-Roc1 ubiquitin ligases. *Nat Cell Biol* 5, 1001-1007.

Gallagher, R., Collins, S., Trujillo, J., McCredie, K., Ahearn, M., Tsai, S., Metzgar, R., Aulakh, G., Ting, R., Ruscetti, F. et al. (1979). Characterization of the continuous, differentiating myeloid cell line (HL-60) from a patient with acute promyelocytic leukemia. *Blood* 54, 713-733.

Gang Wang, Z., Delva, L., Gaboli, M., Rivi, R., Giorgio, M., Cordon-Cardo, C., Grosveld, F. and Paolo Pandolfi, P. (1998). Role of PML in Cell Growth and the Retinoic Acid Pathway. *Science* 279, 1547-1551.

Gareau, J. R. and Lima, C. D. (2010). The SUMO pathway: emerging mechanisms that shape specificity, conjugation and recognition. *Nat Rev Mol Cell Biol* 11, 861-871.

Geng, Y., Monajembashi, S., Shao, A., Cui, D., He, W., Chen, Z., Hemmerich, P. and Tang, J. (2012). Contribution of the C-terminal regions of Promyelocytic leukemia protein (PML) isoform II and V to PML nuclear body formation. *Journal of Biological Chemistry* First Published on July 7, 2012, doi:10.1074/jbc.M112.374769

Geoffroy, M.-C. and Hay, R. T. (2009). An additional role for SUMO in ubiquitin-mediated proteolysis. *Nat Rev Mol Cell Biol* 10, 564-568.

Geoffroy, M.-C., Jaffray, E. G., Walker, K. J. and Hay, R. T. (2010). Arsenic-Induced SUMO-Dependent Recruitment of RNF4 into PML Nuclear Bodies. *Molecular Biology of the Cell* 21, 4227-4239.

Geyer, R., Wee, S., Anderson, S., Yates Iii, J. and Wolf, D. A. (2003). BTB/POZ Domain Proteins Are Putative Substrate Adaptors for Cullin 3 Ubiquitin Ligases. *Molecular Cell* 12, 783-790.

Ghavamzadeh, A., Alimoghaddam, K., Rostami, S., Ghaffari, S. H., Jahani, M., Iravani, M., Mousavi, S. A., Bahar, B. and Jalili, M. (2011). Phase II Study of Single-

Agent Arsenic Trioxide for the Front-Line Therapy of Acute Promyelocytic Leukemia. *Journal of Clinical Oncology* 29, 2753-2757.

Giorgi, C., Ito, K., Lin, H. K., Santangelo, C., Wieckowski, M. R., Lebiedzinska, M., Bononi, A., Bonora, M., Duszynski, J., Bernardi, R. et al. (2010). PML regulates apoptosis at endoplasmic reticulum by modulating calcium release. *Science* 330, 1247-51.

Giuliano, K. A., DeBiasio, R. L., Dunlay, R. T., Gough, A., Volosky, J. M., Zock, J., Pavlakis, G. N. and Taylor, D. L. (1997). High-Content Screening: A New Approach to Easing Key Bottlenecks in the Drug Discovery Process. *Journal of Biomolecular Screening* 2, 249-259.

Goldenberg, S. J., Cascio, T. C., Shumway, S. D., Garbutt, K. C., Liu, J., Xiong, Y. and Zheng, N. (2004). Structure of the Cand1-Cul1-Roc1 Complex Reveals Regulatory Mechanisms for the Assembly of the Multisubunit Cullin-Dependent Ubiquitin Ligases. *Cell* 119, 517-528.

Golebiowski, F., Matic, I., Tatham, M. H., Cole, C., Yin, Y., Nakamura, A., Cox, J., Barton, G. J., Mann, M. and Hay, R. T. (2009). System-wide changes to SUMO modifications in response to heat shock. *Sci Signal* 2, ra24.

Gong, L. and Yeh, E. T. H. (1999). Identification of the Activating and Conjugating Enzymes of the NEDD8 Conjugation Pathway. *Journal of Biological Chemistry* 274, 12036-12042.

Goto, E., Tomita, A., Hayakawa, F., Atsumi, A., Kiyoi, H. and Naoe, T. (2011). Missense mutations in PML-RARA are critical for the lack of responsiveness to arsenic trioxide treatment. *Blood* 118, 1600-1609.

Gresko, E., Ritterhoff, S., Sevilla-Perez, J., Roscic, A., Frobius, K., Kotevic, I., Vichalkovski, A., Hess, D., Hemmings, B. A. and Schmitz, M. L. (2008). PML

tumor suppressor is regulated by HIPK2-mediated phosphorylation in response to DNA damage. *Oncogene* 28, 698-708.

Grimwade, D., Jovanovic, J. V., Hills, R. K., Nugent, E. A., Patel, Y., Flora, R., Diverio, D., Jones, K., Aslett, H., Batson, E. et al. (2009). Prospective Minimal Residual Disease Monitoring to Predict Relapse of Acute Promyelocytic Leukemia and to Direct Pre-Emptive Arsenic Trioxide Therapy. *Journal of Clinical Oncology* 27, 3650-3658.

Gripon, P., Rumin, S., Urban, S., Le Seyec, J., Glaise, D., Cannie, I., Guyomard, C., Lucas, J., Trepo, C. and Guguen-Guillouzo, C. (2002). Infection of a human hepatoma cell line by hepatitis B virus. *Proceedings of the National Academy of Sciences* 99, 15655-15660.

Grisolano, J. L., Wesselschmidt, R. L., Pelicci, P. G. and Ley, T. J. (1997). Altered Myeloid Development and Acute Leukemia in Transgenic Mice Expressing PML-RARalpha Under Control of Cathepsin G Regulatory Sequences. *Blood* 89, 376-387.

Gurrieri, C., Capodieci, P., Bernardi, R., Scaglioni, P. P., Nafa, K., Rush, L. J., Verbel, D. A., Cordon-Cardo, C. and Pandolfi, P. P. (2004). Loss of the tumor suppressor PML in human cancers of multiple histologic origins. *Journal of the National Cancer Institute* 96, 269-79.

Haagenson, K. K., Tait, L., Wang, J., Shekhar, M. P., Polin, L., Chen, W. and Wu, G. S. (2012). Cullin-3 protein expression levels correlate with breast cancer progression. *Cancer Biol Ther* 13.

Haglund, K. and Dikic, I. (2005). Ubiquitylation and cell signaling. *EMBO Journal* 24, 3353-3359.

Haglund, K., Sigismund, S., Polo, S., Szymkiewicz, I., Di Fiore, P. P. and Dikic, I. (2003). Multiple monoubiquitination of RTKs is sufficient for their endocytosis and degradation. *Nat Cell Biol* 5, 461-466.

Hannon, G. J. and Rossi, J. J. (2004). Unlocking the potential of the human genome with RNA interference. *Nature* 431, 371-8.

Hasan, S. K., Mays, A. N., Ottone, T., Ledda, A., La Nasa, G., Cattaneo, C., Borlenghi, E., Melillo, L., Montefusco, E., Cervera, J. et al. (2008). Molecular analysis of t(15;17) genomic breakpoints in secondary acute promyelocytic leukemia arising after treatment of multiple sclerosis. *Blood* 112, 3383-3390.

Hattersley, N., Shen, L., Jaffray, E. G. and Hay, R. T. (2011). The SUMO protease SENP6 is a direct regulator of PML nuclear bodies. *Molecular Biology of the Cell* 22, 78-90.

Hay, R. T. (2005). SUMO: A History of Modification. *Molecular Cell* 18, 1-12.

Hay, R. T. (2007). SUMO-specific proteases: a twist in the tail. *Trends in Cell Biology* 17, 370-376.

Hayakawa, F. and Privalsky, M. L. (2004). Phosphorylation of PML by mitogen-activated protein kinases plays a key role in arsenic trioxide-mediated apoptosis. *Cancer Cell* 5, 389-401.

He, L.-Z., Tribioli, C., Rivi, R., Peruzzi, D., Pelicci, P. G., Soares, V., Cattoretti, G. and Pandolfi, P. P. (1997). Acute leukemia with promyelocytic features in PML/RARα transgenic mice. *Proceedings of the National Academy of Sciences* 94, 5302-5307.

Hecker, C.-M., Rabiller, M., Haglund, K., Bayer, P. and Dikic, I. (2006). Specification of SUMO1- and SUMO2-interacting Motifs. *Journal of Biological Chemistry* 281, 16117-16127.

Hochstrasser, M. (2009). Origin and function of ubiquitin-like proteins. *Nature* 458, 422-429.

Huang, D. T., Ayrault, O., Hunt, H. W., Taherbhoy, A. M., Duda, D. M., Scott, D. C., Borg, L. A., Neale, G., Murray, P. J., Roussel, M. F. et al. (2009). E2-RING Expansion of the NEDD8 Cascade Confers Specificity to Cullin Modification. *Molecular Cell* 33, 483-495.

Huang, M., Ye, Y., Chen, S., Chai, J., Lu, J., Zhoa, L., Gu, L. and Wang, Z. (1988). Use of all-trans retinoic acid in the treatment of acute promyelocytic leukemia. *Blood* 72, 567-572.

Huang, O. W., Ma, X., Yin, J., Flinders, J., Maurer, T., Kayagaki, N., Phung, Q., Bosanac, I., Arnott, D., Dixit, V. M. et al. (2012). Phosphorylation-dependent activity of the deubiquitinase DUBA. *Nat Struct Mol Biol* 19, 171-5.

Huntzinger, E. and Izaurralde, E. (2011). Gene silencing by microRNAs: contributions of translational repression and mRNA decay. *Nat Rev Genet* 12, 99-110.

Isakson, P., Bjørås, M., Bøe, S. O. and Simonsen, A. (2010). Autophagy contributes to therapy-induced degradation of the PML/RARA oncoprotein. *Blood* 116, 2324-2331.

Ishov, A. M., Sotnikov, A. G., Negorev, D., Vladimirova, O. V., Neff, N., Kamitani, T., Yeh, E. T. H., Strauss, J. F. and Maul, G. G. (1999). Pml Is Critical for Nd10 Formation and Recruits the Pml-Interacting Protein Daxx to This Nuclear Structure When Modified by Sumo-1. *The Journal of Cell Biology* 147, 221-234.

Jackson, A. L., Burchard, J., Leake, D., Reynolds, A., Schelter, J., Guo, J., Johnson, J. M., Lim, L., Karpilow, J., Nichols, K. et al. (2006a). Position-specific chemical modification of siRNAs reduces “off-target” transcript silencing. *RNA* 12, 1197-1205.

Jackson, A. L., Burchard, J., Schelter, J., Chau, B. N., Cleary, M., Lim, L. and Linsley, P. S. (2006b). Widespread siRNA “off-target” transcript silencing mediated by seed region sequence complementarity. *RNA* 12, 1179-1187.

Jackson, A. L. and Linsley, P. S. (2010). Recognizing and avoiding siRNA off-target effects for target identification and therapeutic application. *Nat Rev Drug Discov* 9, 57-67.

Jang, M.-S., Ryu, S.-W. and Kim, E. (2002). Modification of Daxx by small ubiquitin-related modifier-1. *Biochemical and Biophysical Research Communications* 295, 495-500.

Jeanne, M., Lallemand-Breitenbach, V., Ferhi, O., Koken, M., Le Bras, M., Duffort, S., Peres, L., Berthier, C., Soilihi, H., Raught, B. et al. (2010). PML/RARA Oxidation and Arsenic Binding Initiate the Antileukemia Response of As2O3. *Cancer Cell* 18, 88-98.

Jensen, K., Shiels, C. and Freemont, P. (2001a). PML protein isoforms and the RBCC/TRIM motif. *Oncogene* 20, 7223 - 7233.

Jensen, K., Shiels, C. and Freemont, P. S. (2001b). PML protein isoforms and the RBCC/TRIM motif. *Oncogene* 20, 7223-33.

Johnson, E. S. and Gupta, A. A. (2001). An E3-like Factor that Promotes SUMO Conjugation to the Yeast Septins. *Cell* 106, 735-744.

Johnson, E. S., Ma, P. C. M., Ota, I. M. and Varshavsky, A. (1995). A Proteolytic Pathway That Recognizes Ubiquitin as a Degradation Signal. *Journal of Biological Chemistry* 270, 17442-17456.

Ju, J. S., Fuentealba, R. A., Miller, S. E., Jackson, E., Piwnica-Worms, D., Baloh, R. H. and Weihl, C. C. (2009). Valosin-containing protein (VCP) is required for autophagy and is disrupted in VCP disease. *Journal of Cell Biology* 187, 875-88.

Jul-Larsen, Å., Grudic, A., Bjerkvig, R. and Ove Bøe, S. (2009). Cell-cycle regulation and dynamics of cytoplasmic compartments containing the promyelocytic leukemia protein and nucleoporins. *Journal of Cell Science* 122, 1201-1210.

Kakizuka, A., Miller, W., Umesono, K., Warrell, R., Frankel, S., Murty, V., Dmitrovsky, E. and Evans, R. (1991). Chromosomal translocation t(15;17) in human acute promyelocytic leukemia fuses RAR alpha with a novel putative transcription factor, PML. *Cell* 66, 663 - 674.

Kamitani, T., Kito, K., Nguyen, H. P., Wada, H., Fukuda-Kamitani, T. and Yeh, E. T. (1998). Identification of three major sentrinization sites in PML. *Journal of Biological Chemistry* 273, 26675-82.

Kamura, T., Sato, S., Haque, D., Liu, L., Kaelin, W. G., Conaway, R. C. and Conaway, J. W. (1998). The Elongin BC complex interacts with the conserved SOCS-box motif present in members of the SOCS, ras, WD-40 repeat, and ankyrin repeat families. *Genes & Development* 12, 3872-3881.

Kassner, P. D. (2008). Discovery of novel targets with high throughput RNA interference screening. *Comb Chem High Throughput Screen* 11, 175-84.

Kastner, P., Perez, A., Lutz, Y., Rochette-Egly, C., Gaub, M. P., Durand, B., Lanotte, M., Berger, R. and Chambon, P. (1992). Structure, localization and transcriptional properties of two classes of retinoic acid receptor alpha fusion proteins in acute promyelocytic leukemia (APL): structural similarities with a new family of oncoproteins. *EMBO Journal* 11, 629-42.

Kayagaki, N., Phung, Q., Chan, S., Chaudhari, R., Quan, C., O'Rourke, K. M., Eby, M., Pietras, E., Cheng, G., Bazan, J. F. et al. (2007). DUBA: a deubiquitinase that regulates type I interferon production. *Science* 318, 1628-32.

Kerscher, O. (2007). SUMO junction[mdash]what's your function? *EMBO Rep* 8, 550-555.

Kim, A. Y., Bommeljé, C. C., Lee, B. E., Yonekawa, Y., Choi, L., Morris, L. G., Huang, G., Kaufman, A., Ryan, R. J. H., Hao, B. et al. (2008). SCCRO (DCUN1D1) Is an Essential Component of the E3 Complex for Neddylation. *Journal of Biological Chemistry* 283, 33211-33220.

Kim, W., Bennett, E. J., Huttlin, E. L., Guo, A., Li, J., Possemato, A., Sowa, M. E., Rad, R., Rush, J., Comb, M. J. et al. (2011). Systematic and quantitative assessment of the ubiquitin-modified proteome. *Molecular Cell* 44, 325-40.

Knipscheer, P., Flotho, A., Klug, H., Olsen, J. V., van Dijk, W. J., Fish, A., Johnson, E. S., Mann, M., Sixma, T. K. and Pichler, A. (2008). Ubc9 Sumoylation Regulates SUMO Target Discrimination. *Molecular Cell* 31, 371-382.

Koegl, M., Hoppe, T., Schlenker, S., Ulrich, H. D., Mayer, T. U. and Jentsch, S. (1999). A novel ubiquitination factor, E4, is involved in multiubiquitin chain assembly. *Cell* 96, 635-44.

Koken, M. H., Linares-Cruz, G., Quignon, F., Viron, A., Chelbi-Alix, M. K., Sobczak-Thepot, J., Juhlin, L., Degos, L., Calvo, F. and de The, H. (1995). The PML growth-suppressor has an altered expression in human oncogenesis. *Oncogene* 10, 1315-24.

Koken, M. H. M. (1994). The t(15;17) translocation alters a nuclear body in a retinoic acid-reversible fashion. *EMBO Journal* 13, 1073-1083.

Komander, D. (2009). The emerging complexity of protein ubiquitination. *Biochemical Society Transactions* 37, 937-53.

Kurahashi, H., Akagi, K., Inazawa, J., Ohta, T., Niikawa, N., Kayatani, F., Sano, T., Okada, S. and Nishisho, I. (1995). Isolation and characterization of a novel gene deleted in DiGeorge syndrome. *Human Molecular Genetics* 4, 541-549.

Kurz, T., Chou, Y.-C., Willems, A. R., Meyer-Schaller, N., Hecht, M.-L., Tyers, M., Peter, M. and Sicheri, F. (2008). Dcn1 Functions as a Scaffold-Type E3 Ligase for Cullin Neddylation. *Molecular Cell* 29, 23-35.

Kurz, T., Ozlu, N., Rudolf, F., O'Rourke, S. M., Luke, B., Hofmann, K., Hyman, A. A., Bowerman, B. and Peter, M. (2005). The conserved protein DCN-1/Dcn1p is required for cullin neddylation in C. elegans and S. cerevisiae. *Nature* 435, 1257-1261.

Lallemand-Breitenbach, V., Jeanne, M., Benhenda, S., Nasr, R., Lei, M., Peres, L., Zhou, J., Raught, B. and de Thé, H. (2008). Arsenic degrades PML or PML-RARα through a SUMO-triggered RNF4/ ubiquitin-mediated pathway. *Nature Cell Biology* 10, 547-555.

Lallemand-Breitenbach, V., Zhu, J., Chen, Z. and de Thé, H. (2012). Curing APL through PML/RARA degradation by As2O3. *Trends in Molecular Medicine* 18, 36-42.

Lallemand-Breitenbach, V., Zhu, J., Puvion, F., Koken, M., Honoré, N., Doubeikovsky, A., Duprez, E., Pandolfi, P. P., Puvion, E., Freemont, P. et al. (2001). Role of promyelocytic leukemia (PML) sumolation in nuclear body formation, 11S proteasome recruitment, and As2O3-induced PML or PML/retinoic acid receptor α degradation. *Journal of Experimental Medicine* 193, 1361-1371.

Lång, E., Grudic, A., Pankiv, S., Bruserud, Ø., Simonsen, A., Bjerkvig, R., Bjørås, M. and Bøe, S. O. (2012). The arsenic-based cure of acute promyelocytic leukemia promotes cytoplasmic sequestration of PML and PML/RARA through inhibition of PML body recycling. *Blood* doi:10.1182/blood-2011-10-388496.

Lang, M., Jegou, T., Chung, I., Richter, K., Münch, S., Udvarhelyi, A., Cremer, C., Hemmerich, P., Engelhardt, J., Hell, S. W. et al. (2010). Three-dimensional

organization of promyelocytic leukemia nuclear bodies. *Journal of Cell Science* 123, 392-400.

Lanotte, M., Martin-Thouvenin, V., Najman, S., Balerini, P., Valensi, F. and Berger, R. (1991). NB4, a maturation inducible cell line with t(15;17) marker isolated from a human acute promyelocytic leukemia (M3). *Blood* 77, 1080-1086.

Lengfelder, E., Hofmann, W. K. and Nowak, D. (2012). Impact of arsenic trioxide in the treatment of acute promyelocytic leukemia. *Leukemia* 26, 433-42.

Liakopoulos, D., Doenges, G., Matuschewski, K. and Jentsch, S. (1998). A novel protein modification pathway related to the ubiquitin system. *EMBO Journal* 17, 2208-2214.

Lin, D.-Y., Huang, Y.-S., Jeng, J.-C., Kuo, H.-Y., Chang, C.-C., Chao, T.-T., Ho, C.-C., Chen, Y.-C., Lin, T.-P., Fang, H.-I. et al. (2006). Role of SUMO-Interacting Motif in Daxx SUMO Modification, Subnuclear Localization, and Repression of Sumoylated Transcription Factors. *Molecular Cell* 24, 341-354.

Lin, H. K., Bergmann, S. and Pandolfi, P. P. (2004). Cytoplasmic PML function in TGF-beta signalling. *Nature* 431, 205-11.

Lipinski, M. M., Hoffman, G., Ng, A., Zhou, W., Py, B. F., Hsu, E., Liu, X., Eisenberg, J., Liu, J., Blenis, J. et al. (2010). A genome-wide siRNA screen reveals multiple mTORC1 independent signaling pathways regulating autophagy under normal nutritional conditions. *Dev Cell* 18, 1041-52.

Lu, X., Meng, X., Morris, C. A. and Keating, M. T. (1998). A novel human gene, WSTF, is deleted in Williams syndrome. *Genomics* 54, 241-9.

Maerki, S., Olma, M. H., Staubli, T., Steigemann, P., Gerlich, D. W., Quadroni, M., Sumara, I. and Peter, M. (2009). The Cul3–KLHL21 E3 ubiquitin ligase targets Aurora B to midzone microtubules in anaphase and is required for cytokinesis. *The Journal of Cell Biology* 187, 791-800.

Martens, J. H. A., Brinkman, A. B., Simmer, F., Francoijs, K. J., Nebbioso, A., Ferrara, F., Altucci, L. and Stunnenberg, H. G. (2010). PML-RARα/RXR Alters the Epigenetic Landscape in Acute Promyelocytic Leukemia. *Cancer Cell* 17, 173-185.

Matic, I., Schimmel, J., Hendriks, I. A., van Santen, M. A., van de Rijke, F., van Dam, H., Gnad, F., Mann, M. and Vertegaal, A. C. O. (2010). Site-Specific Identification of SUMO-2 Targets in Cells Reveals an Inverted SUMOylation Motif and a Hydrophobic Cluster SUMOylation Motif. *Molecular Cell* 39, 641-652.

Matic, I., van Hagen, M., Schimmel, J., Macek, B., Ogg, S. C., Tatham, M. H., Hay, R. T., Lamond, A. I., Mann, M. and Vertegaal, A. C. O. (2008). In Vivo Identification of Human Small Ubiquitin-like Modifier Polymerization Sites by High Accuracy Mass Spectrometry and an in Vitro to in Vivo Strategy. *Molecular & Cellular Proteomics* 7, 132-144.

Mays, A. N., Osheroff, N., Xiao, Y., Wiemels, J. L., Felix, C. A., Byl, J. A. W., Saravanamuttu, K., Peniket, A., Corser, R., Chang, C. et al. (2010). Evidence for direct involvement of epirubicin in the formation of chromosomal translocations in t(15;17) therapy-related acute promyelocytic leukemia. *Blood* 115, 326-330.

Meister, G. and Tuschl, T. (2004). Mechanisms of gene silencing by double-stranded RNA. *Nature* 431, 343-349.

Melchior, F., Schergaut, M. and Pichler, A. (2003). SUMO: ligases, isopeptidases and nuclear pores. *Trends in Biochemical Sciences* 28, 612-618.

Melo, R. A. M., De Vasconcellos, J. F., Melo, F. C. B. C., Machado, C. G. F., Lacerda, T. M. S. and Souto, F. R. (2006). PML–RARα fusion gene transcripts and biological features in acute promyelocytic leukemia patients. *Clinical and Laboratory Haematology* 28, 126-129.

Meyer-Schaller, N., Chou, Y. C., Sumara, I., Martin, D. D., Kurz, T., Katheder, N., Hofmann, K., Berthiaume, L. G., Sicheri, F. and Peter, M. (2009). The human Dcn1-like protein DCNL3 promotes Cul3 neddylation at membranes. *Proceedings of the National Academy of Sciences of the United States of America* 106, 12365-70.

Mistry, A. R., Felix, C. A., Whitmarsh, R. J., Mason, A., Reiter, A., Cassinat, B., Parry, A., Walz, C., Wiemels, J. L., Segal, M. R. et al. (2005). DNA Topoisomerase II in Therapy-Related Acute Promyelocytic Leukemia. *New England Journal of Medicine* 352, 1529-1538.

Mohr, S., Bakal, C. and Perrimon, N. (2010). Genomic screening with RNAi: results and challenges. *Annual Review of Biochemistry* 79, 37-64.

Muller, S., Matunis, M. J. and Dejean, A. (1998). Conjugation with the ubiquitin-related modifier SUMO-1 regulates the partitioning of PML within the nucleus. *EMBO Journal* 17, 61-70.

Nacak, T. G., Leptien, K., Fellner, D., Augustin, H. G. and Kroll, J. (2006). The BTB-kelch Protein LZTR-1 Is a Novel Golgi Protein That Is Degraded upon Induction of Apoptosis. *Journal of Biological Chemistry* 281, 5065-5071.

Nacerddine, K., Lehembre, F., Bhaumik, M., Artus, J., Cohen-Tannoudji, M., Babinet, C., Pandolfi, P. P. and Dejean, A. (2005). The SUMO Pathway Is Essential for Nuclear Integrity and Chromosome Segregation in Mice. *Developmental Cell* 9, 769-779.

Nagai, M., Seki, S., Kitahara, T., Abe, T., Minato, K., Watanabe, S. and Shimoyama, M. (1984). A novel human myelomonocytoid cell line, P39/Tsugane, derived from overt leukemia following myelodysplastic syndrome. *Gann* 75, 1100-7.

Occhionorelli, M., Santoro, F., Pallavicini, I., Gruszka, A., Moretti, S., Bossi, D., Viale, A., Shing, D., Ronzoni, S., Muradore, I. et al. (2011). The self-association

coiled-coil domain of PML is sufficient for the oncogenic conversion of the retinoic acid receptor (RAR) alpha. *Leukemia* 25, 814-820.

Orvedahl, A., Sumpter, R., Jr., Xiao, G., Ng, A., Zou, Z., Tang, Y., Narimatsu, M., Gilpin, C., Sun, Q., Roth, M. et al. (2011). Image-based genome-wide siRNA screen identifies selective autophagy factors. *Nature* 480, 113-7.

Osaka, F., Kawasaki, H., Aida, N., Saeki, M., Chiba, T., Kawashima, S., Tanaka, K. and Kato, S. (1998). A new NEDD8-ligating system for cullin-4A. *Genes and Development* 12, 2263-2268.

Perez-Torrado, R., Yamada, D. and Defossez, P. A. (2006). Born to bind: the BTB protein-protein interaction domain. *Bioessays* 28, 1194-202.

Petroski, M. D. and Deshaies, R. J. (2005). Function and regulation of cullin-RING ubiquitin ligases. *Nat Rev Mol Cell Biol* 6, 9-20.

Pichler, A., Gast, A., Seeler, J. S., Dejean, A. and Melchior, F. (2002). The Nucleoporin RanBP2 Has SUMO1 E3 Ligase Activity. *Cell* 108, 109-120.

Pintard, L., Willems, A. and Peter, M. (2004). Cullin-based ubiquitin ligases: Cul3-BTB complexes join the family. *EMBO Journal* 23, 1681-1687.

Pintard, L., Willis, J. H., Willems, A., Johnson, J.-L. F., Srayko, M., Kurz, T., Glaser, S., Mains, P. E., Tyers, M., Bowerman, B. et al. (2003). The BTB protein MEL-26 is a substrate-specific adaptor of the CUL-3 ubiquitin-ligase. *Nature* 425, 311-316.

Pritchard, C. C., Cheng, H. H. and Tewari, M. (2012). MicroRNA profiling: approaches and considerations. *Nat Rev Genet* 13, 358-369.

Quimby, B. B., Yong-Gonzalez, V., Anan, T., Strunnikov, A. V. and Dasso, M. (2006). The promyelocytic leukemia protein stimulates SUMO conjugation in yeast. *Oncogene* 25, 2999-3005.

Rabellino, A., Carter, B., Konstantinidou, G., Wu, S.-Y., Rimessi, A., Byers, L. A., Heymach, J. V., Girard, L., Chiang, C.-M., Teruya-Feldstein, J. et al. (2012). The SUMO E3-ligase PIAS1 Regulates the Tumor Suppressor PML and Its Oncogenic Counterpart PML-RARA. *Cancer Research* 72, 2275-2284.

Ravandi, F., Estey, E., Jones, D., Faderl, S., O'Brien, S., Fiorentino, J., Pierce, S., Blamble, D., Estrov, Z., Wierda, W. et al. (2009). Effective Treatment of Acute Promyelocytic Leukemia With All-Trans-Retinoic Acid, Arsenic Trioxide, and Gemtuzumab Ozogamicin. *Journal of Clinical Oncology* 27, 504-510.

Richly, H., Rape, M., Braun, S., Rumpf, S., Hoege, C. and Jentsch, S. (2005). A series of ubiquitin binding factors connects CDC48/p97 to substrate multiubiquitylation and proteasomal targeting. *Cell* 120, 73-84.

Rodier, F. and Campisi, J. (2011). Four faces of cellular senescence. *The Journal of Cell Biology*.

Rodrigo-Brenni, M. C. and Morgan, D. O. (2007). Sequential E2s drive polyubiquitin chain assembly on APC targets. *Cell* 130, 127-39.

Rodriguez, M. S., Dargemont, C. and Hay, R. T. (2001). SUMO-1 Conjugation in Vivo Requires Both a Consensus Modification Motif and Nuclear Targeting. *Journal of Biological Chemistry* 276, 12654-12659.

Sachse, C. and Echeverri, C. J. (2004). Oncology studies using siRNA libraries: the dawn of RNAi-based genomics. *Oncogene* 23, 8384-8391.

Saha, A. and Deshaies, R. J. (2008). Multimodal Activation of the Ubiquitin Ligase SCF by Nedd8 Conjugation. *Molecular Cell* 32, 21-31.

Salomoni, P. and Pandolfi, P. P. (2002). The Role of PML in Tumor Suppression. *Cell* 108, 165-170.

Sarkaria, I., O-charoenrat, P., Talbot, S. G., Reddy, P. G., Ngai, I., Maghami, E., Patel, K. N., Lee, B., Yonekawa, Y., Dudas, M. et al. (2006). Squamous Cell

Carcinoma Related Oncogene/DCUN1D1 Is Highly Conserved and Activated by Amplification in Squamous Cell Carcinomas. *Cancer Research* 66, 9437-9444.

Schulman, B. A., Carrano, A. C., Jeffrey, P. D., Bowen, Z., Kinnucan, E. R. E., Finnin, M. S., Elledge, S. J., Harper, J. W., Pagano, M. and Pavletich, N. P. (2000). Insights into SCF ubiquitin ligases from the structure of the Skp1–Skp2 complex. *Nature* 408, 381-386.

Scott, D. C., Monda, J. K., Grace, C. R. R., Duda, D. M., Kriwacki, R. W., Kurz, T. and Schulman, B. A. (2010). A Dual E3 Mechanism for Rub1 Ligation to Cdc53. *Molecular Cell* 39, 784-796.

Seelig, H. P., Moosbrugger, I., Ehrfeld, H., Fink, T., Renz, M. and Genth, E. (1995). The major dermatomyositis-specific Mi-2 autoantigen is a presumed helicase involved in transcriptional activation. *Arthritis and Rheumatism* 38, 1389-99.

Sharma, S. and Rao, A. (2009). RNAi screening: tips and techniques. *Nat Immunol* 10, 799-804.

Shen, T. H., Lin, H.-K., Scaglioni, P. P., Yung, T. M. and Pandolfi, P. P. (2006). The Mechanisms of PML-Nuclear Body Formation. *Molecular Cell* 24, 331-339.

Shen, Z.-X., Chen, G.-Q., Ni, J.-H., Li, X.-S., Xiong, S.-M., Qiu, Q.-Y., Zhu, J., Tang, W., Sun, G.-L., Yang, K.-Q. et al. (1997). Use of Arsenic Trioxide (As2O3) in the Treatment of Acute Promyelocytic Leukemia (APL): II. Clinical Efficacy and Pharmacokinetics in Relapsed Patients. *Blood* 89, 3354-3360.

Siqueira-Neto, J. L., Moon, S., Jang, J., Yang, G., Lee, C., Moon, H. K., Chatelain, E., Genovesio, A., Cechetto, J. and Freitas-Junior, L. H. (2012). An Image-Based High-Content Screening Assay for Compounds Targeting Intracellular Leishmania donovani Amastigotes in Human Macrophages. *PLoS Negl Trop Dis* 6, e1671.

Song, J., Zhang, Z., Hu, W. and Chen, Y. (2005). Small Ubiquitin-like Modifier (SUMO) Recognition of a SUMO Binding Motif. *Journal of Biological Chemistry* 280, 40122-40129.

Soucy, T. A., Smith, P. G., Milhollen, M. A., Berger, A. J., Gavin, J. M., Adhikari, S., Brownell, J. E., Burke, K. E., Cardin, D. P., Critchley, S. et al. (2009). An inhibitor of NEDD8-activating enzyme as a new approach to treat cancer. *Nature* 458, 732-736.

Sowa, M. E., Bennett, E. J., Gygi, S. P. and Harper, J. W. (2009). Defining the human deubiquitinating enzyme interaction landscape. *Cell* 138, 389-403.

Sternsdorf, T., Jensen, K. and Will, H. (1997). Evidence for Covalent Modification of the Nuclear Dot–associated Proteins PML and Sp100 by PIC1/SUMO-1. *The Journal of Cell Biology* 139, 1621-1634.

Stogios, P., Downs, G., Jauhal, J., Nandra, S. and Prive, G. (2005). Sequence and structural analysis of BTB domain proteins. *Genome Biology* 6, R82.

Sumara, I. and Peter, M. (2007). A Cul3-Based E3 Ligase Regulates Mitosis and is Required to Maintain the Spindle Assembly Checkpoint in Human Cells. *Cell Cycle* 6, 3004-3010.

Sumara, I., Quadroni, M., Frei, C., Olma, M. H., Sumara, G., Ricci, R. and Peter, M. (2007). A Cul3-Based E3 Ligase Removes Aurora B from Mitotic Chromosomes, Regulating Mitotic Progression and Completion of Cytokinesis in Human Cells. *Developmental Cell* 12, 887-900.

Swords, R. T., Kelly, K. R., Smith, P. G., Garnsey, J. J., Mahalingam, D., Medina, E., Oberheu, K., Padmanabhan, S., O'Dwyer, M., Nawrocki, S. T. et al. (2010). Inhibition of NEDD8-activating enzyme: a novel approach for the treatment of acute myeloid leukemia. *Blood* 115, 3796-3800.

Tan, M., Li, Y., Yang, R., Xi, N. and Sun, Y. (2011). Inactivation of SAG E3 Ubiquitin Ligase Blocks Embryonic Stem Cell Differentiation and Sensitizes Leukemia Cells to Retinoid Acid. *PLoS ONE* 6, e27726.

Tatham, M. H., Geoffroy, M. C., Shen, L., Plechanovová, A., Hattersley, N., Jaffray, E. G., Palvimo, J. J. and Hay, R. T. (2008). RNF4 is a poly-SUMO-specific E3 ubiquitin ligase required for arsenic-induced PML degradation. *Nature Cell Biology* 10, 538-546.

Tatham, M. H., Jaffray, E., Vaughan, O. A., Desterro, J. M. P., Botting, C. H., Naismith, J. H. and Hay, R. T. (2001). Polymeric Chains of SUMO-2 and SUMO-3 Are Conjugated to Protein Substrates by SAE1/SAE2 and Ubc9. *Journal of Biological Chemistry* 276, 35368-35374.

Thrower, J. S., Hoffman, L., Rechsteiner, M. and Pickart, C. M. (2000). Recognition of the polyubiquitin proteolytic signal. *EMBO Journal* 19, 94-102.

Tresse, E., Salomons, F. A., Vesa, J., Bott, L. C., Kimonis, V., Yao, T. P., Dantuma, N. P. and Taylor, J. P. (2010). VCP/p97 is essential for maturation of ubiquitin-containing autophagosomes and this function is impaired by mutations that cause IBMPFD. *Autophagy* 6, 217-27.

Ventii, K. H. and Wilkinson, K. D. (2008). Protein partners of deubiquitinating enzymes. *Biochemical Journal* 414, 161-175.

Vernier, M., Bourdeau, V., Gaumont-Leclerc, M.-F., Moiseeva, O., Bégin, V., Saad, F., Mes-Masson, A.-M. and Ferbeyre, G. (2011). Regulation of E2Fs and senescence by PML nuclear bodies. *Genes & Development* 25, 41-50.

Vertegaal, A. C. O., Andersen, J. S., Ogg, S. C., Hay, R. T., Mann, M. and Lamond, A. I. (2006). Distinct and Overlapping Sets of SUMO-1 and SUMO-2 Target Proteins Revealed by Quantitative Proteomics. *Molecular & Cellular Proteomics* 5, 2298-2310.

Wang, Z.-G., Ruggero, D., Ronchetti, S., Zhong, S., Gaboli, M., Rivi, R. and Pandolfi, P. P. (1998). Pml is essential for multiple apoptotic pathways. *Nature Genetics* 20, 266-272.

Wang, Z.-Y. and Chen, Z. (2008). Acute promyelocytic leukemia: from highly fatal to highly curable. *Blood* 111, 2505-2515.

Weidtkamp-Peters, S., Lenser, T., Negorev, D., Gerstner, N., Hofmann, T. G., Schwanitz, G., Hoischen, C., Maul, G., Dittrich, P. and Hemmerich, P. (2008). Dynamics of component exchange at PML nuclear bodies. *Journal of Cell Science* 121, 2731-2743.

Westervelt, P., Lane, A. A., Pollock, J. L., Oldfather, K., Holt, M. S., Zimonjic, D. B., Popescu, N. C., DiPersio, J. F. and Ley, T. J. (2003). High-penetrance mouse model of acute promyelocytic leukemia with very low levels of PML-RARα expression. *Blood* 102, 1857-1865.

Wickliffe, K. E., Williamson, A., Meyer, H.-J., Kelly, A. and Rape, M. (2011). K11-linked ubiquitin chains as novel regulators of cell division. *Trends in Cell Biology* 21, 656-663.

Wilson, C. J., Si, Y., Thompsons, C. M., Smellie, A., Ashwell, M. A., Liu, J.-F., Ye, P., Yohannes, D. and Ng, S.-C. (2006). Identification of a Small Molecule That Induces Mitotic Arrest Using a Simplified High-Content Screening Assay and Data Analysis Method. *Journal of Biomolecular Screening* 11, 21-28.

Windheim, M., Peggie, M. and Cohen, P. (2008). Two different classes of E2 ubiquitin-conjugating enzymes are required for the mono-ubiquitination of proteins and elongation by polyubiquitin chains with a specific topology. *Biochemical Journal* 409, 723-9.

Wu, G., Xu, G., Schulman, B. A., Jeffrey, P. D., Harper, J. W. and Pavletich, N. P. (2003). Structure of a β-TrCP1-Skp1-β-Catenin Complex: Destruction Motif

Binding and Lysine Specificity of the SCFβ-TrCP1 Ubiquitin Ligase. *Molecular Cell* 11, 1445-1456.

Wu, H. and Leng, R. P. (2011). UBE4B, a ubiquitin chain assembly factor, is required for MDM2-mediated p53 polyubiquitination and degradation. *Cell Cycle* 10, 1912-5.

Wu, H., Pomeroy, S. L., Ferreira, M., Teider, N., Mariani, J., Nakayama, K. I., Hatakeyama, S., Tron, V. A., Saltibus, L. F., Spyracopoulos, L. et al. (2011). UBE4B promotes Hdm2-mediated degradation of the tumor suppressor p53. *Nature Medicine* 17, 347-55.

Xu, L., Wei, Y., Reboul, J., Vaglio, P., Shin, T.-H., Vidal, M., Elledge, S. J. and Harper, J. W. (2003). BTB proteins are substrate-specific adaptors in an SCF-like modular ubiquitin ligase containing CUL-3. *Nature* 425, 316-321.

Xu, P., Duong, D. M., Seyfried, N. T., Cheng, D., Xie, Y., Robert, J., Rush, J., Hochstrasser, M., Finley, D. and Peng, J. (2009). Quantitative Proteomics Reveals the Function of Unconventional Ubiquitin Chains in Proteasomal Degradation. *Cell* 137, 133-145.

Ye, Y., Meyer, H. H. and Rapoport, T. A. (2001). The AAA ATPase Cdc48/p97 and its partners transport proteins from the ER into the cytosol. *Nature* 414, 652-6.

Yin, Y., Seifert, A., Chua, J. S., Maure, J. F., Golebiowski, F. and Hay, R. T. (2012). SUMO-targeted ubiquitin E3 ligase RNF4 is required for the response of human cells to DNA damage. *Genes and Development* 26, 1196-208.

Yip, K. W., Cuddy, M., Pinilla, C., Giulanotti, M., Heynen-Genel, S., Matsuzawa, S.-I. and Reed, J. C. (2011). A High-Content Screening (HCS) Assay for the Identification of Chemical Inducers of PML Oncogenic Domains (PODs). *Journal of Biomolecular Screening* 16, 251-258.

Yoshimura, K., Kitagawa, H., Fujiki, R., Tanabe, M., Takezawa, S., Takada, I., Yamaoka, I., Yonezawa, M., Kondo, T., Furutani, Y. et al. (2009). Distinct function of 2 chromatin remodeling complexes that share a common subunit, Williams syndrome transcription factor (WSTF). *Proceedings of the National Academy of Sciences of the United States of America* 106, 9280-5.

Yu, J., Lan, J., Wang, C., Wu, Q., Zhu, Y., Lai, X., Sun, J., Jin, C. and Huang, H. (2010). PML3 interacts with TRF1 and is essential for ALT-associated PML bodies assembly in U2OS cells. *Cancer Letters* 291, 177-86.

Yuan, W.-C., Lee, Y.-R., Huang, S.-F., Lin, Y.-M., Chen, T.-Y., Chung, H.-C., Tsai, C.-H., Chen, H.-Y., Chiang, C.-T., Lai, C.-K. et al. (2011). A Cullin3-KLHL20 Ubiquitin Ligase-Dependent Pathway Targets PML to Potentiate HIF-1 Signaling and Prostate Cancer Progression. *Cancer Cell* 20, 214-228.

Zhang, D. D., Lo, S.-C., Cross, J. V., Templeton, D. J. and Hannink, M. (2004). Keap1 Is a Redox-Regulated Substrate Adaptor Protein for a Cul3-Dependent Ubiquitin Ligase Complex. *Molecular and Cellular Biology* 24, 10941-10953.

Zhang, F.-P., Mikkonen, L., Toppari, J., Palvimo, J. J., Thesleff, I. and Jänne, O. A. (2008). Sumo-1 Function Is Dispensable in Normal Mouse Development. *Molecular and Cellular Biology* 28, 5381-5390.

Zhang, J.-H., Chung, T. D. Y. and Oldenburg, K. R. (1999). A Simple Statistical Parameter for Use in Evaluation and Validation of High Throughput Screening Assays. *Journal of Biomolecular Screening* 4, 67-73.

Zhang, R., Poustovoitov, M. V., Ye, X., Santos, H. A., Chen, W., Daganzo, S. M., Erzberger, J. P., Serebriiskii, I. G., Canutescu, A. A., Dunbrack, R. L. et al. (2005). Formation of MacroH2A-Containing Senescence-Associated Heterochromatin Foci and Senescence Driven by ASF1a and HIRA. *Developmental Cell* 8, 19-30.

Zhang, X. W., Yan, X. J., Zhou, Z. R., Yang, F. F., Wu, Z. Y., Sun, H. B., Liang, W. X., Song, A. X., Lallemand-Breitenbach, V., Jeanne, M. et al. (2010). Arsenic trioxide controls the fate of the PML-RARα

oncoprotein by directly binding PML. *Science* 328, 240-243.

Zheng, N., Schulman, B. A., Song, L., Miller, J. J., Jeffrey, P. D., Wang, P., Chu, C., Koepp, D. M., Elledge, S. J., Pagano, M. et al. (2002). Structure of the Cul1-Rbx1-Skp1-F boxSkp2 SCF ubiquitin ligase complex. *Nature* 416, 703-9.

Zheng, N., Wang, P., Jeffrey, P. D. and Pavletich, N. P. (2000). Structure of a c-Cbl–UbcH7 Complex: RING Domain Function in Ubiquitin-Protein Ligases. *Cell* 102, 533-539.

Zhong, S., Salomoni, P. and Pandolfi, P. P. (2000). The transcriptional role of PML and the nuclear body. *Nat Cell Biol* 2, E85-E90.

Zhu, J., Koken, M. H. M., Quignon, F., Chelbi-Alix, M. K., Degos, L., Wang, Z. Y., Chen, Z. and de Thé, H. (1997). Arsenic-induced PML targeting onto nuclear bodies: Implications for the treatment of acute promyelocytic leukemia. *Proceedings of the National Academy of Sciences, USA* 94, 3978-3983.

Zhuang, M., Calabrese, M. F., Liu, J., Waddell, M. B., Nourse, A., Hammel, M., Miller, D. J., Walden, H., Duda, D. M., Seyedin, S. N. et al. (2009). Structures of SPOP-substrate complexes: insights into molecular architectures of BTB-Cul3 ubiquitin ligases. *Molecular Cell* 36, 39-50.

Zimmerman, E. S., Schulman, B. A. and Zheng, N. (2010). Structural assembly of cullin-RING ubiquitin ligase complexes. *Current Opinion in Structural Biology* 20, 714-721.